NILU
Norsk institutt for luftforskning
Norwegian Institute for Air Research

Atmospheric Degradation of Amines (ADA)

Summary Report:
Photo-Oxidation of Methylamine,
Dimethylamine and Trimethylamine
CLIMIT project no. 201604

Claus Jørgen Nielsen, Barbara D'Anna, Matthias Karl, Marius Aursnes,
Antoinette Boreave, Rossana Bossi, Arne Joakim Coldevin Bunkan,
Marianne Glasius, Mattias Hallquist, Anne-Maria Kaldal Hansen,
Kasper Kristensen, Tomas Mikoviny, Mihayo Musabila Maguta,
Markus Müller, Quynh Nguyen, Jonathan Westerlund, Kent Salo,
Henrik Skov, Yngve Stenstrøm and Armin Wisthaler

Scientific report

Atmospheric Degradation of Amines (ADA)

Summary Report:

Gas Phase Photo-Oxidation of Methylamine, Dimethylamine and Trimethylamine

Claus Jørgen Nielsen, Barbara D'Anna, Matthias Karl, Marius Aursnes, Antoinette Boreave, Rossana Bossi, Arne Joakim Coldevin Bunkan, Marianne Glasius, Anne-Maria Kaldal Hansen, Mattias Hallquist, Kasper Kristensen, Tomas Mikoviny, Mihayo Musabila Maguta, Markus Müller, Quynh Nguyen, Jonathan Westerlund, Kent Salo, Henrik Skov, Yngve Stenstrøm, Armin Wisthaler
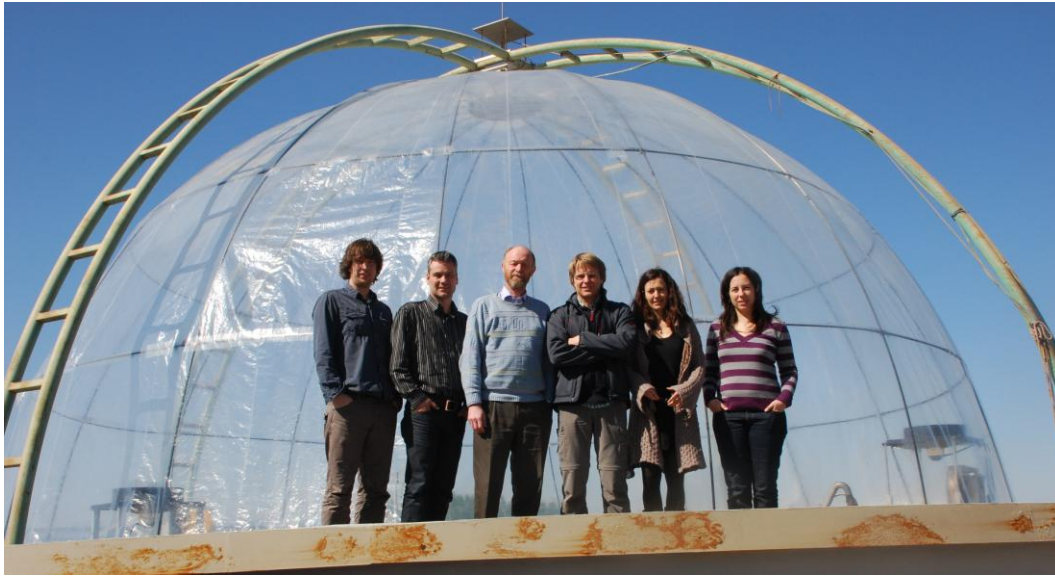
The EUPHORE Team (March 2010). From left: Tomas Mikoviny, Mattias Hallquist,
Claus Jørgen Nielsen, Armin Wisthaler, Barbara D'Anna and Monica Moreno Vazquez.

Preface

Studies on the emission from amine-based CO_2 capture mimic facilities indicate the simple alkane-amines as process degradation products of the more complex amines used in CO_2 capture. These small amines will therefore always be emitted with the cleaned flue gas to the atmosphere no matter which parent amine is used in the absorber, and they may present the major environment and human health problem linked to the implementation of amine-based CO_2 capture. The *Atmospheric Degradation of Amines* project – ADA – has undertaken a systematic experimental study of the atmospheric photo-oxidation of methylamine (CH_3NH_2, CAS: 74-89-5), dimethylamine (($CH_3)_2NH$, CAS: 124-40-3), and trimethyl-amine (($CH_3)_3N$, CAS: 75-50-3) including their contribution to the formation of new particles.

The overall objective of the ADA-2010 project was to contribute to the understanding of the atmospheric degradation of amines emitted to the atmosphere from CO_2 capture plants. The specific targets were:

- To identify the gas phase photochemical degradation products resulting from emission of amines under natural atmospheric conditions.

- To quantify the main products in the gas phase photo-oxidation of amines emitted to air.

- To verify/update existing atmospheric photo-oxidation schemes for amines to account for all products formed under natural conditions.

- To assess the conditions for aerosol formation during the gas phase degradation of amines emitted to air, and to characterize and quantify the aerosol formation.

The present report summarises the findings and conclusions from the ADA-2010 study on the atmospheric photo-oxidation of methylamine, dimethylamine and trimethylamine. The project has achieved its targets.

This page is intentionally left blank

Table of Contents

Executive Summary

The atmospheric gas phase photo-oxidation of methylamine (CH_3NH_2), dimethyl-amine ((CH_3)$_2$NH) and trimethylamine ((CH_3)$_3$N) has been studied under pseudo natural conditions at the European Photochemical Reactor, EUPHORE, in Valencia, Spain. The experiments were carried out under different, relevant NOx conditions and initial gas phase mixing ratios of 100 to 300 ppbV. The photo-oxidation was monitored *in situ* by FT-IR and on-line by PTR-TOF-MS, HT-PTR-MS and cryotrap GC-MS, and samples were collected on various adsorbents for subsequent off-line analysis. The formation of particles was monitored by SMPS, TEOM, AMS and VTDMA on-line instruments and filter sampling followed by analysis with HPLC-qTOF-MS.

Atmospheric photo-oxidation is dominated by the OH radical which reacts with the amines by abstracting a hydrogen atom. All major photo-oxidation products have been identified and quantified, and detailed photo-oxidation schemes including branching ratios have been obtained. Based on the results from on-line and *in situ* instrumentation it is found that around 25 % of the reaction between methylamine and OH radicals takes place at the amino group (–NH_2), and that the nitramine, CH_3NHNO_2, is formed directly as a result of this. For dimethyl-amine the present study confirms previous results by Lindley *et al*. (*Chem. Phys. Lett*. *67*, (1979) 57-62) that around 40 % of the reaction with OH radicals takes place at the amino group (–NH), and that the nitrosamine, (CH_3)$_2$NNO, and the nitramine, (CH_3)$_2$NNO$_2$, are formed as a result of this. For trimethylamine the study shows that around 60 % of the reaction with OH radicals has the potential to form of the nitrosamine, (CH_3)$_2$NNO, and the nitramine, (CH_3)$_2$NNO$_2$. The amounts of nitrosamine and nitramines depend upon the mixing ratio of NOx. For rural regions with NOx levels of 0.2-10 ppbV and with a NO_2:NO ratio of 2:1, less that 0.4 % of the atmospheric oxidation of methylamine will result in the nitramine (CH_3NHNO_2). For dimethylamine less than 2.5 % will end up as nitramine ((CH_3)$_2$NNO$_2$), and for trimethylamine less than 5 % will end up as nitramine ((CH_3)$_2$NNO$_2$). The amount of nitrosamine, (CH_3)$_2$NNO, formed in the atmosphere depends not only on the ambient amounts of NO and NO_2, but also on the amount of oxidizing radicals and the actinic flux. The conditions vary during the time of day and throughout year, and because NDMA is constantly formed and destructed through photolysis is the amount of NDMA present in the atmosphere that is of interest, and this can be derived from steady-state considerations. Taking an annual average oxidant activity (OH at daytime, NO_3 at night-time) corresponding to [OH] = 5×10^5 cm^{-3} and an annual average actinic flux corresponding to j_{NO2} = 6×10^{-5} s^{-1} mimicking conditions at Mongstad results in a steady-state nitrosamine concentration of less than 0.6 % of photo-oxidized dimethylamine and less than 1.1 % of photo-oxidized trimethylamine.

The major primary products in atmospheric photo-oxidation of methylamine, dimethylamine and trimethylamine are imines (methanimine and N-methyl-methanimine) and amides (formamide, *N*-methyl formamide and *N,N*-dimethyl formamide). The atmospheric fate of imines is not yet completely understood;

hydrolysis in the atmospheric aqueous phase is most likely a dominant sink in which methanimine and *N*-methyl methanimine hydrolyses to formaldehyde and ammonia, respectively methylamine. The atmospheric photo-oxidation of formamide leads to isocyanic acid, while the major product from atmospheric photo-oxidation of *N*-methyl formamide and *N,N*-dimethyl formamide is methyl-isocyanete. Small amounts of nitramines are also formed in the atmospheric photo-oxidation of *N*-methyl formamide and *N,N*-dimethyl formamide. As the atmospheric lifetimes of these amides are of the order 1 day in the Mongstad area, they will be so dispersed that the concentrations of secondary products in the amine photo-oxidation will be negligible.

The aerosol formation potential of the three methylamines was found to be substantial. Total aerosol yields obtained in EUPHORE experiments were between 8 and 14%. The total aerosol yield in the photo-oxidation of N-methyl methanimine was estimated using the aerosol model MAFOR to be 18% and aerosol forming in the photo-oxidation of N-methyl methanimine had a very low volatility. In general, aerosol particles that formed in methylamine photo-oxidation experiments consisted of two major fractions: a nitrate salt fraction (aminium nitrates of the respective methylamine and other nitrates) which showed a relative high volatility and secondary produced organics which showed intermediate to low volatility. In experiments under low NO_x conditions, representative for rural air, secondary organic aerosol (SOA) was the dominant fraction in the aerosol. Once aminium nitrate salt particles are formed in the atmosphere, they can re-volatilize, undergo particle-phase reactions, or serve as a site for condensation of other organic species. Aminium nitrate from dimethylamine was found to be more stable when indicated by the thermodynamic solid/gas equilibrium. Possibly, condensation of organics onto the produced aerosol formed a barrier that prevented the salts from re-volatilization. The enhanced stability of particles produced by dimethylamine should be taken into account when performing atmospheric dispersion model calculation on the fate of emitted dimethylamine.

The major uncertainties in the understanding of the fate of amines emitted to the atmosphere is related to night-time chemistry (NO_3 radicals), to the chemistry of imines such as $CH_2=NH$ and $CH_2=NCH_3$, and to chemistry in the aqueous aerosol. It is suggested that research on the gas phase kinetics of NO_3 reactions with simple amines be initiated. It is further suggested that research on aqueous phase chemistry of amines and amine photo-oxidation products be initiated. Research on the atmospheric chemistry of imines should be continued.

Gas Phase Photo-Oxidation of Methylamine, Dimethylamine and Trimethylamine

1 State of the art

Compounds emitted into the atmosphere are removed again from the atmosphere by wet and dry deposition, photolysis, and chemical reaction. Aliphatic amines show absorption at 230-250 nm extending to shorter wave-lengths;[1] they will therefore not undergo photolysis in the troposphere. Wet and dry depositions of organic compounds are controlled by their vapour-particle partitioning,[2] which in turn depends on their vapour pressure and Henry's Law constants, and on the particle and droplet size and number density. Organics with vapour pressure $\approx 10^{-4}$ Pa will partition roughly 50:50 between the parti-culate and gas phases in areas with 100 μg m^{-3} background aerosol.[2] Methyl-amine (CAS: 74-89-5), dimethylamine (CAS: 124-40-3) and trimethylamine (CAS: 75-50-3) are all gases at STP and will only partition to particulate matter if this is acidic. Further, the Henry's Law constants for the three amines are reported to be only 36[3] - 90[4], 31[3] - 57[4] and 9.6[4] for methylamine, dimethylamine and trimethylamine, respectively. Accordingly, these three amines will preferentially undergo photo-oxidation in the gas phase.

Aliphatic amines have almost been left out of atmospheric and environmental sciences due to their low ppbV-range mixing ratios and their short lifetimes.[5] Consequently, the frequently used mechanistic database for modelling atmospheric photo-oxidation of organics, the Master Chemical Mechanism (MCM, http://mcm.leeds.ac.uk/MCM/home.htt),[6] does currently not include degradation schemes for amines.

Reaction with OH radicals is the dominant loss process for the majority of the tropospheric trace gases.[7] Compounds such as aldehydes and ketones undergo direct photolysis, and reactions with O_3 and NO_3 radicals are important for many unsaturated hydrocarbons. In marine areas reactions with Cl atoms may also constitute an important sink. Currently there are no kinetic data for the reactions of amines with Cl atoms and NO_3 radicals.

Tropospheric O_3 stems from *in situ* photochemical formation and from downward transport from the stratosphere.[8] Mixing ratios of O_3 in the lower troposphere ranges for 10 - 40 ppbV in clean remote areas[9] and may reach levels above 100 ppmV in urban/suburban sites.[10]

The presence of ozone in the troposphere leads to the formation of OH radicals through the photolysis of O_3 (λ < 320 nm). Because OH radicals are produced photolytically, they are only present in significant amounts during the daytime and exhibit a maximum around midday. A diurnally, seasonally, and annually averaged global tropospheric OH concentration of 9.7×10^5 molecules cm^{-3} has been derived from observations of methyl chloroform.[11] However, large seasonal, latitudinal and altitudinal variations exist.[12]

Average Cl atom concentrations in coastal areas have been derived from variability-lifetime relationships for selected non-methane hydrocarbons (NMHC) in surface air at Maine, USA, placing estimates of Cl⬚concentrations of 2.2 - 5.6 ×⬚10^4 cm^{-3}.[13] It has been suggested that an average Cl atom concentration of around 6×10^4 cm^{-3} is representative for the polluted North Atlantic air mass.[14]

The NO_3 radical is formed in the reactions of NO and NO_2 with O_3. Because the NO_3 radical photolyzes rapidly,[15] the NO_3 radical concentrations are low during the daytime. The NO_3 radical has been observed at mixing rations up to 350 pptV in night-time ambient atmospheres over the United States and Europe.[16] Recent measurements place night-time mixing ratios around 4-5 pptV in rural areas,[17] and around 10 pptV in polluted marine environment.[18]

1.1 CH_3NH_2

Atkinson et $al.$[19] studied the kinetics of the OH radical reaction with CH_3NH_2 over the temperature range 299 – 426 K and reported a *negative* Arrhenius activation energy, $k_{OH}(T) = 1.02 \times 10^{-11} \times exp\{(230 \pm 150)K/T\}$ and $k_{OH} = (2.20 \pm 0.22) \times 10^{-11}$ cm^3 molecule^{-1} s^{-1} at 298 K. Carl and Crowley[20] reported later a room temperature value, $k_{OH} = (1.73 \pm 0.11) \times 10^{-11}$ cm^3 molecule^{-1} s^{-1}, which is ca. 30% lower. The absolute value of Atkinson et $al.$[19] depends on a calibrated gas whereas Carl and Crowley[20] used the UV cross-section of the amine for calibration, and they suggest that the earlier results suffer from a calibration error. Tuazon et al.[21] have determined the rate constant for reaction of methylamine with O_3 to be $k_{O3} = (7.4 \pm 2.4) \times 10^{-21}$ cm^3 molecule^{-1} s^{-1} at 298 K.

Rudic et $al.$[22] studied the product branching and dynamics of the reaction between methylamine and Cl atoms employing REMPI spectroscopy with TOF-MS detection. They found branching ratios for the C-H : N-H and the C-D : N-D abstractions of 0.48 : 0.52 and 0.58 : 0.42 in CH_3NH_2 and CD_3ND_2, respectively. Since OH radicals and Cl atoms often show similar selectivity in their reactions, one may expect that also hydrogen abstraction in primary amines by OH radicals will occur from both C and N.

Galano and Alvarez-Idaboy have calculated the rate constant for the methylamine reaction with OH radicals using Canonical Variational Therory employing results from CCSD(T)/6-311++G(2d,2p)//BHandHLYP/6-311++G(2d,2p) calculations. Their result are $k_{OH}(T) = 5.89 \times 10^{-11} \times exp(-757/RT)$ cm^3 molecule^{-1} s^{-1} and $k_{OH} = 5.20 \times 10^{-12}$ at 298 K;[23] they predict a *positive* Arrhenius activation energy. They also predict a branching ratio for the C-H : N-H abstractions of 0.80 : 0.20 at 298 K. Tian et $al.$[24] have presented results from similar theoretical calculations at the CCSD(T)/6-311++G(2d,2p)// CCSD/6-31G(d) level of theory followed by improved canonical variational transition state theory incorporating small-curvature tunnelling. Tian et $al.$[24] predict a *negative* Arrhenius activation energy at atmospheric temperatures, a positive Arrhenius activation energy at higher temperatures, and $k_{OH} = 2.98 \times 10^{-11}$ cm^3 molecule^{-1} s^{-1} at 298 K. They further report the theoretical branching ratio for the C-H : N-H abstractions to be 0.74 : 0.26 at 298 K.

There are no literature data on the products formed in the atmospheric photo-oxidation of methylamine. Schade and Crutzen speculated on the atmospheric degradation mechanism for the OH initiated photo-oxidation of CH_3NH_2 in a study of the emission of aliphatic amines from animal husbandry,[25] Scheme 1.1.
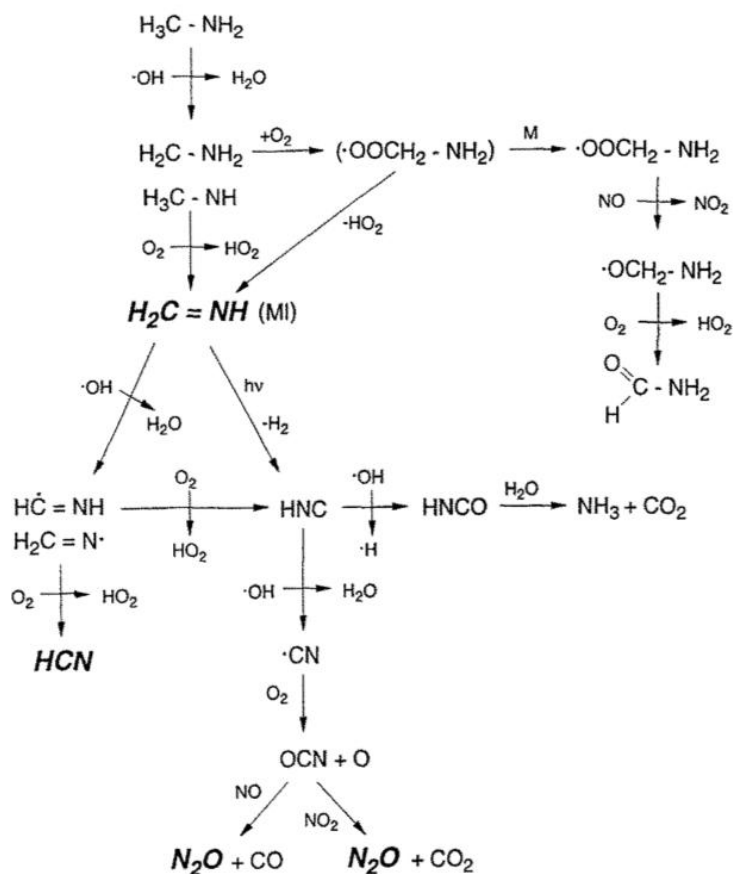
Scheme 1.1. Possible methylamine gas phase chemistry, leading to N_2O or HCN. (From Schade and Crutzen, Ref. 25).

Murphy et al.[26] carried out 3 experiments in which the oxidant precursor(s) were i) NO_2, ii) H_2O_2/NO and iii) O_3. They found that nearly 100% of the aerosol formed during a photo-oxidation experiment with CH_3NH_2 consisted of methyl-ammonium nitrate (salt) and that less than 1% was non-salt organics. Though the formation of non-salt aerosol was small, the relative importance of non-salt organic aerosol increased through the course of the experiments.

1.2 $(CH_3)_2NH$

Atkinson et al.[27] studied the kinetics of the OH radical reaction with $(CH_3)_2NH$ over the temperature range 299 – 426 K and reported a *negative* Arrhenius activation energy, $k_{OH}(T) = 2.89 \times 10^{-11} \times \exp\{(245 \pm 150)K/T\}$ and $k_{OH} = (6.54 \pm 0.66) \times 10^{-11}$ cm^3 molecule^{-1} s^{-1} at 298 K. Carl and Crowley[20] reported a room temperature value in perfect agreement with the results of Atkinson et al., $k_{OH} = (6.49 \pm 0.64) \times 10^{-11}$ cm^3 molecule^{-1} s^{-1}.

Pitts et al.[28] employed a 50 m^3 outdoor chamber to carry out an exploratory study of the products formed when a mixture of 500 ppbV $(CH_3)_2NH$, 80 ppbV NO

and 160 ppbV NO_2 was subjected to natural sunlight conditions. They found $(CH_3)_2NNO_2$ (dimethylnitramine) and $CHON(H)CH_3$ (*N*-methyl formamide) as gas phase products, but did not quantify the amounts. About 1% yield of $(CH_3)_2NNO$ (dimethylnitrosamine) was formed in the dark and subsequently destroyed in sunlight. Aerosol was formed during the photo-oxidation but was not analyzed. There is no report on the mass balance in the $(CH_3)_2NH$ photo-oxidation experiment.

Hanst *et al.*[29] were the first to report formation of $(CH_3)_2NNO$ under dark, humid conditions when dimethylamine was mixed HONO, NO and NO_2 in air. As mentioned above, Pitts *et al.*[28] found a similar, but smaller nitrosation reaction of dimethylamine in the dark. A later control experiment by Glasson,[30] however, suggests that the apparent gas phase nitrosation in reality may be a surface reaction. A theoretical study of the gas phase reaction between HONO and dimethylamine[31] suggests a barrier to the direct reaction of more than 90 kJ mol^{-1}, *i.e.* the reaction will not take place at atmospheric conditions: <u>HONO is not a gas phase nitrosation agent under atmospheric conditions</u>.

Grosjean has outlined the routes of OH reaction with $(CH_3)_2NH$,[32] Scheme 1.2.
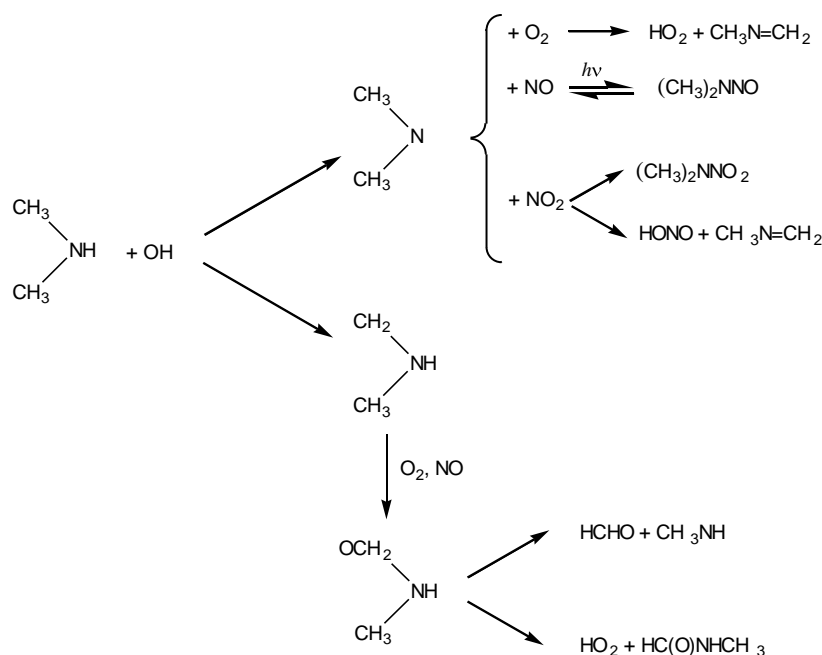
Scheme 1.2. Reaction of OH with dimethylamine. (From Grosjean, Ref. 32).

The branching ratio in the initial hydrogen abstraction by OH radicals was determined by Lindley *et al.*[33] who reported $k_{1a}/(k_{1a}+k_{1b}) = 0.37 \pm 0.05$

$$(CH_3)_2NH + OH \rightarrow (CH_3)_2N + H_2O \qquad (1a)$$

$$\rightarrow CH_3NHCH_2 + H_2O \qquad (1b)$$
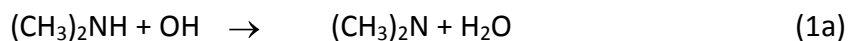
Galano and Alvarez-Idaboy have calculated the rate constant for the dimethylamine reaction with OH radicals using Canonical Variational Therory employing results from CCSD(T)/6-311++G(2d,2p)//BHandHLYP/6-311++G(2d,2p) calculations. Their results are $k_{OH}(T) = 2.72 \times 10^{-11} \times \exp(200/RT)$ cm^3 $molecule^{-1}$

s^{-1} and k_{OH} = 5.20 × 10^{-12} at 298 K;[23] they predict a *negative* Arrhenius activation energy and a branching ratio for the C-H:N-H abstractions of 0.48 : 0.52 at 298 K.

Tuazon *et al.*[21] have determined the rate constant for reaction of dimethylamine with O_3 to be k_{O3} = (1.67 ± 0.20) × 10^{-18} cm^3 molecule^{-1} s^{-1} at 298 K. They reported $CH_3N=CH_2$, CH_3NO_2, CH_2O, HCOOH, $(CH_3)_2NCHO$ and CH_3NHCHO as products in the reaction; *N*-methyl methanimine was reported formed with the largest yield. Tuazon *et al.* proposed a reaction mechanism for the amine – ozone reaction, Scheme 1.3.
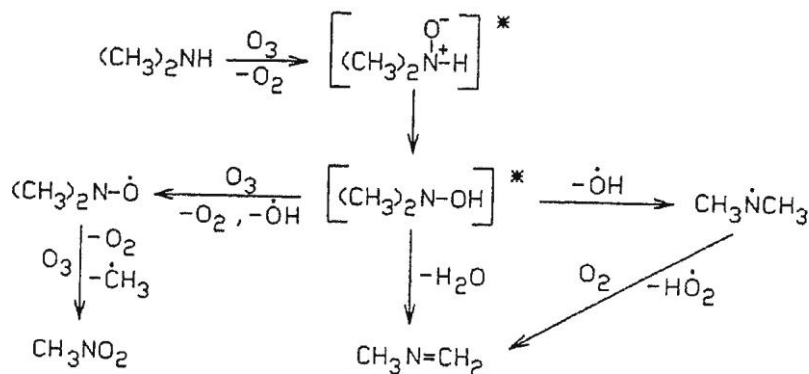
Scheme 1.3. Proposed mechanism for the reaction of ozone with dimethylamine (From Tuazon *et al.*, Ref. 21).

Derek Price has in a recent MSc-thesis reported results from studies of the NO_3 radical initiated atmospheric oxidation of $(CH_3)_2NH$ in a 20 m^3 indoor smog chamber.[34] The gas phase was monitored by PTR-MS and the following inter-pretation of the major PTR-MS ion signals $[MH]^+$ was offered: *m/z* 44, CH_3NCH_2 (methyl-methanimine); *m/z* 45, CH_3CHO (acetaldehyde); *m/z* 46, $(CH_3)_2NH$ (dimethylamine); *m/z* 58, CH_3NCHCH_3 (*N*-methyl ethanimine); *m/z* 59, $(CH_3)_2CO$ (acetone) and/or CH_3CH_2CHO (propanal); *m/z* 60, $(CH_3)_3N$ (trimethylamine) and or CH_3CH_2NO (nitrosoethane), *m/z* 62, CH_3NO_2 (nitromethane); *m/z* 91, $(CH_3)_2NNO_2$ (dimethyl-nitramine). There was no attempt to relate the compounds mentioned to any specific degradation mechanism in the thesis.

In the exploratory study by Pitts *et al.*[28] aerosol was formed during the photo-oxidation of $(CH_3)_2NH$, but it was not analyzed. Derek Price[34] also analyzed the aerosol formed in the $(CH_3)_2NH/O_3/NOx$ oxidation experiments by HR-TOF-AMS. The major ion peaks observed of the aerosol included *m/z* 30.034 (CH_4N^+), *m/z* 44.050 ($C_2H_6N^+$), *m/z* 58.066 ($C_3H_8N^+$), *m/z* 86.099 ($C_5H_{12}N^+$), and *m/z* 101.114 ($C_6H_{15}N^+$), which represent the backbone amine fragments. Fragments of large hydrocarbons including *m/z* 72.094 ($C_5H_{12}^+$), *m/z* 86.11 ($C_6H_{14}^+$), and *m/z* 94.078 ($C_7H_{10}^+$) were detected, with evidence of oxidation in *m/z* 72.058 ($C_4H_8O^+$) and *m/z* 97.065 ($C_6H_9O^+$). The thesis offers no further interpretation of the results.

1.3 $(CH_3)_3N$

Atkinson *et al.*[27] studied the kinetics of the OH radical reaction with $(CH_3)_3N$ over the temperature range 299 – 426 K and reported a *negative* Arrhenius activation energy, $k_{OH}(T)$ = 2.62×10^{-11} × exp{(250 ± 150)K/T} and k_{OH} = (6.09 ± 0.61) × 10^{-11}

cm^3 molecule^{-1} s^{-1} at 298 K. Carl and Crowley[20] presented a room temperature value for k_{OH} = (3.58 ± 0.22) × 10^{-11} which differ by a factor of 2. The absolute value of Atkinson *et al.*[27] depends on a calibrated gas whereas Carl and Crowley[20] used the UV cross section of the amine for calibration, and the latter authors suggest that the earlier results suffer from a calibration error.

Pitts *et al.*[28] employed a 50 m^3 outdoor chamber to carry out an exploratory study of the products formed when a mixture of 500 ppb $(CH_3)_3N$, 80 ppb NO and 160 ppb NO_2 was subjected to natural sunlight conditions. They found $(CH_3)_2NNO_2$ (dimethylnitramine) and $(CH_3)_2NCHO$ (*N,N*-dimethylformamide) as gas phase products, but they did not quantify the amounts formed. Large amounts (370 ppb) of HCHO (formaldehyde) were detected in the gas phase. Only trace amounts of $(CH_3)_2NNO$ (dimethylnitrosamine) were reported. There was no report on the mass balance in their $(CH_3)_3N$ photo-oxidation experiments.

Tuazon *et al.*[21] have determined the rate constant for reaction of trimethylamine with O_3 to be k_{O3} = (7.84 ± 0.87) × 10^{-18} cm^3 molecule^{-1} s^{-1} at 298 K. They observed $(CH_3)_2NCHO$, $CH_3N=CH_2$, CH_3NO_2, CH_2O and HCOOH as products in the reaction. Formaldehyde was formed with the largest yield, followed by *N*-methyl methanimine. A reaction mechanism for the amine − ozone reaction was proposed, Scheme 1.4.
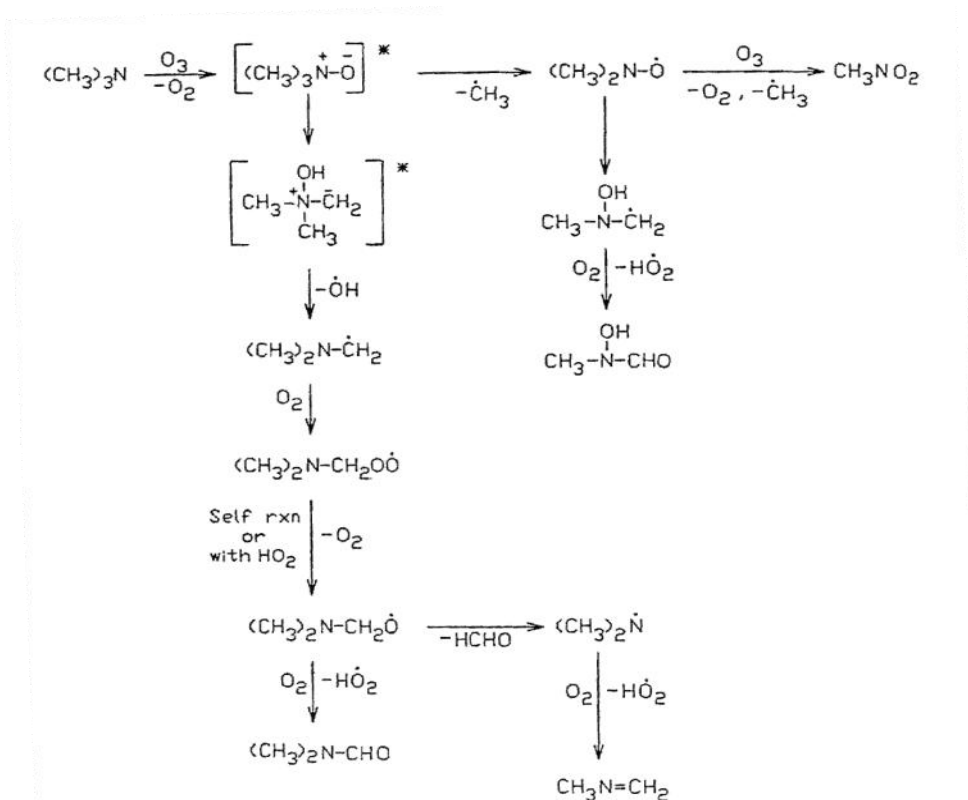
Scheme 1.4. Proposed mechanism for the reaction of ozone with trimethylamine (From Tuazon *et al.*, Ref. 21).

Grosjean outlined the mechanism for atmospheric photo-oxidation of $(CH_3)_3N$, in 1991.[32] In 1995 Schade and Crutzen speculated on the atmospheric degradation mechanism in a study of the emission of aliphatic amines from animal husbandry and their atmospheric photo-oxidation reactions,[25] Scheme 1.5.

$(CH_3)_3N$

$\cdot OH \quad | \leftarrow H_2O$

$\cdot CH_2N(CH_3)_2$

$O_2+M \quad |$
$NO \quad | \leftarrow NO_2$

$\cdot OCH_2N(CH_3)_2$

$O_2 \swarrow \quad \searrow -HCHO$
HO_2

$OCH-N(CH_3)_2$ (DMF) $\qquad (CH_3)_2N\cdot$

$O_2 | \leftarrow HO_2$

$OCN-CH_3 \leftarrow|\cdot OH \quad CN-CH_3 \xleftarrow[-H_2]{h\nu} H_3C-N=CH_2$ (MMI)

$\cdot OH | \qquad H\cdot \qquad \cdot OH |$

$NO \searrow \quad O_2/-H_2O \qquad -CO_2 \qquad +M \qquad -H_2O$
$\qquad \searrow NO_2 \qquad \qquad -HCHO \quad O_2 \swarrow NO_2$
$\qquad \qquad \qquad \qquad \qquad \qquad NO$

$OCN+HCHO \qquad H_3C-\dot{N}H \qquad \cdot N=CH_2+HCHO$

$NO_x | \qquad O_2|\leftarrow HO_2 \qquad O_2|\leftarrow HO_2$

$N_2O \qquad H_2C=NH \qquad HCN$

$|$
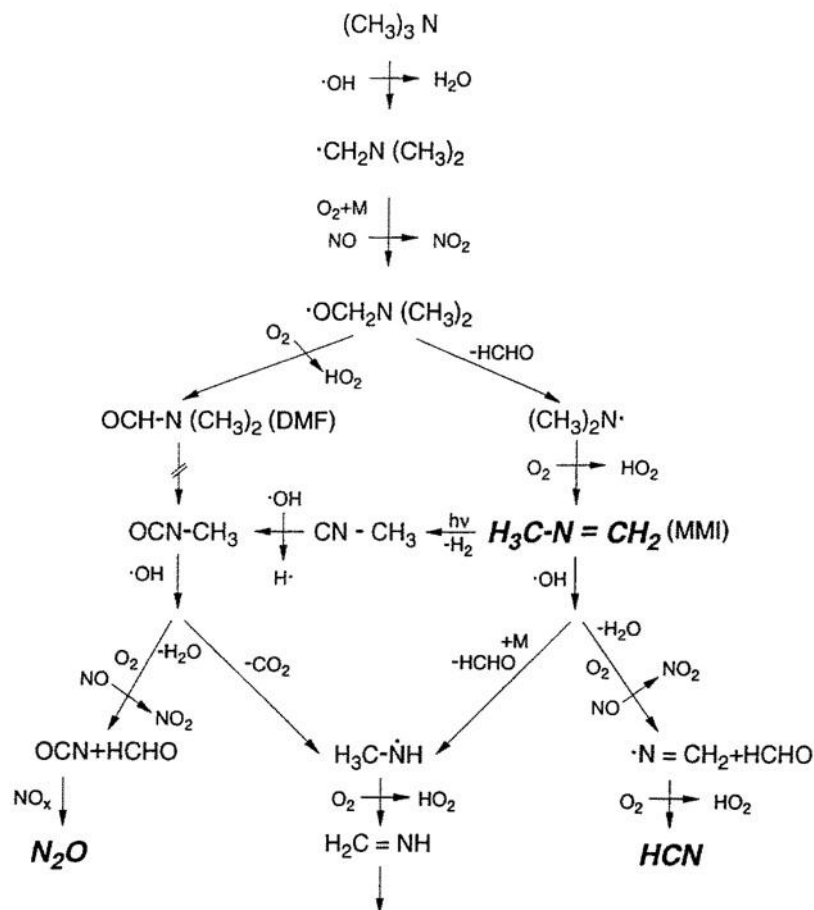
Scheme 1.5. Possible trimethylamine gas phase chemistry, leading to N_2O or HCN. (From Schade and Crutzen, Ref. 25).

Europe *et al.*[35] investigated the NO_3 initiated oxidation of TMA including secondary organic aerosol formation in a 90 m^3 indoor smog chamber. The NO_3 radicals were produced *in situ* by adding NO to a mixture of trimethylamine with excess O_3 under dark conditions, and the gas phase VOCs were monitored by PTR-MS. Their interpretation of the major ion masses [MH]$^+$ was as follows: *m/z* 31, HCHO (formaldehyde); *m/z* 33, CH_3OH (methanol); *m/z* 44, $CH_3N=CH_2$ (*N*-methyl methanimine); *m/z* 45, CH_3CHO (acetaldehyde); *m/z* 47, HCOOH (formic acid) and/or CH_3OH (methanol); *m/z* 59, $(CH_3)_2CO$ (acetone) and/or CH_3CH_2CHO (propanal); *m/z* 60, $(CH_3)_3N$ (trimethylamine); *m/z* 61, CH_3COOH (acetic acid) and/or $CH_3CH_2CH_2OH$ (propanol); *m/z* 62, CH_3NO_2 (nitromethane); *m/z* 74, $(CH_3)_2NCHO$ (dimethylformamide); *m/z* 75, $(CH_3)_2NNO$ (dimethylnitrosamine); *m/z* 88, $CH_3N(CHO)_2$ (methyldiformamide) *m/z* 90, $CH_2OH(CH_3)NCHO$ (hydroxy-methyl-methylformamide); *m/z* 91, $(CH_3)_2NNO_2$ (dimethylnitramine); *m/z* 102, $(CHO)_3N$ (triformamide). Scheme 1.6 shows their proposed mechanism for the reaction of trimethylamine with the nitrate radical and includes the trimethyl-amine oxidation by O_3 previously proposed by Tuazon *et al.*[21]
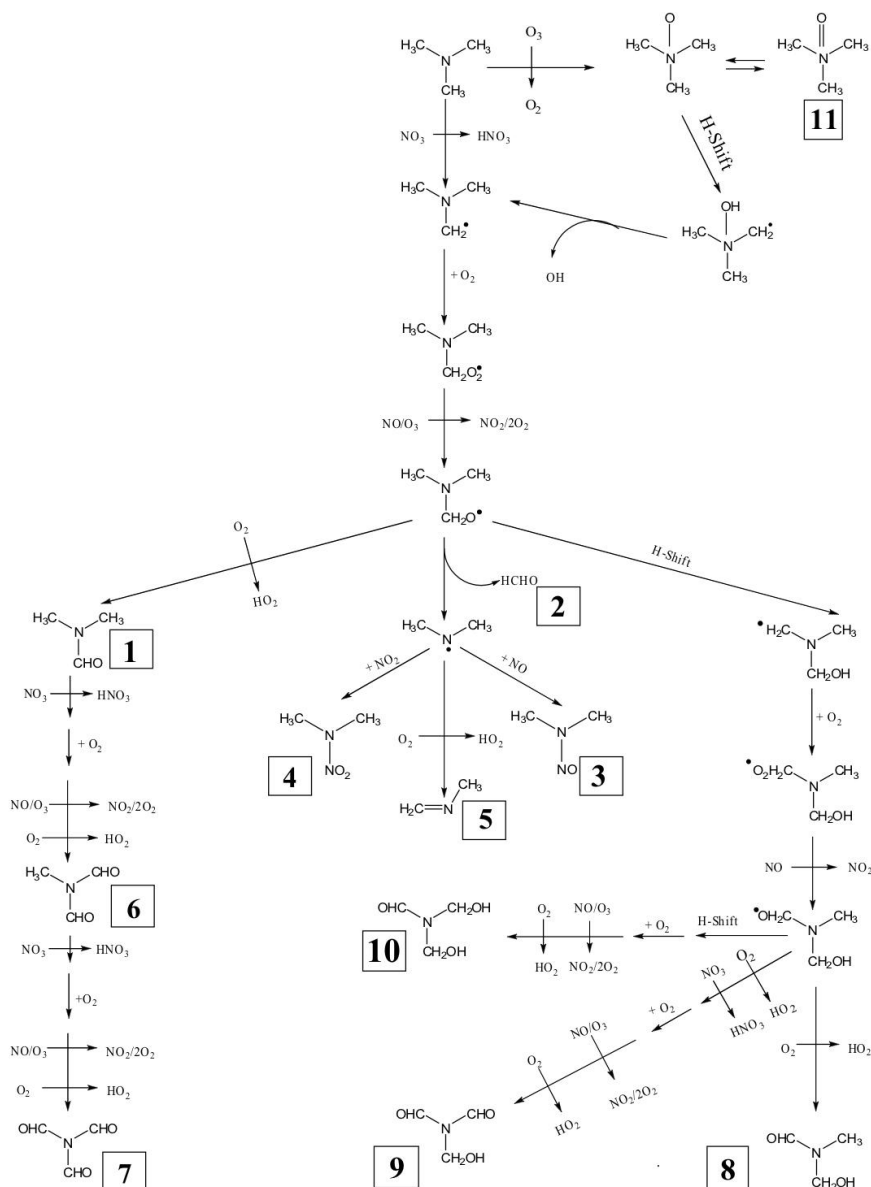
Scheme 1.6. Proposed mechanism for the reaction of trimethylamine with the nitrate radical and the trimethylamine oxidation by O_3 (From Europe *et al.*, Ref. 35)

In the exploratory $(CH_3)_3N$ photo-oxidation study by Pitts *et al.*[28] the aerosol formed contained ca. 3 µg m^{-3} (1.6 ppb) $CHONH_2$ (formamide) and another amide-like compound with M=87 was detected but not identified and quantified. Schade and Crutzen[25] suggested that this mass could correspond to $CHO-N(CH_3)-CHO$ (*N*-formyl, *N*-methylformamide). Murphy *et al.*[26] reported that the aerosol formed in high-NOx photo-oxidation experiments with $(CH_3)_3N$ mainly consisted of trimethylammonium nitrate salt. The nitrate particles were generated in an acid-base equilibrium reaction between nitric acid and $(CH_3)_3N$. Non-salt organic particles were reported formed with a mass yield of 23%.

Europe *et al.*[35] reported ion peaks from the aerosol at *m/z* 44.052 ($C_2H_6N^+$) and *m/z* 58.066 ($C_3H_8N^+$) represent amine backbone fragments while *m/z* 58.030

($C_2H_4NO^+$), 76.040 ($C_2H_6NO_2^+$), *m/z* 88.037 ($C_3H_6NO_2^+$) and *m/z* 104.040 ($C_3H_6NO_3^+$) represent fragments of amines that have been oxidized.

In summary, the amine reactions with OH radicals are fast, with room-temperature rate constants being in the range ~10^{-11} cm^3 molecule^{-1} s^{-1}, Table 1.1. The *average global lifetimes* of amines with respect to reaction with OH radicals will therefore be of the order of one day or less. The corresponding O_3 reactions are slower, and these reactions will only be relevant under extreme conditions. There are no experimental kinetic data for the reactions of amines with Cl atoms and NO_3 radicals, which both react with saturated compounds in H-abstraction reactions; the latter forming nitric acid, see *e.g.* the reviews by Atkinson[36] and by Wayne *et al.*[15]

Table 1.1. Summary of experimental rate constants at 295-300 K (/cm^3 molecule^{-1} s^{-1}) for the reactions of OH radicals and O_3 with amines.

Compound	k_{OH}	Ref.	k_{O3}	Ref.
CH_3NH_2	$(2.20 \pm 0.22) \times 10^{-11}$	19	$(7.4 \pm 2.4) \times 10^{-21}$	21
	$(1.73 \pm 0.11) \times 10^{-11}$	20		
$(CH_3)_2NH$	$(6.54 \pm 0.66) \times 10^{-11}$	27	$(1.67 \pm 0.20) \times 10^{-18}$	21
	$(6.49 \pm 0.64) \times 10^{-11}$	20		
$(CH_3)_3N$	$(6.09 \pm 0.61) \times 10^{-11}$	27	$(7.84 \pm 0.87) \times 10^{-18}$	21
	$(3.58 \pm 0.22) \times 10^{-11}$	20		

The two aerosol formation studies in which NO_3 radicals were used to initiate the degradation of amines[34,35] show many of the same types of products as found in the OH-initiated photo-oxidation studies, *i.e.* amides, nitrosamines and nitramines. It can be concluded that the night-time gas phase degradation of amines will result in the same compounds as the daytime photo-oxidation. However, the relative amounts of the different products may be different.

1.4 Amine photo-oxidation products

All atmospheric amine (photo)oxidation experiments show that imines, amides, nitramines and nitrosamines constitute the major products. The following sections summarize the available, relevant information on the atmospheric chemistry of these compounds.

1.4.1 Nitrosamines and nitramines

Experiments show that the atmospheric oxidation of secondary and tertiary amines results in the formation on photo-labile *N*-nitroso amines (nitrosamines) and photo-stable *N*-nitro amines (nitramines). Tuazon *et al.*[37] studied the reactions of OH radicals with ($CH_3)_2NNO$ (NDMA) and ($CH_3)_2NNO_2$ (DMN) by long-path FTIR employing CH_3OCH_3 as reference and found $k_{OH+NDMA}/k_{OH+CH3OCH3} = 0.85 \pm 0.05$ and $k_{OH+DMN}/k_{OH+CH3OCH3} = 1.29 \pm 0.05$. Taking today's recommended absolute value for $k_{OH+CH3OCH3} = 2.8 \times 10^{-12}$ cm^3 molecule^{-1} s^{-1} at 298 K,[38] places
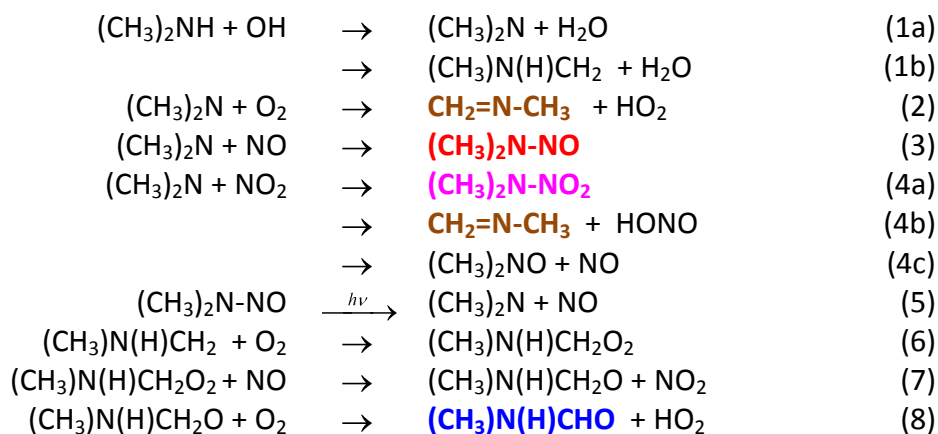
$k_{OH+NDMA} = (2.4 \pm 0.4) \times 10^{-12}$ and $k_{OH+DMN} = (3.6 \pm 0.5) \times 10^{-12}$ cm³ molecule⁻¹ s⁻¹. Later Zabarnick *et al.*[39] reported a 50% higher rate constant for dimethyl-nitrosamine reaction with OH radicals from experiments employing the two-laser photolysis/LIF probe technique, $k_{OH+NDMA} = (3.6 \pm 0.1) \times 10^{-12}$ cm³ molecule⁻¹ s⁻¹ at 296 K. Accordingly, the *average global atmospheric lifetimes* of NMDA and DMN with respect to reaction with OH are of the order of days.

The gas phase photolysis of *N*-nitroso dimethylamine (NDMA) was studied by Bamford,[40] Lindley *et al.*,[33] Geiger *et al.*,[41] Geiger and Huber[42] and by Tuazon *et al.*,[37] who determined the photolysis rate of NDMA relative to that of NO₂ to be $j_{NDMA}/j_{NO2} = 0.53 \pm 0.03$. Geiger *et al.*[41,42] report a quantum yield to photo-dissociation of NDMA following $S_1(n\pi^*) \leftarrow S_0$ excitation to be 1 ± 0.1. Photolysis of NDMA (and presumably also of other nitrosamines) is therefore fast and NDMA has an atmospheric lifetime of less than 1 hour during summer.

Tuazon *et al.*[37] found 33% CH₃NO₂, 38% HCHO and 2% CO in addition to 65% (CH₃)₂NNO₂ in their experiment and could account for ~100% of the carbon and ~95% of the nitrogen and states that the amount of (CH₃)₂NNO₂ formed in the photolysis experiment is in agreement with the relative rates k_2/k_{4a} and k_{4b}/k_{4a} determined by Lindley *et al.*[33], see below. It should be noted, however, that they employed a large excess O₃ in their photolysis experiments to prevent back-reaction of NO with the dimethylamino radical. This was at a time when it was not realized that the NO₃ radical is formed under such conditions and that this radical might also contribute to the loss of NDMA. Their result for j_{NDMA}/j_{NO2} is therefore an *upper* limit to the nitrosamine relative photolysis rate.

Lindley *et al.*[33] studied the gas phase reactions of the (CH₃)₂N radical following photolysis of NDMA with O₂, NO and NO₂, and also derived the relative rates $k_2/k_3 = (1.48 \pm 0.07) \times 10^{-6}$, $k_2/k_{4a} = (3.90 \pm 0.28) \times 10^{-7}$ and $k_{4b}/k_{4a} = 0.22 \pm 0.06$. Lazarou *et al.*[43] studied the reactions of the (CH₃)₂N radical with NO and NO₂ by the Very Low Pressure Reactor (VLPR) technique and reported absolute rates of reaction $k_3 = (8.53 \pm 1.42) \times 10^{-14}$, $k_{4a} = (3.18 \pm 0.48) \times 10^{-13}$, and $k_{4c} = (6.36 \pm 0.74) \times 10^{-13}$ cm³ molecule⁻¹ s⁻¹ at 300 K.

The products observed were explained by the following series of reactions:

(CH₃)₂NH + OH	→	(CH₃)₂N + H₂O	(1a)
	→	(CH₃)N(H)CH₂ + H₂O	(1b)
(CH₃)₂N + O₂	→	**CH₂=N-CH₃** + HO₂	(2)
(CH₃)₂N + NO	→	**(CH₃)₂N-NO**	(3)
(CH₃)₂N + NO₂	→	**(CH₃)₂N-NO₂**	(4a)
	→	**CH₂=N-CH₃** + HONO	(4b)
	→	(CH₃)₂NO + NO	(4c)
(CH₃)₂N-NO	$\xrightarrow{h\nu}$	(CH₃)₂N + NO	(5)
(CH₃)N(H)CH₂ + O₂	→	(CH₃)N(H)CH₂O₂	(6)
(CH₃)N(H)CH₂O₂ + NO	→	(CH₃)N(H)CH₂O + NO₂	(7)
(CH₃)N(H)CH₂O + O₂	→	**(CH₃)N(H)CHO** + HO₂	(8)

Nitramines, such as DMN, do not undergo photolysis in the troposphere, and virtually nothing is known about their environmental fate. Nitramines have been

reported as products in the studies of secondary and tertiary amines, but results from ADA-2009 [44] also show that nitramines are also formed in photo-oxidation of primary aliphatic amines. From a theoretical point of view, the photo-oxidation of nitramines should result in the formation of *N*-nitro amides, R-C(O)-N(R')NO$_2$, for which no atmospheric chemistry data exist.

It should be noted that there is only kinetic information for one, single nitramine reaction with OH radicals – DMN. It should also be noted that there is only gas phase photolysis rate data for one, single nitrosamine – NDMA.

It is well established from condensed phase chemistry that secondary amines readily form stable nitrosamines, and that nitrosamines from primary aliphatic amines are very unstable [45]. This has lead to the general assumption that primary aliphatic amines do not form nitrosamines [28]. However, quantum chemistry calculations suggest that primary amines form nitrosamines in exactly the same way as secondary amines, and that the primary nitrosamines themselves are stable in oxygen-free environments.[46] However, in the gas phase the primary nitrosamines isomerizes to hydroxylimines, which react with O$_2$ to give the corresponding imines, Figure 1.1.
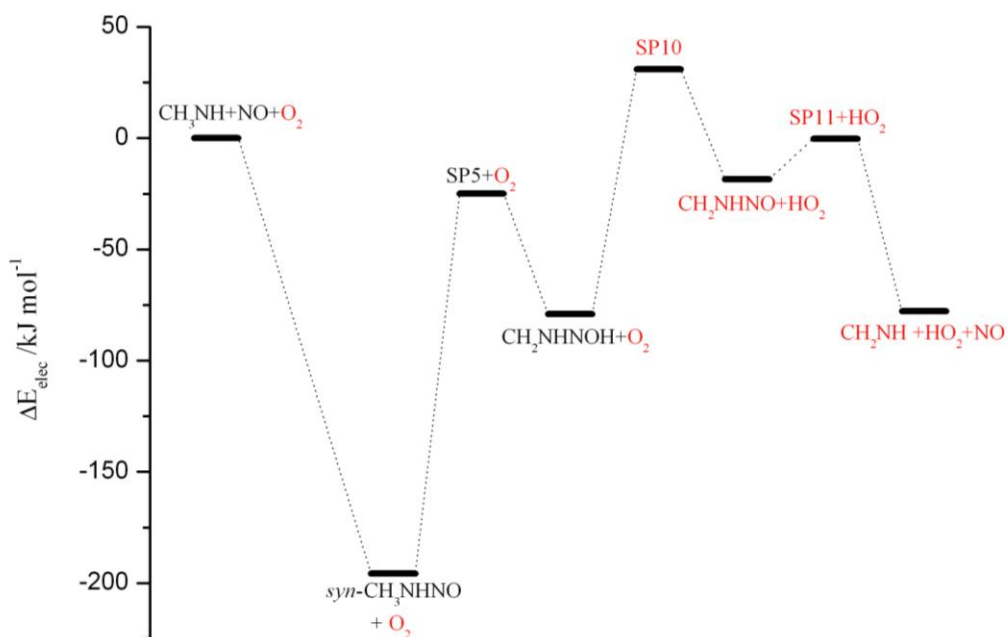
Figure 1.1. Formation of *N*-nitroso methylamine, isomerisation and subsequent reaction with O$_2$. From Tang *et al.*, Ref. 46

Although the barrier to reaction of the hydroxylamine with O$_2$ is calculated to be quite high, around 25 kJ mol^{-1}, and consequently the rate constant small, less than 10^{-17} cm^3 molecule^{-1} s^{-1}, the amount of O$_2$ in the atmosphere is so high that the lifetime of the hydroxylamine will be less than 1 s at atmospheric conditions.

1.4.2 Amides

The gas phase UV absorption cross-sections have been determined for a series of amides: *N,N*-dimethyl formamide, *N,N*-dimethyl acetamide, *N,N*-dimethyl propionamide and 1-methyl-2-pyrrolidone.[47] The spectra are structureless and show low absorption cross-sections beyond 270 nm. Consequently, tropospheric photolysis of amides will not be an important loss process.

Table 1.2. Amides reported as products in dimethyl- and trimethylamine gas phase oxidation experiments.

Parent amine	Oxidant	Amides reported		Ref.
		Gas phase	Aerosol	
$(CH_3)_2NH$	OH	CH_3NHCHO		28
$(CH_3)_2NH$	O_3	CH_3NHCHO		21
$(CH_3)_3N$	OH	$(CH_3)_2NCHO$	$CHONH_2$	28
			$CH_3N(CHO)_2$	
$(CH_3)_3N$	O_3	$(CH_3)_2NCHO$		21
$(CH_3)_3N$	O_3/NO	$(CH_3)_2NCHO$		35
		$CH_3N(CHO)_2$		
		$CH_2OH(CH_3)NCHO$		
		$(CHO)_3N$		

There are three kinetic studies of OH radical reactions with amides. Koch *et al.*[48] studied 4 amides with the aim of testing/extending a commonly used structure-activity relationship (SAR)[5] for prediction of OH rate constants. The reactions were found to show *negative* Arrhenius temperature dependencies and to conflict with the SAR predictions. Solignac *et al.*[49] studied the OH and Cl reaction kinetics of 3 amides; the results support that the reactivity of amides deviate from the SAR predictions. Finally, Aschmann and Atkinson[50] studied the reactions of 1-methyl-2-pyrolidone at 296 K.

There are two kinetic studies of NO_3 radical reaction with amides. Aschmann and Atkinson[50] studied the reactions of 1-methyl-2-pyrolidone at 296 K, Dib and Chakir[51] studied the temperature dependence of the NO_3 reaction with 4 amides. The kinetic results relevant to the present study are summarized in Table 1.3.

Table 1.3. Rate constants at 298-300 K (/cm^3 molecule^{-1} s^{-1}) and activation energies (/K) for the reaction of OH radicals with selected amides.

Compound	$k_{OH}/10^{-11}$	E_a/R	$k_{Cl}/10^{-11}$	$k_{NO3}/10^{-14}$	E_a/R
NH_2CHO	≈ 0.4 [a]		4.5 ± 0.5 [b]	<1 [a]	
CH_3NHCHO	0.86 ± 0.24 [c]		9.7 ± 1.7 [c]		
$(CH_3)_2NCHO$	1.4 ± 0.3 [c]		19 ± 3 [c]	4.5 ± 1.1 [d]	1600 ± 300 [d]

[a] Estimated by Barnes *et al.*, Ref. 52 [b] From Barnes *et al.* 52 [c] From Solignac *et al.*, Ref. 49. [d] From Dib and Chakir, Ref. 51.

The amide-OH reactions are relatively fast, and the *average global lifetimes* of amides with respect to reaction with OH radicals will be of the order of a few days. Although the reactions of amides with Cl atoms are faster that the

corresponding OH reactions, the average global atmospheric concentration of OH radicals is so much higher than that of Cl atoms that the atmospheric amide loss is dominated by OH reactions.

There is only one report on the products in the reactions between OH radicals and the relevant amides; Barnes et al.[52] have recently presented results from photo-oxidation studies of NH_2CHO, CH_3NHCHO, and $(CH_3)_2NCHO$. Scheme 1.7 shows a summary of their findings for this group of compounds.
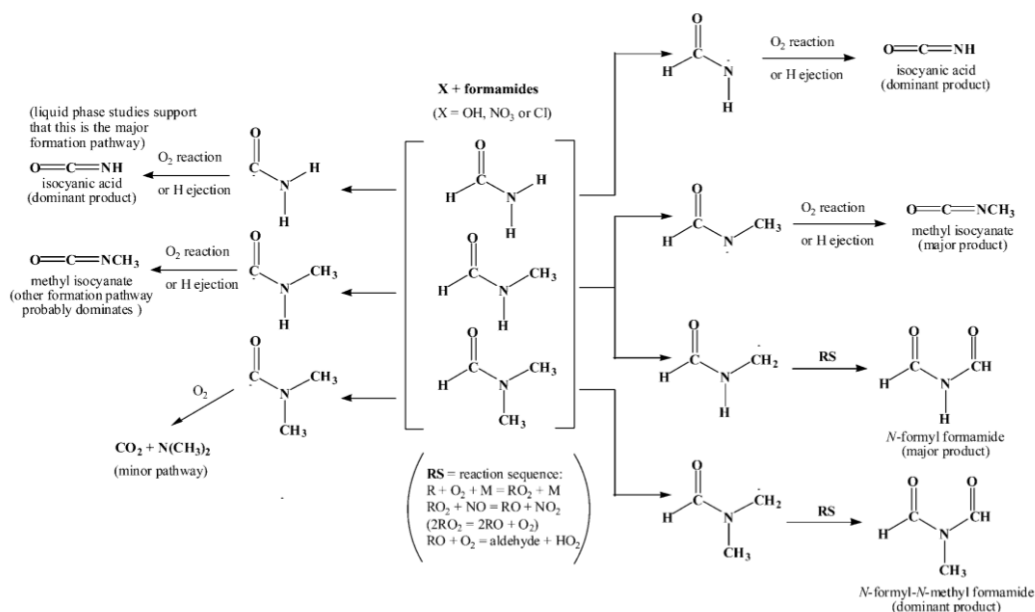
Scheme 1.7. Simplified overall reaction mechanism for the main abstraction pathways involved in the oxidation of formamide and its N-methylated derivates by atmospheric oxidants X, X = OH, NO_3 or Cl atoms. (From Barnes et al., Ref. 52).

1.4.3 Imines

Imines, $R_1N=CR_2R_3$, are reported as major products in amine gas phase photo-oxidation experiments. There are no experimental data available for the gas phase reactions of imines. Imines are, however, known to hydrolyse in aqueous solution resulting in amines and carbonyl compounds.[53] Imine hydrolysis is also expected to occur on surfaces.

$$R_1N=CR_2R_3 + H_2O \ (het., l) \quad \rightarrow \quad R_1NH_2 + R_2R_3CO \quad (9)$$
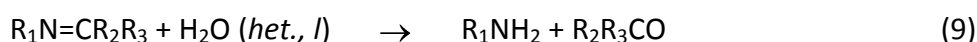
There is a single study of the electronic spectrum of $CH_2=NH$ in the region 235 to 260 nm showing a broad and structureless absorption with maximum near 250 nm.[54] There is no information concerning the spectrum in the region of relevance to tropospheric chemistry ($\lambda > 300$ nm). It is possible, however, that the absorption band stretches into this region such that photolysis may occur in the troposphere in which case the products will be HCN and H_2.[54,55]

Heterogeneous condensation reactions between imines and amines have been reported,[56] *e.g.* methanimine, $CH_2=NH$, may react with methanamine, CH_3NH_2 to give methyl methanimine and ammonia:

$$CH_2=NH + CH_3NH_2 \ (het.) \quad \rightarrow \quad CH_2=NCH_3 + NH_3 \tag{10}$$
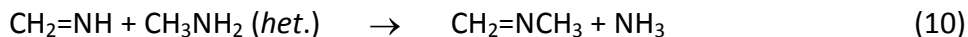
1.4.4 *Isocyanic acid and methyl isocyanate.*

Isocyanic acid, HNCO, and methyl isocyanate, CH_3NCO, are reported as major products in amide gas phase photo-oxidation. The reaction of isocyanic acid with OH radicals was studied by Tully *et al.* in the 624 – 875 K range,[57] and later by Glarborg et al. in the 1025 – 1425 K range,[58] and by Woolridge et al. in the 620 – 1860 K range.[59] The latter authors summarised the available experimental results to give $k_{OH}(T) = 6.03 \times 10^{-17} \times T^{1.50} \times \exp(-1809/T)$, from which one may extrapolate $k_{OH} \approx 7 \times 10^{-16}$ cm^3 $molecule^{-1}$ s^{-1} at 298 K. Assuming an average global OH concentration of 10^6 cm^{-3} implies $\tau_{OH} \approx 45$ years. Isocyanic acid and aliphatic isocyanates show continuous absorption with long wavelength limits at 224, 255 and 248 nm for isocyanic acid, methylisocyanate and ethylisocyanate, respectively.[60] The dominant atmospheric loss process of HNCO will therefore be wet and dry deposition. In the aqueous phase HNCO hydrolyse to form ammonia:

$$HNCO + H_2O \ (aq.) \quad \rightarrow \quad CO_2 + NH_3 \tag{11}$$
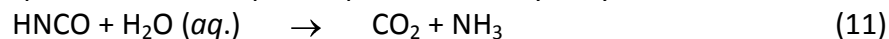
There are no kinetic data available for methyl isocyanate. To a first approximation one may assume that the OH rate constant for reaction with CH_3NCO is of the same order of magnitude as that of CH_3CN, that is $k_{OH} \approx 2 \times 10^{-14}$ cm^3 $molecule^{-1}$ s^{-1} at 298 K.[61] The estimated atmospheric lifetime, $\tau_{OH} \approx 1.5$ years, implies that wet and dry deposition will also be the dominant atmospheric loss process for methyl isocyanate. In the aqueous phase CH_3NCO hydrolyse to form methylamine:

$$CH_3NCO + H_2O \ (aq.) \quad \rightarrow \quad CO_2 + CH_3NH_2 \tag{12}$$
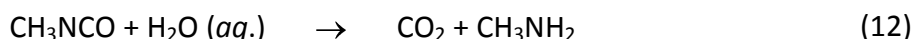
2 Simplified theoretical photo-oxidation schemes

Detailed theoretical schemes for the atmospheric photo-oxidation of methylamine (MMA), dimethylamine (DMA) and trimethylamine (TMA) have been derived from quantum chemistry calculations during the ADA-2010 project.[62,63] The schemes are based on generic atmospheric photo-oxidation pathways for hydrocarbons[5,64] and experimental data for amines from the literature.[19-21,28,32,33,37,42,65-72] Schemes 2.1 - 2.3 show the expected major reaction routes following the initial hydrogen abstraction. Intermediate compounds are highlighted in colour coded boldface types (**carbonyls**: expected lifetime >1 day at 60° N; **amides**: expected atmospheric lifetime >1 day at 60° N; **imines**: expected lifetime < 1 day at 60° N; **nitramines**: expected lifetime >3 days at 60° N; **nitrosamines**: short photolysis lifetimes, but expected to be extremely carcinogenic).

The main primary products expected in the photo-oxidation of MMA are: **NH_2CHO** (formamide), **$CH_2=NH$** (methanimine) and **CH_3NHNO_2** (N-nitro methylamine), Scheme 2.1.
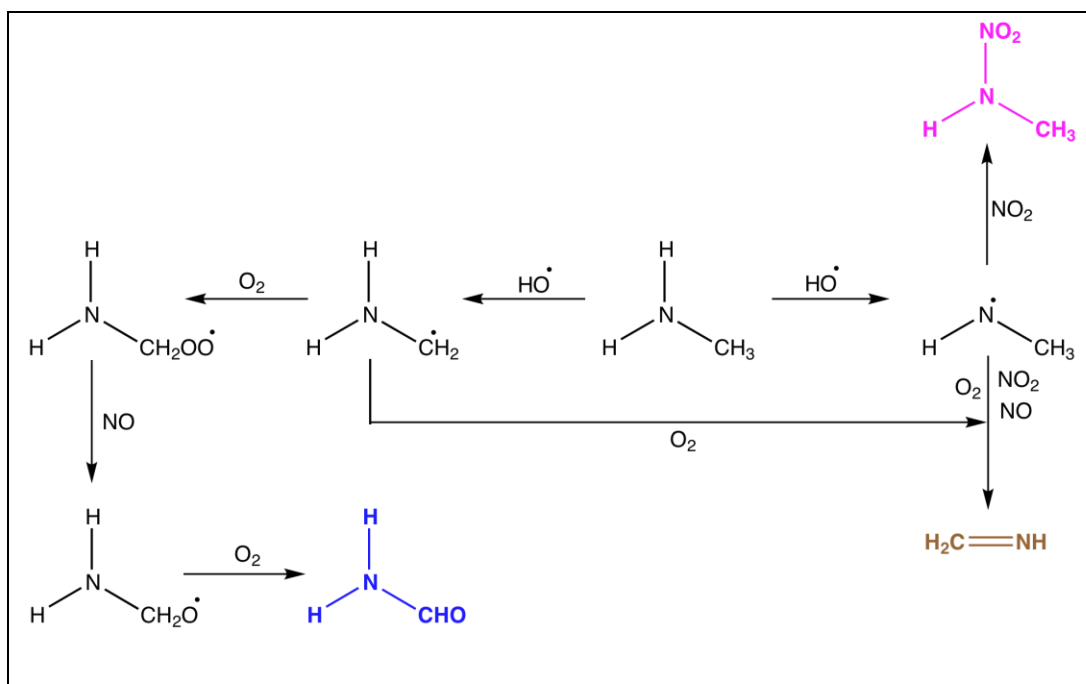
Scheme 2.1. Main routes of the atmospheric methylamine photo-oxidation.

The main primary products expected in the photo-oxidation of DMA are: **CH₃NHCHO** (*N*-methyl formamide), **(CH₃)₂NNO** (*N*-nitroso dimethylamine, NDMA), **(CH₃)₂NNO₂** (*N*-nitro dimethylamine), and **CH₃N=CH₂** (N-methyl methanimine), Scheme 2.2.

**Scheme 2.2**. Main routes of the atmospheric dimethylamine photo-oxidation.
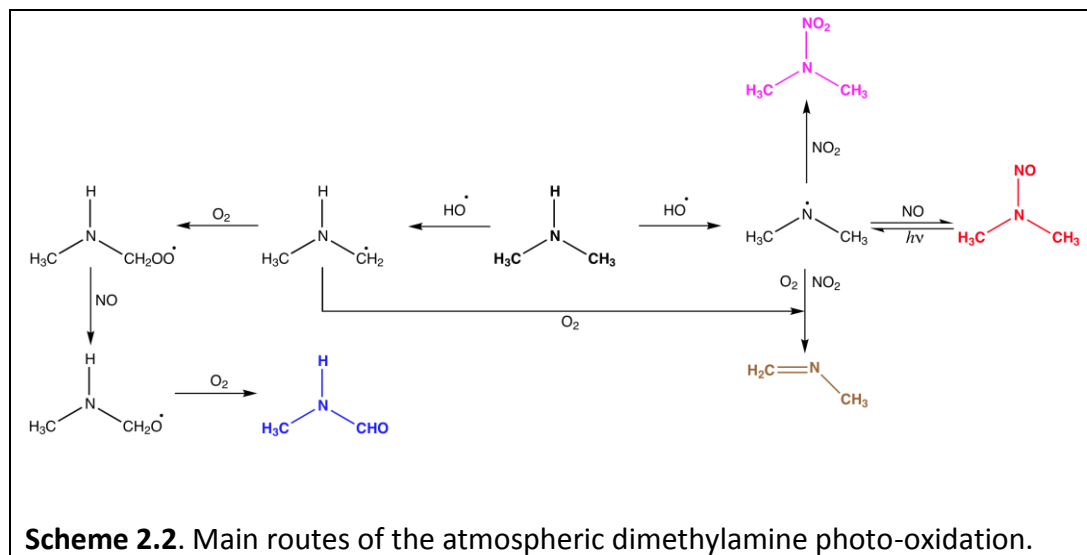
Finally, the main primary products expected in the photo-oxidation of TMA are: **(CH₃)₂NCHO** (*N,N*-dimethyl formamide), **CH₃N=CH₂** (N-methyl methanimine), **(CH₃)₂NNO** (*N*-nitroso dimethylamine, NDMA) and **(CH₃)₂NNO₂** (*N*-nitro dimethylamine), Scheme 2.3.

Scheme 2.3. Main routes of the atmospheric trimethylamine photo-oxidation.
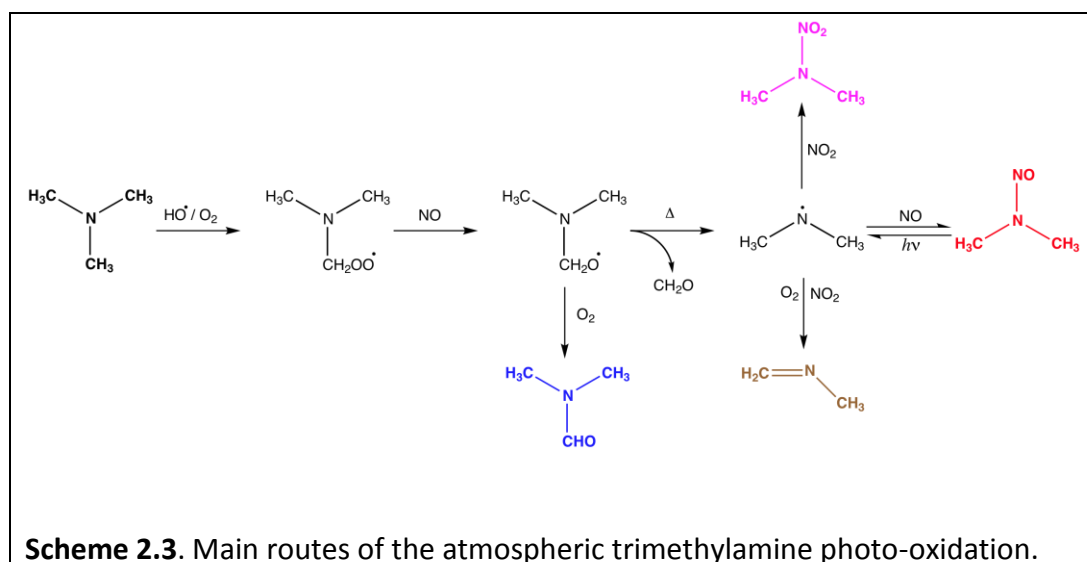
3   Aerosol model

3.1   Introduction

In the atmosphere, methylamines (mono-, di-, and trimethyl amine) may contribute to particle formation and growth via the following processes:

1. Nucleation (stable clusters) involving methylamines and nitric acid (HNO_3) or sulphuric acid;
2. Growth of particles by condensation of aminium nitrate salts;
3. Growth of particles by condensation of low volatile secondary products;
4. Formation of secondary organic aerosol (SOA);
5. Mass transfer into aqueous aerosols followed by dissociation in the liquid (not considered in ADA-2010).

For more details on relevant aerosol dynamics and aerosol chemistry processes of amine-related aerosols, with regards to the lifecycle of aerosols formed by the processing of amine emissions it is referred here to a recent review by Karl.[73]

To model the chemical composition of the aerosol, the *number size distribution function* (*n(r)*) has to be constructed and assumptions about the mixing of chemical components within individual aerosol particles have to be made. In this context, a "chemical component" refers for example to sulphate, soot, organic, soil dust, or sea salt aerosol. One can then characterize the aerosol size distribution by the *number size distribution function $n_N(r)$* (particles μm^{-1} cm^{-3}) such that $n_N(r)dr$ represents the number of particles per cm^3 of air in the radius size range [*r, r+dr*]. The *number size distribution function* can be integrated to determine the total number concentration, total mass concentration, and other features of the aerosol over selected size ranges or over the entire size distribution.

3.2   Description of the model

MAFOR (Marine Aerosol Formation model) is a recently developed NILU in-house sectional aerosol dynamics model, primarily designed to study aerosol evolution in the marine boundary layer.[74,75] MAFOR is a 0-dimensional Lagrangian type sectional aerosol box model which includes gas phase and aqueous phase chemistry in addition to aerosol dynamics.

The aerosol general dynamic equation (GDE) in terms of particle volume *v* governing the size distribution of spherical particles, *n(v,t),* in a non-advected well-mixed 0-dimensional box is generally written:

$$\frac{\partial n(v,t)}{\partial t} = \left(\frac{\partial n(v,t)}{\partial t}\right)_{nucl} + \left(\frac{\partial n(v,t)}{\partial t}\right)_{emis} + \left(\frac{\partial n(v,t)}{\partial t}\right)_{coag} + \left(\frac{\partial n(v,t)}{\partial t}\right)_{cond} + \left(\frac{\partial n(v,t)}{\partial t}\right)_{dep} \quad \text{(I)}$$

In this equation, *n(v; t)* is defined such that *n(v; t)dv* is the number of particles in the size range *v* to *v+dv* per unit volume at time t. Equation (I) represents the change in the particle number size distribution due to emission, nucleation, coagulation, condensation/evaporation and loss by dry and wet deposition. The

second term in the right side in Eq. (I), representing emissions of primary particles (sea salt and/or organic particles) is omitted in MAFOR. Growth of particles occurs through condensation of inorganic or organic vapours onto particles.

The numerical solution to the *general dynamic equation* for aerosols in atmospheric models is done by either of two approaches, the *sectional method* or the *moments method*. In the *sectional method* one divides the aerosol size distribution into discrete size bins and discretizes Equation (I) over each size bin, Figure 3.1.
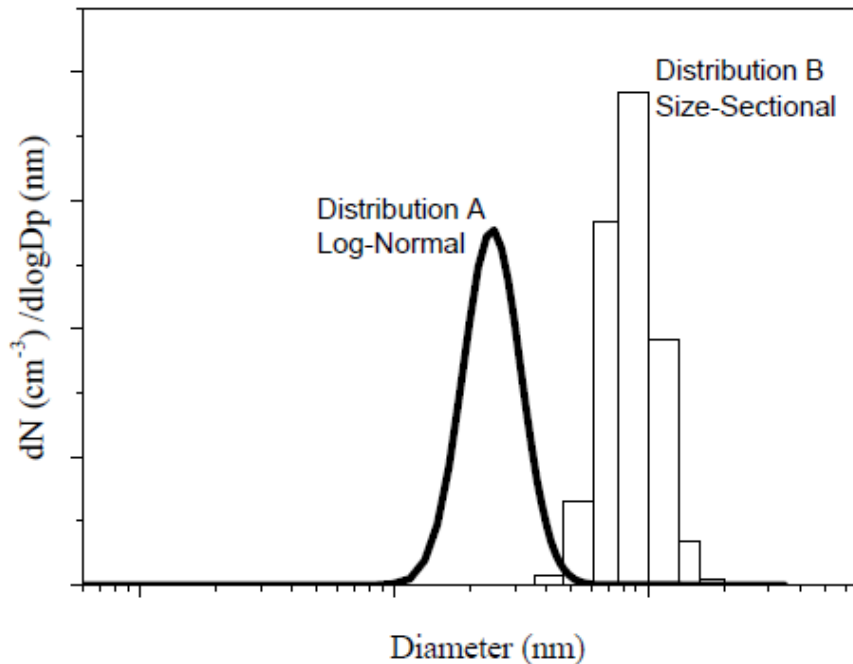

Figure 3.1. Two different schematic aerosol size distributions; one represented as a log-normal distribution, the other a size-sectional distribution.

In MAFOR, the aerosol GDE is solved using a sectional approach with a fixed sectional grid. The various aerosol dynamical processes are treated by modelling the number concentration and component mass concentrations of each size section.

MAFOR has been further extended to simulate chamber experiments on photo-oxidation of methylamines to include gas-phase chemistry of each methylamine as well as condensation/evaporation and nucleation of vapours produced in the oxidation of methylamines. Implemented aerosol processes and chemical components are the same as in the monodisperse aerosol dynamics model MONO32.[76-78] MAFOR has been thoroughly evaluated by comparison both with simulation results from MONO32 and with field measurements.[75] Monodisperse models such as MONO32 are not appropriate for the modelling of continuous (several hours) or more intense nucleation events, unless a new aerosol mode is inserted to allocate the new evolving 1 nm size particles. Hence, the sectional model MAFOR was mainly developed to overcome the limitations of MONO32 with respect to modelling of the nucleation mode evolution.

The number of size sections in MAFOR can be selected by the user; usually 60 size bins are used to represent the aerosol size distribution. The kinetic pre-processor (KPP) solver package[#] is used to generate Fortran95 code for the chemistry module and the Rosenbrock 3 solver[79] is used to integrate the differential equation system of gas phase reactions and dN/dt is solved with forward finite differences. Change of number and mass concentration of particles is solved subsequent to the integration of the gas phase/liquid phase chemistry. The time step for the integration of chemistry and of the aerosol processes is 10 s.

In the following, we denote methylamines as R_nNH_{3-n}, where R is the methyl group (CH_3) and n=1, 2, or 3 signifies mono-, di-, or trimethylamine. To describe the photo-oxidation of a selected methylamine in the EUPHORE chamber, the following processes were implemented into the model: 1) methylamine gas phase chemistry, 2) wall sources of gases, 3) condensation of aminium nitrate ($R_nNH_{4-n}NO_3$) onto pre-existing particles, 4) SOA-partitioning of two organic oxidation products of different volatility, 5) nucleation of methylamine and HNO_3 to form new 1nm-sized particles, 6) wall losses of gases and particles. The flexible structure of the program facilitates later implementation of other aerosol processes and allows switching on/off certain aerosol processes for test purposes. Due to the use of a chemical pre-compiler, new chemical compounds and reactions can be easily included.

3.3 Chamber-specific processes

The wall source of nitrous acid (HONO) in EUPHORE is well studied.[80] The HONO wall source was found to be a strong function of the photolysis frequency of NO_2, $j(NO_2)$, and also depends on temperature (T) and relative humidity (RH). The source is parameterized for dry and humid conditions:

$$S_{dry}(\text{HONO}) = a \times j_{NO_2} \times \exp(-T_0/T)$$

$$S_{humid}(\text{HONO}) = S_{dry}(\text{HONO}) + b \times j_{NO_2} \times RH^q$$

$$(\text{II})$$

The parameters a, T_0 and b and q are 7.3×10^{21} cm^{-3}, 8945 K^{-1}, and 5.8×10^8 cm^{-3}, and 0.36, respectively. RH is used as percentage value. Since the concentration of HONO was not monitored during the experiments in May, the wall source of HONO was one of the fit parameters in the model simulation:

$$S_{exp}(\text{HONO}) = F_{HONO} \times S_{humid}(\text{HONO})$$

$$(\text{III})$$

Where F_{HONO} is a fit parameter to scale the HONO wall source in the simulation of the experiments. In addition, a light-dependent ($j(NO_2)$-dependent) wall source of formaldehyde (HCHO) is considered.[80]

During the experiments, all compounds are diluted by the replenishment flow. The replenishment flow is added to ensure a constant chamber volume by replacing air that is lost due to outtake by the connected instruments and

---

[#] http://people.cs.vt.edu/~asandu/Software/Kpp/

through the Teflon foil. The rate constant for dilution was determined from the first order decay of acetonitrile or SF_6 during the experiment period. First order rate constants for MA wall loss and dilution were determined to be in the range between $6\text{-}8\times10^{-6}$ s^{-1} and $2\text{-}7\times10^{-5}$ s^{-1}, respectively. A wall loss rate for NO_2 of 2.3×10^{-5} s^{-1} and for HNO_3 of 2.0×10^{-5} s^{-1} have been used in the simulation of experiments.

A size-dependent parameterization of the wall loss of particles in the chamber is included in the model to reproduce the particle loss. The parameterization is according to Naumann[81] and takes into account the geometry of the EUPHORE chamber.

3.4 The total budget of methylamines

Concentration changes with time of a condensing and/or nucleating compound i in the gas phase are predicted using the following equation:

$$\frac{dC_{g,i}}{dt} = Q_i - 4\pi D_i \sum_{j=1}^{Nb} N_j r_j \beta_{ij} \times \left[C_{g,i} - Ke_i C_{g,eq,i}\right] - J_{nucl} \times \frac{v_{p,1}}{v_i}$$

(IV)

$C_{g,i}$ is the vapour concentration of compound i in the gas phase, and $C_{g,eq,i}$, its concentration over a flat solution of the same composition as the particle, respectively, Q_i is the net gas phase chemical production rate as the sum of production and loss processes in the gas phase. Kelvin effect Ke_i is considered for the condensation/evaporation of the organic oxidation products and $R_nNH_{4-n}NO_3$ on particles, β_{ij} is the transitional correction factor, and D_i is the gas phase diffusion coefficient, r_j the particle's radius, and N_j the number concentration of particles in size section j. The second term on the right hand side (RHS) in Eq. (IV) is its condensation/evaporation flux to a particle population. The condensation rate of condensable vapours in each size bin is calculated each time step. Mass transfer of gas molecules to particles is calculated using the Analytical Predictor of Condensation scheme.[82] The third term on the RHS represents the loss term due to nucleation of new aminium nitrate particles and J_{nucl} is the nucleation rate.

3.5 Formation of aminium nitrate particles

In the gas phase, nitric acid (HNO_3) is produced by reaction of NO_2 with OH radicals. Destruction of gas phase HNO_3 occurs by reaction with OH, by photolysis, and by wall loss. Gas phase MA and nitric acid can react to form the corresponding methylaminium nitrate, $R_nNH_{4-n}NO_3$, salt:

$$R_nNH_{3-n}(g) + HNO_3(g) \quad \leftrightharpoons \quad R_nNH_{4-n}NO_3(s) \qquad (13)$$

The reaction is assumed to be in equilibrium. Depending on the ambient relative humidity, $R_nNH_{4-n}NO_3$ may exist as a solid or as an aqueous solution of MAH$^+$ and NO_3^-. At low humidity as it was the case in the chamber experiments, when $R_nNH_{4-n}NO_3$ is a solid salt, the dissociation constant K_d for this equilibrium reaction can be calculated by integration of the van't Hoff equation. At the moment, a fixed - not temperature-dependent - dissociation constant is used in

the model. Formation of the $R_nNH_{4-n}NO_3$ salt is limited by the availability of the least abundant of the two species. Any excess methylamine may then react with HNO_3 to form the methylaminium nitrate. The equilibrium HNO_3 concentration, corresponding to $C_{g,eq}$ in Eq. (IV) can be calculated:

$$\left[HNO_3(eq)\right] = \frac{1}{K_d}\left(\left(\frac{\left[R_nNH_{3-n}\right]-\left[HNO_3\right]}{2}\right)+\sqrt{\frac{\left[R_nNH_{3-n}\right]-\left[HNO_3\right]^2}{4}+K_d}\right) \quad (V)$$

Here the squared brackets denote gas phase concentrations (in [molecules cm^{-3}]. The dissociation constant, K_d, is equal to the product of the partial pressures of MA and HNO_3.

3.6 Nucleation of aminium nitrate particles

Methylamines and nitric acid are involved in the formation of new particles during the experiments. The rate of formation of new particles is expressed by the nucleation rate J_{nucl}. It is assumed that nucleation proceeds via homogenous heteromolecular nucleation between nitirc acid and methylamine vapour molecules, or one of the vapours activating the clusters composed around a molecule of the other vapour.

The parameterization for the nucleation process involving methylamines and nitric acid developed in this work is:

$$J_{nucl} = K_{nucl} \times [MA] \times [HNO_3]$$
$$\left[R_nNH_{3-n}\right]\times\left[HNO_3\right] > K_d \times 10$$
$$J_{nucl} = 0$$
$$\left[R_nNH_{3-n}\right]\times\left[HNO_3\right] < K_d \times 10 \quad (VI)$$

Values of the nucleation parameter K_{nucl} (units [cm^3 molecules^{-1} s^{-1}]) and the aminium salt dissociation constant K_d (here in units [(molecules cm^{-3})^2]) are fit parameters and were adjusted for each experiment to match observed particle formation (mass and number concentration) and observed gas phase concentrations of MA and its major photo-oxidation products.

3.7 Gas phase / particle partitioning of organic products

Gas-phase compounds have a saturation vapour pressure (p^0_L), a pressure at which the vapour is in equilibrium with the liquid. Several gas-phase compounds that form in the oxidation of methylamines (amides, imines, nitrosamines, and nitramines) have vapour pressures in an intermediate regime such that they exist (in the atmosphere) in part in the gas phase and partially associated with particles. Such a compound is commonly referred to as a *semi-volatile organic compound* (SVOC). By partitioning into the particulate phase they constitute *secondary organic aerosol* (SOA).

Observations of particle growth at vapour pressures less than saturation lead to the formulation of the *gas/particle partitioning theory* for SOA growth (*e.g.* Odum *et al.*[83]). Some aerosol models, particularly those with multiple aerosol species (as most of the current aerosol dynamic models), calculate explicitly the

condensation/evaporation driving force, which is the difference between the species concentration in the bulk gas and the concentration just above the particle surface.[76,84,85] However, the theory of (heterogeneous) *condensation* of semi-volatile and non-volatile VOCs does not consider any potential for a species to adsorb to a particles surface or absorb into the existing organic phase of the particle itself. Pankow has shown that the partitioning of a species does not require saturation and could occur at concentrations well below the saturation concentration of the species.[86,87] This is because SOA compounds form an organic solution into which other organic molecules may partition (absorb).

Hybrids of the partitioning and condensation methods exist, where partitioning theory is used to calculate the gas-phase concentration above the particle surface, which is then implemented into a condensation-like flux equation.[88] MAFOR uses a hybrid method of condensation and partitioning to treat formation of SOA from the photo-oxidation of methylamines. Since the specific condensing oxidation products that form in the photo-oxidation of methylamines are only vaguely known, the model uses a simplified approach of two products ("two-product model"), one less volatile and one more volatile SVOC that can partition to the aerosol phase. The two products, termed SOAN1 and SOAN2, are formed in the initial reaction of gas-phase R_nNH_{3-n} and the hydroxyl radical (OH),

$$R_nNH_{3-n} + OH \quad \rightarrow \quad \alpha_1 \text{ SOAN1} \tag{14a}$$

$$\rightarrow \quad \alpha_2 \text{ SOAN2} \tag{14b}$$

with the stoichiometric yield α_1 and α_2, respectively. The partitioning of a condensable compound i between the gas phase and the aerosol phase is described by the gas/particle partitioning coefficient $K_{p,i}$ for absorptive uptake into the particle phase (*e.g.* Seinfeld and Pankow[89]):

$$K_{p,i} = \frac{C_{a,i}}{C_{g,i}M_t} = \frac{10^{-6}RTf}{MW\zeta_i p^0_{L,i}} \tag{VII}$$

Where $p^0_{L,i}$ is the pure compound's vapour pressure in atm, T is temperature in K, $C_{g,i}$ (ng/m^3) is the concentration in the gas phase, $C_{a,i}$ (ng/m^3) is the concentration in the (organic) material aerosol phase, R is the universal gas constant (8.206×10^{-5} m^3 atm mol^{-1} K^{-1}), f is the absorptive mass fraction, ζ_i is the activity coefficient of compound i in that particulate phase, and 10^{-6} is a conversion factor (g/µg). The activity coefficient ζ_i describes the non-ideal interaction between the dissolved species i and the other components of the (organic) particulate phase. An ideal solution was assumed here and hence ζ_i equals unity. For SOAN1 the temperature-dependent saturation vapour pressure of succinic acid is used (log($p^0_{L,succinic\_acid}$)[Pa] = -7196.8T/[K]+19.8; [90]). The vapour pressure of SOAN2 is a factor of 100 lower. The yields α_1 and α_2 were adjusted for each experiment to match the mass concentration of organics observed by AMS.

4   Experimental

The ADA-2010 project included several experimental activities: photo-oxidation studies in the Innsbruck, Oslo and at EUPHORE chambers; chemical kinetic studies, organic synthesis of reactants and reference compounds including *N*-nitroso and *N*-nitro amines, recording of absolute UV and infrared absorption cross-sections, development of on-line analytical instrumentation, development of off-line analytical methods, analytical software development, and development of aerosol modelling tools.

4.1   HSE

Safety precautions, synthesis: All synthetic work has been done in an inert atmosphere (N$_2$) in a well-ventilated fume hood. Usual precautions have been implemented when working with organic synthesis, *i.e.* use of gloves, laboratory coat and safety goggles. Compounds specially suspected to be cancer promoting or explosive is treated wet and destroyed according to standard laboratory practice. All chemical waste has been sealed in special flasks and sent to authorized companies for destruction of such materials. For safety reasons the synthesis procedures will not be described in the present, public report.

Safety precautions, transport and experiments: Nitrosamines and nitramines were only transported in sealed glass ampoules containing < 0.25 g. The glass ampoules were packed in individual PET bottles, enclosed in a sealed soft steel canister protected by isopor for transportation between laboratories. Usual precautions have been implemented in the laboratory work, *i.e.* use of gloves, laboratory coat and safety goggles. The nitrosamine samples were cooled to liquid nitrogen temperature before the ampoules were opened and transferred to standard vacuum ampoules or to impingers for subsequent transfer to the reaction chambers in a stream of air. All transfer lines and glassware were subsequently cleaned in 1 M sulphuric acid for 2 days before disposal. No accident or spillage has occurred during the project lifetime.

4.2   The Innsbruck and Oslo photo-chemistry reactors

The "Oslo reactor" reactor is a 2.2 m long, 250 L electro-polished stainless steel chamber equipped with a White type multiple reflection mirror system with a 128 m optical path length for rovibrationally resolved infrared spectroscopy. The reaction chamber is equipped with UV photolysis lamps mounted in a quartz tube inside the chamber. Infrared spectra were recorded with a Bruker IFS 66vs FTIR instrument employing LN2-cooled MCT and InSb detectors, and the light intensity was reduced to ensure linear detector response.

The "Innsbruck-reactor" is a 480 L Teflon coated reaction chamber made of glass and surrounded by 18 UV/VIS lamps ($\lambda \geq 300$ nm) to simulate sunlight. Analytical instrumentation includes a high-resolution proton-transfer-reaction time-of-flight mass spectrometer (PTR-TOF 8000, Ionicon Analytik GmbH) for VOC measurements, a chemiluminescence NO-detection instrument (CLD770 AL ppt, ECO PHYSICS) combined with a photolytic converter (PLC 760 MH, ECO PHYSICS)

for NO$_2$ detection, a UV photometric ozone analyzer (49i, Thermo Scientific) and a temperature / relative humidity sensor (UFT75-AT, MELTEC).

4.3   The EUPHORE photo-chemical reactor

Two European Photochemical Reactor, EUPHORE, in Valencia, Spain (longitude – 0.5, latitude 39.5) is an "open access" large-scale facility established in 1991 as part of the CEAM Centre of Applied Research with financial support from EU, http://www.ceam.es/html/index_i.htm. There are two ~200 m^3 hemispherical chambers for photochemical studies. The chambers are constructed from Teflon film, which have a uniform transmission of sunlight, and are protected by steel canopies, which are opened during the photo-oxidation experiments. After the experiments the chambers are closed and flushed overnight with scrubbed air. The floors of the chambers are cooled to ensure a stable temperature in the chambers during the experiments.

A typical EUPHORE experiment started around 06:00 UT when reagents were added to the chamber. The canopy of the chamber was opened after the reagents were considered to be well mixed, and the first air samples had been collected. Some experiments lasted up to 12 hours after which the canopy was closed, and a large-volume collection of aerosol carried out. The chamber was then flushed overnight with scrubbed air.

Unlike the typical laboratory smog chamber, purified air is constantly added to compensate for leakage, loss through connections, sampling on filters and continuous sampling by ozone, NOx and other monitors, and by the on-line instruments. This is corrected for in the data analysis: SF$_6$ was added to measure the apparent dilution rate by FT-IR.

The EUPHORE facility offers a long range of analytical instrumentation for *in situ* and on-line detection of chemical components and particles in the chamber (FT-IR, GC-MS, SMPS, TEOM, and monitors for actinic flux, CH$_2$O, NOx, NOy, CO, H$_2$O, O$_3$, HONO). A detailed description of the EUPHORE facility and the existing analytical instruments is available in the literature.[91-95]

To complement the in-house instrumentation, users may attach own instrumentation and sample collection. The ADA-2010 project provided four additional on-line instruments: an Aerosol Mass Spectrometer (AMS), a High-Resolution Proton-Transfer-Reaction Time-of-Flight Mass Spectrometer (PTR-TOF-MS), a High-Temperature Proton-Transfer-Reaction Mass Spectrometer (HT-PTR-MS), and a Volatility Tandem Differential Mobility Analysers (VTDMA) system. These instruments are further described below. The high mass resolution of the PTR-TOF-MS instrument allows an (almost) unambiguous determination of the sum formulae of ions detected – structural isomers exempt. In addition, reactor air was sampled several times a day employing various adsorbents for subsequent analysis (nitrosamines, nitramines, carbonyls, amides).

4.4 On-line and *in situ* analytical instrumentation

4.4.1 PTR-TOF-MS/HT-PTR-MS.

Two different on-line mass spectrometers for real-time analysis of the amines and their volatile oxidation products were used:

- a commercial PTR-TOF 8000 proton-transfer-reaction time-of-flight mass spectrometer (PTR-TOF-MS) (Ionicon Analytik GmbH, Innsbruck). This instrument has a mass resolving power of m/Δm of ~ 4000 (FWHM) and a 5-to-10 ppm mass accuracy which allows to determine the exact mass and thus elemental composition of the analyte molecules.[96]

- a home-built prototype High-Temperature Proton-Transfer-Reaction Mass Spectrometer (HT-PTR-MS).[97] This instrument can be operated at the temperatures up to 250°C which minimizes surface adsorption effects typically observed with amines. During the second half of the spring campaign, ammonia was used instead of water as a chemical ionization reagent gas in the HT-PTR-MS. In the June campaign, the HT-PTR-MS instrument was used for high-time-resolution measurements of nitrosamines in photolysis experiments. In late June, the HT-PTR-MS was also used for pilot measurements of particle phase amine oxidation products.

The PTR-TOF-MS was interfaced to the chamber via a PEEK capillary tube (length: 220 cm, inner diameter: 1.01 mm; temperature: 160°C; flow: 0.5 slpm). The HT-PTR-MS was interfaced to the chamber via a Sulfinert®-passivated stainless steel tube (length: 125 cm, inner diameter: 5.33 mm; temperature: 170°C; flow: 10 slpm). Two different instruments with different inlet configurations were used to investigate potential analytical artefacts caused by amine surface adsorption processes.

For particle composition measurements, the HT-PTR-MS instrument was equipped with a monolithic charcoal denuder and an aerosol evaporation cell (similar to the approach described by Hellen *et al.*[98]). In the denuder, gas-phase organics were stripped off the sample air owing to their high diffusion coefficient. Particles with lower diffusivity were mostly transported through the denuder into a heating cell (150-250 °C) where they were vaporized for subsequent analysis by PTR-MS. High temperature operation of both the inlet and the drift tube of the PTR-MS (up to 250 °C) prevented re-condensation of the vaporized aerosol material.

4.4.2 VTDMA.

A volatility tandem differential mobility analysers (VTDMA) system has been developed for measuring the thermal characteristics of SOA particles[99] or fundamental thermal properties of pure compounds.[100] The VTDMA system is useful for observing changes in particle size/volume when exposed to heat.[101-103] The system comprises three main parts: *a)* a DMA, selecting particles of a known size, *b)* an "exposure unit", where the potential size change occurs due to heating *c)* an SMPS system, measuring the residual particle size distribution (Figure 4.1). The heating unit consists of four or eight parallel ovens having a temperature range from 298 to well
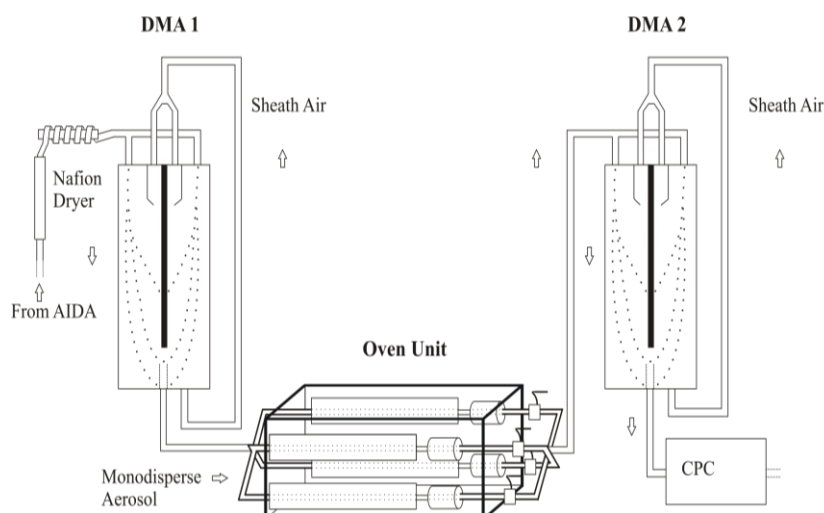
Figure 4.1. Schematic of the VTDMA set-up. (From Jonsson *et al*. Ref. 99)

above 573 K, enabling rapid change of the temperature. The VTDMA has been proven to detect very small changes in volatility that can be attributed to changes in chemical composition.

4.4.3   AMS.

The time-of-flight Aerodyne Aerosol Mass Spectrometer (AMS) is an innovative instrument that allows real-time and *in situ* analysis of fine and ultrafine particles. The instrument investigates size distribution and chemical composition of particles between 0.03 to 1mm on a 1 min basis. The methodology used within c-TOF AMS is fully described in Drewnick *et al*.[104] The particles are sampled through a critical orifice (diameter 100µm) at 80 cm^3 min^{-1} and focused by an aerodynamic lens which blocks all particles larger than 1mm in diameter. Then they enter a vacuum chamber where a mechanical chopper allows a packet of particles (beam chopped) to be accelerated according to their vacuum aerodynamic diameter (D_{va}) and thereby giving size distribution data. The particles are then sent to the vaporization-ionization chamber where the non-refractory (NR) components of the particles are flash-vaporized on a hot surface (~600 °C) and ionized by electron impact (70 eV). Resultant positively charged ions are guided into the time-of-light mass spectrometer. The collected mass spectra (m/z from 4 to >350 in a minute scale) give information on the chemical composition (i.e., nitrate, sulphate, chloride, potassium, ammonium, aliphatic organic, PAHs) using the "fragmentation table". Using default parameters (70 eV for the electron impact ionisation) fragmentation of the aliphatic organic fraction is important. During ADA project we tried to develop and optimize data acquisition at 30 eV in the tentative to reduce the fragmentation of the amines and their degradation products.

High Resolution data analysis by Cumulative Function Distribution. Quantification and identification of the aerosol components is often complicated due to the low resolution (m/Δm=800-1000) of the Compact-Time of Flight MS of the AMS. In the aerosol formed upon amine degradation several signals are often associated to multiple ion fragments. It is the case for m/z 30 (NO^+ fragment at

29.99 and CNH_4^+ 30.04) and m/z 44 (which can contains up to 3 fragments m/z 43.985 CO_2^+, m/z 44.027 $C_2H_4O^+$ and m/z 44.050 $C_2H_6N^+$, respectively). Routine analysis does not allow the separation of these fragments.

Within the frame of ADA project, a new methodology for the analysis and identification of the aerosol composition has been developed. The new
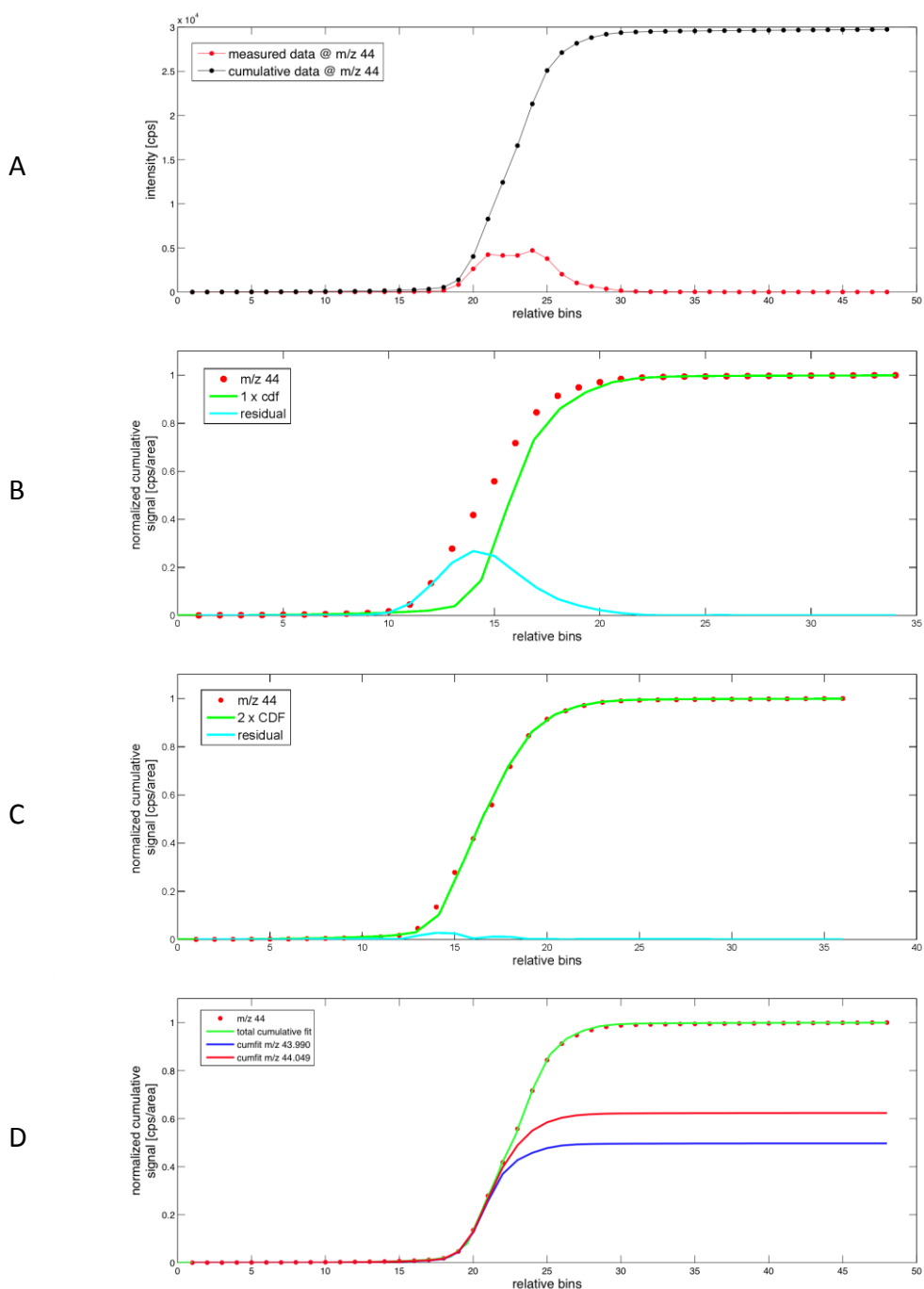

Figure 4.2 Peak detection and quantification by iterative residual analysis. Panel A: measured data around m/z 44 (red dots) and the respective cumulative sum (black dots). Panel B: fit of a previously determined single cumulative distribution function (cdf, green line) and the corresponding residual (blue line). Panel C: fit of a superposition of two similar cdfs with different positions and intensities (green line). Panel D: visualisation of the single ion contributions of m/z 43.985, m/z 44.027 and m/z 44.050.

methodology is based on custom peak de-convolution and quantification routines previously described and applied for PTR-TOF data by Müller *et al.*[105] These routines apply a function of 4 superposed Gaussian peaks to selected single peaks for peak shape determination and time-of-flight (TOF) to m/z calibration. Afterwards an averaged spectrum is analyzed for all ionic peaks utilizing a residual analysis. By fitting superpositions of the previously determined peak shape a peak list is created. This allows the detection of hidden peaks without distinguished peak maxima. According to these results, the routines described by Müller *et al.*[105] were updated and adopted for C-TOF AMS spectral analysis.

Figure 4.2 illustrates how the resolution enhancement routines work. Panel A depicts the measured data bins around m/z 44 (red dots) and the corresponding cumulative sum (black dots). Panels B and C show the residual analysis by fitting one (B) and a superposition of two (C) cumulative peaks. Panel D visualizes the single ionic contributions of a fit of a superposition of three detected peaks. Three ionic signals can be distinguished around m/z 44, m/z 43.985 with 14800 cps (CO_2^+), m/z 44.027 with 3760 cps ($C_2H_4O^+$) and m/z 44.050 with 11200 cps ($C_2H_6N^+$), respectively.

AMS results on the aerosol chemical composition and volatility are discussed in the respective sections on photo-oxidation of CH_3NH_2, $(CH_3)_2NH$, $(CH_3)_3N$, and $CH_2=NCH_3$ (Sections 5.10, 5.11, 5.12, and 5.15). Detailed aerosol analysis results obtained from the AMS set up in photo-oxidation experiments during ADA-2010 are provided in Annex 7.

4.4.4 FT-IR.

The EUPHORE Chamber B is equipped with a Nicolet 6700 FTIR spectrometer coupled with White multi-reflection mirror system for in situ analysis adjusted to give an optical path length of 553.5 m. FTIR spectra were recorded every ten minutes by co-adding 370 interferograms with a resolution of 0.5 cm^{-1}. Boxcar apodization was used in the Fourier transformation. The interferograms were saved for possible later re-processing.

Retrieval of trace gas volume mixing ratios was carried out semi-automatically employing the MALT program.[106] This method simulates the spectrum of the mixture of absorbing species from a set of initial concentrations and reference spectra and then varies the concentrations iteratively to minimize the residual between the measured and simulated spectrum. In the spectrum calculation, true absorption coefficients are used if available, otherwise high resolution spectra can be used as a good approximation. The spectral data needed in the fitting procedure were taken from the HITRAN 2008 database (H_2O, CO, NO, NO_2, CO_2, CH_4);[107] for MMA, DMA, TMA and NDMA experimental IR spectra were used. Retrieval of chemical components from the FT-IR spectra is sensitive to detector non-linearity and interference of compounds with overlapping spectra. For compounds whose spectra only show *PQR*-structure the retrieval procedure has an estimated uncertainty of ±10 %. For compounds showing rotational fine structure the retrieval procedure has an estimated uncertainty of ±5 %.

4.5 Off-line analytical methods

All off-line techniques used in this project collect both gas phase and particulate matter (aerosols). For this reason the off-line analysis results may not be directly comparable with the on-line measurement results. A general picture should be that the off-line measurements are systematically higher in concentrations than the data obtained by on-line techniques.

An important property by the off-line techniques is the inherent higher number of analytical identification points compared to the on-line techniques. This enables the definitive confirmation of the chemical compounds identified by the on-line techniques. The analytical methodologies are briefly outlined in the following.

4.5.1 HPLC-qTOF-MS analysis of particle filters

The filters were extracted in acetonitrile in a cooled ultrasound bath. The solution was filtered into a small beaker and evaporated by gentle N_2–flow. 1 mL of a 5 % acetonitrile solution with 10 mM ammonium acetate was added to the beaker and then transferred to a sample vial. To ensure that all compounds in the glass beaker were dissolved additional 1 mL acetonitrile was added to the beaker and transferred to a sample vial. Finally, the filter was extracted once more to ascertain that all compounds had been extracted from the filter. In addition to the ADA filters, a clean quartz filter was extracted as well, and used as a blank.

High Performance Liquid Chromatography (HPLC). Extracts were analysed by a high-performance liquid chromatograph (HPLC, Dionex) coupled to a quadrupole time-of-flight mass spectrometer (qTOF-MS, Bruker) at Aarhus University. The qTOF-MS has a general mass range from 50 - 20,000 m/z and an accuracy often better than 3-5 ppm deviation.

Several HPLC methods based on literature by Zhao *et al.*[108], Lee *et al.*[109] and Krauss and Hollender[110] were attempted in combination with several different types of columns but none of the methods could retain and effectively separate the compounds from the ADA samples, which all eluted from the column simultaneously within a few minutes.

qTOF MS analysis. Mass spectrometry methods using Electrospray ionisation (ESI) and Atmospheric Pressure Chemical Ionisation (APCI) both operated in positive mode were compared. Methods using APCI showed significantly higher sensitivity regarding low m/z compounds hence this method was preferred during the analysis of the ADA samples.

4.5.2 Nitrosamines and nitramines[#]

For sampling of nitrosoamines and nitroamines Thermosorb/N cartridges (Cambridge Scientific Instruments Ltd., UK) have been employed. Thermosorb/N cartridges are designed and patented for collection of nitrosamines from tobacco smoke (NIOSH, 1994). The solid phase contained in these cartridges has a special

---

[#] Air sampling was also carried out for subsequent off-line analysis of nitrosamines and nitramines by NILU. Methodology and results are collected in Annex 3.

coating which avoids degradation of nitrosamines during collection and thus sampling artefacts. During the first EUPHORE campaign (March 2010) collection on Thermosorb/N has been performed with and without an ozone scrubber (MnO$_2$) in order to evaluate the possible effect of ozone degradation of the target compounds. For Thermosorb/N cartridges a sampling flow of 1 L min^{-1} has been used.

Moreover, charcoal and Tenax cartridges (Markes Int., UK) have also been employed in order to collect a broader spectrum of compounds. Sampling with Thermosorb/N and charcoal cartridges has been performed in parallel at the same flow rate (1 L min^{-1}), while sampling for Tenax cartridges has been performed at a flow rate of 100 mL min^{-1}.

Thermosorb/N and charcoal cartridges have been extracted with solvent, while Tenax cartridges have been extracted by Thermal Desorption.

Analysis of nitroso- and nitroamines by GC-MS. A method has been developed for quantitative analysis of the following target compounds: *N*-nitroso-dimethylamine, *N*-nitro dimethylamine, *N*-nitro methylamine and *N*-ethyl nitrosamine. The compounds have been provided by The Norwegian University of Life Sciences as pure standard (>99%).

The compounds were dissolved in acetonitrile to a concentration of about 1 mg/mL. Individual solutions at 10 µg/mL in dichloromethane were prepared in order to determine the full scan spectrum and the chromatographic retention time for each compound.

Individual solutions were analysed in full scan by GC-MS (Agilent 5975C MSD) with chemical ionization (CI) in both positive (PCI) and negative mode (NCI). Methane was used as reagent gas. The compounds were separated on an RTX-1701 capillary column (30 m, 0.32 mm I.D., 1 µm film) from Restek. The oven was programmed to start at 45°C for 5 minutes, then 5°C/min to 160 °C for 1 minute and 25 °C/min to 260 °C for 5 minutes. The injection volume was 1 µL and the injector temperature 200 °C.

The NCI full scan spectrum showed *m/z* 46 (NO$_2$) as the most intense ion for the three nitroamines. In full scan PCI all compounds had the protonated molecular ion as the most intense ion. N-nitrosodimethylamine could only be analysed by PCI. In Table 4.1 the ions used in selected ion monitoring (SIM) are shown.

Table 4.1. SIM ions for nitroso- and nitroamines in PCI and NCI GC-MS

Compound	Acronym	Molecular Weight	PCI Ions (m/z)	NCI ions (m/z)
N-nitroso dimethylamine	NDMA	74	75	-
N-nitro methylamine	MeNA	76	77	46
N-nitro dimethylamine	DiMeNA	90	91	46
N-nitro ethylamine	EtNA	90	91	46

A better sensitivity was obtained for the three nitroamines by NCI. However, PCI was used for confirmation purposes for nitroamines and for determination of N-nitrosodimethylamine.

Quantification was performed by linear regression with external calibration (standard concentrations ranging from 5 ng mL^{-1} to 400 ng mL^{-1}.

Extraction of Thermosorb/N cartridges. The manufacturer recommends elution of Thermosorb/N with 2 mL methylene chloride/methanol (3:1, v/v) for the analysis of nitrosamines. Before elution of the samples, the elution efficiency was evaluated by spiking Thermosorb/N cartridges with the target compounds (100 ng) and eluting the cartridges with three times 2 mL fractions of methylene chloride or methylene chloride/methanol (3:1, v/v). The three fractions were analysed separately. Methylene chloride/methanol (3:1, v/v) resulted to be the solvent with the best elution efficiency. However, it was necessary to use 4 mL for complete elution of the compounds. The solvent extract was then evaporated under a gentle stream of nitrogen and reconstituted to an exact volume of 1 ml for GC-MS analysis. Unspiked Thermosorb/N cartridges were also eluted in order determine the laboratory background level of the target compounds. No target compounds were found in the laboratory blank. The recovery of the four target compounds was the following: N-nitrosodimethylamine 65%, *N*-nitro dimethyl-amine 85%, *N*-nitro methylamine 76& and *N*-ethyl nitroamine 93%.

In the final method spiking of the cartridges with $^{13}C_2$, D_6-nitrosoamine (100 ng) was introduced for controlling that the cartridge was properly eluted. Concentrations of the target analytes were not corrected for $^{13}C_2$, D_6-nitrosoamine recovery.

Extraction of Charcoal Cartridges. Extraction of charcoal cartridges was carried out with 2 mL methylene chloride/methanol (3:1, v/v). The solvent extract was then evaporated under a gentle stream of nitrogen and reconstituted to an exact volume of 1 ml for GC-MS analysis. Recovery of N-nitrosodimethylamine and *N*-nitro dimethylamine were 37% and 55%, respectively. Recovery of *N*-nitro methylamine was very low (below 5%).

The detection limit for both methods, given a sampling volume of 0.3 m^3 is 0.03 µg/m^3 for *N*-nitro methylamine and *N*-nitro ethylamine, and 0.003 ng/m^3 for *N*-nitrosodimethylamine and *N*-nitro dimethylamine.

Thermal Desorption of Tenax Cartridges. Tenax cartridges were analysed by Thermal Desorption (TD) coupled to GC-MS. The TD unit (Ultra TD, Markes, UK) was programmed to a desorption temperature of 300°C for 10 minutes at 20 mL min^{-1}. The analysis was performed with an Agilent 5973 MSD and a CP-Sil 5 capillary column 50 m x 0.32 mm i.d. (Varian). The oven was programmed from 40°C for 2 minutes, then at 5°C/min to 90°C for 3 minutes, 10°C/min to 150°C for 3 minutes and 10°C/min to 300°C for 3 minutes. The MS was operated in full scan from 35 to 250 amu.

5   Results

5.1   AMS mass spectra of pure MMA-, DMA- and TMA-nitrate salt

Reference compounds (nitrate salts and chloride salts of methyl-, dimethyl- and trimethylamine) were measured with the Aerosol Mass Spectrometer. This procedure is needed since the high volatilization temperature and the high electron energy cause more fragmentation than observed in the reference spectra from NIST or other databases. The spectra were acquired at both 70 eV and 30 eV. The reference spectra from the aqueous solution made in February-March 2010 showed high contributions from ammonium and nitrate fragments and very low contributions from the organic fraction. We inferred that pollution with ammonium had occurred during generation and/or drying of the reference aerosol. We therefore repeated the reference spectra of the amines by sending a stable and particle free flow of air through the pure salt. The sample was slightly warmed up and dried using a nafion dryer for the references taken in solution. The new reference spectra are presented below. This type of analysis has been repeated for all the pure ammonium salts at both 70 and 30 eV (the intensity of the signal is given in ion count rate (Hz)). The peaks in orange correspond to the ammonium fragments, the ones in blue to nitrate and in green to the organic amine fragments (CNH_x^+). As it can be seen the contribution of the organic fraction (CNH_4^+) at the fragment 30 accounts for 40 % for $MMANO_3$, while it decreases to 20 % for $DMANO_3$ and less than 10 % for $TMANO_3$.
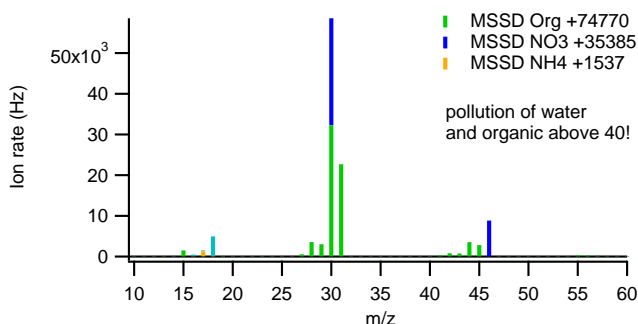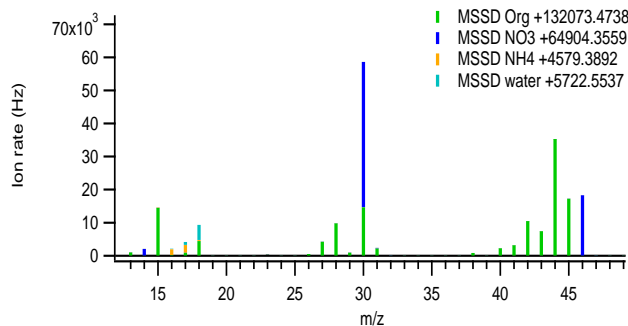
$MMANO_3$ at 70eV
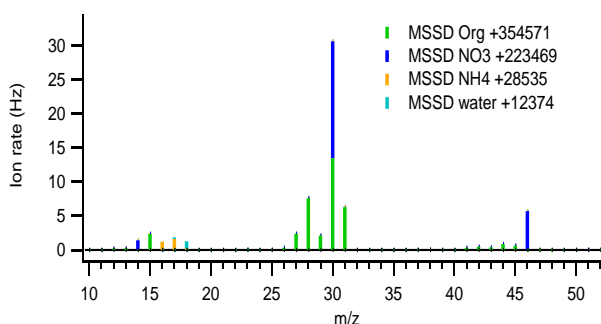
$MMANO_3$ at 30eV

Figure 5.1.   Organic and inorganic contribution to the AMS signals from $CH_3NH_3NO_3$ at 70 and 30 eV.
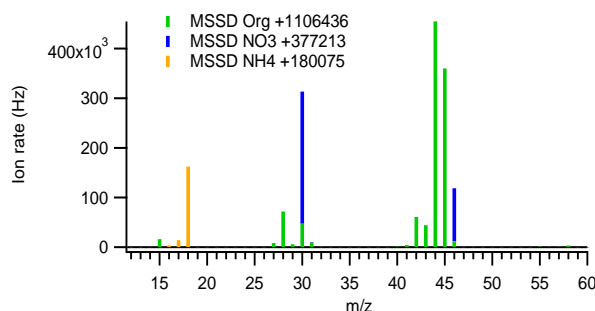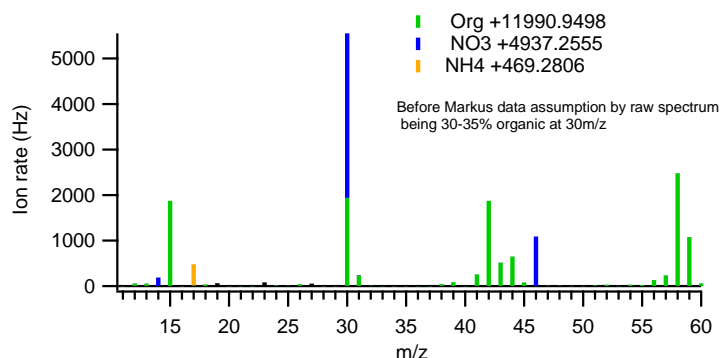
DMANO₃ at 70eV

DMANO₃ at 30eV

Figure 5.2. Organic and inorganic contribution to the AMS signals from $(CH_3)_2NH_2NO_3$ at 70 and 30 eV.

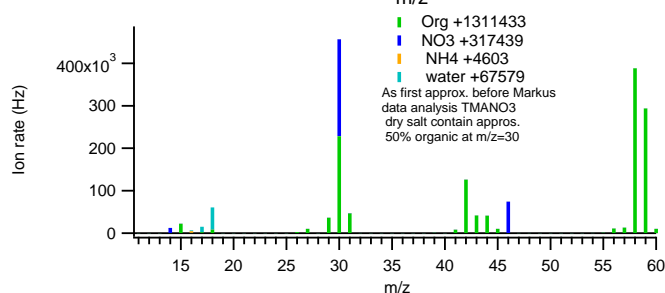TMANO₃ at 70eV

TMANO₃ at 30eV

Figure 5.3. Organic and inorganic contribution to the AMS signals from $(CH_3)_3NHNO_3$ at 70 and 30 eV.

Quantification issue. Different chemical species ionize differently in the ionization chamber. The instrument is carefully calibrated against the nitrate anion which defines the standard Ionization Efficiency. The ionization efficiency of all the other species is relative to the nitrate ion and therefore their ionization efficiency is a called Relative Ionization Efficiency (RIE).

5.2 Density of pure MMA-, DMA- and TMA- nitrate salt

A correct quantification of the aerosol formed during the experiment is possible only if a certain number of parameters are known (density, collection efficiency, ionization efficiency). These parameters have been determined using pure amine nitrate salts. The SMPS (Scanning Mobility Particle Sizer) measures the concentration of the particles between 15 to 1000nm, the results are given in number concentration (N/cm^3). The mass loading can then be derived if the density of the system is known. Therefore we carefully determined the density of the pure salts. To ensure reliable results the density of the pure MMA-, DMA- and TMA- nitrate salt has been determined using two methods, the results are shown in Table 5.1.

Table 5.1. Density and effective density values, the methods are explained in the paragraphs below.

	Method 1	Method 1	Method 2	Method 2
	100503 effective density (g/cm^3)	100323 effective density (g/cm^3)	Room T (water absorbed) real density (g/cm^3)	At 85C real density (g/cm^3)
$MMANO_3$	1.21	1.27	1.4	1.40-1.42
$DMANO_3$	1.2-1.23	1.20-1.23	1.2	1.23-1.30
$TMANO_3$	1.25	1.28	1.3	1.24-1.30
NH_4NO_3			1.79	1.74-1.76

Method 1. The effective density can be measured by comparison of the size distribution derived by the AMS and the SMPS data. The AMS measures an aerodynamic diameter (D_{va}) due to the acceleration of the particles in the vacuum, while the SMPS measures the mobility diameter (D_m) at 1 atm. The two diameters are related through density (ρ_p of the particle) and shape factor (Sp=1 for spherical particles and Sp<1 for non –spherical ones ex. NH_4NO_3 has shape factor 0.8):

$$D_{va}/D_m = S_p \cdot \rho_p = \rho_{eff} \tag{VIII}$$

Method 2. It consists on a direct measurement of the salt volume using a BET surface apparatus.[111] The procedure is the following: the empty volume (V_0) of a cell is determined by introduction of N_2; then a known amount of a salt is placed in the cell; a primary vacuum is then applied at room temperature until the pressure is stable. N_2 is finally introduced and a new volume V_1 is determined. The differences V_0-V_1 provides the salt volume. From the known mass (weighted before the experiment) the density is derived: $\rho = m/V$.

Since salts can adsorb water we repeated the same measurements heating the sample at 85°C under primary vacuum for 1h 30 min (Table 5.1, column 4).

As can be seen in Table 5.1 the density determination has been repeated twice for each method. Column 1 and 2 present the results of effective density, while columns 3 and 4 present the direct density evaluation from a volumetric method.

The results are comparable for the two methods with the exception of the MMANO$_3$ salt, indicating that this salt behave as non-spherical particles when accelerated in the particle Time-of-Flight of the AMS (size distribution). For MMANO$_3$ a shape factor of approximately 0.9 is derived while for DMANO$_3$ and TMANO$_3$ its value is approximately 1.

5.3   Thermal study of amine nitrate particles.

Short alkyl chain aliphatic amines have relatively high vapour pressures and their presence in the aerosol phase is thus most likely to occur in the form of alkyl aminium salts. The physical data on vapour pressure of amine nitrate particles are scarce. In order to provide aerosol models with fundamental data the vapour pressure and corresponding heat of vaporization were derived using our VTDMA set-up in analogue to the work described in Salo *et al.*[112] In short the VTDMA system is useful for observing changes in particle size/volume when exposed to heat. In these experiments the vaporisation of three nitrate amine salts was evaluated, in addition to the evaporation of ammonium nitrate as a reference compound. Figure 5.4 shows, in addition to data for ammonium nitrate, an example of a thermogram for one of the amine nitrates (dimethyl aminium nitrate). The thermograms shown are in the form of calculated volume fraction remaining, assuming spherical particles, as a function of temperature of the evaporation unit. In order to extract and calculate vapour pressures from these data a number of other physical parameters were needed (see Table 5.2 and equation IX).

$$p^0 = -\frac{\rho_i RT}{4 D_{i,air} \Delta t M_i} \int_{D_{p,i}}^{D_{p,f}} \frac{D_p}{f(Kn_i, \alpha)} \exp\left(\frac{-4\gamma_i M_i}{D_p \rho_i RT}\right) dD_p$$

(IX)

Where ρ_i is the particle density see Table 5.2, R is the gas constant, T is the temperature $D_{i,air}$ is the diffusivity of molecule i in air which can be calculated with parameters σ_{ii} and ε_{ii} fromTable 5.2, Δt is the residence time in the oven calculated by assuming a plugflow, M_i is the molar mass. In the second term $D_{p,i}$ is the initial and $D_{p,f}$ is the final particle diameter, $f(Kn_i, \alpha)$ is a correction term for particle diameters in the transition regime calculated according to Salo *et al.*[112] where Kn_i is the Knudsen number and α is the accommodation coefficient. In the third term γ_i is the surface free energy, seeTable 5.2.

Further details on how to derive the vapour pressures from these data and associated uncertainties are described in Salo *et al.*[112] In addition a comprehensive sensitivity analysis was carried out similar to that of Mønster *et al.*[113] giving an upper limit on systematic errors of ± 21%. Figure 5.5 shows the resulting vapour pressures (P^o) as a function of evaporating temperature T in a Clausius–Clapeyron type of plot (log P^o *versus* 1/T). The resulting heat of vaporization and estimated vapour pressure at 298 K are shown in Table 5.3. It should be noted that this is heat of vaporisation and not heat of sublimation, i.e. evaporation is from a liquid and not from a crystalline phase. Furthermore, ΔH$_{vap}$ was obtained by assuming that it is constant over the studied temperature interval.
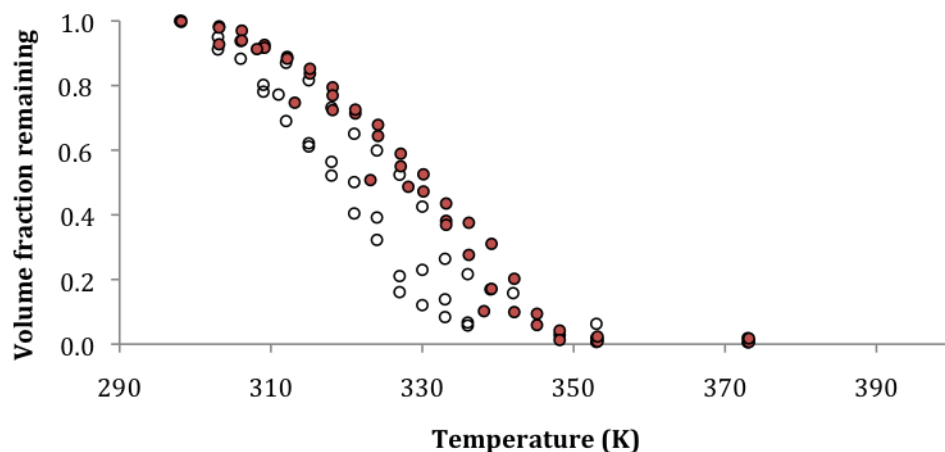
Figure 5.4. Volume fraction remaining versus evaporative temperature (thermograms) for three dimethyl aminium nitrate experiments (red circles) and three ammonium nitrate experiments (open circles).
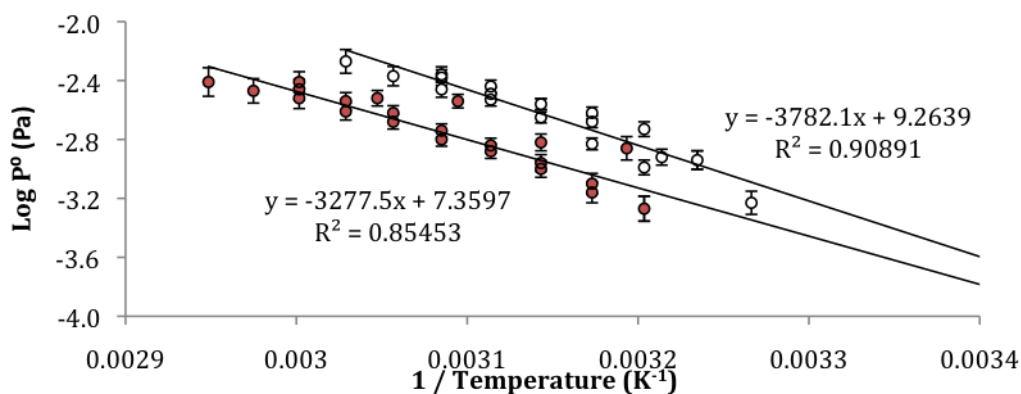

Figure 5.5. Clausius–Clapeyron plot for Dimethyl aminium nitrate (red circles) and Ammonium Nitrate (open circles) extrapolated to 298 K. Shown also is the linear regression fit to the data with stated slope, intercept and R^2.

Table 5.2. Physical properties used in vapour pressure calculations for the four compounds investigated in this work.

Compound	M /g mol^{-1}	Density[a] /g cm^{-3}	Melting point /K	γ[b] /J m^{-2}	Vc[c] /cm^3 mol^{-1}	σ_{ii}[d] /Å	ε_{11}/kb[e] /K
NH_4NO_3	80.04	1.74-1.76	443[f]	0.1[n]	146[q] 155[r]	4.43	850.56
$CH_3NH_3NO_3$	94.07	1.40-1.42	383[g]	0.1[n]	201[q] 202[r]	4.93	735.36
$(CH_3)_2NH_2NO_3$	106.09	1.23-1.30	350[h]	0.1[n]	256[q] 251[r]	5.34	672
$(CH_3)_3NHNO_3$	122.12	1.24-1.30	428[i]	0.1[n]	311[q] 302[r]	5.70	821.76

[a] This study see section 5.2. [b] Surface free energy. [c] Critical volume. [d] Interparticle distance where potential is zero. Calculated according to Bird et al.[114] [e] Depth of the potential energy well calculated according to Bird et al.[114] [f] Product data sheet. [g] Mylrajan et al.[115] [h] Walden et al.[116] [i] Cottrell and Gill.[117] [n] Estimated. [q] Calculated according to Lydersen et al.[118] [r] Calculated according to Nannoolal et al.[119]

Table 5.3. Heat of vaporization and calculated vapour pressures. Vapour pressures were extrapolated to 298 K. Stated errors are at the 95% confidence level. In addition, any systematic errors are estimated to be not more than 21%.

Compound	This study		Literature	
	$p^o_{(298\,K)}$ $/10^{-4}$ Pa	ΔH_{vap} /kJ mol^{-1}	$p^o_{(298\,K)}$ $/10^{-4}$ Pa	ΔH_{vap} / kJ mol^{-1}
NH$_4$NO$_3$	3.84–1.0+1.3	72 ± 5.4 (309 – 330^a K)	14.3^c 30.1^c 17.5^d	89.9^{*,c}, 83.4^c 97.2 ± 12.6^{*,e} (332.8 – 360.4 K)
CH$_3$NH$_3$NO$_3$	2.17–0.5+0.7	61 ± 3.4 (318 – 345^a K)	n.a.	n.a.
(CH$_3$)$_2$NH$_2$NO$_3$	2.35–0.8+1.1	63 ± 5.6 (315 – 339^a K)	n.a.	n.a.
(CH$_3$)$_3$NHNO$_3$	3.32–0.7+0.8	63 ± 3.8 (308 – 333^a K)	n.a.	n.a.

^{a} Temperature interval used to calculate heat of vaporization. ^{c} Brandner *et al.*[120] ^{d}Extrapolated using Clausius Clapeyron plot provided by Hildenbrand *et al.*[121] ^{e}Hildenbrand *et al.*[121] *heat of sublimation

5.4   Quantum Chemistry studies

Quantum chemistry calculations have been used to obtain very detailed mechanisms for the OH-initiated atmospheric photo-oxidations of methyl-, dimethyl and trimethylamine in the ADA-2010 project.[62] Reaction enthalpies for every elementary step have been derived in G3 calculations[122] employing the Gaussian 03 suite of programs.[123] In addition, systematic studies of the potential energy surfaces for a number of ostensibly simple elementary reactions have provided new insight and understanding of the complex amine photo-oxidation. This work, however, is part of VISTA project 6157 "*Study of the formation and stability N-nitrosamines, N-nitramines and N-nitroamides resulting from degradation of amines emitted to the atmosphere*" and details will be reported elsewhere.

The mechanistic development is intended to comply with the Master Chemical Mechanism, MCM. (http://mcm.leeds.ac.uk/MCM/home.htt)[6] For simplicity only the major routes in the photo-oxidation the three amines to their primary products have been included in the simplified photo-oxidation schemes in section 2 (page 21).

Proton affinities were calculated as the enthalpy for the reaction A + H$^+$ → AH$^+$ at 298 K and 1 atm using the G3 model chemistry.[124] Dipole moments and isotropic polarizabilities were obtained in DFT calculations using B3LYP functional[125-128] and the aug-cc-pVTZ basis set.[129] All calculations were performed in Gaussian 09.[123] The results are summarized in Annex 2.

5.5   Infrared reference spectra

Reference FT-IR spectra (4000-400 cm^{-1}) of pure vapours in 23.0 ± 0.1 cm gas cell with KBr windows were recorded at 298 ± 2 K using a Bruker IFS 66vs spectrometer employing nominal resolutions of 1.0, 0.5 and 0.25 cm^{-1}. A Ge/KBr beamsplitter was used to cover the spectral region, and a DTGS detector was

chosen because of its linear response. Background spectra of the empty gas cell were recorded before and after each sample spectrum to check for baseline drift. The pressure was measured by CERAVAC CTR 100 Transmitters with an accuracy of 0.2% of reading (Oerlicon Leybold Vacuum). As standard, spectra were obtained by co-adding 128 interferograms and employing Boxcar apodization in the Fourier transformation. Additional spectra of the compounds diluted in Argon at 1013 ± 5 hPa were obtained with a spectral resolution of 0.25 cm^{-1}. These spectra were calibrated against the reference spectra and used in the analyses of the IR spectra from EUPHORE.

Integrated IR absorption intensities and calibration. From Beer-Lambert's law, the absorption cross-section of a compound *J* at a specific wave number $\tilde{\nu}$ is given by $\sigma(\tilde{\nu}) = A_e / n_J l$, $A_e = -\ln \tau$ where is the napierian absorbance, τ is the transmittance, n_J is the number density of *J* and *l* is the path length over which the absorption takes place. The integrated absorption intensity, S_{int}, is given by:

$$S_{int} = \int_{Band} \sigma(\tilde{\nu}) d\tilde{\nu}$$

Infrared reference spectra of samples with low vapour pressures were obtained employing the "Oslo-reactor" (optical pathlength 128 ± 0.6 m) equipped with windows of KBr. These spectra were recorded in the 4000-600 wave number region using a Bruker IFS 66v FTIR spectrometer employing a nominal resolution of 0.25 cm^{-1}. LN2-cooled MCT and InSb detectors were used and the light intensity was reduced to ensure linear detector response. Single channel spectra (background or sample) were recorded averaging 128 interferograms and applying a Boxcar apodization.

The absolute infrared absorption cross-section of gaseous MMA, DMA, TMA and NDMA were obtained from the FT-IR spectra using the CH stretching band region for the calibration. The integrated cross-section of the CH stretching band region was determined by plotting the integrated absorbance intensities against the product of the number density and path length. Conservative estimates of systematic errors are: sample pressure (<5 %), path length (<1 %), temperature (<1 %), and definition of the baseline in the integration procedure (<5 %). The estimated accuracy of the absolute absorption cross section is believed to be better than ± 7 % including possible baseline offset.

The reference spectra and absolute cross-sections obtained are collected in Annex 6.

5.6 UV absorption cross-section of (CH$_3$)$_2$NNO

UV spectra were obtained of the pure gas at 295 ± 2 K in a cell of 8.000 ± 0.002 cm length equipped with windows of quartz. The spectra were recorded in the 190-1100 nm region using an Agilent 8453 spectrophotometer.

The partial pressures of the gases in the cell ranged from 0.1 to 5 hPa and were measured using CERVAC CTR 100 Transmitters with a stated accuracy of ± 0.2 %. The amounts of low pressure compounds were determined by weight with an accuracy of ± 0.1 mg. The absorption cross-sections were obtained from the absorbance spectra assuming that the gas was ideal.
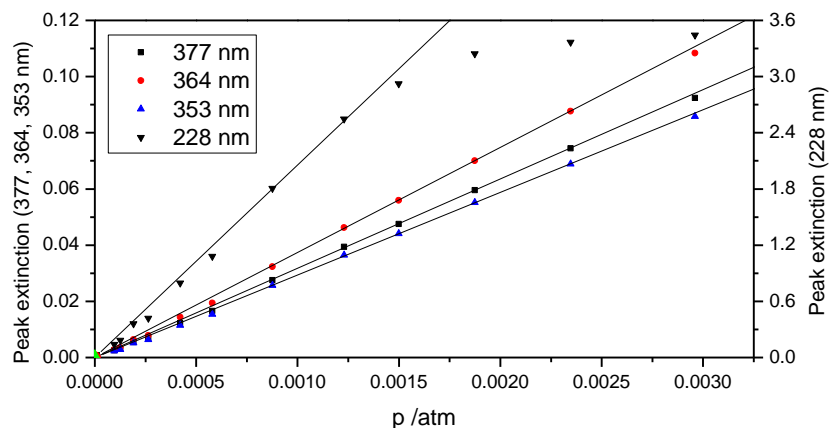
Figure 5.6. Peak absorbance for the distinct bands in the UV-VIS spectrum of *N*-nitroso dimethylamine.

In UV-VIS spectroscopy the tradition has been to present molar extinction coefficients, $\varepsilon(\lambda) = N_A \times \sigma(\lambda)$, where $\sigma(\lambda) = A_{10}/n_J \cdot l$, and $A_{10} = -\log_{10} \tau(\lambda)$ is the Briggs' absorbance, τ is the transmittance, n_J is the number density of *J* and *l* is the path length over which the absorption takes place.

The UV-VIS calibration curves given in Figure 5.6 displays the linear relationship between number density times path length and the peak absorbance of the distinct bands in the spectrum of *N*-nitroso dimethylamine. The data show a linear relationship for the weak bands and and for the strong band at 228 nm up to an absorbance of 3 (0.001 is the photometric accuracy of the instrument).

The UV-VIS molar extinction of N-nitroso dimethylamine is shown in Figure 5.7; the present results are compared with previous data in Table 5.5. The new gas phase data compare well with the previous solution results, while the gas phase results of Geiger *et al.*[41] appear to be too low.

Table 5.4. Comparison of experimental molar extinction coefficients (/L mol^{-1} cm^{-1}) of *N*-nitroso dimethylamine.

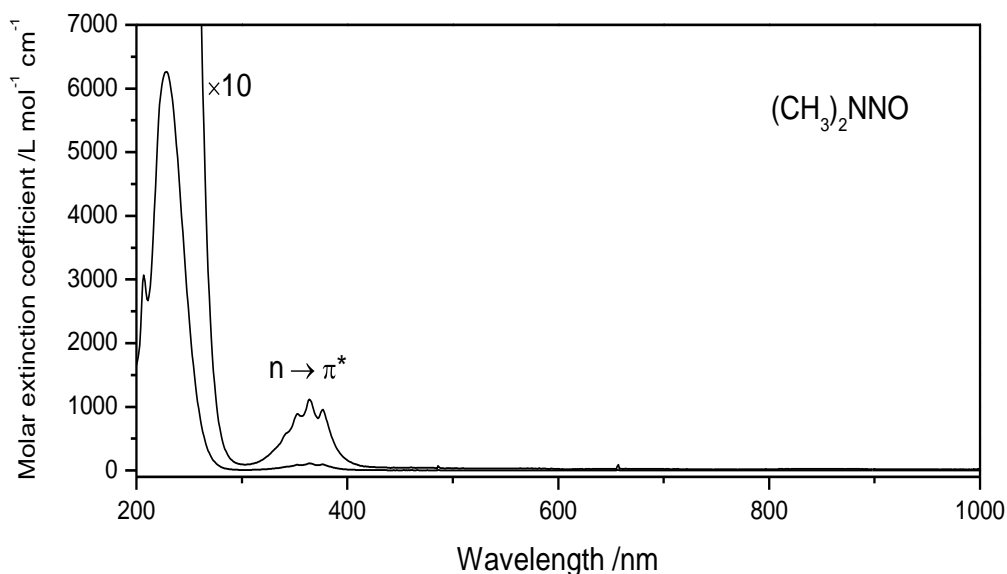| Wave length /nm	This work Gas phase	Geiger *et al.*[41] Gas phase	Haszeldine and Jander[130] Light Petroleum	Chow *et al.*[131] Methyl cyclohexane	Plumlee and Reinhard [132] Water
377	97		105		
364	114	68	125	≈130	≈100
353	89		98		
228	6240	4600	5900	≈6000	≈8000

Figure 5.7. UV-VIS molar extinction (L mol^{-1} cm^{-1}) of *N*-nitroso dimethylamine.

5.7 Off-line analysis

The results for analysis of nitroso- and nitroamines collected on Thermosorb/N catridges are summarized in Table 5.5.

Table 5.5. Concentrations (μg/m^3) of nitroso- and nitroamines collected on Thermosorb/N cartridges.

Date	Cartridge Nr.	O$_3$ scrubber	NDMA /μg m^{-3}	MeNA /μg m^{-3}	DiMeNA /μg m^{-3}
09.03.2010	G65452	Yes	0.06	<0.03	14.9
09.03.2010	G65503	No	0.05	<0.03	11.6
11.03.2010	G65448	Yes	0.16	0.75	25.3
11.03.2010	G65459	No	0.12	0.75	24.2
15.03.2010	G65454	Yes	0.18	4.25	5.65
15.03.2010	G65455	No	0.15	4.50	4.93
17.03.2010	G65445	Yes	0.01	3.58	2.39
17.03.2010	G65446	No	0.01	3.63	2.73
25.03.2010	G65443	Yes	0.12	12.3	24.4
25.03.2010	G65444	No	0.10	13.0	23.4
26.03.2010	G65453	Yes	0.03	0.64	1.00
26.03.2010	G65457	No	<0.003	0.73	1.24

Analysis of field blank and laboratory blank revealed only traces of dimethyl-nitroamine (9 ng/sample). Parallel sampling with and without ozone scrubber showed that collection of nitroso- and nitroamines is not affected by the presence of ozone. Moreover an excellent repeatability between the two parallel sampling has been obtained.

The results obtained with Thermosorb/N are compared with those obtained with charcoal cartridges In Table 5.6. Much higher concentrations were found on

Charcoal compared to Thermosorb/N cartridges. This is most probably due to heterogeneous oxidation of the amines on the charcoal cartridges, as observed by Padhye et al.[133] The lower concentrations observed for MeNA in charcoal cartridges are probably due to a much lower recovery of this compound from charcoal, as noted in section 4.5.2 (page 35). For DiMeNA the paired values are more in agreement when DiMeNA concentrations are below 10 µg m^{-3}, while charcoal concentrations are higher than Thermosorb/N concentrations at DiMeNA concentrations higher than 10 µg m^{-3}. As DiMeNA concentrations might have exceeded the capacity of Thermosorb/N cartridges, it was postulated that the lower concentrations observed for Thermosorb/N could be due to breakthrough of this compound during sampling. In order to check this hypothesis, it was decided to place a backup cartridge during the next sampling campaign and to elute the two cartridges separately.

Table 5.6. Comparison between concentrations (/µg m^{-3}) of nitroso- and nitramines collected on Thermosorb/N and charcoal cartridges in March 2010. Average values from the same day are used for Thermosorb/N results.

Date	NDMA		MeNA		DiMeNA	
	Thermo [a] /µg m^{-3}	Charcoal /µg m^{-3}	Thermo /µg m^{-3}	Charcoal /µg m^{-3}	Thermo /µg m^{-3}	Charcoal /µg m^{-3}
09.03.2010	0.06	39.4	<0.03	0.17	13.3	74.0
11.03.2010	0.14	13.3	0.75	0.03	24.7	47.5
15.03.2010	0.17	12.2	4.37	0.18	5.29	6.54
17.03.2010	0.01	0.74	3.61	0.12	2.56	3.56
25.03.2010	0.11	17.6	12.7	2.54	23.9	47.9
26.03.2010	0.03	1.44	0.68	0.10	1.12	1.41
31.03.2010	0.17	8.08	1.46	0.84	10.5	15.1

[a] Abbreviation: Thermo, Thermosorb/N.

Much higher concentrations were found on Charcoal compared to Thermosorb/N cartridges. This is most probably due to heterogeneous oxidation of the amines on the charcoal cartridges, as observed by Padhye et al. (2010). The lower concentrations observed for MeNA in charcoal cartridges are probably due to a much lower recovery of this compound from charcoal, as noted in section 4.5.2 (page 35). For DiMeNA the paired values are more in agreement when DiMeNA concentrations are below 10 µg m^{-3}, while charcoal concentrations are higher than Thermosorb/N concentrations at DiMeNA concentrations higher than 10 µg m^{-3}. As DiMeNA concentrations might have exceeded the capacity of Thermosorb/N cartridges, it was postulated that the lower concentrations observed for Thermosorb/N could be due to breakthrough of this compound during sampling. In order to check this hypothesis, it was decided to place a backup cartridge during the next sampling campaign and to elute the two cartridges separately.

Tenax cartridges were analysed by TD-GC-MS. No target compounds were found on these cartridges. The main reason for the absence of the target analytes

might be the thermal degradation of the compounds that occurs during desorption at 300°C.

Results from the July campaign. For the campaign in July only Thermosorb/N and charcoal cartridges were used for sampling. The sampling time was decreased from 5 hours to 1 hours (0.06 m^{-3} total sampling volume), since the observed concentrations of MeNA and DiMeNA observed in the first campaign could exceed the capacity of the cartridges. The use of the ozone scrubber was excluded since its use had no effect on analytes concentrations, as observed in the first campaign.

Nitroso- and nitroamines concentrations collected on Thermosorb/N and charcoal cartridges are summarized in Table 5.6. Separate analysis of the backup cartridges used for Thermosorb/N did not show any breakthrough of the compounds.

Table 5.7. Comparison between concentrations (µg/m^3) of nitroso- and nitroamines collected on Thermosorb/N and charcoal cartridges in July 2010.

Date	NDMA		MeNA		DiMeNA	
	Thermo [a] µg/m^{-3}	Charcoal µg/m^{-3}	Thermo µg/m^{-3}	Charcoal µg/m^{-3}	Thermo µg/m^{-3}	Charcoal µg/m^{-3}
06.07.2010	<0.02	<0.02	4.0	0.3	0.75	0.50
12.07.2010	<0.02	<0.02	5.9	1.0	2.1	1.4
13.07.2010	<0.02	<0.02	16.6	<0.15	1.8	1.1
14.07.2010	<0.02	6.4	1.1	0.6	22.2	15.1
15.07.2010	<0.02	18.2	3.1	1.3	79.8	119.9
16.07.2010	<0.02	5.1	14.9	2.1	27.4	18.2
19.07.2010	<0.02	<0.02	35.3	14.4	20.1	15.5
21.07.2010	<0.02	0.67	<0.15	0.3	<0.02	1.3
22.07.2010	<0.02	1.2	<0.15	<0.15	<0.02	<0.02

[a] Abbreviation: Thermo, Thermosorb/N.

For NDMA concentration it was again observed higher concentrations for charcoal cartridges, confirming the occurrence of artefacts. The concentrations of MeNA were lower for charcoal cartridges, as previously observed in March. A much better agreement between Thermosorb/N and charcoal concentrations was again observed for DiMeNA.

Full scan GC-MS analysis of sample extracts. Sample extracts from both Thermosorb/N and charcoal have been analysed in full scan by GC-MS. Full scan analyses allow to obtain full spectra of compounds present in the sample and thus attempt an identification of other compounds in addition to the target analytes. The scope of this kind of analysis is only qualitative. Since the sensitivity of the mass spetrometer decreases by about a factor 100 if compared to selected ion monitoring (SIM), only compounds present in the extract at a concentration over 1 µg/mL can be detected.

Sample extracts were first analysed by positive and negative CI. CI is a soft ionization technique which gives a little fragmentation of the molecule.

However, the spectra cannot be directly compared to libraries such as e.g. the NIST library of spectra, which are obtained by Electron Impact (EI). Thus the extracts were also analyzed by GC-MS with EI in order to compare the spectra to the NIST library.

qTOF MS analysis of particle filters. Several MS acquisitions were performed on each sample with three APCI$^+$ MS methods developed for this specific purpose. MS spectra of the analysed ADA samples were compared with the blank sample to exclude artifact compounds from the quartz filters. The results of the analyses are shown in Table 5.8.

Table 5.8. APCI$^+$ Ions (m/z) and molecular weight of compounds found in the ADA samples (and not present in the blank sample).

Experiment Date	Comments	APCI$^+$ ions(m/z)	Molecular weight /u	Molecular formula
2010/03/09	DMA-experiment. High-NOx experiment, dry conditions. Starting conditions: ~100 ppbV NO_2 and 20 ppbV NO.	46.07	45.07	$C_2H_7N_1$
		58.07	57.07	$C_3H_7N_1$
		72.05	71.05	$C_3H_5O_1N_1$
		101.07	100.07	?
2010/03/11	DMA-experiment. Low-NOx experiment, dry conditions. H_2O_2 as OH precursor. NOx kept constant at 10 ppbV.	44.06	43.06	?
		46.07	45.07	$C_2H_7N_1$
		55.06	54.06	C_4H_6
		58.07	57.07	$C_3H_7N_1$
		60.06	59.06	$C_2H_5N_1O_1$
		62.07	61.07	CH_5N_2O
		72.05	71.05	$C_3H_5N_1O_1$
		74.10	73.10	$C_3H_7N_1O_1$
		101.07	100.07	?
2010/03/22	MMA-experiment. Low-NOx experiment, dry conditions. H_2O_2 as OH precursor. NOx kept constant at 10 ppbV.	44.06	43.06	?
		46.08	45.08	$C_2H_7N_1$
		55.06	54.06	C_4H_6
		72.05	71.05	$C_3H_5N_1O_1$
		74.10	73.10	$C_3H_7N_1O_1$
		79.06	78.06	?
		85.08	84.08	?
		101.07	100.07	?
		107.10	106.10	?
		114.10	113.10	$C_5H_7N_1O_2$
2010/03/25	TMA-experiment. High-NOx experiment, dry conditions, Starting conditions: ~100 ppbV NO_2, 20 ppbV NO. NOx kept constant at 120 ppbV.	60.06	59.06	$C_2H_5N_1O_1$
		72.05	71.05	$C_3H_5N_1O_1$
		89.07	88.07	?
		101.07	100.07	?
		114.10	113.10	$C_5H_7N_1O_2$

The m/z shown in Table 5.8 were only present in samples from the first extraction of the filters thus indicating that all of the compounds have been successfully extracted from the filters into sample solution. Some of the ions present may be due to fragmentation during ionization in the mass spectrometer.

5.8 On-line chemical analysis of aerosol during the July campaign by PTR-MS.

Proof-of-principle measurements of this on-line particle analysis method were carried out during the ADA-2010 summer campaign. While more work remains to be done on method optimization and validation, exemplary data have been produced that demonstrate the utility of the new approach. Figure 5.8 displays the time trace of particle mass concentration (as measured by SMPS assuming unit density) and of the two major ion signals detected by the particle PTR-MS (pPTR-MS) instrument during a trimethylamine oxidation experiment.
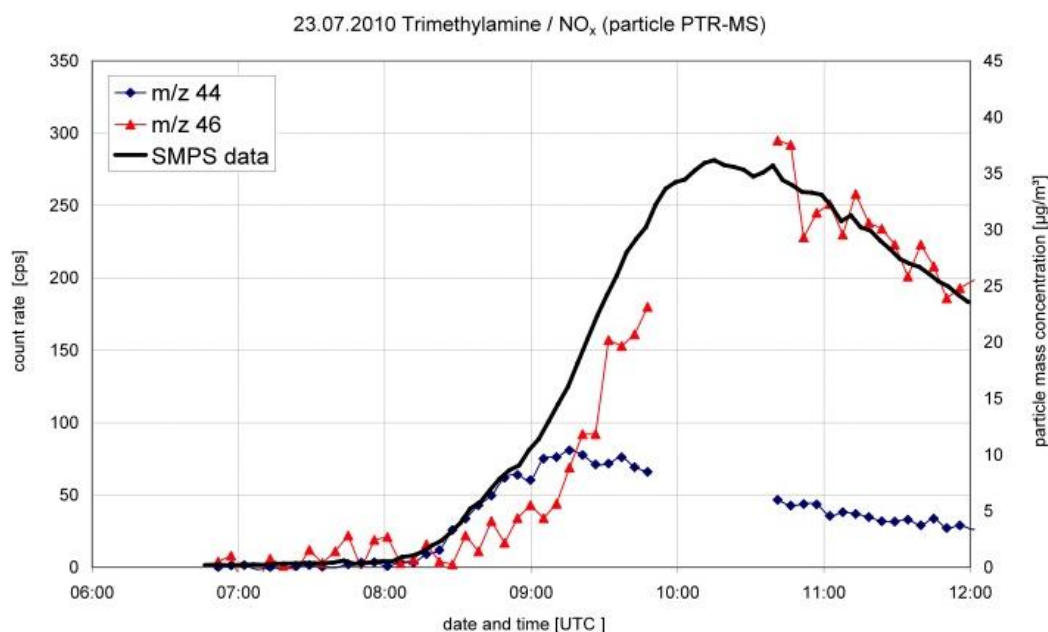
Figure 5.8. Time trace of particle mass concentration (SMPS) and of the two major ion signals detected by the particle PTR-MS instrument during a trimethylamine oxidation experiment on July 23, 2010.

The initial increase of particle mass concentration correlates with the increase of the m/z 44 ion signal. Our preliminary and tentative interpretation of this observation is that N-methyl methanimine (detected in its protonated form at m/z 44) is involved in initial particle formation via condensation reactions. At a later photo-oxidation stage, the m/z 46 signal dominates the mass spectrum. Our current interpretation is that this signal arises from formamide which is produced by thermal decomposition of yet unknown precursors on the aerosol within the aerosol evaporation cell.

Our preliminary pPTR-MS data also indicate that nitrosopiperazine formed in the photo-oxidation of piperazine is found in the secondary organic aerosol. A thorough data analysis and further tests are necessary to confirm this finding.

5.9 Analytical methods validation / intercomparison.

The quantitative detection of amines and amine degradation products is a challenging analytical task. Since there were no routine methods available to meet the analytical needs of ADA-2010, the project involved substantial method development and optimization work. Comparison of results from different methods (based on different measurement principles; independently calibrated) provided a solid test for the analytical reliability of the obtained results. Table 5.9 lists all analytical techniques that were available for method intercomparison.

Table 5.9. Overview of analytical techniques available for method intercomparison.

	On-line CEAM FT-IR (1)	On-line CEAM Hartzsch AL-4021	On-line UIBK PTR-TOF	On-line UIBK HT-PTR (2)	Off-line NERI Thermosorb/N- GC-MS	Off-line NERI Charcoal GC-MS (3)	Off-line NILU Thermosorb/N HPLC-MS	Off-line NILU DNPH-Silica HPLC-MS	Off-line NILU Thermosorb/N- GC-TEA	Off-line CEAM Thermosorb/N- GC-FID / SPME LC-MS	Off-line CEAM DNPH LC-MS	Off-line CEAM Cryotrap GC-MS
Alkylamines	X		X	X						X(6)		
Nitrosamines	X		X	X	X	X	X(4)		X(5)	X(6)		
Nitramines			X	X	X	X	X(5)	X(4)		X(6)		
Amides			X	X						X(6)		X(6)
$CH_3N=CH_2$, $CH_2=NH$		X	X	X								
HCOOH, CH_3COOH			X									
CH_3CHO, $CH_3C(O)CH_3$			X								X	
HCHO	X	X	X								X	
NH_3	X		X									

(1) data analyzed by UiO, (2) selected experiments only, (3) exploratory measurements, (4) spring campaign, (5) summer campaign, (6) qualitative data only

It was beyond the scope and time constraints of the ADA-2010 project to conduct a comprehensive and formal intercomparison exercise. In our analysis, we thus focused on the target compounds of ADA-2010 which are alkylamines, nitrosamines and nitramines. Exemplary intercomparison results are shown here – additional examples are given in the Annex 8.

Alkylamines: FT-IR / PTR-TOF

Figure 5.9 shows that PTR-TOF and FT-IR results for the three alkylamines were in excellent agreement. Both techniques detected initial amine levels of 250 ppbV which corresponds to the amount of amine that was nominally injected into the chamber. FT-IR data of methylamine and dimethylamine are reported only for the period when the chamber was kept in the dark since interferant compounds were formed under sunlight conditions.
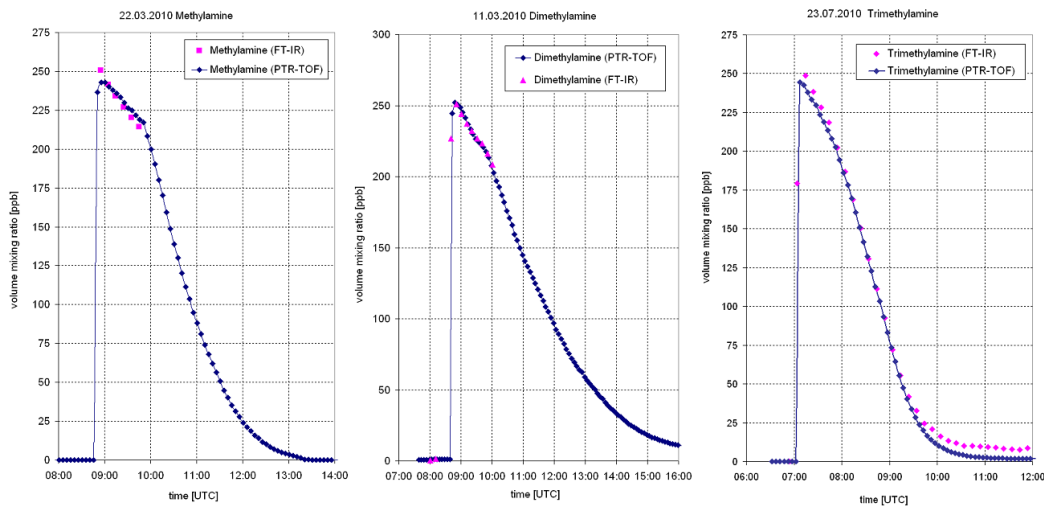
Figure 5.9. Comparison of FT-IR and PTR-TOF results for CH_3NH_2, $(CH_3)_2NH$ and $(CH_3)_3N$.

Nitrosamines: FT-IR / PTR-TOF / HT-PTR-MS

Figure 5.10 shows that the agreement between PTR-TOF, HT-PTR-MS and FT-IR results for dimethylnitrosamine was better than $\pm\,10\,\%$.
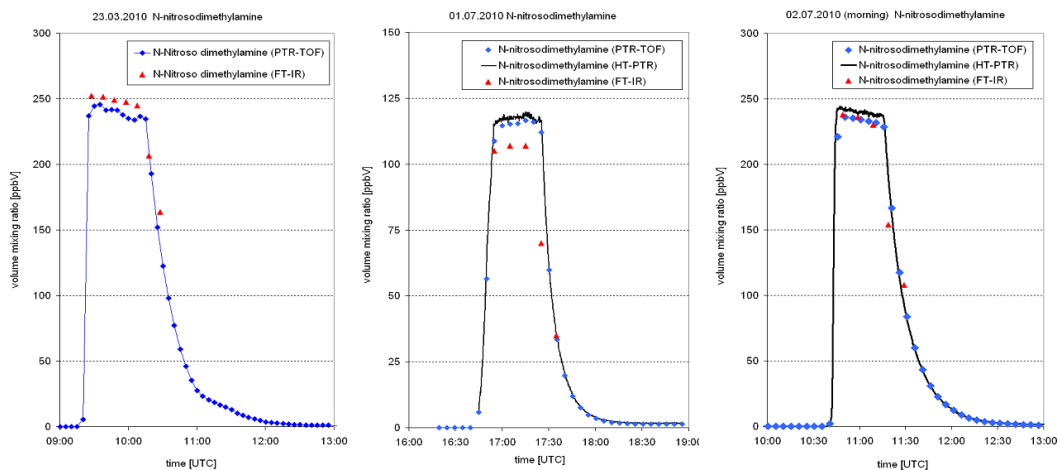
Figure 5.10. Comparison between FT-IR and PTR-TOF results for $(CH_3)_2NNO_2$.

Nitrosamines: **Offline / PTR-TOF**
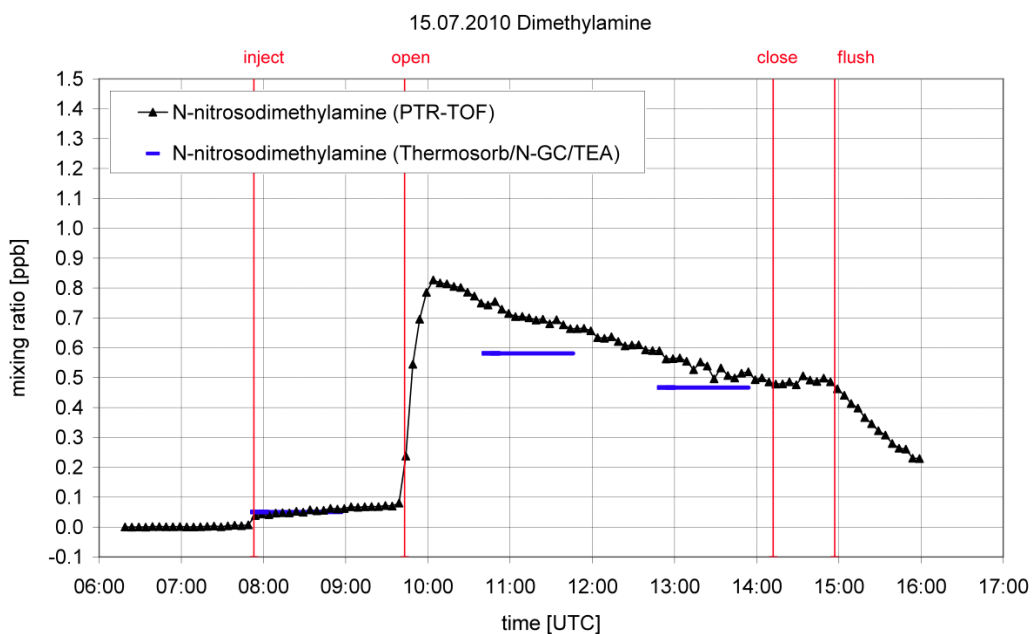
Figure 5.11. Comparison between PTR-TOF and NILU's off-line results for $(CH_3)_2NNO$.

Figure 5.11 indicates that the discrepancy between PTR-TOF and NILU's off-line results for nitrosamines was less than 15 %. This good agreement was achieved only after NILU had switched to the GC-TEA method for the analysis of the summer campaign data. NILU's spring campaign data for $(CH_3)_2NNO$ were significantly higher than the results reported both by the PTR-TOF and DMU's offline analysis. Figure 5.12 shows that PTR-TOF and DMU's off-line results for nitrosamines agreed to within 12 %. DMU reported $(CH_3)_2NNO$ data only for the spring campaign. In summer, the detection limit was insufficient because the sampling interval had been reduced to one hour.
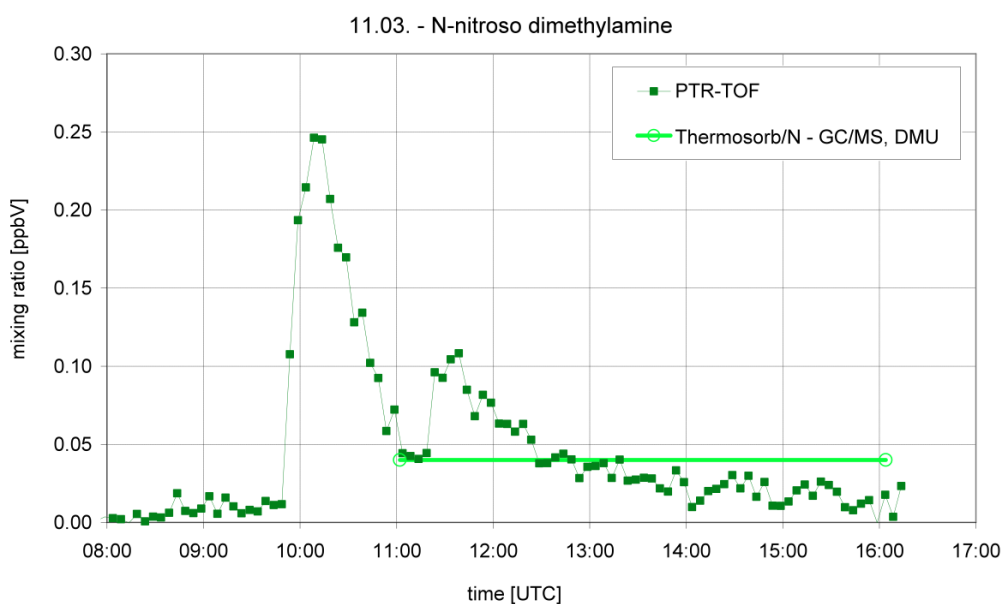
Figure 5.12. Comparison between PTR-TOF and DMU's off-line results for $(CH_3)_2NNO$.

Nitramines: **Offline / PTR**

Figure 5.13 and Figure 5.14 indicate that the agreement between the PTR-TOF and DMU's off-line results for N-nitrodimethylamine was better than 15 %. NILU did not report N-nitrodimethylamine data.
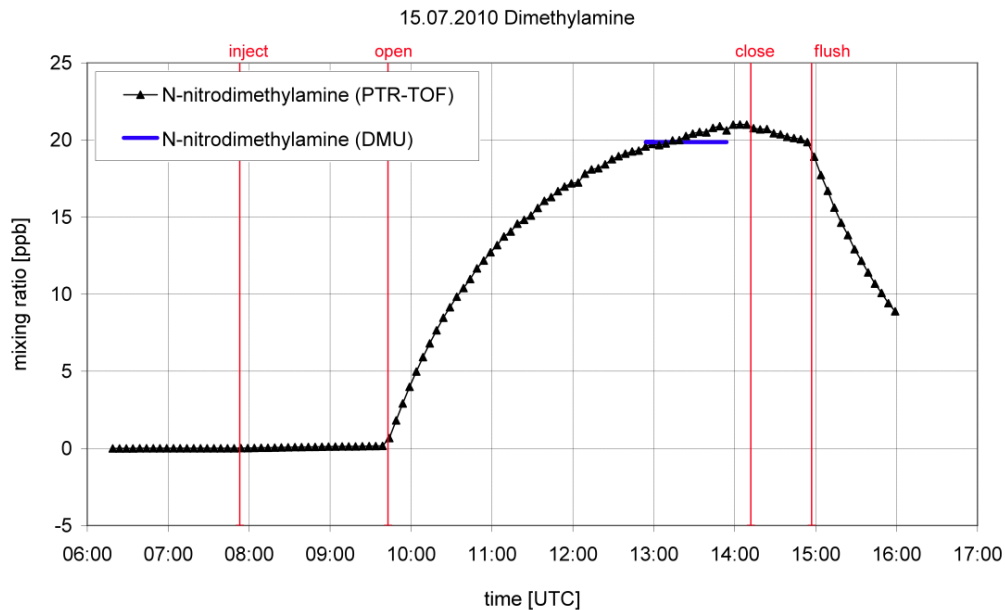
Figure 5.13. Comparison between PTR-TOF and DMU's off-line results for $(CH_3)_2NNO_2$.
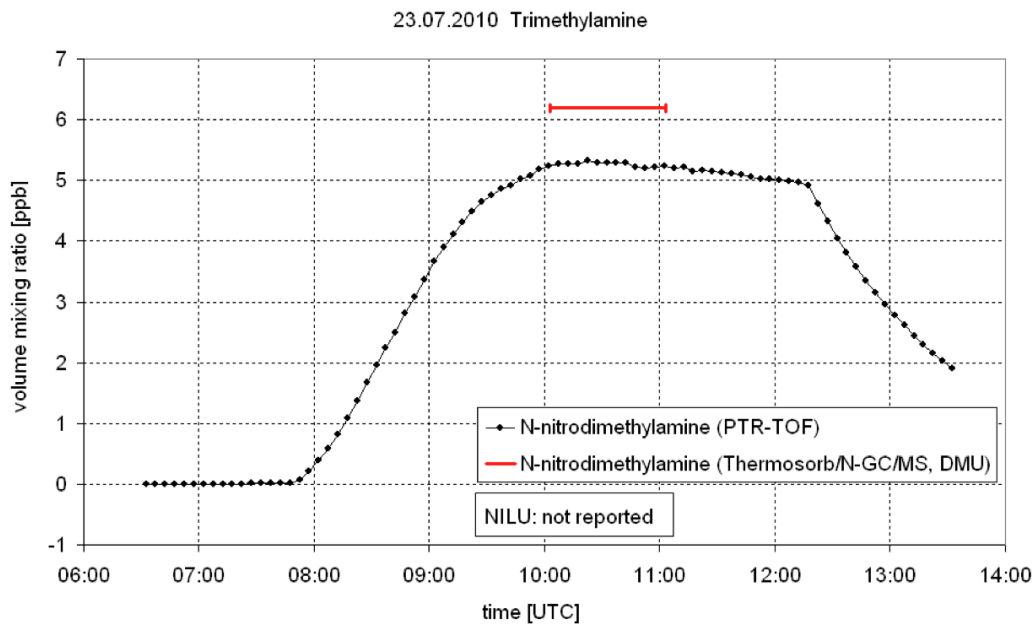
Figure 5.14. Comparison between PTR-TOF and DMU's off-line results for $(CH_3)_2NNO_2$.

The given exemplary results indicate that the obtained experimental data are of high analytical quality. ADA-2010 produced first-time-ever data on amines and amine degradation products (incl. nitrosamines and nitramines) that are i) on-line, ii) in the 10-ppt-to-250 ppb range, and iii) validated by independently calibrated methods.

5.10 CH₃NH₂ photo-oxidation studies

Three MMA photo-oxidation studies, carried out 2010, have been selected for more detailed analysis:

Date	Experimental conditions	Monitor data
2010/03/22	Low-NOx experiment: NOx constant ~10 ppbV.	Annex 11
2010/07/13	High-NOx experiment. Starting conditions: ~100 ppbV NO₂, ~5 ppbV NO.	Annex 18
2010/07/22	High-NOx. Starting conditions: ~100 ppbV NO₂, ~20 ppbV NO.	Annex 22

The 2010/03/22 experiment was carried out under low-NOx conditions: the NOx-level was kept constant at 10 ppbV by adding NO. To increase the OH radical production around 350 ppbV H_2O_2 was added to the chamber (H_2O_2 + hν → 2 OH).

The 2010/07/13 experiment was carried out under high-NOx conditions. Around 3.5 ppmV H_2O_2 was added to increase the OH concentration in the experiment. This resulted in interfering reactions in the PTR drift-tube making quantification of absolute yields difficult. The aerosol study was not affected.

The 2010/07/22 experiment was carried out under high-NOx conditions. A small amount of H_2O_2 was added at start of the experiment (around 350 ppbV). This resulted only in minor interfering reactions in the PTR drift-tube.

The theoretical photo-oxidation mechanism of methylamine (Scheme 2.1, Page 21), is shown again below indicating the major photo-oxidation products to be formamide (H₂NCHO), methanimine (HN=CH₂) and *N*-nitro methylamine (CH₃NHNO₂).
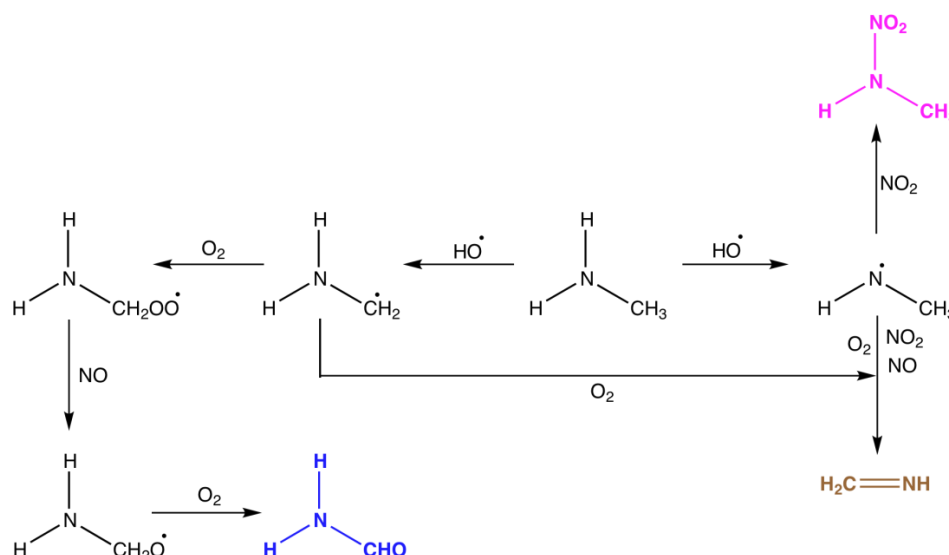
Scheme 2.1. Main routes of the atmospheric methylamine photo-oxidation.

Figure 5.15 shows the time-integrated molar increase in CH₃NH₂ photo-oxidation products (detected in their protonated forms at m/z 18.034, 30.034, 31.018, 44.050 and 45.029) relative to the time-integrated decrease of methylamine

(detected in its protonated form at m/z 32.0495) during the first 30 minutes of the photolysis experiment on 2010/03/22. Only products with a relative increase > 1 % have been included in the figure. The observed ion signals are assigned as follows: m/z 18.034 (protonated ammonia), m/z 30.034 (protonated methan-imine), m/z 31.019 (protonated formaldehyde), and m/(z 44.050 (protonated *N*-methyl methanimine); *N*-nitro methylamine was observed with less than 1% yield in this experiment. In addition, ions from spill-over from a previous dimethylamine experiment, and acetaldehyde, formic acid and acetic acid were observed. The latter compounds are typically formed in any smog chamber photo-oxidation experiments.
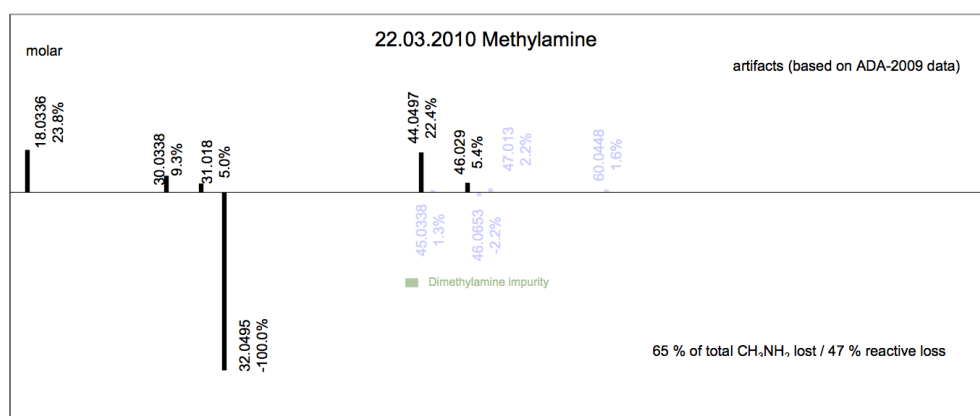
Figure 5.15. Mass spectral difference measured during the photo-oxidation of methylamine on March 22. Mass peaks of intensity < 1 % of $\Delta I_{32.0495}$ are omitted.

Figure 5.16 shows the time evolution of the major ion signals during the photo-oxidation of methylamine under low-NOx conditions, while Table 5.10 summarizes the ions observed during the selected experiments, their relative molar increase and the interpretation.

N-methylmethanimine, $CH_3-N=CH_2$, and not methanimine, $CH_2=NH$, is the major product observed under low-NOx conditions. Methaneimine shows the typical time-profile of an intermediate in the photo-oxidation of methylamine, Figure 5.16, while *N*-methyl methanimine, containing more carbon atoms than the reactant methylamine, and which obviously cannot be a product of the photo-oxidation *per se*, shows the time-profile of a primary product. Obviously, methanimine undergoes faster heterogeneous reactions than gas phase reactions with i.e. OH radicals.

Ammonia, NH_3, is also observed to increase during the experiment and we suggest that both *N*-methylmethanimine and NH_3 originate in heterogeneous reactions of the expected major product methanimine with water and methylamine:
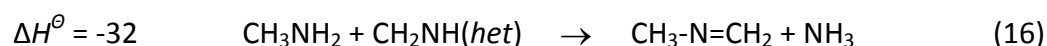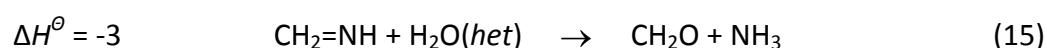
$$\Delta H^{\ominus} = -3 \qquad CH_2=NH + H_2O(het) \quad \rightarrow \quad CH_2O + NH_3 \qquad (15)$$

$$\Delta H^{\ominus} = -32 \qquad CH_3NH_2 + CH_2NH(het) \quad \rightarrow \quad CH_3-N=CH_2 + NH_3 \qquad (16)$$

The reaction enthalpies listed ($\Delta H^{\ominus}$ /kJ mol^{-1}) refer to 298 K and to the lowest energy conformations of the species involved and stem from G3 calculations.[122]
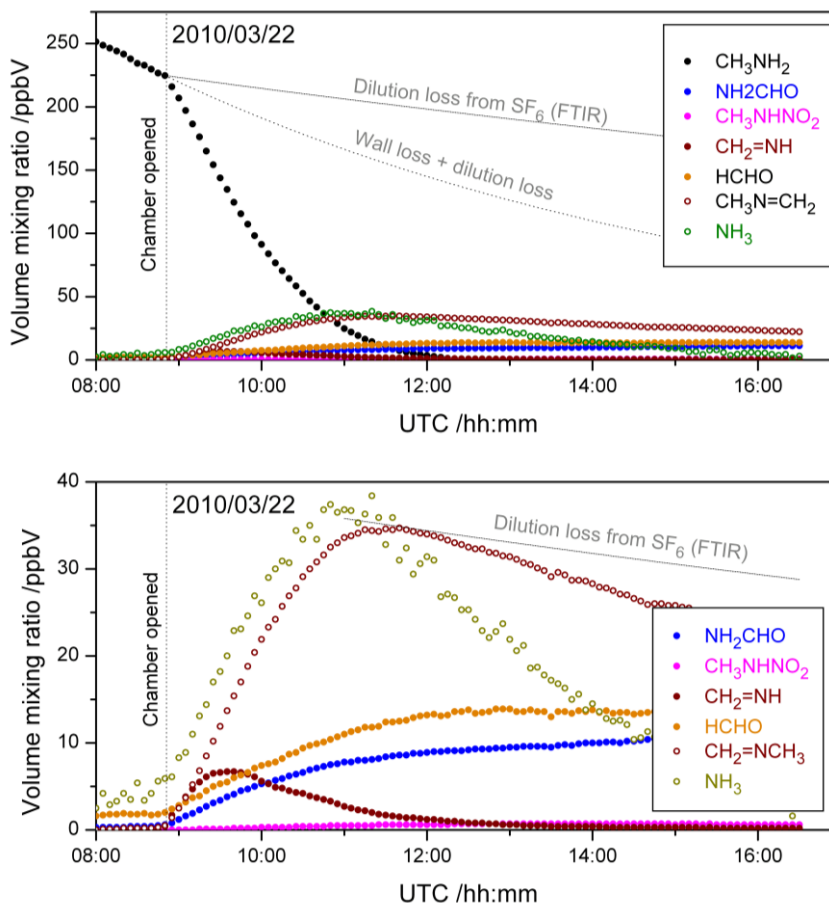
Figure 5.16. Top: Time evolution of ion signals observed in the 2010/03/22 low-NOx experiment. Bottom: Time evolution of the product ion signals.

Figure 5.17 shows the time profiles of the products formed under high-NOx conditions in the experiment on 2010/07/22. The experiment was carried out early in the morning (low actinic flux) and consequently the reactive loss of methylamine was low. It can, however, be seen from Figure 5.17 that relatively more methylnitramine was formed in the high-NOx experiment.
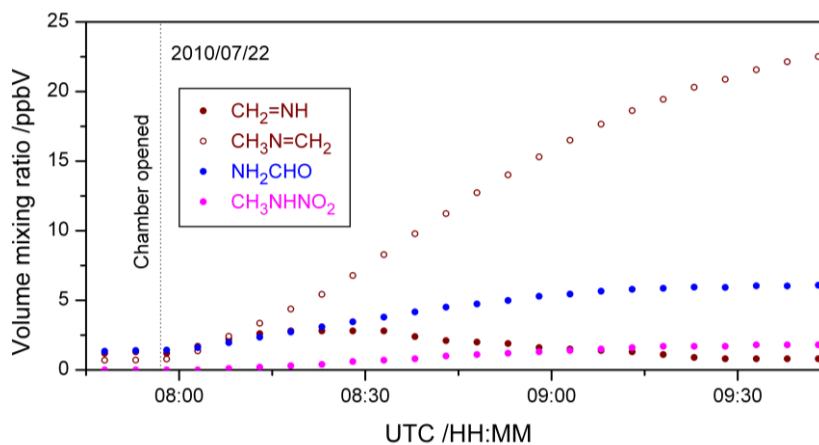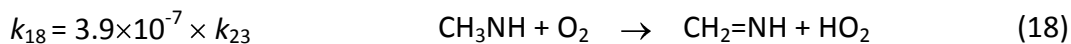

Figure 5.17. Time evolution of the product ion signals observed in the 2010/07/22 High-NOx experiment.

The heterogeneous reactions makes it impossible to model the gas phase reactions of CH$_2$=NH (and CH$_2$=NCH$_3$) in detail. The chemistry of methanimine is currently unsettled and only two products can be considered reliable markers of the experiments: CH$_3$NHNO$_2$ (*N*-nitro methanamine, methylnitramine) and NH$_2$CHO (formamide).

The products observed are are thus in agreement with the theoretical gas phase chemistry model. The data have therefore been analysed in terms of the following scheme:
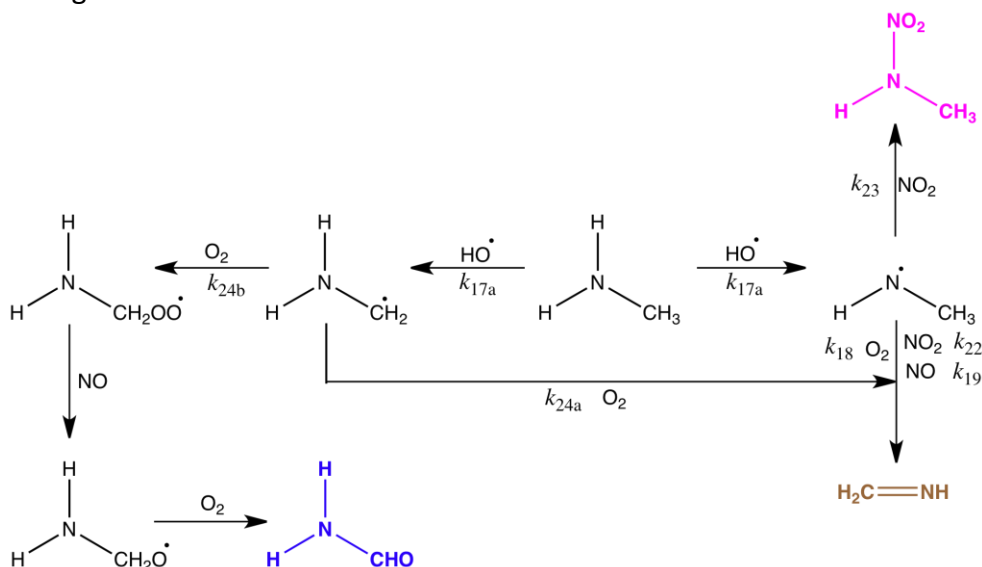
Scheme 5.1. Updated scheme with rate constants for the atmospheric photo-oxidation of methylamine.
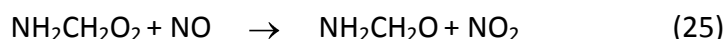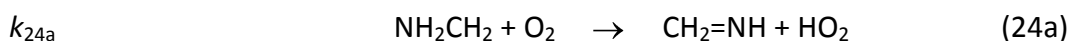
In modelling the gas phase chemistry it was initially assumed a C-H : N-H branching ratio in the initial OH reaction equal to that of the Cl reaction (0.48 : 0.52).[22] Further, initial values for the the rate constants of the CH$_3$NH radical reactions with O$_2$, NO and NO$_2$ (volume mixing ratios X_{O2}, X_{NO} and X_{NO2}) were taken to be the same as those of the (CH$_3$)$_2$N radical,[33] (see section 1.4.1, page 15), but taking into account that the primary nitrosamine, CH$_3$NHNO, isomerizes and reacts fast with O$_2$ to form the imine.[46]

k_{17a}	CH$_3$NH$_2$ + OH	$\rightarrow$	CH$_2$NH$_2$ + H$_2$O	(17a)
k_{17b}		$\rightarrow$	CH$_3$NH + H$_2$O	(17b)
$k_{18} = 3.9 \times 10^{-7} \times k_{23}$	CH$_3$NH + O$_2$	$\rightarrow$	CH$_2$=NH + HO$_2$	(18)
$k_{19} \propto 0.26 \times k_{23}$	CH$_3$NH + NO	$\rightarrow$	CH$_3$NHNO	(19)
Fast equilibrium	CH$_3$NHNO	$\leftrightarrows$	CH$_2$NHNOH	(20)
Fast	CH$_2$NHNOH + O$_2$	$\rightarrow$	CH$_2$=NH + NO + HO$_2$	(21)
$k_{22} \propto 0.22 \times k_{23}$	CH$_3$NH + NO$_2$	$\rightarrow$	CH$_2$=NH + HONO	(22)
k_{23}		$\rightarrow$	CH$_3$NHNO$_2$	(23)
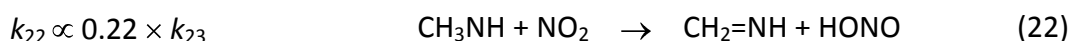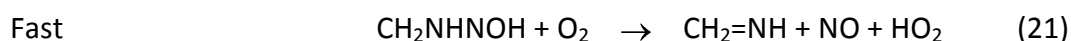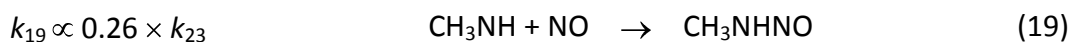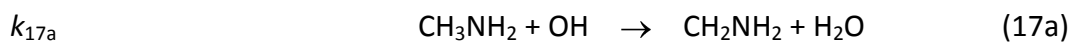
The NOx concentration in the 2010/03/22 experiment was low (< 10 ppbV) and reactions (19)-(22) can be neglected in comparison to reaction (18). Given the volume fractions, X_{NO} and X_{NO2} (see Annex 11), the observed concentration time

profile of CH_3NHNO_2 will therefore determine the ratio k_{18}/k_{23} relative branching ratio of reaction (18) for a given initial N-H:C-H branching ratio in reaction (17). The NOx concentration in the 2010/07/22 experiment was high (15-40 ppbV NO and >75 ppbV NO_2) and the time profiles of CH_3NHNO_2 in this and the 2010/03/22 experiment, will therefore determine the initial N-H:C-H branching ratio in reaction (17).

The branching of the NH_2CH_2 radical reactions with O_2 can then be determined from the time profiles of the NH_2CHO formation:

$$k_{24a} \qquad\qquad\qquad NH_2CH_2 + O_2 \quad \rightarrow \quad CH_2=NH + HO_2 \qquad\qquad (24a)$$

$$k_{24b} \qquad\qquad\qquad\qquad\qquad\qquad \rightarrow \quad NH_2CH_2O_2 \qquad\qquad (24b)$$

$$NH_2CH_2O_2 + NO \quad \rightarrow \quad NH_2CH_2O + NO_2 \qquad\qquad (25)$$

$$NH_2CH_2O + O_2 \quad \rightarrow \quad NH_2CHO + HO_2 \qquad\qquad (26)$$
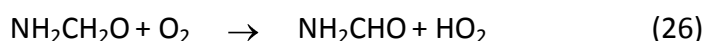
The best fit to the data shown in Figures 5.16 and 5.17 are obtained for $k_{17a}/k_{17} = 0.25$, $k_{24b}/k_{24} = 0.15$, $k_{18}/k_{23} = 2.0\times10^{-6}$, $k_{22}/k_{23} = 4$, and $k_{19}/k_{23} = 0.75$ (constrained at the value obtained for the corresponding reaction of the dimethylamino radical, see section 5.11, page 67, and section 5.13, page 98). The estimated error in the ratios given is $\pm15\%$. Considering the differences in electronic structure between the CH_3NH and $(CH_3)_2N$ radicals the kinetic parameters of the two systems are remarkably like.

Table 5.10. Ions observed by PTR-TOF-MS during the methylamine photo-oxidation and their time integrated molar increase in the experiments.

m/z	Ion formula	2010.03.22	2010.07.22	Confirmation	Potential neutral precursor
18.0334	NH_4^+	23.8		FTIR	ammonia
30.0338	CH_3N^+	9.3			methanimine
31.0180	CH_3O^+	5.0		FTIR, DNPH	formaldehyde
32.0495	CH_6N^+	-100			methylamine
44.0133	CH_2NO^+				isocyanic acid
44.0497	$C_2H_6N^+$	22.4			*N*-methyl methanimine
45.0338	$C_2H_5O^+$	CA^a	CA		acetaldehyde
46.0289	CH_4NO^+	5.4		SPME	formamide
46.0653	$C_2H_8N^+$	CAO			dimethylamine
47.0130	$CH_3O_2^+$				formic acid
59.0494	$C_2H_7O^+$	CA		DNPH	acetone
60.0448	$C_2H_6NO^+$	COA		SPME	*N*-methylformamide
61.0289	$C_2H_5O_2^+$	CA			acetic acid
77.0349	$C_2H_5N_2O_2^+$	<1		ThermoN	*N*-nitro methylamine
91.0509	$C_2H_7N_2O_2^+$				*N*-nitro dimethylamine

[a] Abbreviations: CA, Chamber Artifact; COA, Confirmed in Off-line Analysis; FTIR, Fourier Transform Infrared; DNPH, Di-Nitro-Phenyl-Hydrazine cartridges; SPME, Solid Phase Micro-Extraction; ThermoN, Themosorb-N cartridges.

5.10.1 Analysis of aerosol formation

The experiment on March 22, 2010, illustrates particle formation during photo-oxidation of methylamine (MMA) under low NOx conditions (a mixture of about 250 ppbV MMA and H_2O_2 / NO_2 was exposed to sunlight). The chamber canopy was opened at 09:51 UTC. The SMPS recording stopped due to instrument failure at 09:43 UTC and for this reason the onset of the particle burst that very likely followed the opening was not monitored (Figure 5.18). At 11:27 UTC the SMPS instrument was successfully restarted.
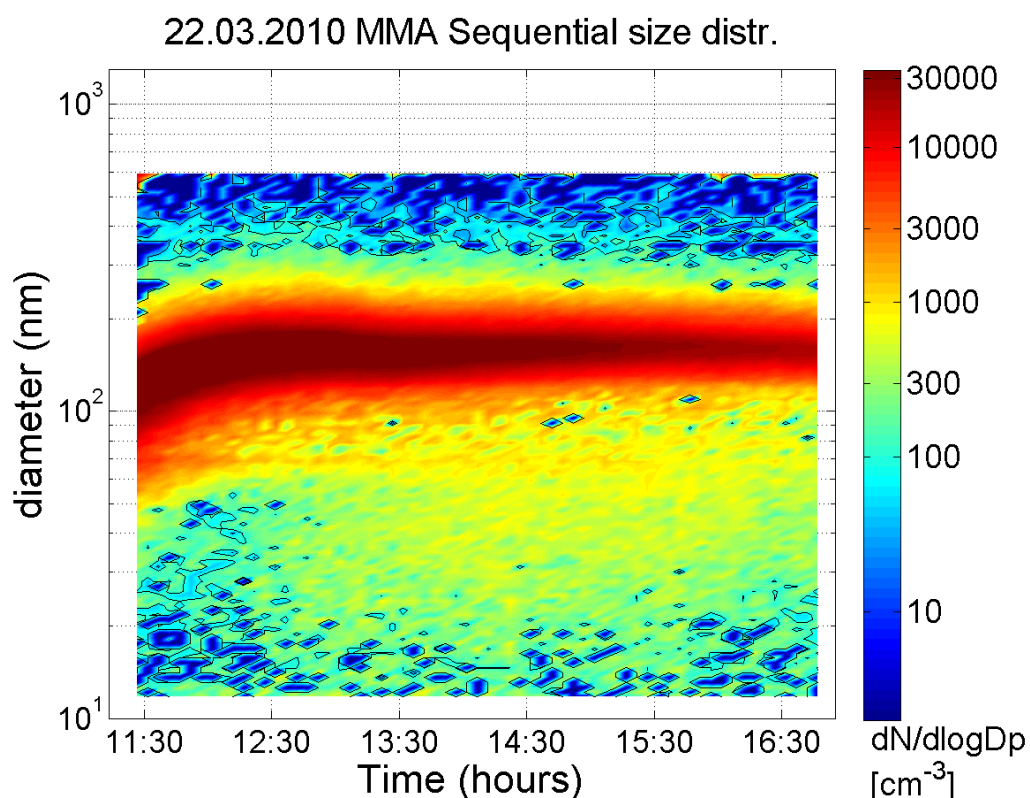
Figure 5.18. Sequential number size distribution (dN/DlogDp in # cm^{-3}) as recorded by SMPS during the experiment on March 22, 2010. Instrument failure from 09:43 to 11:27 UTC. SMPS lower cut-off is at 11.8 nm.

After the chamber is exposed to sunlight, the OH-initiated oxidation of methylamine (short: MMA) started and MMA to a large extent degraded by chemical reaction with the OH radical (93% according to model results). Monitored time series of NO and NO_2 concentration as well as temperature and the photolysis rate of j_{NO2} are input to the coupled gas phase / aerosol model MAFOR. HONO is produced at the chamber wall and following photolysis is a primary source of OH radicals in EUPHORE. Measured concentration time series of MMA, ozone, and HONO are well reproduced by the model (Figure 5.19).
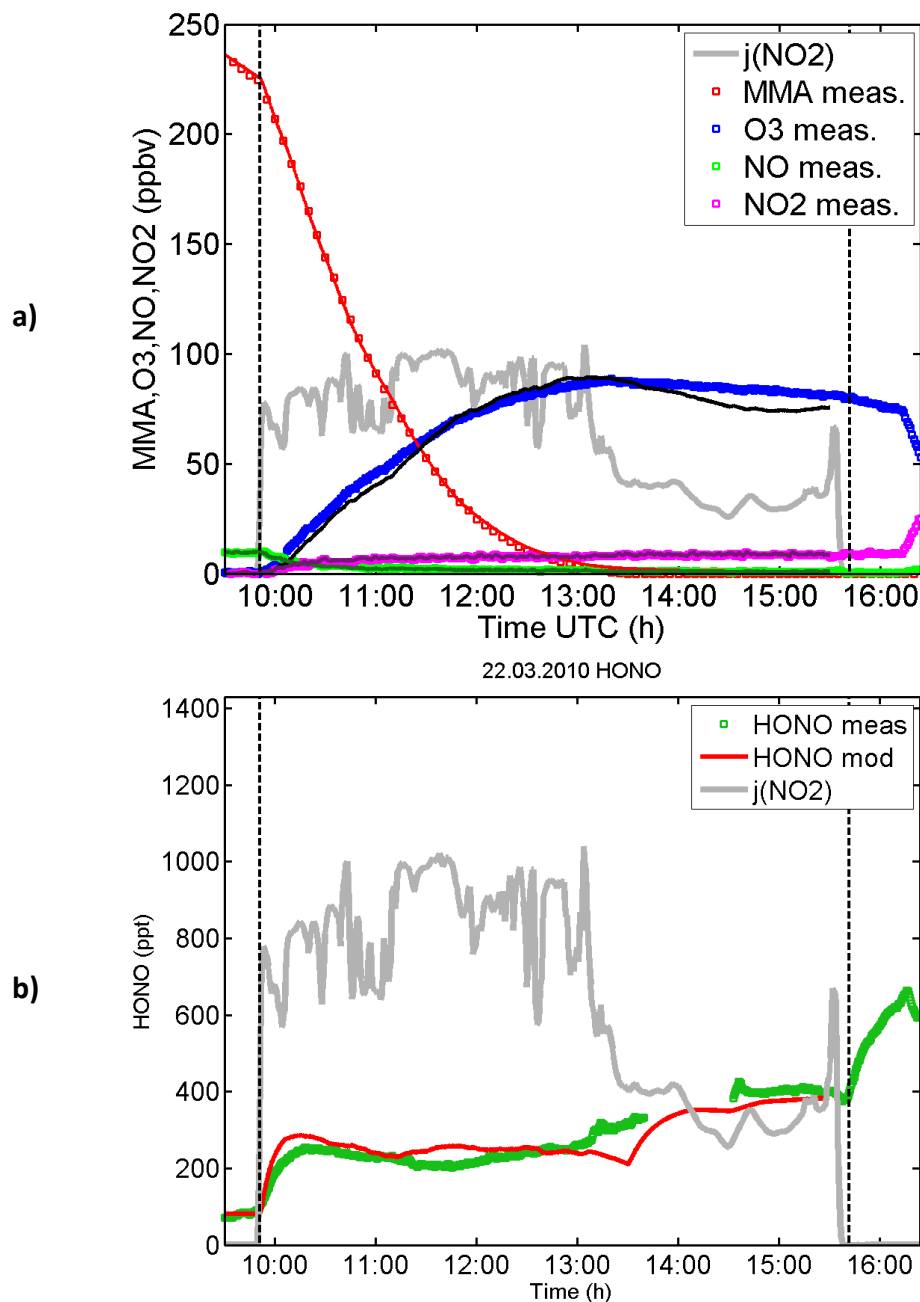
Figure 5.19. Modelled (solid lines) versus measured (squares) gas phase concentrations during the experiment on March 22, 2010, a) methylamine (red squares; measured by PTR-MS), ozone (blue squares), NO (green squares), NO_2 (magenta squares) in ppbV b) HONO (green squares; measured by LOPAP) in pptv. Grey line indicates photolysis frequency of $j(NO_2)$ (scaled to displayed concentrations). The time period between the vertical (dashed) lines is the sunlit experiment.

Model results from MAFOR indicate that immediately after opening of the canopy nucleation of new particles occurs (assumed to be methylaminium nitrate salt particles). The model predicts that nucleation occurs during a period of half an hour after chamber opening and then stops completely (Figure 5.20a). The particle burst generated in the model simulation largely resembles the one recorded by SMPS. Modelling allows in this case to "re-construct" the particle

burst both at small particle diameters (SMPS cut-off at 11.8 nm) and during the period of missing data at the start of the experiment.
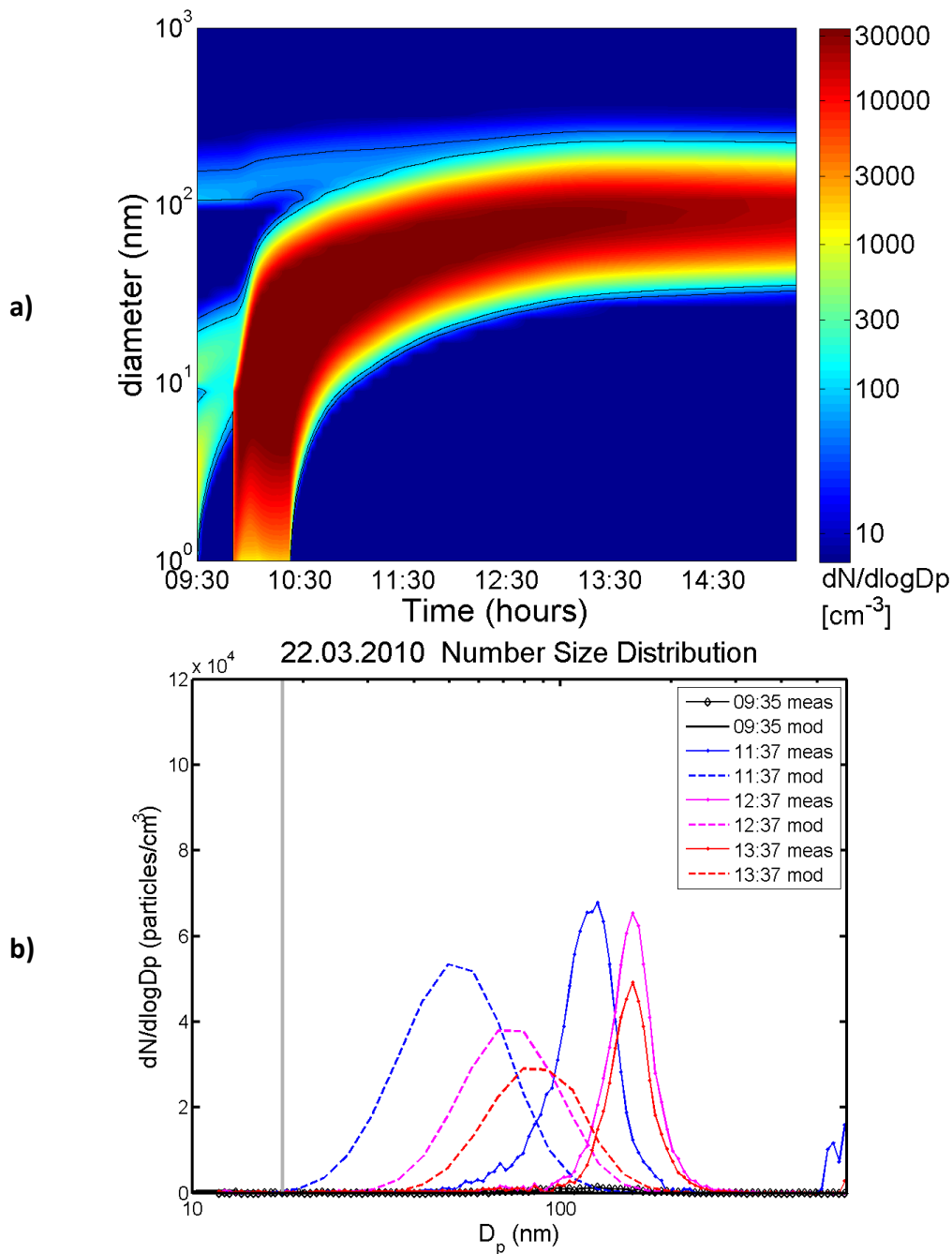
Figure 5.20. Modelled number size distribution (dN/DlogDp in # cm-3) during the experiment on March 22, 2010, a) as 2-dimensional plot for the diameter range 1-1000 nm, b) as snapshots at 11:37, 12:37, 13:37 UTC. Modelled peaks are broader than the peaks recorded by SMPS, a possible reason being numerical diffusion in the model.

Growing aerosol particles reached maximum diameters of about 200 nm and after about 12:20 UTC no further growth was observed and a decrease of total particle numbers can be seen. The total aerosol mass concentration as provided by SMPS and AMS instruments (using an effective particle density of ~1200

kg/m^3) increased up to ~25 µg/m^3 during the experiment. Figure 5.21 depicts the evolution of the AMS and the SMPS data during the experiment. Two thermograms were performed with the AMS during 12:57 – 13:22 UTC and 16:16 – 16:34 UTC. During these thermograms the temperature was varied in 4 steps from 25°C to 110°C. From 13:22 until 16:16 UTC no quantitative AMS data is available due to instrumental testing.
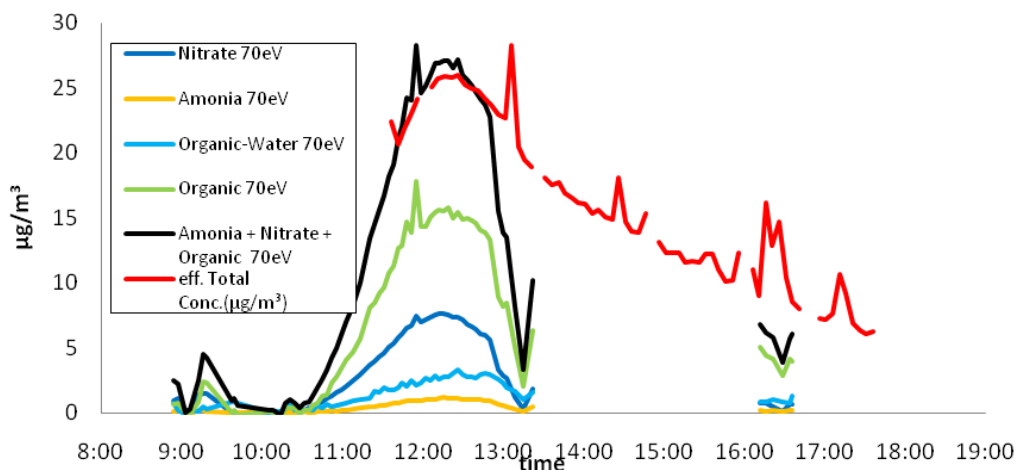
Figure 5.21. AMS mass loading for nitrate, ammnium, organics and organic-water for 70 eV and effective SMPS total concentration during the experiment on March 22, 2010.

By applying an effective density D_{va}/D_m between 1.16 at 11:40 UTC to 1.26 at 12:50 UTC to the SMPS data, the AMS total aerosol mass (ammonia + nitrate+ organics) and the D_{va}/D_m corrected SMPS total concentration show good agreement. According to the AMS records, at 12:20 UTC about 58 % of the total loading contributed as organics, about 28 % as nitrate. By using pure reference spectra of methylaminium nitrate (MMANO$_3$), the fragmentation pattern of MMANO$_3$ for 70 eV electron impact ionization and 600°C vaporizer temperature was determined. Accordingly, the most significant organic fragments of MMA are CH$_4$N$^+$ and CH$_5$N$^+$. By inter-comparison of the fragmentation pattern of these two ions with the nitrate time-series, an upper limit for the pure MMANO$_3$ can be calculated.

Figure 5.22 depicts the evolution of total nitrate, pure MMANO$_3$ nitrate and non MMANO$_3$ nitrate. The pure MMANO$_3$ salt is dominating the initial phase of the experiment with about 65% contribution to the total nitrate. Later on during photo-oxidation other salts become more important and the MMANO$_3$ salt contribution to the total nitrate decreases to 40% at 13:20 UTC. Five ions with a similar time series as the non MMANO$_3$ nitrate could be identified, HCO$^+$, C$_2$H$_2$N$^+$, C$_2$H$_4$N$^+$, C$_3$H$_6$O$^+$ and C$_3$H$_7$O$^+$ respectively.

Detailed analysis revealed high volatility comparable to the nitrate volatility for C$_3$H$_6$O$^+$ and C$_3$H$_7$O$^+$. Due to the time-series and the volatility information it is very likely that these two ions are fragments of the organic part of a secondary salt. By taking the organic part of the MMANO$_3$ salt into account and the additional

assumption, that the organic part of the non MMANO$_3$ nitrate salt has an average m/z ratio of 59 (C$_3$H$_7$O$^+$), a total salt contribution between 35 % and 40 % of the organic mass fraction can be estimated. The remaining 60 % to 65 % of the total aerosol mass must be attributed to secondary organic aerosol components.
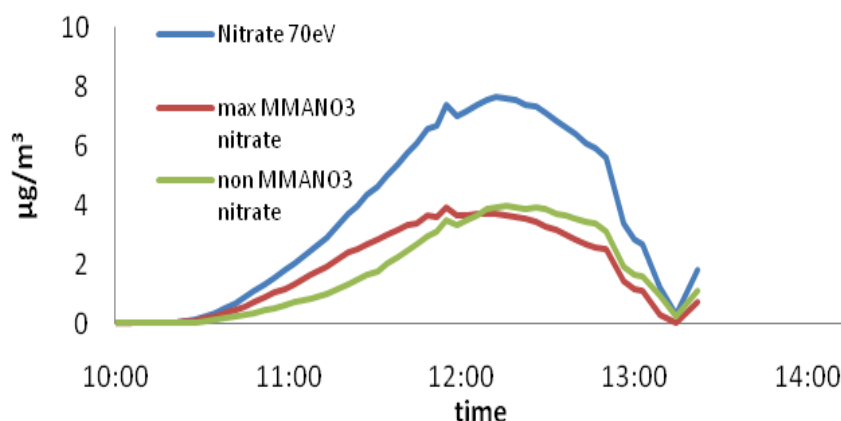

Figure 5.22. Time series of total nitrate, maximum nitrate from pure the MMANO$_3$ salt and the non MMANO$_3$ nitrate during MMA 2010/03/22.

Three experiments on MMA were evaluated for thermal properties of the aerosol produced (see Figure 5.23) using the VTDMA set up. After the chamber had been open for 1 hour all experiments produced an aerosol with similar volatility. Although the aerosol in the low NOx-experiment had a higher volume fraction remaining at high temperatures.
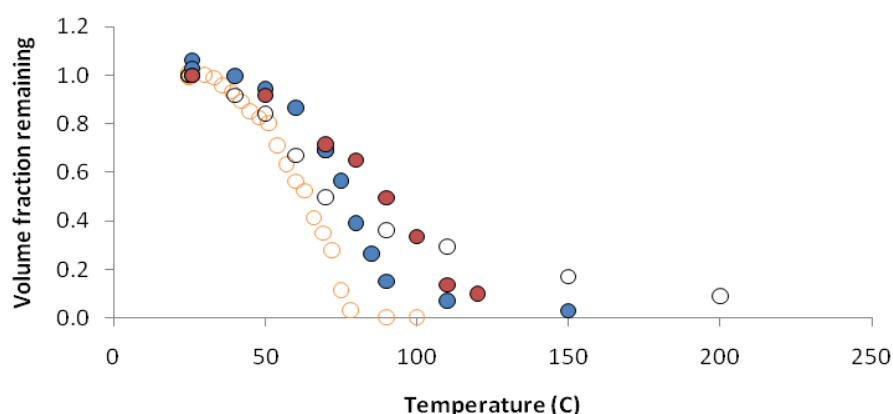
Figure 5.23. Volume fraction remaining versus evaporative temperature for three experiments on monomethylamine. One low NO$_x$-experiment on March 22, 2010 (open circles), two high NO$_x$-experiments on July 22, 2010 (red circles) and on July 13, 2010 (blue circles). The thermograms were made 1 hour after the chamber was opened. Shown is also an experiment on pure monomethylamine nitrate particles produced from a nebulizer (open yellow circles, see also section 5.3, page 41).

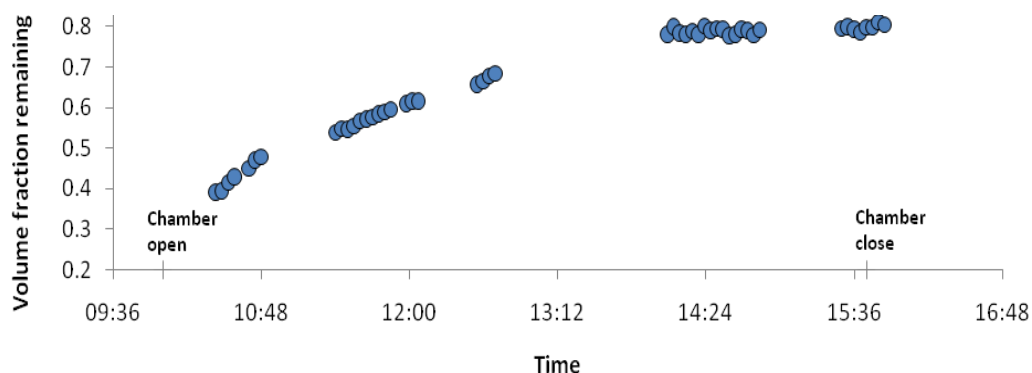All experiments on MMA showed a typical aging of the aerosol (see example in Figure 5.24).

Figure 5.24. Volume fraction remaining at 70 $^{\circ}$C versus time during a low NO$_x$ - monomethylamine experiment on March 22, 2010.

Immediately after monomethylamine was added to the chamber already containing NO$_x$ and H$_2$O$_2$ nucleation was initiated producing a very volatile aerosol probably consisting of significant fraction of methyl aminium nitrate (see Figure 5.25). After opening the chamber oxidation was initiated and gradually replacing the volatile salt with less volatile material. The decrease in volatility was most rapid initially followed by a less step change until it stabilizes. This feature was seen in most experiments except for the N-methylmethanimine experiments where instead the volatility increased after opening the chamber (see section 5.15, page 107).
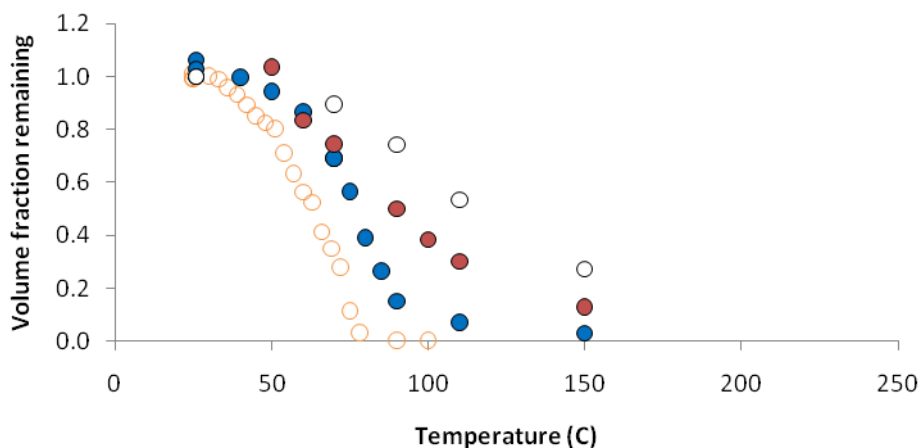

Figure 5.25. Volume fraction remaining versus evaporative temperature for the monomethylamine high NO$_x$-experiment on July 13, 2010, measured at 1 (blue circles), 3.3 (red circles) and 4 (open circles) hours after the chamber was opened, respectively. Shown is also an experiment on pure monomethylamine nitrate particles produced from a nebulizer (open yellow circles, see section 5.3).

Figure 5.26 depicts the results for thermogram 1 (12:57 – 13:22 UTC) obtained with the AMS set up during the experiment on March 22, 2010. Two thermograms have been measured during this experiment during 12:57 – 13:22

UTC and 16:16 – 16:34 UTC. The volatility of the aerosol decreasesd with time. Indeed for thermogram 1 79 % of the initial aerosol mass is evaporated at 110°C whereas for thermogram 2 only 43 %. In both AMS thermograms indicate the nitrate fraction is negligible at 110°C indicating the high volatility of the primary and secondary formed nitrate salts.
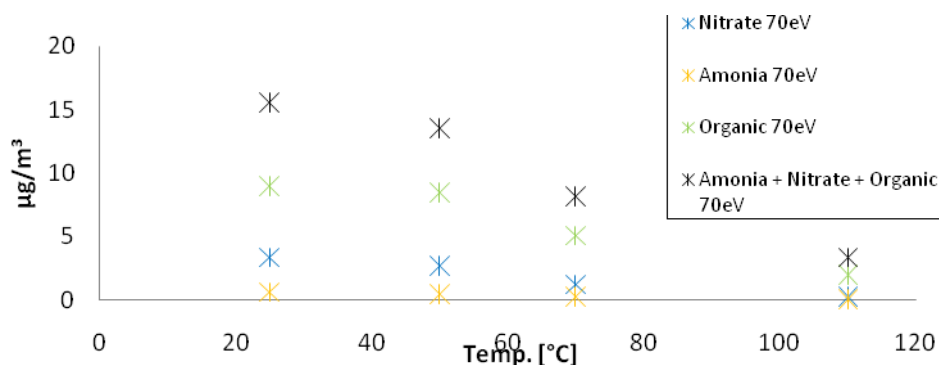

Figure 5.26. Thermogram 1 containing 4 temperature steps measured during 12:57 - 13:22 UTC.

It is concluded from modelling of the observed aerosol evolution, is that the formed particles -– assumed in the model to be methylaminium nitrate salt particles - are rather unstable and as the concentration of MMA decreases during the experiment, the particles re-volatilized. The dissociation coefficient K_d of MMANO$_3$ obtained by adjusting the model to measured particle mass concentrations of nitrate and measured particle number distributions was 3×10^{-8} Pa^2 (at the average temperature of the experiment, 297.6 K). This model-derived value is in very good agreement with the K_d value of 4.54×10^{-8} Pa^2 (at 298 K; for the pure salt) given in a recent review by Ge *et al*.[134] The high volatility of the formed nitrate particles was also confirmed in the AMS thermograms.

The low NOx experiment on March 22, 2010, showed similar amounts of initially formed "pure" MMANO$_3$ salt and one or more secondary produced nitrate salt(s). During this experiment, the aerosol production was significantly slower than in the high NO$_x$ experiments with MMA on July 13 and 22, 2010. Half an hour after the chamber was opened, a significant contribution from the non-MMA nitrate salt(s) was observed in the produced aerosol. In the high NOx / high H$_2$O$_2$ experiment (July 13, 2010) mainly the "pure" MMANO$_3$ was formed initially, whereas in the high NO$_x$ experiment (July 22, 2010) a very slow increase of the "pure" MMANO$_3$ salt was observed initially. Both MMANO$_3$ and non MMANO$_3$ salts were found to have high volatility.

A total nitrate (salt) contribution between 35 % and 40 % of the organic mass fraction was estimated in the MMA experiment on March 22, 2010. Secondary organic aerosol (SOA) was formed from MMA in significant amounts and was the dominating fraction of the formed aerosol in this low NO$_x$ experiment. MAFOR predicted a mass-based yield of ~8% SOA to be formed in the oxidation of MMA under low NO$_x$-conditions. The total aerosol yield in the photo-oxidation of MMA was estimated to be 9%.

5.11 (CH₃)₂NH photo-oxidation studies

Four DMA photo-oxidation studies, carried out in 2010, have been selected for more detailed analysis:

Date	Experimental conditions	Monitor data
2010/03/09	High-NOx experiment. Starting conditions: ~100 ppbV NO_2 and 20 ppbV NO.	Annex 9
2010/03/11	Low-NOx experiment. NOx constant ~10 ppbV.	Annex 10
2010/07/14	Low-NOx experiment. Constant NOx ~10 ppbV.	Annex 19
2010/07/15	High-NOx experiment. Starting conditions: ~200 ppbV NO_2, 50 ppbV NO. Constant NOx ~250 ppbV.	Annex 20

The 2010/03/09 experiment was carried out under high to medium level NOx conditions. The NOx-level was initially around 60 ppbV NO_2 and 10 ppbV NO before opening the chamber canopy when it instantaneously changed to around 30 and 40 ppbV. From then on, the mixing ratios decreased monotonously to around 25 and 5 ppbV, respectively, at the end of the experiment.

The 2010/03/11 experiment was carried out under low-NOx conditions. Sufficient OH radical production was accomplished in the early phase of the experiment by adding around 300 ppbV H_2O_2 to the chamber ($H_2O_2 + h\nu \rightarrow 2$ OH).

The 2010/07/14 experiment was carried out under low-NOx conditions. Around 3.5 ppmV of H_2O_2 was added to increase the OH concentration in the experiment. This resulted in interfering reactions in the PTR drift-tube making quantification of absolute yields difficult.

The 2010/07/15 experiment was carried out under high-NOx conditions. A small amount of H_2O_2 was added to increase the OH concentration in the experiment. This resulted in minor interfering reactions in the PTR drift tube.

The simplified theoretical photo-oxidation mechanism of dimethylamine (Scheme 2.2, Page 22) is shown again below suggesting the major photo-oxidation products to be *N*-methyl formamide (CH_3NHCHO), *N*-methyl methanimine ($CH_3N=CH_2$) and *N*-nitro dimethylamine (($CH_3)_2NNO_2$).

The expected compounds are indeed observed as the major products in the experiments. *N*-nitroso dimethylamine is only a very minor product in the experiments except under high-NOx conditions. Figure 5.27 shows the time evolution of the major ion signals during the photo-oxidation of dimethylamine. In addition the figure includes the *N*-nitroso dimethylamine signal. It can be seen from Figure 5.27 that the *N*-methyl methanimine signal continues to increase after the signals of *N*-methyl formamide and *N*-nitro dimethylamine have started to level off. This indicates that *N*-methyl methanimine is both a primary and a secondary product in the photo-oxidation of dimethylamine.
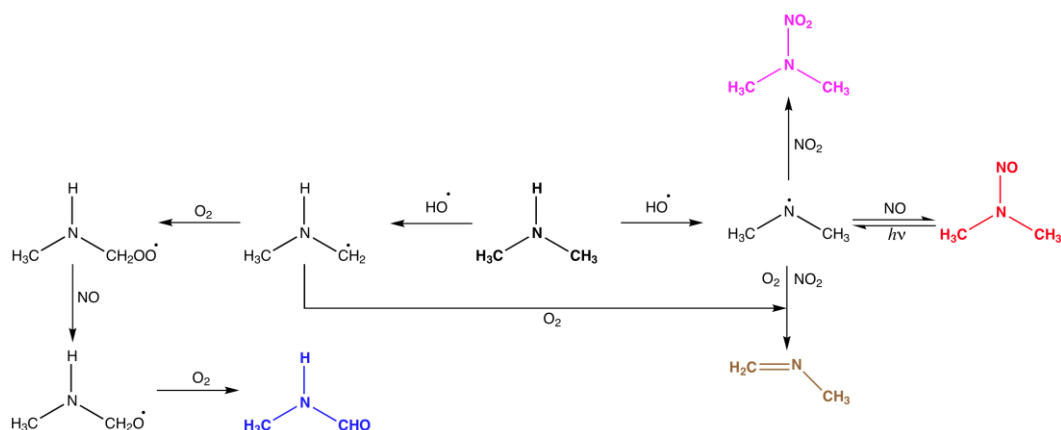
Scheme 2.2. Main routes of the atmospheric dimethylamine photo-oxidation.

The amount of *N*-methyl formamide formed in the atmospheric photo-oxidation of dimethylamine depends not only on the initial C-H:N-H branching in the OH reaction, but also on the followeing branching in the O_2 reactions of the CH_3NHCH_2 alkyl radical:

$\Delta H^\ominus$ = -143 $\qquad$ $CH_3NHCH_2 + O_2$ $\qquad \rightarrow \qquad$ $CH_3NHCH_2O_2$ $\qquad$ (27a)

$\Delta H^\ominus$ = -64 $\qquad\qquad\qquad\qquad\qquad \rightarrow \qquad$ $CH_3N=CH_2 + HO_2$ $\qquad$ (27b)

The reaction enthalpies listed ($\Delta H^\ominus$ /kJ mol^{-1}) refer to 298 K and to the lowest energy conformations of the species involved and stems from G3 calculations.[122]

Significant amounts of NH_3 (ammonia), CH_2O (formaldehyde) and HCOOH (formic acid) are observed in addition to the major expected products. Minor amounts of NH_2CHO (formamide) and $(CH_3)_2NCHO$ (*N,N*-dimethyl formamide) are also observed in amounts exceeding normal chamber artifacts. Table 5.11 summarises the ion signals changing during the photo-oxidation of dimethyl-amine and the interpretation.
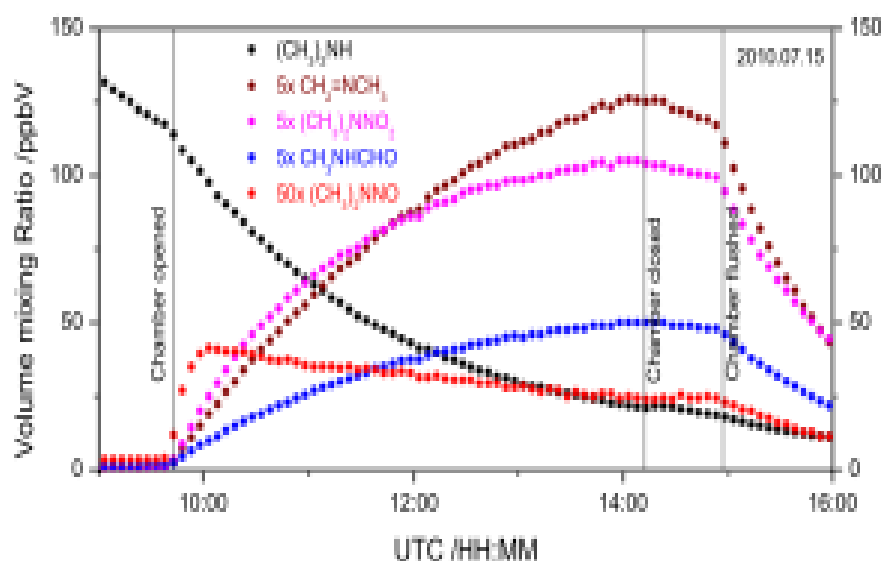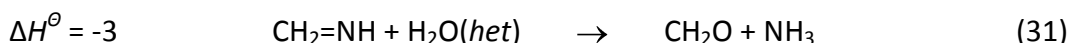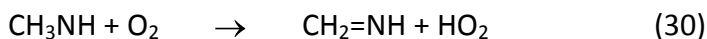

Figure 5.27. Time evolution of the major ion signals during photo-oxidation of dimethylamine under high-NOx conditions. The ion signal of *N*-nitroso dimethyl-amine (minor product) is included.

The formation of formaldehyde and ammonia is explained by the unimolecular, thermal dissociation of the CH_3NHCH_2O radical, which is endothermic by only ca. 38 kJ mol^{-1} and therefore expected to compete with the O_2 H-abstraction reaction (28):
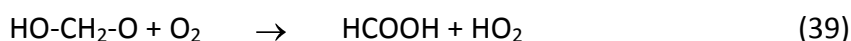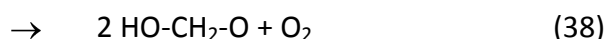
$\Delta H^{\ominus} = 38$ $\qquad$ $CH_3NHCH_2O \xrightarrow{\Delta} CH_3NH + CH_2O$ $\qquad$ (28)

$\qquad$ $CH_3NHCH_2O + O_2 \rightarrow \textbf{\textcolor{blue}{CH_3NHCHO}} + HO_2$ $\qquad$ (29)

$\qquad$ $CH_3NH + O_2 \rightarrow CH_2=NH + HO_2$ $\qquad$ (30)

$\Delta H^{\ominus} = -3$ $\qquad$ $CH_2=NH + H_2O(het) \rightarrow CH_2O + NH_3$ $\qquad$ (31)
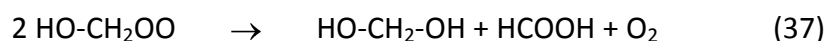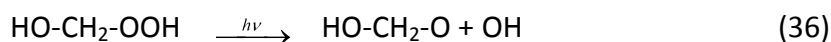
Methanimine may also react heterogeneously with dimethylamine:

$\Delta H^{\ominus} = -13$ $\qquad$ $CH_2=NH + (CH_3)_2NH(het) \rightarrow CH_3N=CH_2 + CH_3NH_2$ $\qquad$ (32)
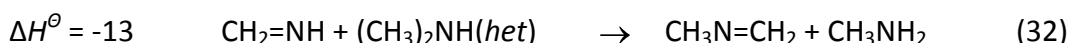
HO_2 radicals are always formed in photo-oxidation reactions, and formic acid is formed in the gas-phase reaction between formaldehyde and HO_2 radicals. The first step is that HO_2 radicals enter a reversible reaction to form a formaldehyde adduct:[135-141]
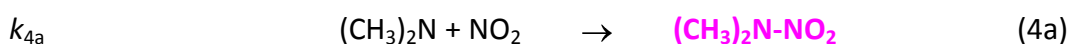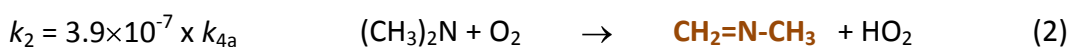
$\qquad$ $CH_2O + HO_2 \leftrightarrow HOO-CH_2O \leftrightarrow HO-CH_2OO$ $\qquad$ (33)

This adduct can react irreversibly in several ways, of which the most important under the conditions in the reactor are:[135,136]

$\qquad$ $HO-CH_2OO + HO_2 \rightarrow HO-CH_2-OOH + O_2$ $\qquad$ (34)

$\qquad$ $\rightarrow HCOOH + H_2O + O_2$ $\qquad$ (35)

$\qquad$ $HO-CH_2-OOH \xrightarrow{h\nu} HO-CH_2-O + OH$ $\qquad$ (36)

$\qquad$ $2 HO-CH_2OO \rightarrow HO-CH_2-OH + HCOOH + O_2$ $\qquad$ (37)

$\qquad$ $\rightarrow 2 HO-CH_2-O + O_2$ $\qquad$ (38)

$\qquad$ $HO-CH_2-O + O_2 \rightarrow HCOOH + HO_2$ $\qquad$ (39)
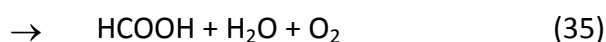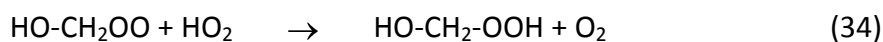
The formation of small amounts $(CH_3)_2NCHO$, *i.e.* a compound with more carbon atoms than the substrate under study itself, can be explained by a heterogeneous condensation reactions between dimethylamine and formic acid:

$\qquad$ $(CH_3)_2NH + HCOOH(het) \rightarrow (CH_3)_2NCHO + H_2O$ $\qquad$ (40)
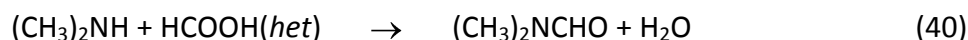
Again, the heterogeneous reactions makes it difficult to model the gas phase reactions of $CH_2=NH$ and $CH_2=NCH_3$ in detail. The chemistry of methylmethanimine and methanimine is unresolved and only three products can be considered reliable markers of the experiments: $(CH_3)_2NNO$, $(CH_3)_2NNO_2$ and CH_3NHCHO. The reactions relevant to nitrosamine and nitramine formation are:

$0.37 \times k_1$ $\qquad$ $(CH_3)_2NH + OH \rightarrow (CH_3)_2N + H_2O$ $\qquad$ (1a)

$0.63 \times k_1$ $\qquad$ $\rightarrow (CH_3)N(H)CH_2 + H_2O$ $\qquad$ (1b)

$k_2 = 3.9\times10^{-7} \times k_{4a}$ $\qquad$ $(CH_3)_2N + O_2 \rightarrow \textbf{\textcolor{brown}{CH_2=N-CH_3}} + HO_2$ $\qquad$ (2)

$k_3 = 0.26 \times k_{4a}$ $\qquad$ $(CH_3)_2N + NO \rightarrow \textbf{\textcolor{red}{(CH_3)_2N-NO}}$ $\qquad$ (3)

k_{4a} $\qquad$ $(CH_3)_2N + NO_2 \rightarrow \textbf{\textcolor{magenta}{(CH_3)_2N-NO_2}}$ $\qquad$ (4a)

$K_{4b}= 0.22 \times k_{4a}$ $\rightarrow$ $CH_2=N\text{-}CH_3$ + HONO (4b)

j_{NDMA} $(CH_3)_2N\text{-}NO$ $\xrightarrow{h\nu}$ $(CH_3)_2N$ + NO (5)

The updated reaction scheme for DMA gas phase photo-oxidation is presented in Scheme 5.2. In modelling the gas phase reactions we have taken the initial C-H : N-H branching ratio to be 0.37 : 0.63, and assumed the branching ratios of the subsequent reactions of the dimethylamino radical with O_2, NO and NO_2 to be as reported by Lindley et al.,[33] and the photolysis rate constant, $j_{NDMA} = 0.53 \times j_{NO2}$, reported by Tuazon et al.[37] This gas phase chemistry model, based on literature values, results in a relatively large discrepancy with the experiment, Figure 5.28.
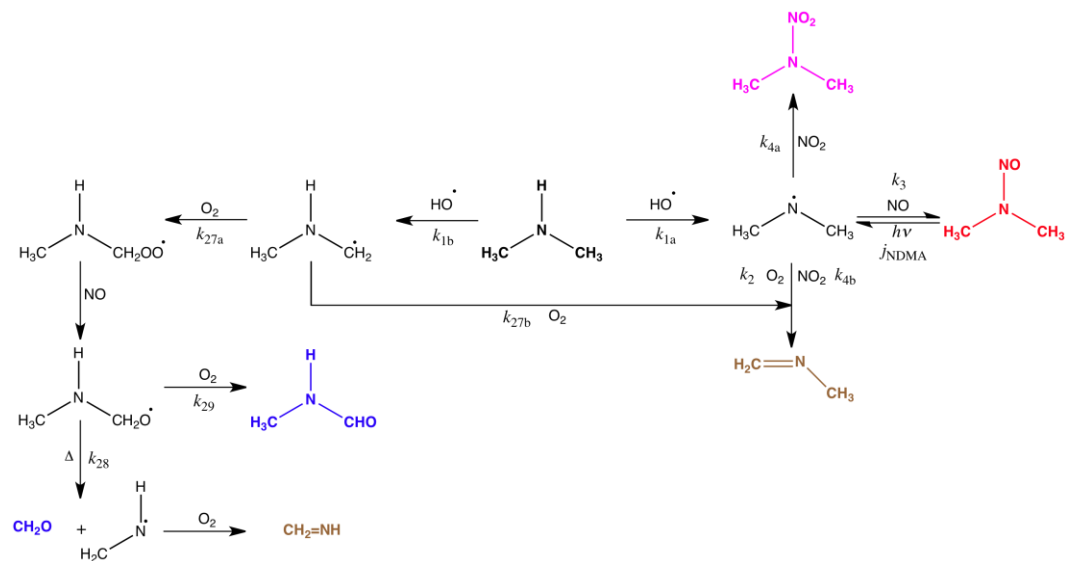
Scheme 5.2. Updated scheme with rate constants for the atmospheric photo-oxidation of dimethylamine.

To reproduce the observed time profiles of $(CH_3)_2NNO_2$ requires first of all a slightly higher branching towards the initial N-H abstraction by OH: the value of N-H:C-H of 0.37:0.63 reported by Lindley et al.[33] had to be slightly adjusted to 0.42:0.58. Second, k_2 in the branching of the dimethylamino radical has to be slightly lower. The best fit to the observed data is obtained employing a value of
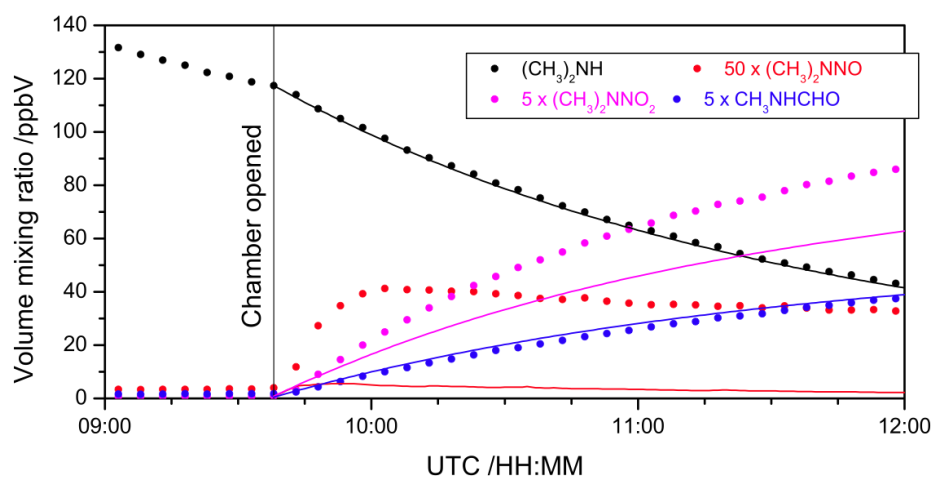

Figure 5.28. Observations (●) and literature model results (—) of time evolution of dimethylamine and primary product ion signals during photo-oxidation of dimethylamine under high-NOx conditions.

3.0×10^{-7}. To fit the time profile of $(CH_3)_2NNO$ requires a significantly larger k_3 and/or a lower photolysis rate constant j_{NDMA}. A best fit to the dimethylamine photolysis experiments and to the *N*-nitroso dimethylamine photolysis experiments, see section 5.13 (page 98), is obtained for $k_3 = 0.75 \times k_{4a}$ and $j_{NDMA} = 0.25 \times j_{NO2}$. The estimated error in the ratios given is $\pm 15\%$.

Figure 5.29 compares the observations and model results for the 2010/07/15 high-NOx experiment while Figure 5.30 compares the observations and model results for the 2010/03/11 low-NOx experiment.
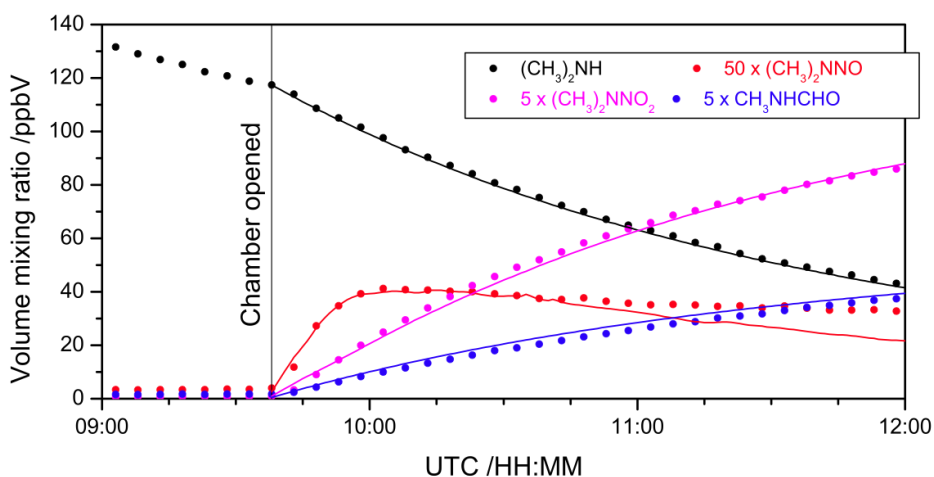

Figure 5.29. Observations (●) and literature model results (—) of time evolution of dimethylamine and primary product ion signals during photo-oxidation of dimethylamine under high-NOx conditions.

Finally, the concentration time profiles of formaldehyde and *N*-methyl formamide are determined by the branching of the CH_3NHCH_2 radical reaction with O_2, and the branching of the CH_3NHCH_2O radical dissociation *vs*. reaction with O_2. Ratios of of $k_{28}/k_{29} = 0.5$ and $k_{27a}/k_{27} = 0.45$ give the best agreement with observations, Figures 5.29 and 5.20.
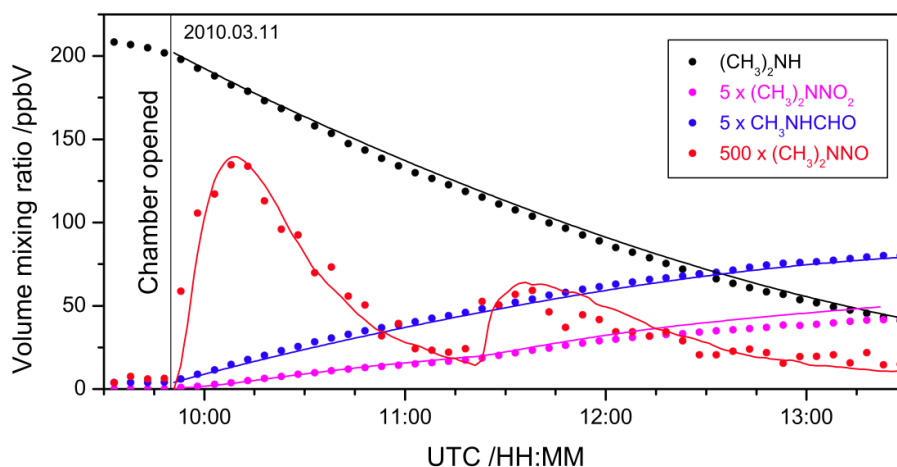

Figure 5.30. Observations (●) and literature model results (—) of time evolution of dimethylamine and primary product ion signals during photo-oxidation of dimethylamine under high-NOx conditions.

Table 5.11. Ions observed by PTR-TOF-MS during dimethylamine photo-oxidation experiments. Mass peaks of intensity < 1 % of $\Delta I_{46.0656}$ and ^{13}C isotope signals are omitted.

m/z	Ion formula	2010.03.09	2010.03.11	2010.07.15	Confirm.	Potential neutral precursor
18.0340	NH_4^+			6.2	FTIR	Ammonia
31.0184	CH_3O^+	2.5		9.5	FTIR, DNPH	Formaldehyde
33.0337	CH_5O^+					Methanol
43.0181	$C_2H_3O^+$	CA[a]	CA	CA		Acetic acid (acetyl ion fragment)
44.0135	CH_2NO^+					Isocyanic acid
44.0501	$C_2H_6N^+$	19.9		20.4		*N*-methylmethanimine
45.0338	$C_2H_5O^+$	CA	CA	CA	DNPH	Acetaldehyde
46.0294	CH_4NO^+	6.3		5.1		Formamide, Nitrosomethane
46.0656	$C_2H_8N^+$					Dimethylamine
47.0131	$CH_3O_2^+$	5.1		10.0		Formic acid
58.0292	$C_2H_4NO^+$					*N*-methylideneformamide
59.0494	$C_2H_7O^+$	CA	CA	CA	DNPH	Acetone
60.045	$C_2H_6NO^+$	7.3		9.5	SPME	*N*-methylformamide
61.0288	$C_2H_5O_2^+$	CA	CA	CA		Acetic acid
62.0244	$CH_4NO_2^+$			1.7		Nitromethane
74.0243	$C_2H_4O_2N^+$					?
74.0606	$C_3H_8NO^+$			1.1	SPME	*N,N*-dimethyl formamide
75.0556	$C_2H_7N_2O^+$			1.5	ThermoN	*N*-nitroso dimethylamine
91.0504	$C_2H_7N_2O_2^+$	8.0		25.0	ThermoN	*N*-nitro dimethylamine

[a] Abbreviations: CA, chamber artifact;

5.11.1 Analysis of aerosol formation

The aerosol evolution in two dimethylamine (short: DMA) photo-oxidation experiments, under high NO_x conditions on March 09, 2010, and under low NO_x conditions on March 11, 2010, were studied in more detailed, including modelling with the aerosol model MAFOR.

Photo-oxidation experiment with DMA under high NO_x conditions.

A high NO_x experiment (about 120 ppb NO_x) was performed on March 09, 2010. The chamber canopy was opened at 10:11 UTC followed by weak new particle formation which rapidly ceased after less than 15 minutes. After 11:00 UTC continuous formation and growth of ultrafine particles was observed (Figure 5.31). The total aerosol mass concentration increased up to ~20 µg/m^3 during the experiment. The chamber canopy was closed at 16:35 UTC. In summary, no pronounced new particle formation was observed. Instead continuous nucleation seems to occur throughout the experiment at low intensity.
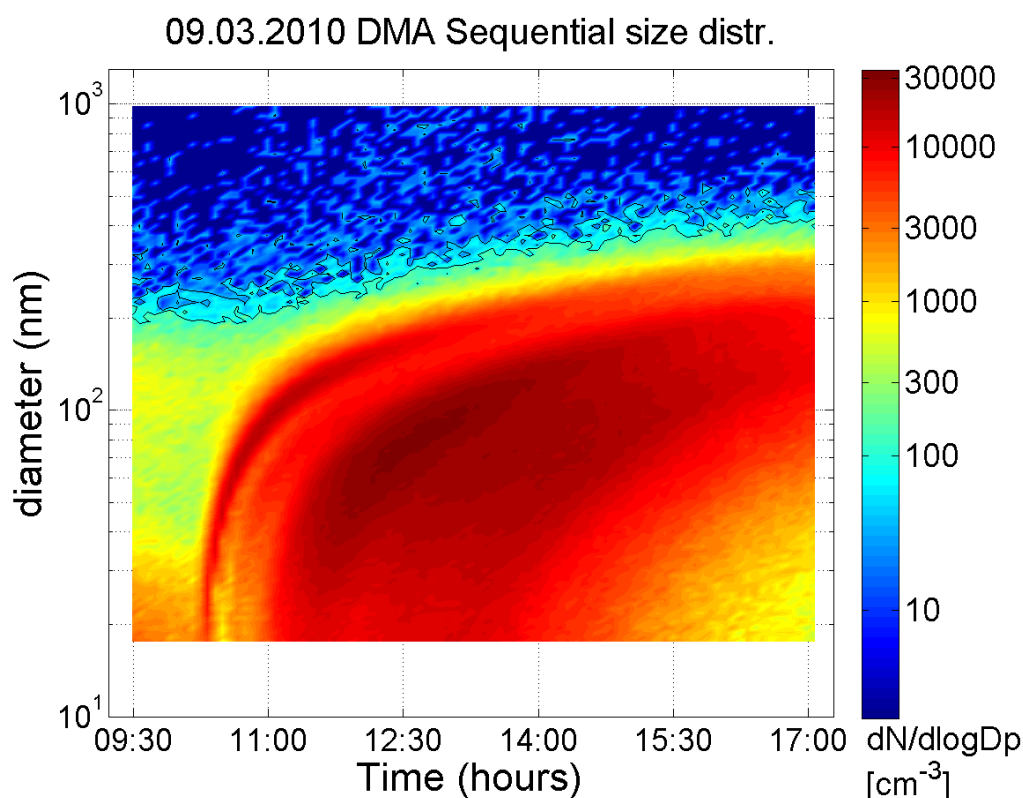

Figure 5.31. Sequential number size distribution (dN/dlogDp in # cm^{-3}) as recorded by SMPS during the experiment on March 09, 2010.

The aerosol model MAFOR can reproduce this feature of continuous nucleation, Figure 5.32. The dissociation coefficient K_d of dimethylamine nitrate (DMANO$_3$) obtained by adjusting the model to measured particle mass concentrations of nitrate and measured particle number distributions was 3×10^{-11} Pa^2 (at the average temperature of the experiment, 290.4 K) and thus lower than the K_d value of 6.27×10^{-8} Pa^2 (at 298 K; for the pure salt) given in a recent review by Ge

et al.[134] The nitrate aerosol in the experiment is thus more stable than would be expected from the thermodynamics properties of the pure nitrate salt. It could be that secondary organics have been mixed into the nitrate salt particles and stabilized the aerosol. Another explanation could be, that other (less volatile) nitrate salts than DMANO$_3$ have been formed in the experiment.
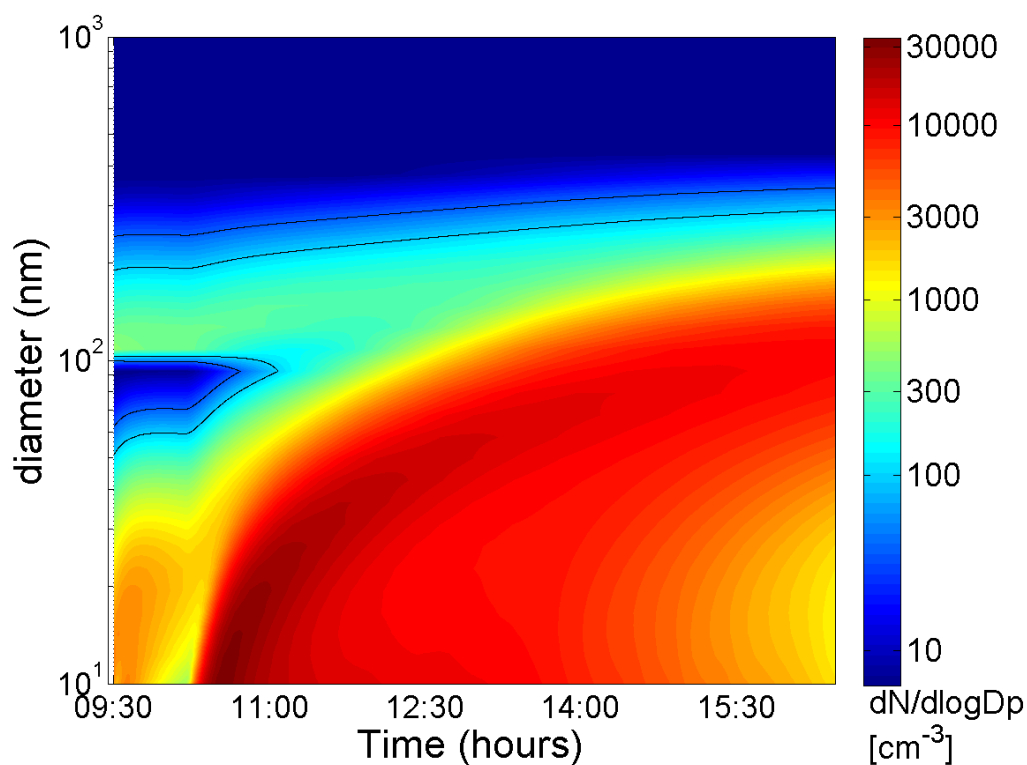

Figure 5.32. Modelled number size distribution (dN/DlogD$_p$ in # cm^{-3}) during the experiment on March 09, 2010, as 2-dimensional plot for the diameter range 10-1000 nm.

Figure 5.33 depicts the evolution of the AMS and the SMPS data during this experiment. During the first part of the experiment instrumental testing (e.g. variation of the vaporizer temperature) has been performed. Therefore only the AMS data between 15:30 and 16:38 show quantitative results.

The AMS mass spectra (Figure 5.34) taken during the experiment on March 9, 2010, are quite similar and the organic fragments are the same but it is not clear why in the pure salt spectra, obtained from nebulisation of an aqueous solution followed by drying, ammonium fragments are detected while in the chamber experiment these fragments are not visible. In addition at both 70 eV and 30 eV at the end of the chamber experiment there is some signal at m/z above 50. This can be associated to formation of molecules at molecular weight larger than the pure salt.
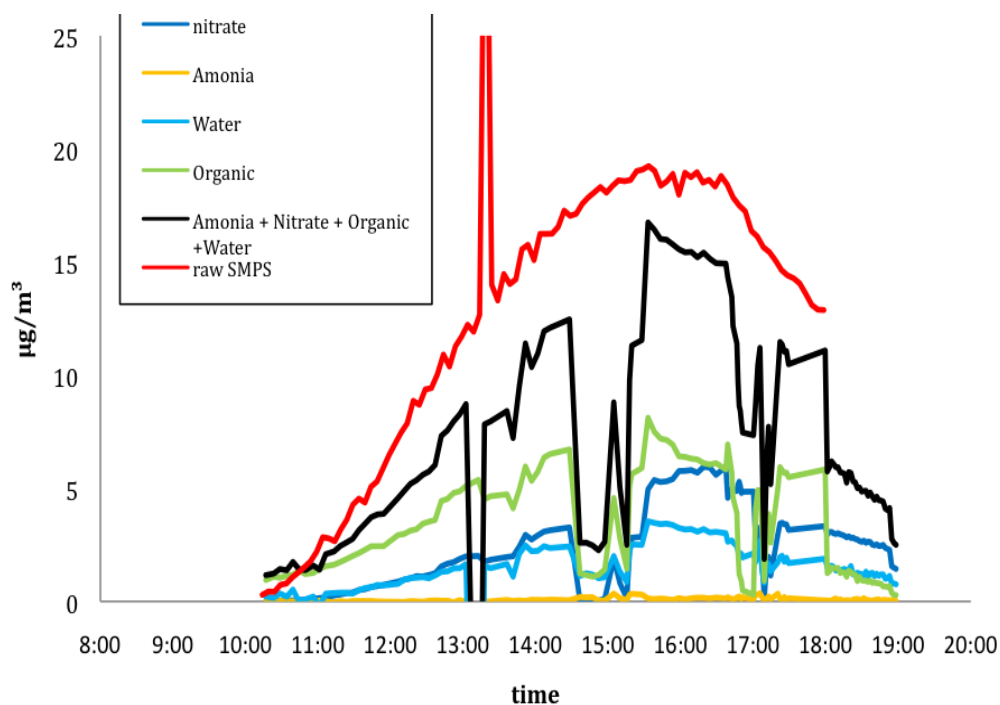
Figure 5.33. Mass loading for Nitrate, Amonia, Organics and Organic-Water for 70 eV and effective SMPS total concentration during the low-NO_x DMA experiment on March 09, 2010.

Modelled particle mass concentrations obtained in a MAFOR simulation of the experiment on March 09, 2010, of organics (including DMA) and nitrate ($DMANO_3$) are in excellent agreement with measured particle mass concentrations obtained by AMS (Figure 5.34). The mass-based yield of SOA in this experiment was 9%. According to the model, only 1.4% of the initial DMA amount were converted into particulate matter., while 49% of the initial DMA amount was lost to the chamber walls.

By using pure reference spectra of $DMANO_3$, the fragmentation pattern of $DMANO_3$ for 70 eV electron impact ionization and 600°C vaporizer temperature was determined (experimental settings between 15:30 and 16:38 UTC). Accordingly, the most significant organic fragments of DMA are CH_4N^+, $C_2H_4N^+$, $C_2H_6N^+$ and $C_2H_7N^+$. By inter-comparison of the fragmentation pattern of these four ions with the nitrate time-series, an upper limit for the pure $DMANO_3$ can be calculated. In a further DMA experiment under high NO_x conditions, on July 15, 2010, the nature of the nitrate aerosol produced has been investigated in more detail. By using pure reference spectra of $DMANO_3$, the fragmentation pattern of $DMANO_3$ for 30 eV electron impact ionization and 600°C vaporizer temperature was determined. Accordingly, the most significant organic fragments of DMA were CH_4N^+, $C_2H_4N^+$, $C_2H_6N^+$ and $C_2H_7N^+$. By inter-comparison of the fragmentation pattern of these four ions with the nitrate time-series, an upper limit for the pure $DMANO_3$ can be calculated. Figure 5.35 depicts the evolution of total nitrate, pure $DMANO_3$ nitrate and non $DMANO_3$ nitrate in the experiments on March 09, 2010 (top panel) and July 15, 2010 (bottom panel). On July 15,

2010, the DMANO$_3$ nitrate was present with a maximum of 3.5 µg/m³, about 60% of the total nitrate signal (bottom panel).
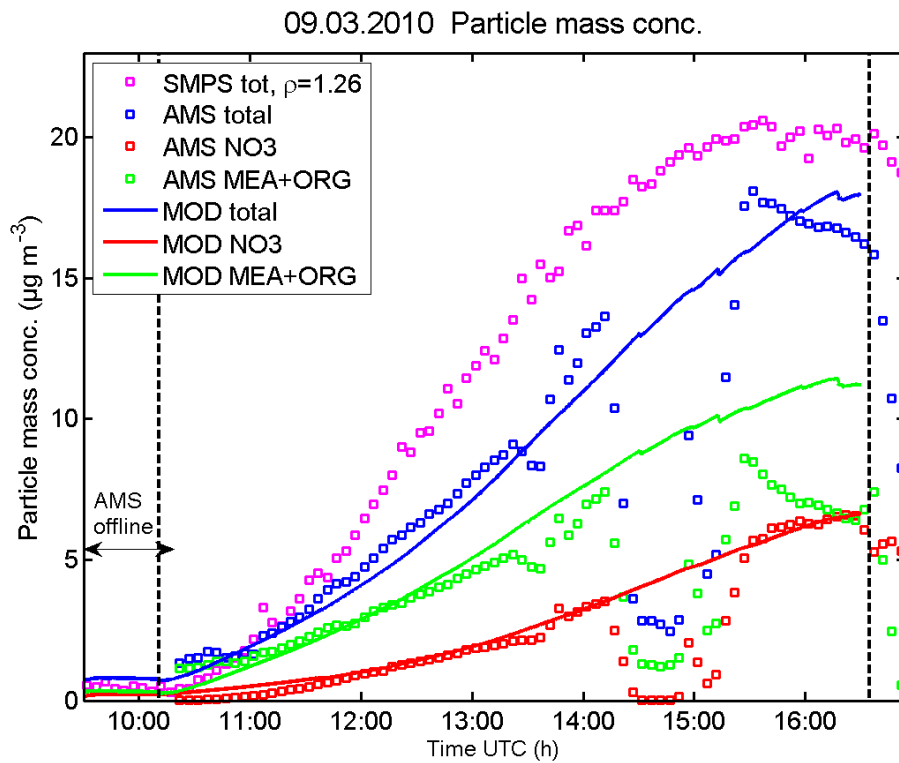

Figure 5.34. Comparison of modelled particle mass concentration (in µg m^{-3}) of aerosol components with measured mass concentrations by AMS (red, green an blue squares), and by SMPS (magenta squares) for the DMA experiment on March 09, 2010. Increase of modelled particle mass concentration of total organics including DMA (green line) and modelled mass concentration of total nitrate (red line) are in excellent agreement with the mass concentrations measured by AMS.
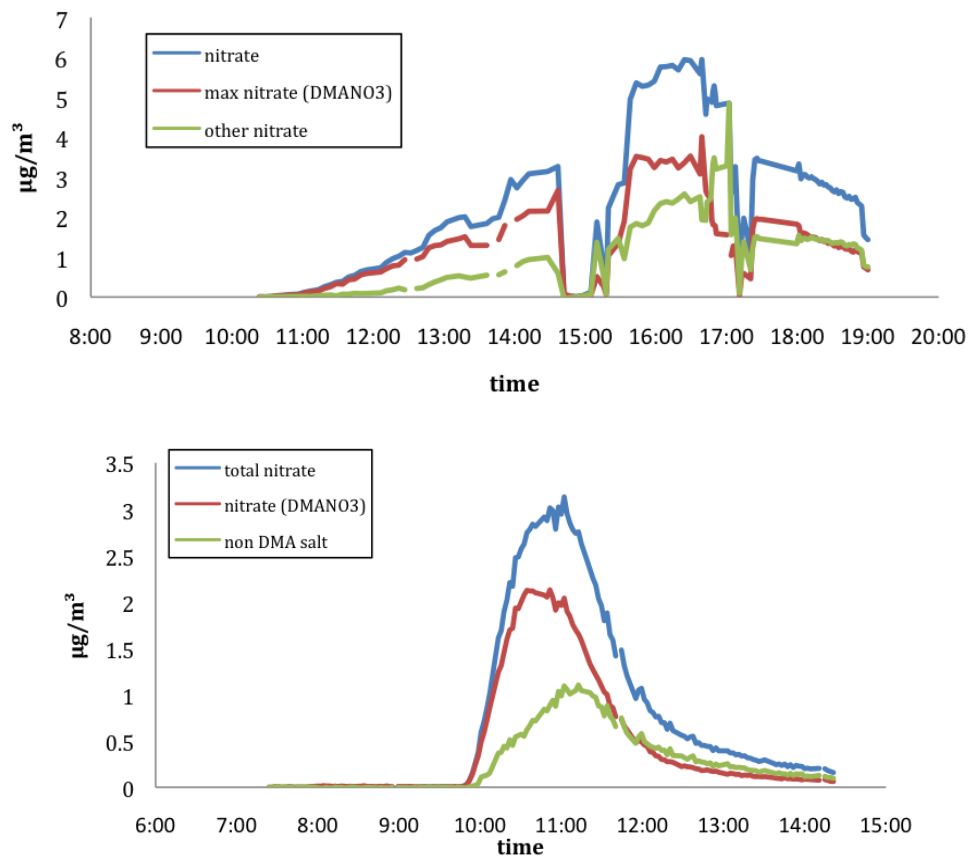
Figure 5.35. Time series of total Nitrate, maximum nitrate from pure the DMANO$_3$ salt and the non DMANO$_3$ nitrate during the high-NO$_x$ DMA experiments. Top panel: March 09, 2010 (70 eV data), bottom panel: July 15, 2010 (30 eV data).
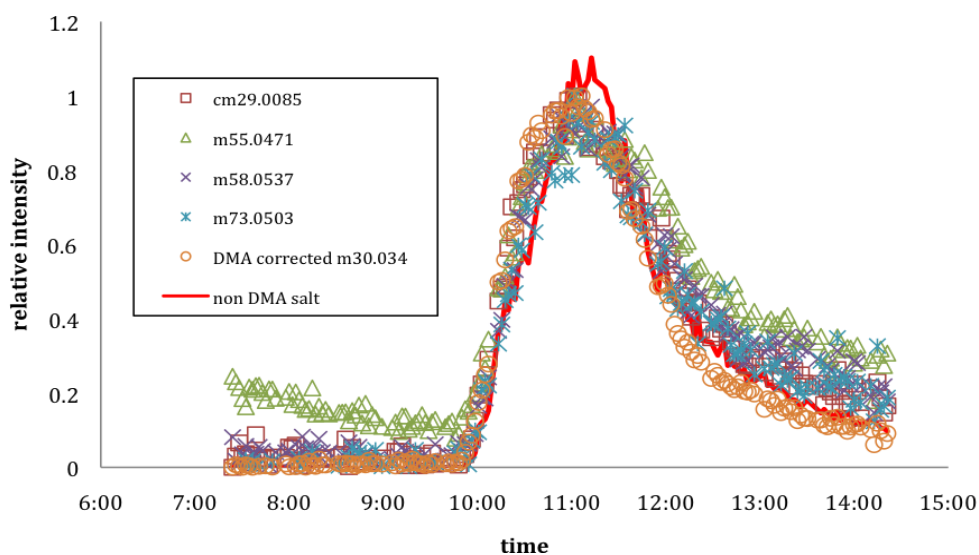

Figure 5.36. Time series of the non DMANO$_3$ nitrate during the high-NOx MDA experiment on July 15, 2010, compared with the best correlating ions m/z 29.01, m/z 55.05, m/z 58.06, m/z 73.05 and m/z 30.03 (DMA interference corrected), HCO$^+$, C$_3$H$_5$N$^+$, C$_3$H$_8$N$^+$, C$_3$H$_8$NO$^+$ and CH$_4$N$^+$, respectively.

Similar to the other high NO_x experiments, the nitrate signal in the experiment on July 15, 2010, was initially dominated by the pure $DMANO_3$ salt. Secondary non-$DMANO_3$ nitrates are slowly increasing reaching a stable relative contribution to the nitrate signal of about 60 % at 12:30 UTC, shortly after the chamber was closed. Figure 5.36 depicts all m/z ratios with a good correlation to the secondary nitrate salt, m/z 29.008 (HCO), m/z 55.047 (C_3H_5N), m/z 58.054 (C_3H_8N), m/z 73.05 (C_3H_7NO) and m/z 30.034 (CH_4N; corrected from the expected DMA interference).

Photo-oxidation experiment with DMA under low NO_x conditions.

In the photo-oxidation experiment with DMA under low NO_x conditions on March 11, 2010, a mixture of about 250 ppbV DMA and H_2O_2 / NO_2 was exposed to sunlight. The chamber canopy was opened at 09:50 UTC followed by a weak new particle formation which rapidly ceased after less than 15 minutes. It was followed by a stronger particle burst at about 10:30 UTC with peak number concentrations at about 11:30 UTC (Figure 5.37). In this experiment a broad but clear banana-type growth curve was obtained. The total aerosol mass concentration increased up to 25 µg/m^3 during the experiment. The chamber canopy was closed at 16:14 UTC.
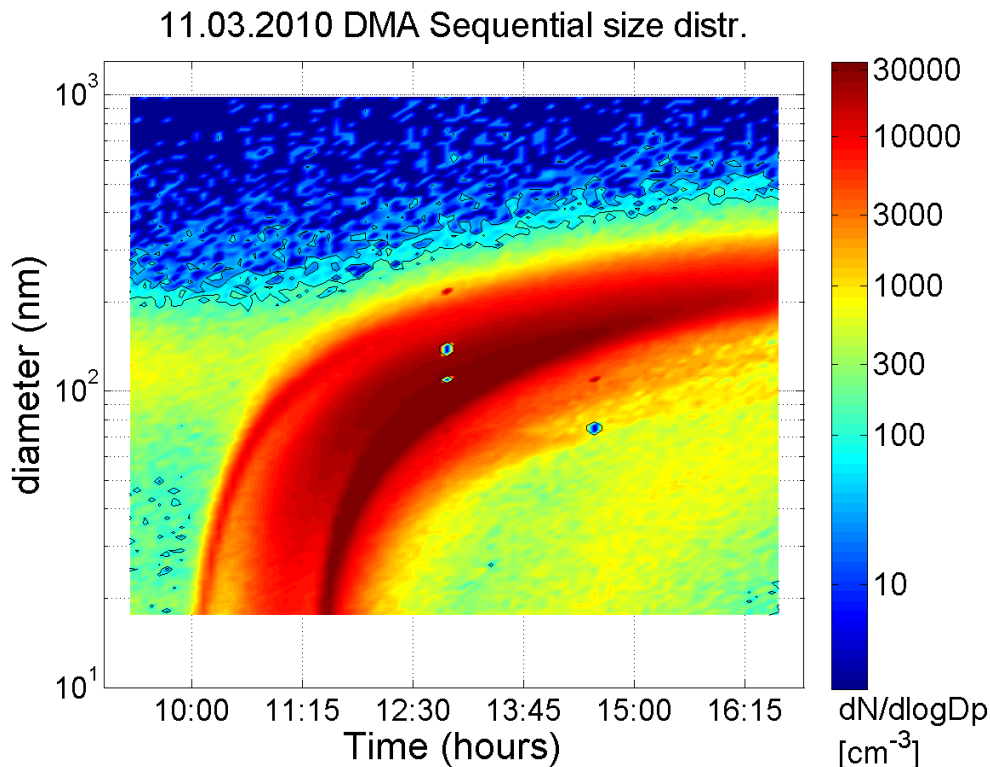

Figure 5.37. Sequential number size distribution (dN/dlogD$_p$ in # cm^{-3}) as recorded by SMPS during the experiment on March 11, 2010.

The much stronger particle formation in this DMA experiment - associated with higher number concentrations and a larger growth rate - compared the "high

NO$_x$" experiment is tentatively explained by the formation of secondary organic aerosol (SOA) compounds that are less volatile than the particulate aminium nitrate salts forming under "high NO$_x$" conditions.

The aerosol model MAFOR reproduced the nucleation event in the experiment on March 11, 2010. The nitrate aerosol is found to be more volatile than in the high-NO$_x$ experiment on March 09, 2010. The dissociation coefficient K_d of dimethylamine nitrate (DMANO$_3$) obtained by adjusting the model to measured particle mass concentrations of nitrate and measured particle number distributions was 8×10^{-10} Pa^2 (at the average temperature of the experiment, 289.9 K). The nitrate aerosol in the experiment is thus more stable than would be expected from the thermodynamics properties of the pure nitrate salt. It could be that secondary organics have been mixed into the nitrate salt particles and stabilized the aerosol. Another explanation could be, that other (less volatile) nitrate salts than DMANO$_3$ have been formed in the experiment.
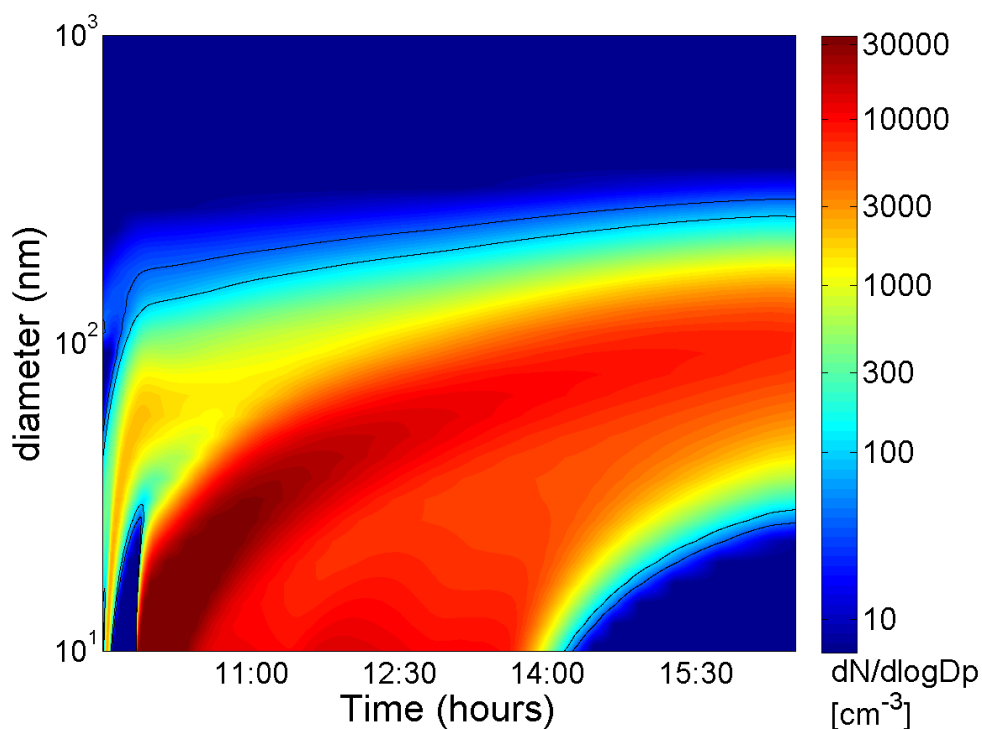

Figure 5.38. Modelled number size distribution (dN/DlogD$_p$ in # cm^{-3}) during the low NO$_x$ experiment on March 11, 2010, as 2-dimensional plot for the diameter range 10-1000 nm.

A maximum aerosol mass loading of about 27 µg/m³ has been detected around 15:30 UTC, about 5h 40min after the chamber was initially opened. At this time 09:09 about 77% of the total loading is formed by organics, about 23% as nitrate, 20.4 µg/m³ and 6.6 µg/m³ respectively. By using pure reference spectra of DMANO$_3$, the fragmentation pattern of DMANO$_3$ for 70 eV electron impact ionization and 600°C vaporizer temperature was determined.
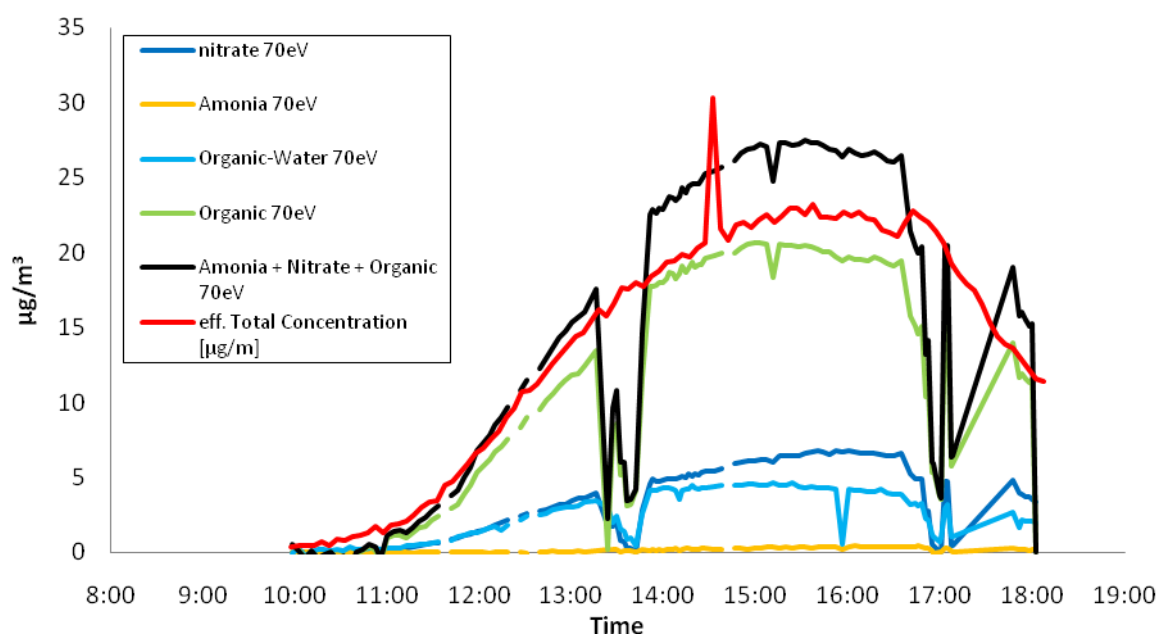
Figure 5.39. Mass loading for Nitrate, Amonia, Organics and Organic-Water for 70 eV and effective SMPS total concentration during the DMA 2010/03/11 experiment.

Modelled nitrate mass concentrations obtained in a MAFOR simulation of the experiment on March 11, 2010 underestimate the nitrate mass concentrations measured by AMS (Figure 5.40). Modelled organic mass concentrations (including DMA) start to increase about 1-2 hours before the measured nitrate mass concentrations increase. Underestimation of measured nitrate indicates that other nitrate salts than $DMANO_3$ (i.e. non $DMANO_3$) are involved in the particle formation during the experiment on March 11, 2010. This was confirmed in a detailed analysis of the nitrate signals recorded by the AMS set up as will be described below.
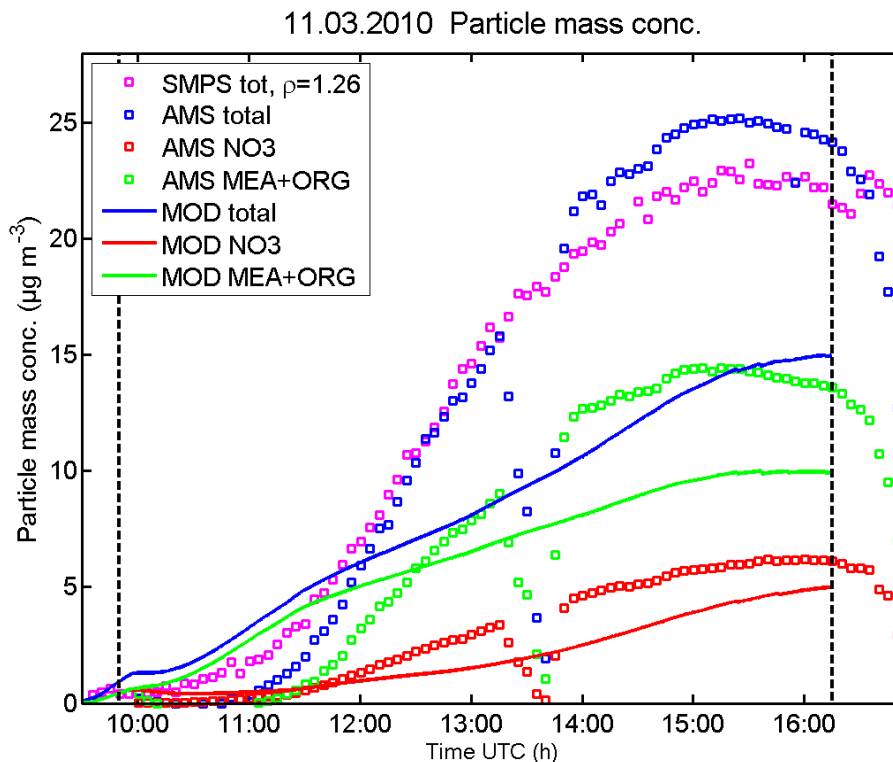
11.03.2010 Particle mass conc.

Figure 5.40. Comparison of modelled particle mass concentration (in µg m^{-3}) of aerosol components with measured mass concentrations by AMS (red, green an blue squares), and by SMPS (magenta squares) for the DMA experiment on March 11, 2010. Increase of modelled particle mass concentration of total organics including DMA (green line) starts earlier than AMS measured organics (green squares). Modelled nitrate mass concentrations (red line) underestimate AMS measured nitrate (red squares).

The most significant organic fragments of DMA on March 11, 2010, were CH_4N^+, $C_2H_4N^+$, $C_2H_6N^+$ and $C_2H_7N^+$. By inter-comparison of the fragmentation pattern of these four ions with the nitrate time-series, an upper limit for the pure $DMANO_3$ can be calculated. Figure 5.41 depicts the evolution of total nitrate, pure $DMANO_3$ nitrate and non $DMANO_3$ nitrate.
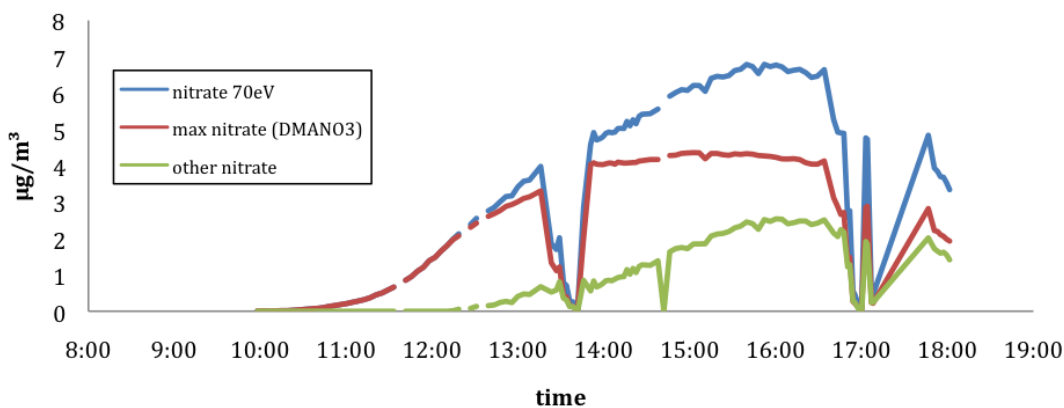

Figure 5.41. Time series of total Nitrate, maximum nitrate from pure the $DMANO_3$ salt and the non $DMANO_3$ nitrate during low-NO$_x$ DMA experiment on March 11, 2010 (70 eV data).

The pure DMANO$_3$ salt is dominating the initial phase of the experiment with about 100% contribution to the total nitrate. Later on (12:30 UTC) during photo-oxidation other salts become more important and the primary DMANO$_3$ salt contribution (i.e. DMANO$_3$) to the total nitrate slowly decreases to 50% at the end of the experiment. One ion with a similar time series as the non DMANO$_3$ nitrate could be identified: C$_3$H$_8$N$^+$.

A detailed analysis of the thermogram 2 indicates a high volatility of the ion (Figure 5.42).Due to the time-series and the volatility information it is very likely that C$_3$H$_8$N$^+$ is a fragment or the parent ion of the organic part of a secondary salt. By taking the organic part of the DMANO$_3$ salt into account and the additional assumption, that the organic part of the non DMANO$_3$ nitrate salt has an average m/z ratio of 58 (C$_3$H$_8$N$^+$, highest identified non DMANO$_3$ salt contributing ion), a total salt contribution of about 25 % of the organic mass fraction can be estimated at 15:30 UTC.
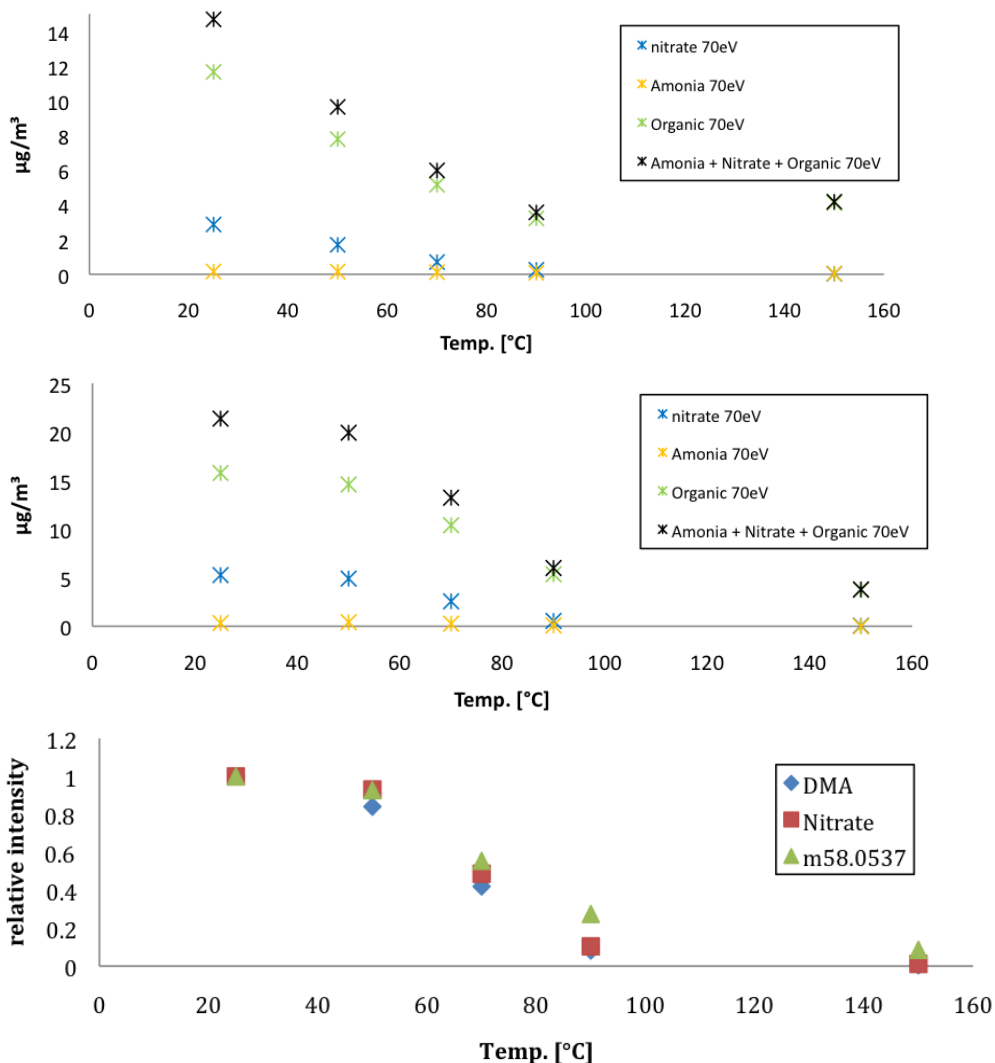

Figure 5.42. 5 temperature step thermograms between 25 and 150°C during the low-NO$_x$ DMA experiment on March 11, 2010 between 13:16 - 13:50 UTC (upper panel) and 16:41 - 17:07 UTC (middle and bottom panel). Bottom panel: relative comparison of the of the volatility of DMA, Nitrate and m/z 58 (identified as C$_3$H$_8$N$^+$).

The remaining fraction of the produced aerosol has to be attributed to SOA. Similar observations were made in other DMA photo-oxidation experiments under low NO_x conditions. For example, in the experiment on July 14, 2010, at around 14:30 UTC (two hours after opening the canopy) secondary organics contributed about 80% to the total loading, whereas nitrates contributed only about 15% to the total loading.

Figure 5.42 depicts the results for thermogram 1 and 2 on March 11, 2010, measured during 13:16 - 13:50 UTC and 16:41 - 17:07 UTC, respectively. The volatility of the aerosol decreases with time. In both thermograms the nitrate fraction is negligible at 110°C indicating the high volatility of the primary and secondary formed nitrate salts.

Summary. Intuitively, the secondary aerosol forming in DMA photo-oxidation experiments under low NO_x and under high NO_x conditions should be significantly different in regards to chemical composition and volatility, because the formation of nitrate salts is favoured under high NO_x-conditions and suppressed under low NO_x conditions, while the formation of low volatile secondary organics is favoured under low NO_x conditions and suppressed under high NO_x-conditions. Partly this is reflected when contrasting the high NO_x experiment on March 09, 2010, with the low NO_x experiment on March 11, 2010. The aerosol mass produced in the high NO_x experiment is (slightly) dominated by nitrates (~60% of the total mass) whereas the low NO_x experiment is clearly dominated by secondary organics (~70-80% of the total mass). SOA produced in DMA experiments can be characterized as relatively low volatile.

The aerosol produced in the low NO_x experiment of July 14, 2010 is consistent with theoretically expected low volatility. However, the aerosol produced in the high resp. low NO_x-experiment in March gave an aerosol of the same volatility (Figure 5.43). The reason for this is not clear but it is consistent with other observation on the effect of NO_x that the result of the experiments on March 09, 2010 and July 14, 2010, is indeed valid.
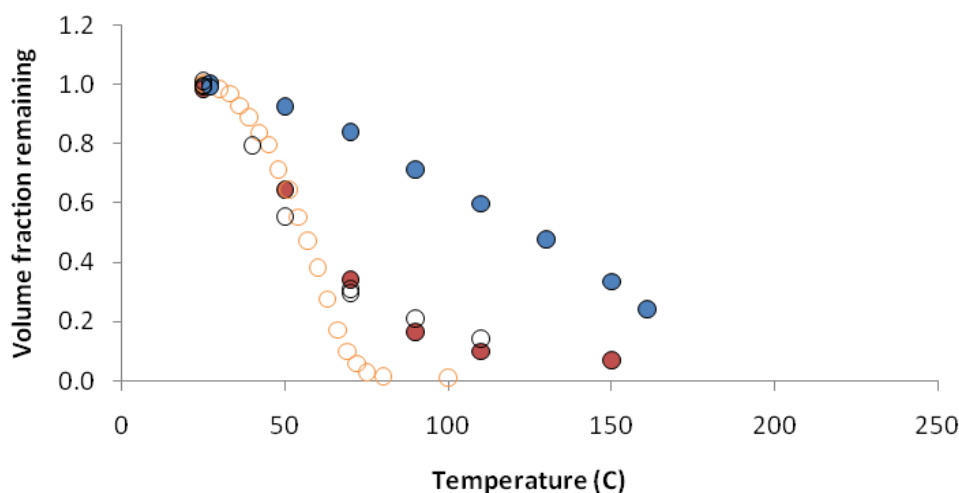
Figure 5.43. Volume fraction remaining versus evaporative temperature for three experiments on dimethylamine. One high NO_x on March 09, 2010 (red circles), two low NO_x experiment on March 11, 2010 (open circles) and on July 14, 2010 (blue circles). Shown is also an experiment on pure dimethylamine nitrate particles produced from a nebulizer (open yellow circles, see also section 5.3, page 41).

Unfortunately, the AMS set up did not record thermograms for the experiment on July 14, 2010. The nitrate salts produced in the low NO_x experiment on March 11, 2010, consisted mainly of $DMANO_3$ ("primary salt") in the initial stages, but in later stages the contribution of non $DMANO_3$ increased. Similar behaviour was observed in high NO_x experiments.

According to the model, only 1-2% of the initial DMA amount was converted into particulate matter, the mass-based yield of SOA in DMA experiments was 8-9% and the total aerosol yield was 6%, all independent of the applied NO_x conditions. Further, the $DMANO_3$ dissociation constant K_d determined by adjustment of the model was 20 times lower in the high NO_x experiment than in the low NO_x experiment. The K_d values derived by the model for the low-NO_x and high-NO_x experiments are both lower than the literature value. The nitrate aerosol in the experiment is thus found to be more stable than would be expected from the thermodynamics properties of the pure nitrate salt, i.e. for true equilibrium conditions. One explanation could be, that less volatile nitrate salts than $DMANO_3$ have been formed in the experiment. However, both primary and secondary nitrate salts were found to have high volatility. Thus a more likely explanation for deviation from equilibrium is that secondary organics condensed onto the nitrate salt particles and stabilized the nitrate aerosol. This explanation is also consistent with the fact that observed volatility of the aerosol produced in DMA experiments decreased with time of the experiment.

5.12 (CH$_3$)$_3$N photo-oxidation studies

Four TMA photo-oxidation studies have been selected for more detailed analysis:

| Date	Experimental conditions	Monitor data
2010/03/24	High-NO$_x$ experiment. HONO as OH precursor.	Annex 13
2010/03/25	High-NOx experiment. Starting conditions: ~100 ppbV NO$_2$, 20 ppbV NO. NOx kept constant at 120 ppbV	Annex 14
2010/07/16	High-NOx conditions. Starting conditions: ~200 ppbV NO$_2$, 50 ppbV NO. Constant NOx = 100 ppbV.	Annex 21
2010/07/23	High-NOx, dry conditions. Starting conditions: ~150 ppbV NO$_2$, 20 ppbV NO.	Annex 23

The 2010/03/24 experiment was carried out under high-NOx conditions on a very cloudy day. HONO was added throughout the experiment as OH precursor. Starting conditions: ~200 ppbV NO$_2$, 100 ppbV NO and 150 ppbV HONO.

The 2010/03/25 trimethylamine experiment was carried out under high-NOx conditions. The NO$_x$-level was initially around 100 ppbV NO$_2$ and 10 ppbV NO before opening the chamber canopy when it instantaneously changed to around 70 and 40 ppbV. From then on the mixing ratios decreased monotonously to around 100 and 10 ppbV, respectively, at the end of the experiment.

The 2010/07/16 experiment was carried out under high-NOx conditions. 1 mL 30 wt% H$_2$O$_2$ was added to as additional OH precursor.

The 2010/07/23 experiment was carried out under high-NOx conditions.

The theoretical photo-oxidation mechanism of trimethylamine (Scheme 2.3, Page 22) is reproduced below showing the major photo-oxidation products to be (CH$_3$)$_2$NCHO (*N,N*-dimethyl formamide), CH$_3$N=CH$_2$ (*N*-methyl methanimine), (CH$_3$)$_2$NNO (*N*-nitroso dimethylamine, NDMA) and (CH$_3$)$_2$NNO$_2$ (*N*-nitro dimethylamine).
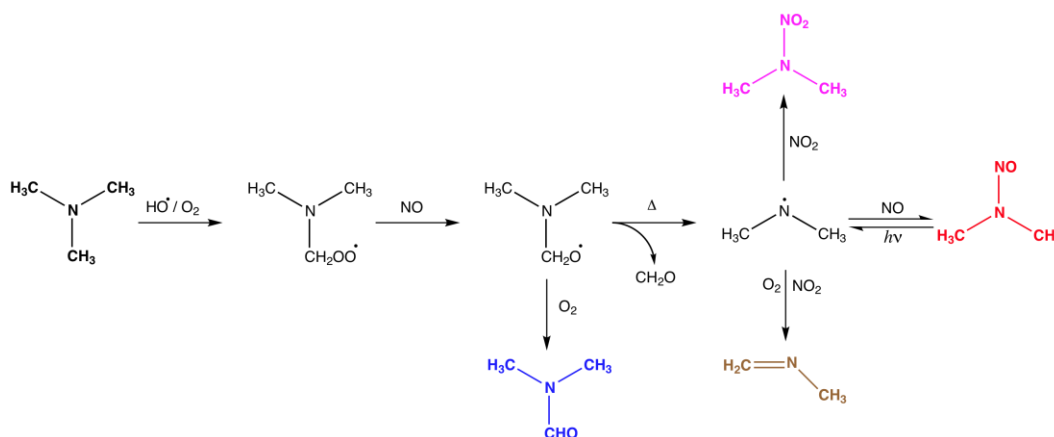
Scheme 2.3. Main routes of the atmospheric trimethylamine photo-oxidation.

Figure 5.44 shows the differences in the mass spectra obtained during the first 60 min. decay of trimethylamine relative to the ion signal at m/z 60.0807 (protonated trimethylamine). Only ion peaks of intensity > 1 % of $\Delta I_{60.0807}$ are included in the figure. Table 5.12 summarises the ion signals changing during the photo-oxidation of trimethylamine and the tentative interpretation.
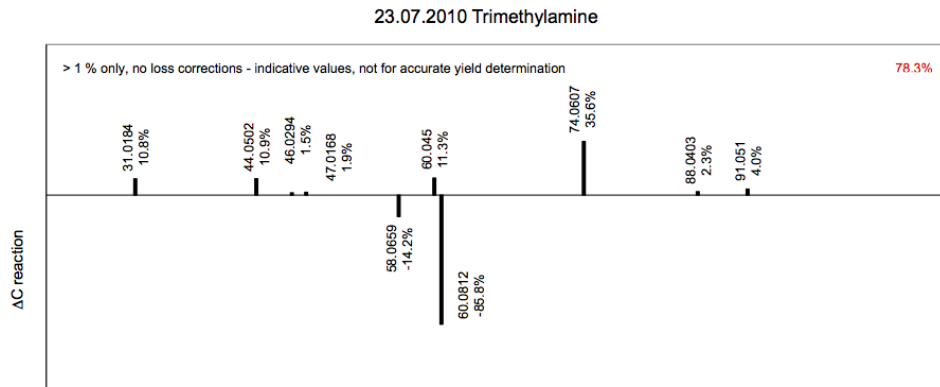
Figure 5.44. Mass spectral difference measured during the photo-oxidation of methylamine on March 22. Mass peaks of intensity < 1 % of $\Delta I_{60.0807}$ are omitted.

The concentration time profiles of the major product ions, observed in the experiment on 2010/07/23 are included in Figure 5.45. In addition to the expected products substantial amounts of NH_2CHO (formamide), HCOOH (formic
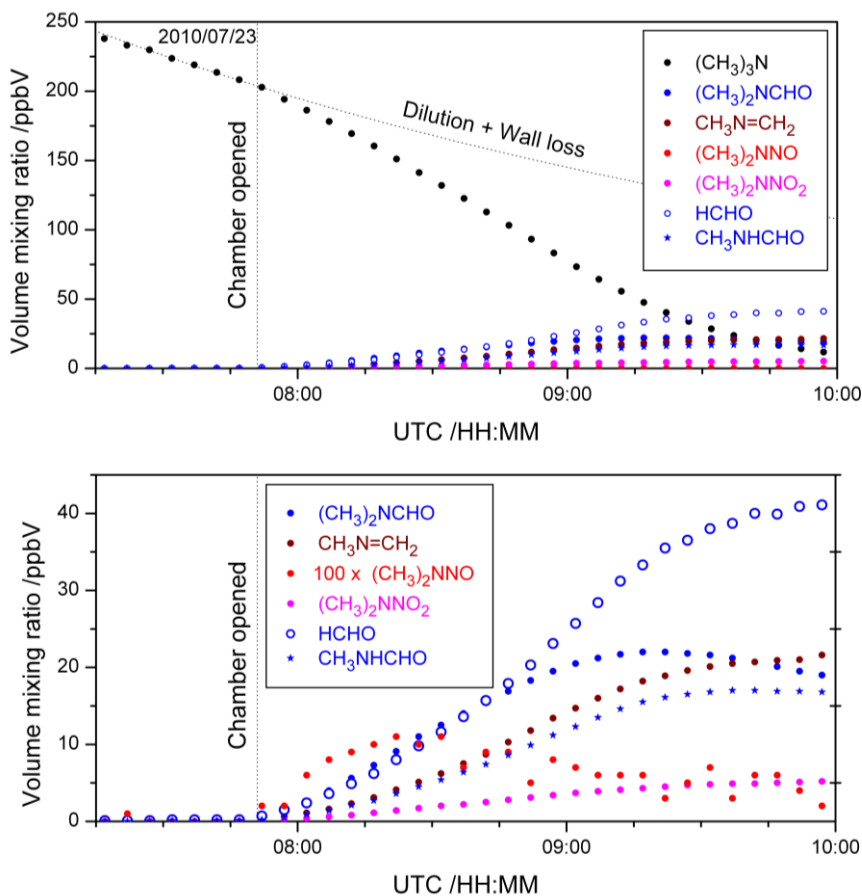
Figure 5.45. Time evolution of the major ion signals observed in the 2010/07/23 trimethylamine photo-oxidation experiment.

acid), $(CH_3)NHCHO$ (*N*-methyl formamide), CH_3NHNO_2 (*N*-nitro methylamine) and $CH_3N(CHO)_2$ (*N*-formyl,*N*-methyl formamide) were observed in this experiment. Formamide was not observed in the similar experiment≈ on 2010/03/25, Figure 5.46, and is considered a spill-over from previous experiments.

Figure 5.46. Time evolution of the major ion signals observed in the 2010/03/25 trimethylamine photo-oxidation experiment.

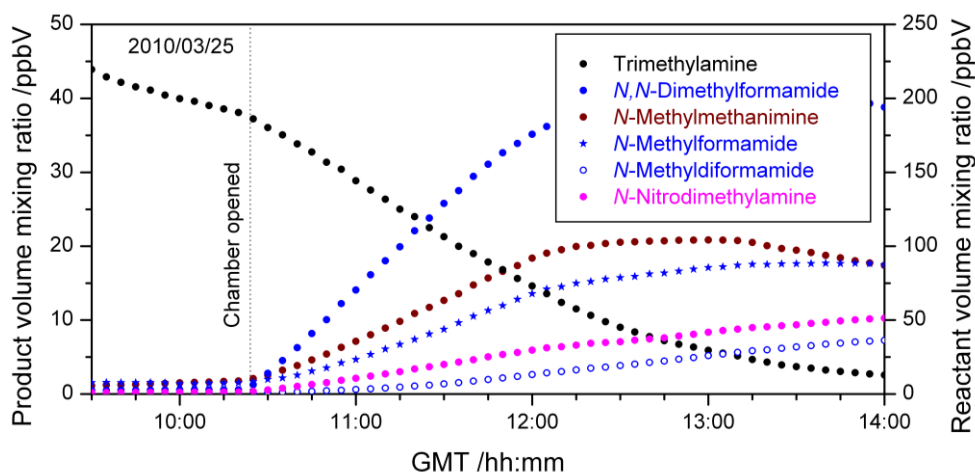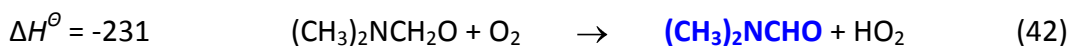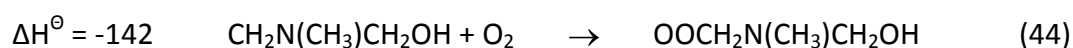Formic acid results from the reaction of HCHO and HO_2 radicals as outlined in section 5.11. $CH_3N(CHO)_2$ is a secondary product and stems from the oxidation of $(CH_3)_2NCHO$, see section 5.19, page 118.

The formation of N-nitroso dimethylamine and N-nitro dimethylamine can be accurately modelled with the relative rates derived from the dimethaylamine photo-oxidation (section 5.11) and *N*-nitroso dimethylamine photolysis (section 5.13) experiments. In this sense there is no additional information to be gained from the trimethylamine photo-oxidation experiments. The concentration time profiles of *N,N*-dimethyl formamide and *N*-nitro dimethylamine are determined by the branching of the $(CH_3)_2NCH_2O$ radical dissociation *vs.* reaction with O_2:

$$\Delta H^{\ominus} = 4 \qquad\qquad (CH_3)_2NCH_2O \xrightarrow{\;\Delta\;} (CH_3)_2N + CH_2O \qquad\qquad (41)$$

$$\Delta H^{\ominus} = -231 \qquad\qquad (CH_3)_2NCH_2O + O_2 \;\longrightarrow\; \textbf{(CH}_3\textbf{)}_2\textbf{NCHO} + HO_2 \qquad\qquad (42)$$

The reaction enthalpies listed ($\Delta H^{\ominus}$ /kJ mol^{-1}) refer to 298 K and to the lowest energy conformations of the species involved and stems from G3 calculations.[122] A best fit to observations is obtained by $k_{41}/k_{42} \approx 0.6$. This means that, on a per molecule basis, the atmospheric photo-oxidation of trimethylamine will result in around 50% more *N*-nitroso dimethylamine and *N*-nitro dimethylamine than dimethylamine itself.

At present we offer no final explanation to the apparent formation of *N*-methyl formamide and *N*-nitro methylamine in the trimethylamine photo-oxidation experiments. Detailed quantum chemistry calculations are underway to confirm the following route in which the $(CH_3)_2NCH_2O$ radicals first undergo internal 1,4-hydrogen shift:

$\Delta H^{\ominus} = -76$ $(CH_3)_2NCH_2O \xrightarrow{1,4-H} CH_2N(CH_3)CH_2OH$ (43)

$\Delta H^{\ominus} = -142$ $CH_2N(CH_3)CH_2OH + O_2 \rightarrow OOCH_2N(CH_3)CH_2OH$ (44)

$\Delta H^{\ominus} = -40$ $OOCH_2N(CH_3)CH_2OH + NO \rightarrow OCH_2N(CH_3)CH_2OH + NO_2$ (45)

$\Delta H^{\ominus} = +41$ $OCH_2N(CH_3)CH_2OH \xrightarrow{\Delta} CH_3NCH_2OH + \mathbf{CH_2O}$ (46)

$\Delta H^{\ominus} = -78$ $CH_3NCH_2OH + O_2 \rightarrow CH_2=NCH_2OH + HO_2$ (47a)

$\Delta H^{\ominus} = -133$ $\rightarrow CH_3N=CHOH + HO_2$ (47b)

$\Delta H^{\ominus} = -43$ $CH_3N=CHOH \xrightarrow{1,4-H} CH_3NHCHO$ (48)

No detailed gas phase chemistry modelling is offered until the above route has been confirmed or rejected.

Table 5.12. Ions observed by PTR-TOF-MS during the photo-oxidation of trimethylamine on March 25, 2010.

Mass	ion formula	Parent molecule	comment
31.0179	CH_3O^+	Formaldehyde	Product, Chamber artifact
33.0336	CH_5O^+	Methanol	Chamber artifact
43.0182	$C_2H_3O^+$	Acetic acid (acetyl ion fragment)	Chamber artifact
44.0498	$C_2H_6N^+$	*N*-methylmethanimine	
45.0337	$C_2H_5O^+$	Acetaldehyde	Chamber artifact
45.9925	NO_2^+	Nitric acid, Organic nitrates	Fragment ion
46.0293	CH_4NO^+	Formamide	
47.0130	$CH_3O_2^+$	Formic acid	Chamber artifact
58.0654	$C_3H_8N^+$	Trimethylamine (fragment)	Reactant
59.0497	$C_2H_7O^+$	Acetone	Chamber artifact
59.0732	$^{13}C\ C_2H_8N^+$	Trimethylamine (fragment)	^{13}C-isotope
60.0447	$C_2H_6NO^+$	*N*-methylformamide	
60.0807	$C_3H_{10}N^+$	Trimethylamine	Reactant
61.0288	$C_2H_5O_2^+$	Acetic acid	Chamber artifact

61.0860	^{13}C $C_2H_{10}N^+$	Trimethylamine	^{13}C-isotope
62.0244	$CH_4NO_2^+$	Nitromethane	
74.0603	$C_3H_8NO^+$	*N,N*-dimethyl formamide	Product
75.0631	$C_2H_7N_2O^+$	*N*-nitroso dimethylamine	Product
77.0349	$CH_5N_2O_2^+$	*N*-nitro methylamine	
88.0398	$C_3H_6NO_2^+$	*N*-methyldiformamide	Product
91.0506	$C_2H_7N_2O_2^+$	*N*-nitro dimethylamine	Product

5.12.1 Analysis of aerosol formation

A further photo-oxidation experiment with trimethylamine (TMA) under high NO$_x$ conditions was performed on July 23,2010. A mixture of about 250 ppbV TMA and 150 ppbV NO$_2$ has been exposed to sunlight. The chamber canopy was opened at 07:53 UTC. A pronounced particle burst was observed immediately after opening, with intense growth until about 10:00 UTC. A second but minor burst occurred at 09:15 (Figure 5.47). The chamber canopy was closed at 10:45 UTC.
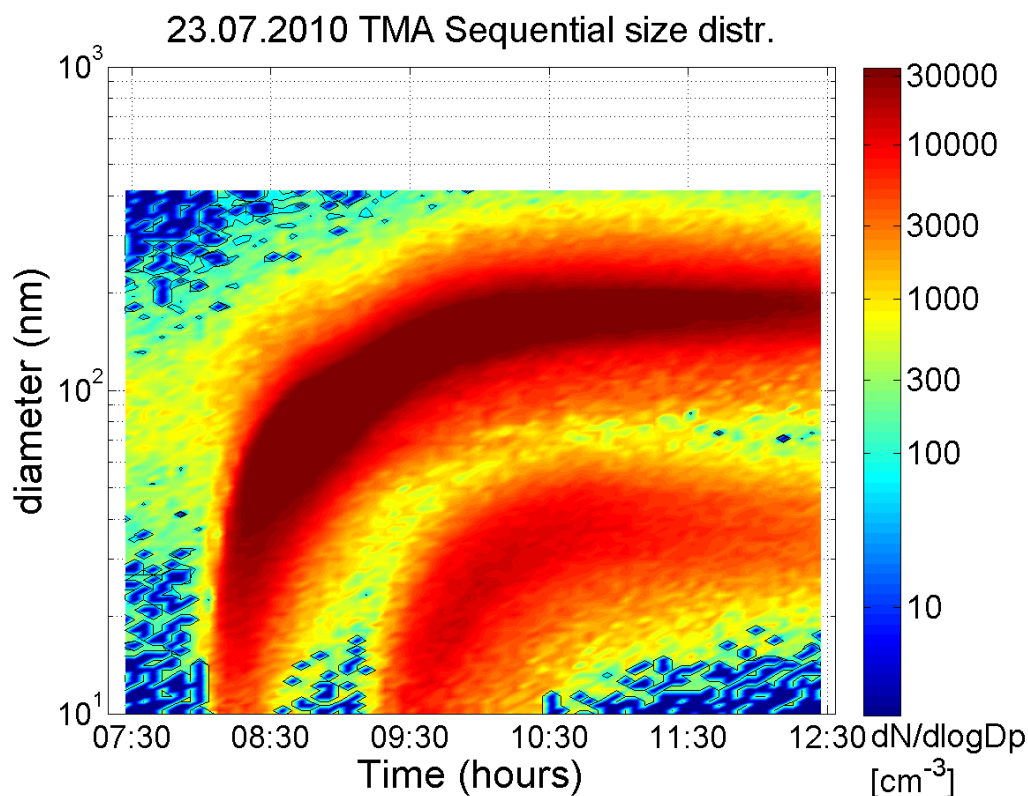

Figure 5.47. Sequential number size distribution (dN/DlogDp in # cm^{-3}) as recorded by SMPS during the experiment on July 23, 2010. SMPS lower size cut-off is at 9.82 nm and upper size cut-off at 414 nm.

The aerosol model MAFOR does not reproduce the first intense particle burst after opening of the canopy. By adjustment of the modelled aerosol evolution to measured aerosol mass concentrations, the timing of the second burst is captured by the model but the modelled curve has the characteristics of the first burst (Figure 5.48). This is a first indication that nucleation of new particles did not occur through formation of the primary trimethylamine nitrate (TMANO$_3$) salt. The model only takes into account formation of the primary salt and does not treat nitrate formation by other compounds than the main reactant (here: TMA).
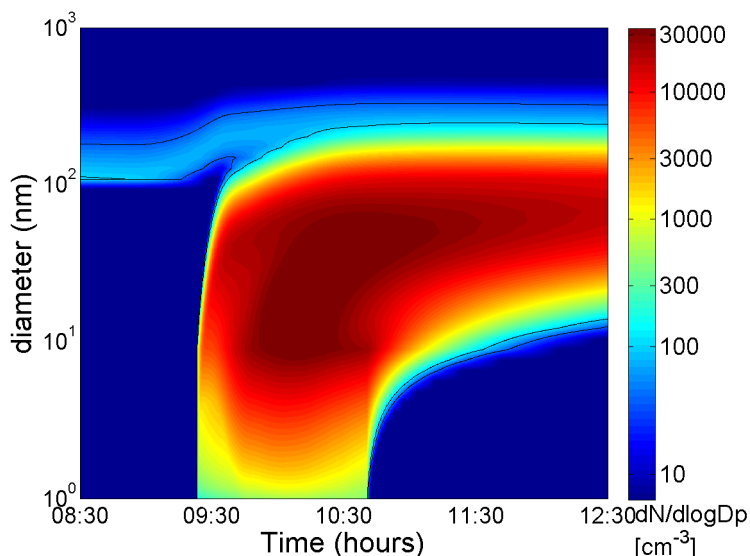
Figure 5.48. Modelled number size distribution (dN/DlogDp in # cm-3) during the experiment on July 23, 2010, as 2-dimensional plot for the diameter range 1-1000 nm.

Figure 5.49 presents the evolution of the total aerosol mass concentrations during the experiment on July 23, 2010, as recorded by AMS and SPMS. At the initial phase of the experiment an impressive agreement between 30 eV and 70 eV data was achieved. Starting at about 09:30 the organic signals at 30 eV and 70 eV started to diverge, resulting in higher mass loadings at 70 eV. This is an indication for a chemical change of the aerosol. The aerosol showed an increasing effective density D_{va}/D_m during the experiment from 1.16 and 1.24 (stable after the chamber was closed); these values were then used to correct the SMPS data. The total aerosol mass concentration as provided by SMPS (using the effective density) increased up to ~45 µg/m^3 during the experiment.
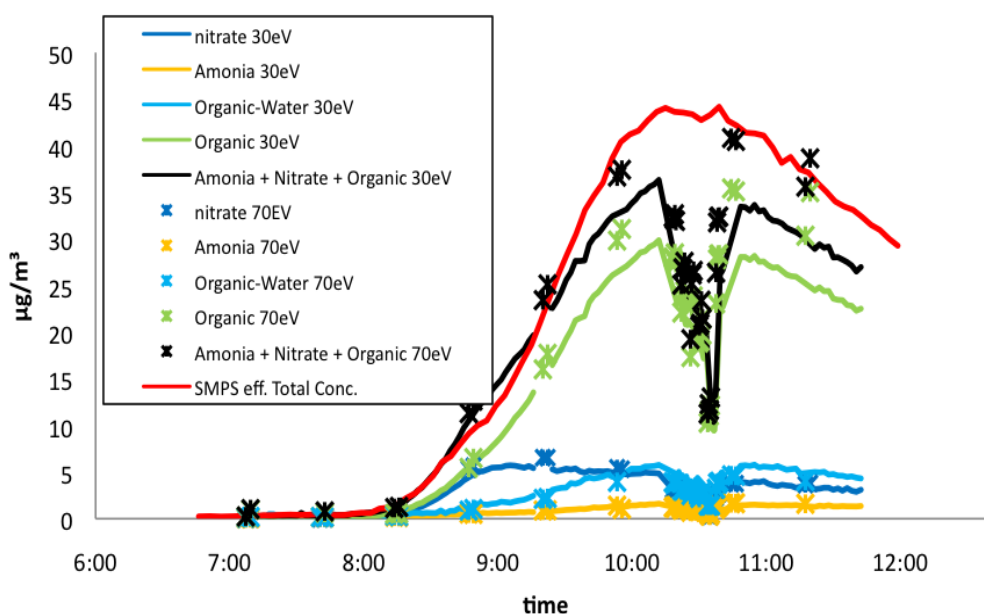

Figure 5.49. Mass loading Nitrate, Ammonium, Organics and Organic-Water for 30eV (solid lines) and 70eV (stars) during the TMA photooxidation experiment on July 23, 2010.

Modelled particle mass concentrations obtained in a MAFOR simulation of the experiment on July 23, 2010, starting short after exposure to sunlight, overestimate the slope of the concentration increase of secondary organics (Figure 5.50). Modelled nitrate aerosol mass concentrations lag the observed concentrations by approximately one hour in time. This is a second indication from modelling, that the first nucleation event occurring after opening of the canopy is not due to newly formed $TMANO_3$ particles, and more probably due to nitrate salt particles formed by other compounds, likely TMA oxidation products. Maximum mass loadings obtained in the model simulation agree with the AMS data but underestimate the maximum loadings derived by SMPS.
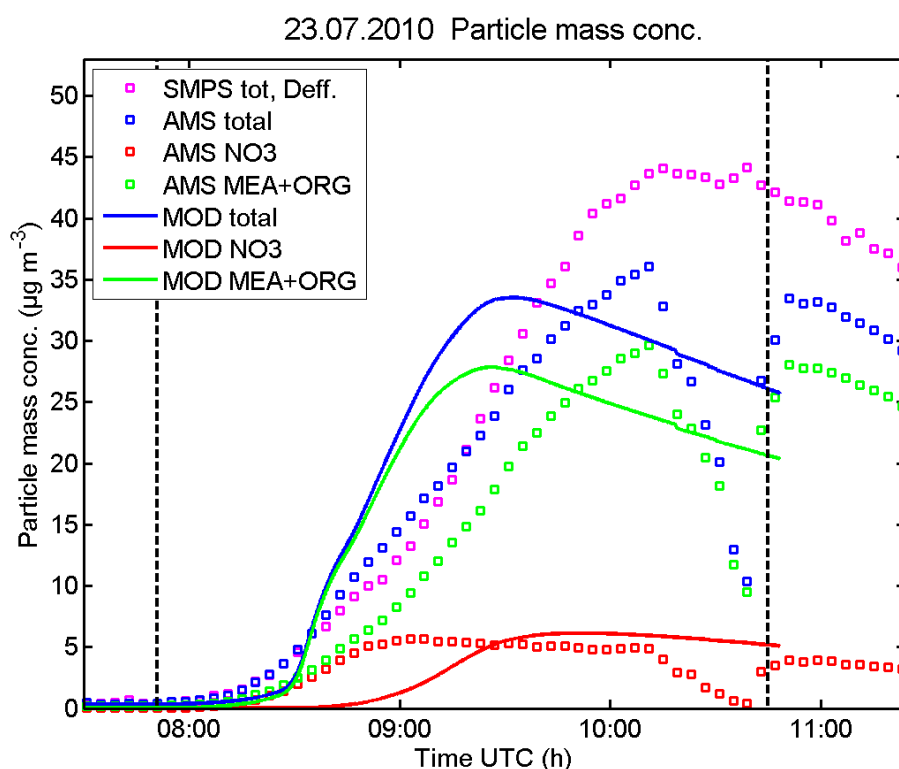
Figure 5.50. Comparison of modelled particle mass concentration (in $\mu g\ m^{-3}$) of aerosol components with measured mass concentrations by AMS (red, green an blue squares), and by SMPS (magenta squares) for the TMA experiment on July 23, 2010. Increase of modelled particle mass concentration of total organics including TMA (green line) shows a steeper slope than AMS measured organics (green squares). A time lag of about 1 hour is found between modelled (red line) and observed (red squares) nitrate mass concentrations.

By using the AMS reference spectrum of $TMANO_3$ shown in section 5.1 (page 38), the fragmentation pattern of $TMANO_3$ was determined in the AMS data. Accordingly, the most important organic fragments of TMA are m/z $C_3H_8N^+$_at m/z 58.05 and $C_3H_9N^+$_at m/z 59.06. By intercomparison of the fragments patterns of these two ions with the nitrate time series (NO_2^+ at m/z 45.99 as a proxy), the $TMANO_3$ contribution can be calculated.

Figure 5.51a below shows the results: approximately 30% of the total nitrate originates from TMANO₃, the remaining fraction consists of nitrate salts formed by other compounds. It also shows that the nitrate aerosol in the initial phase, between about 08:00 UTC and 08:45 UTC, was dominated by other nitrate salts than TMANO₃. In particular, the initial increase of mass loadings due to the other nitrate salt particles was much steeper than the increase due to TMANO₃ particles.

a)

b)
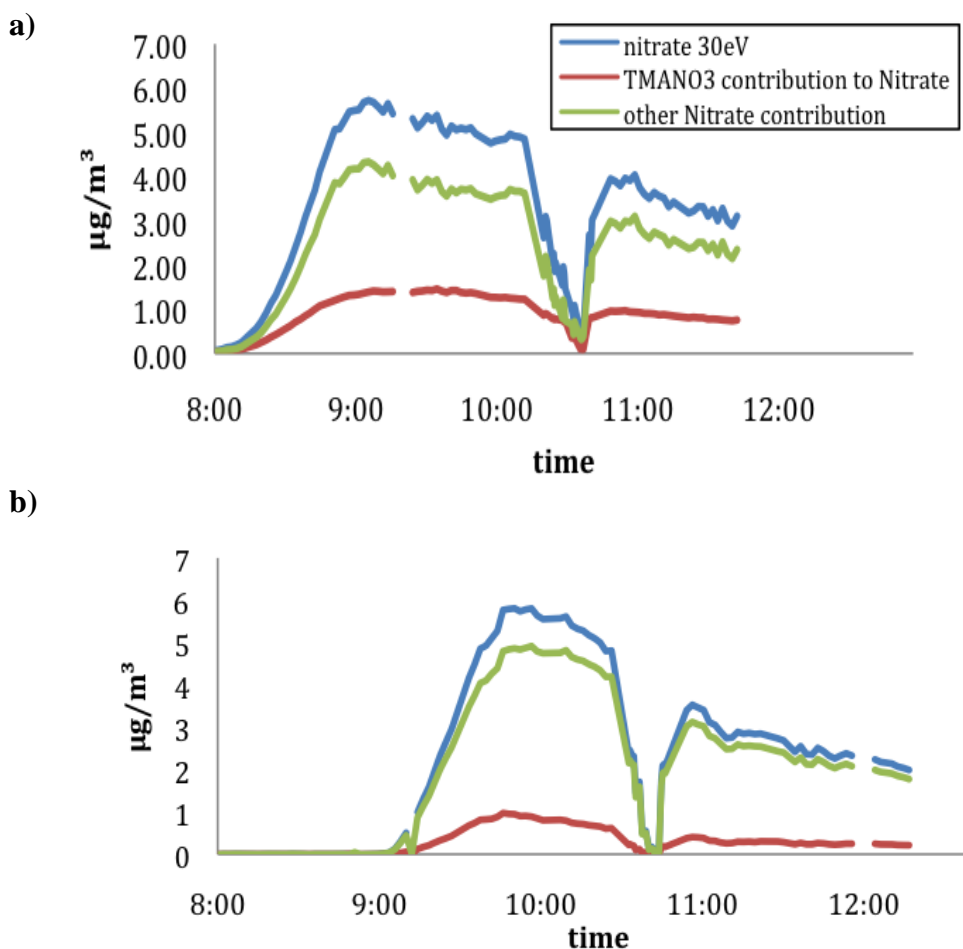
Figure 5.51. Time series of the total nitrate, nitrate from pure TMANO₃ and the non-TMANO₃ nitrate contribution, a) in the experiment on July 23, 2010, b) in the experiment on July 16, 2010.

Possible ions contributing to the non-TMANO₃ nitrate salt on July 23, 2010, were identified by the thermogram and we selected those ions showing the same thermal decomposition of the nitrate signal. Figure 5.52 below presents a list of possible ions participating to all the nitrate salts (the TMANO₃ is included). Approximately 30-40% of the total aerosol mass is in the form of a salt. The fragment at m/z 43.04 (purple line) possibly arises from the N-methylmethan-imine nitrate salt.
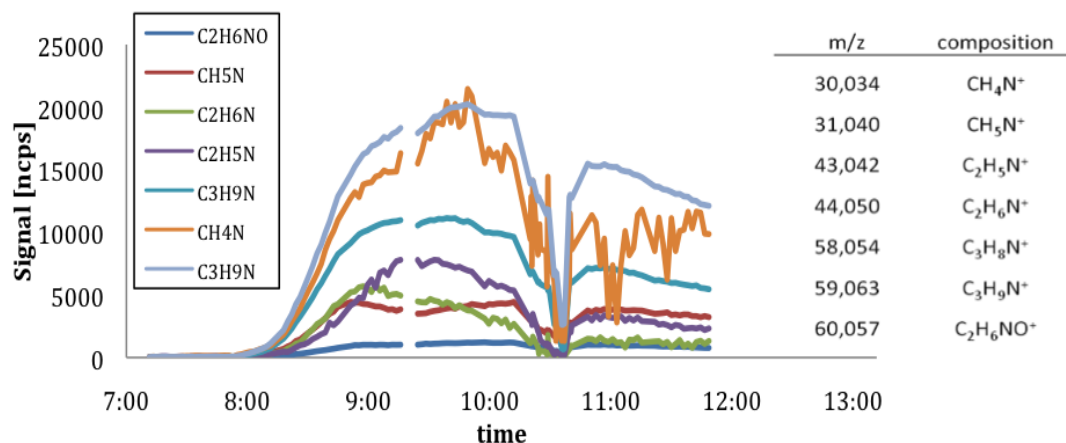
Figure 5.52. Time series of the organic ion fragments showing a similar time evolution and volatility of the nitrate signal (NO_2^+) during the experiment on July 23, 2010.

On-line chemical analysis of aerosol using PTR-MS (described in section 5.8, page 50) gave two major contributions: one at m/z 44 and the other at 46. Here we compare the AMS and PTR-MS results. Figure 5.53 depicts the time series of the most important ion signals arising just after the chamber was opened for the instruments.
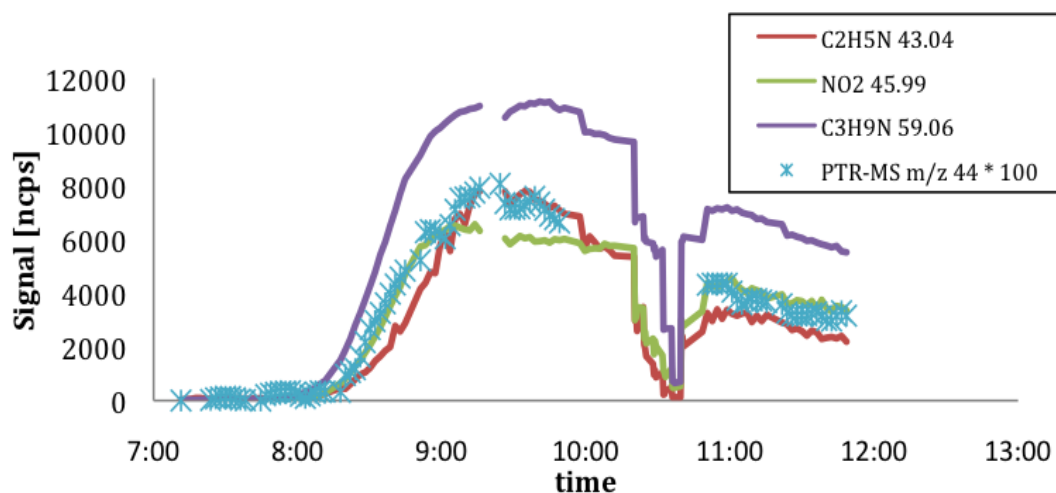
Figure 5.53. Time series of the ions associated to the initially formed aerosol (first particle burst) recorded by AMS (full line) and by the PTR-MS (blue stars) analysis during the experiment on July 23, 2010.

The m/z 44 observed by the PTR-MS (light blue stars) correlates well with the AMS ion signals corresponding to the primary salts (TMANO$_3$) and the N-methylmethanimine signal, this latter should be present in the aerosol in the form of a salt (due to its high proton affinity). The aerosol of the first nucleation event is formed just after 8:00 and reaches a maximum around 9:00 UTC.
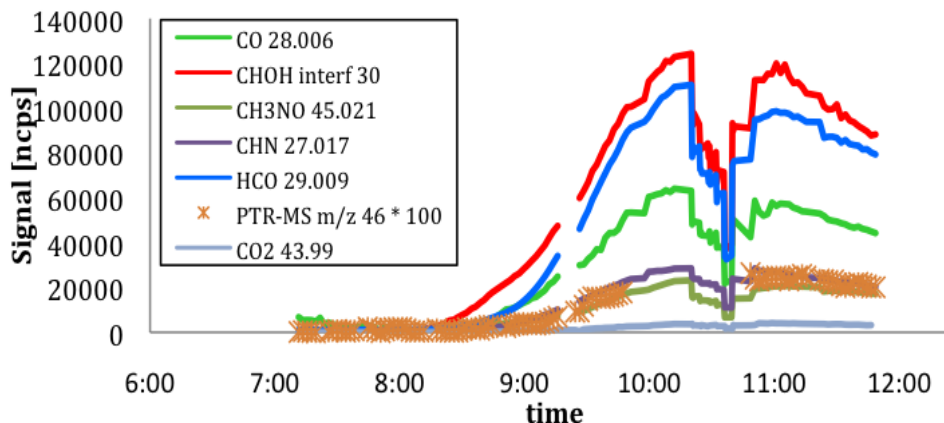
Figure 5.54. Time series evolution of ions associated to the secondary formed organic aerosol for the AMS and the PTR-MS data during the experiment on July 23, 2010.

Figure 5.55 shows the time series evolution of secondary organic aerosol compounds, mainly oxygenated, which are formed approximately one hour after the first particle burst, and reaches its maximum loading around 10:30 UTC. In this experiment the largest fraction of the aerosol correspond to these oxygenated species. PTR-MS identifies a ion at m/z 46 (light-brown stars) which could correspond in the AMS signal the m/z 45.01 assigned to CH_3NO.

The four experiments on TMA that were performed during ADA-2010 were evaluated for thermal properties of the produced aerosol using the VTDMA set up (see Figure 5.55). In three of the experiments, after the chamber had been open for 2 hours, the aerosol produced was very low-volatile or non-volatile. Within the first half hour most of the decrease in volatility had already occurred. Only in the cloudy experiment on March 24, 2010, in which HONO was used as OH-precursor, a different pattern was observed. This aerosol was significantly
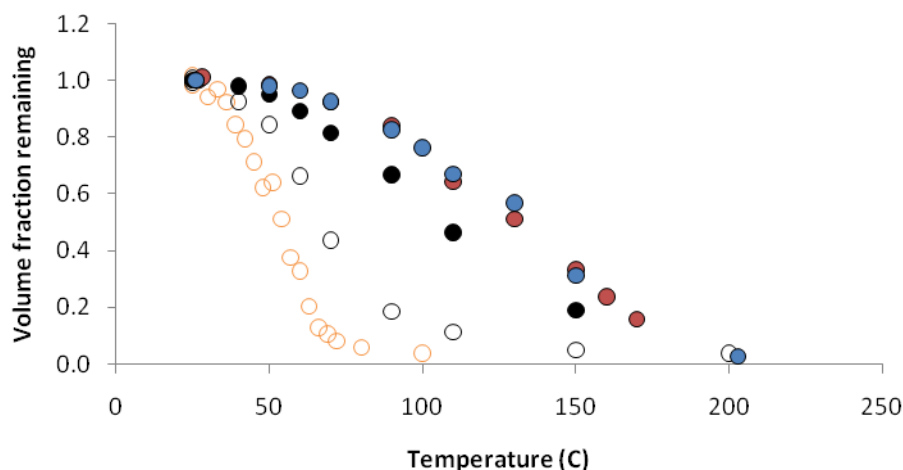
Figure 5.55. Volume fraction remaining versus evaporative temperature for four high NO_x-experiments on trimethylamine (TMA) 2 hours after opening the chamber on March 24 (open circles), March 25 (yellow circles), July 16 (red circles) and July 23 (blue circles), 2010. The experiment on March 24, 2010, was done on a very cloudy day with HONO as OH-precursor. Shown is also an experiment on pure trimethylamine nitrate particles produced from a nebulizer (open yellow circles).

more volatile than the other experiments most likely consisting of trimethyl-amine nitrate while the other experiments produced an aerosol consisting of more oxidized material.

Figure 5.56 depicts the temperature dependent loadings during the experiment on July 23, 2010, measured by the AMS set up at 30 eV and 70 eV. Interestingly the organic signals for 30 eV and 70 eV get more and more equal with increasing temperature. The signal m/z 59.06 (TMANO$_3$) decreases by 93% during the thermogram, this salt is almost completely evaporated at this temperature. At this temperature 40% of the total aerosol mass is still present; it is organic material with low volatility.
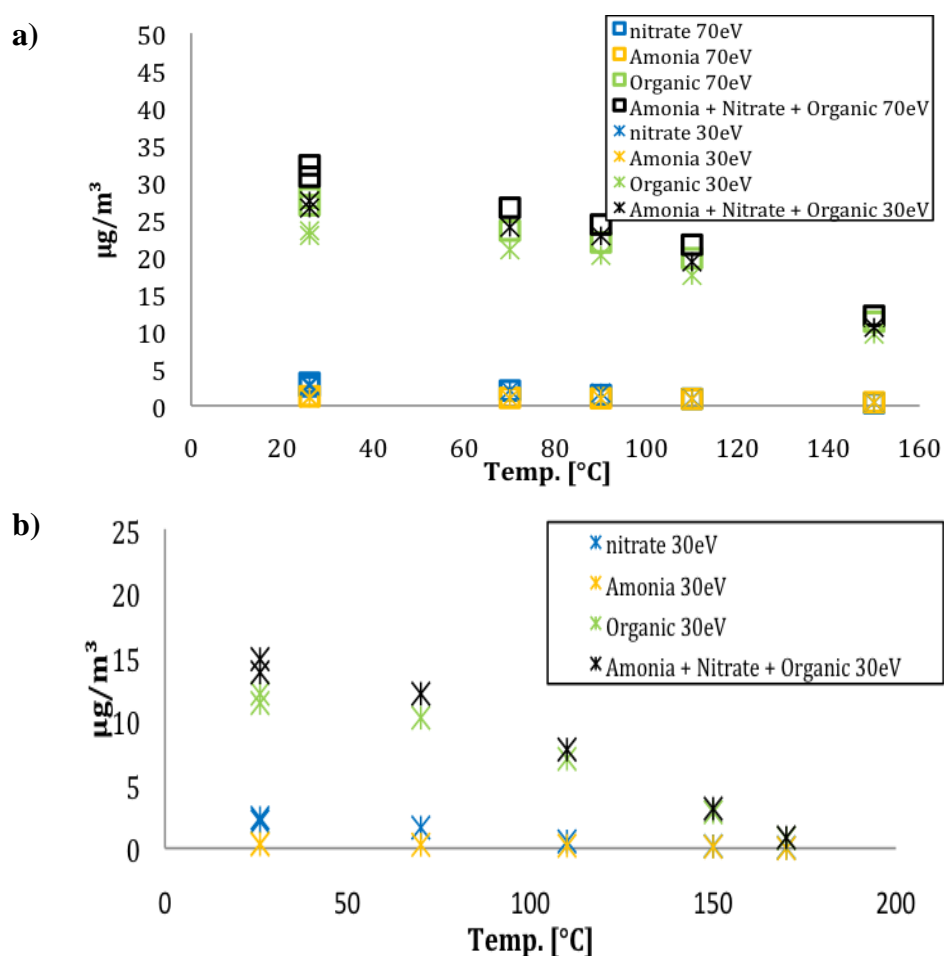
Figure 5.56. A 5-temperature-step thermogram between 25 and 200°C during TMA experiments, a) on July 23, 2010, recorded between 10:30 and 10:45, b) on July 16, 2010, recorded between 10:32 and 10:46.

Summary. The total aerosol mass observed during TMA photo-oxidation experiments contained only small contributions from TMANO$_3$. The total nitrate salt loading corresponded to 30-40% of the total aerosol loading. The nitrate aerosol forming in the TMA photo-oxidation consisted largely of other nitrate salts than TMANO$_3$. In the experiment on July 23, 2010, approximately 30% of the total nitrate mass concentration was associated to the TMA, while the remaining 70 % of the measured nitrate salt was associated to other ions, among

those the N-methylmethanimine seem to be a very good candidate (see section 5.15, page 107) as concurrent measurements with the AMS set up and the newly deployed PTR-MS particulate-phase set up revealed.

Secondary organic aerosol formed in the photo-oxidation of TMA is the dominant aerosol fraction and has a low volatility. The major fraction of the aerosol is formed by oxygenated species, generated approximately one hour after the first burst of particles (primary salt formation) and are associated to low volatile material, approximately 40% the aerosol did not evaporate at 150°C in the AMS set up.

The aerosol model MAFOR overestimated the organic mass concentration increase after opening of the chamber and could not reproduce the first particle burst that was observed after exposure of the TMA/NO_x mixture to sunlight. This implies that initial nucleation event was not caused by the formation of $TMANO_3$ particles; a finding that was confirmed by inspection of the AMS nitrate signals. The dissociation coefficient K_d of $TMANO_3$ obtained by adjusting the model to measured particle mass concentrations of nitrate and measured particle number distributions was 5×10^{-7} Pa^2 (at the average temperature of the experiment, 303.4 K). This model-derived value is still in good agreement with the K_d value of 1.65×10^{-6} Pa^2 (at 298 K; for the pure salt) given in a recent review by Ge et $al.$[134] Note that the K_d value is higher than that of ammonium nitrate (4.48×10^{-7} Pa^2 at 298 K; Ge et al., 2010) while the K_d of other methylamines and ethylamines is at least one order of magnitude smaller than that of ammonium nitrate. The high volatility of the $TMANO_3$ salt is in contrast to the low volatility of the SOA formed in TMA photo-oxidation. MAFOR predicted a mass-based yield of ~14% SOA to be formed in the oxidation of TMA under high NO_x-conditions. The total aerosol yield in the photo-oxidation of TMA was estimated to be 8%.

5.13 (CH₃)₂NNO photolysis studies

Four *N*-nitroso dimethylamine (NDMA) photolysis experiments were carried out with quite different starting conditions:

Date	Experimental conditions	Monitor data
2010/03/23	Very cloudy day. Starting conditions: ~120 ppbV NO$_2$ and 50 ppbV NO.	Annex 12
2010/07/01	Afternoon experiment. Starting conditions: ~0 ppbV NO$_2$ and ~0 ppbV NO.	Annex 15
2010/07/02	Morning experiment. Starting conditions: ~0 ppbV NO$_2$ and ~100 ppbV NO.	Annex 16
2010/07/02	Afternoon experiment. Starting conditions: ~200 ppbV NO$_2$ and ~0 ppbV NO.	Annex 16

In each experiment around 150 mg of NDMA, roughly corresponding to a mixing ratio of 250 ppbV, were introduced into the chamber. In the 2010/07/01 experiment the sample was partly lost upon injection which resulted in a lower NDMA concentration in the chamber. Upon opening of the chamber canopy NDMA underwent swift photolysis and essentially only two compounds, *N*-nitro dimethylamine (DMNA) and *N*-methyl methanimine (MMI), were detected as primary products. In addition, small amounts of nitromethane, CH$_3$NO$_2$, and formaldehyde were observed as primary products in all experiments.

A simplified reaction scheme for photolysis of NDMA suggests the formation of two products, DMNA and MMI. The relative amount of the two products will only depend on the NO$_2$-level. Additional reactions may take place in the presence of OH radicals, but OH reactions with NDMA and DMNA are slow. The OH reaction with MMI is presumably faster, but the rate coefficient is not yet known.
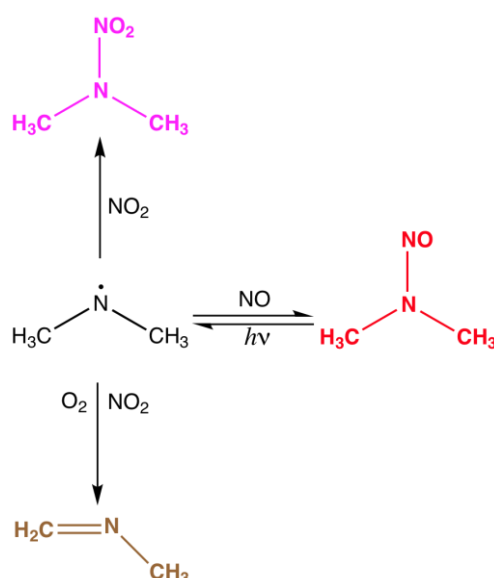
Scheme 5.3. Simplified reaction scheme for the atmospheric photolysis of *N*-nitroso dimethylamine.

Table 5.13 shows the time-integrated molar increase of products (detected in their protonated forms) in the NDMA photolysis experiments relative to the time-integrated decrease of NDMA (detected in its protonated form at m/z 75.0522) during the first 30 minutes of the experiments: only ion peaks of intensity > 1 % of $\Delta I_{75.0522}$ have been included in the table. Figure 5.58. shows the time-profiles of NDMA and its photolysis products as observed in the 2010/03/23 experiment.

Table 5.13. Ions observed by PTR-TOF-MS during photolysis studies of *N*-nitroso dimethylamine. Also given are the derived sum formulas, the observed time-integrated molar increase/decrease during the course of the experiment and the assigned neutral precursor species.

m/z	Ion formula	2010.03.23	2010.07.01	2010.07.02 am	2010.07.02 pm	Potential neutral precursor
31.0180	CH_3O^+	4.5	5.8	4.1	4.0	formaldehyde
44.0497	$C_2H_6N^+$	42.8	63.9	43.3	31.1	*N*-methyl methanimine
46.0292	CH_4NO^+		1.4			formamide
46.0653	$C_2H_8N^+$					dimethylamine
58.0292	$CH_3O_2^+$		1.6			formic acid
60.0449	$C_2H_6NO^+$		1.5			*N*-methylformamide
62.0240	$C_2H_5O_2^+$	1.2	0.6	1.1	1.3	Nitromethane
75.0522	$C_2H_5N_2O_2^+$	-100	-100	-100	-100	*N*-nitroso dimethylamine
91.0500	$C_2H_7N_2O_2^+$	52.0	18.2	45.2	63.0	*N*-nitro dimethylamine

The five time traces shown in Figure 5.57 are clearly correlated indicating that the four products observed are <u>primary</u> products. Furthermore, the correlation between signals observed during the first 30 min of the experiment gives direct information on the branching in the dimethylamino radical reactions – the initial rate method, Figure 5.58. It should, however, be noted that the correlations give no information on the back-reaction of the $(CH_3)_2N$ radical reactions with NO.
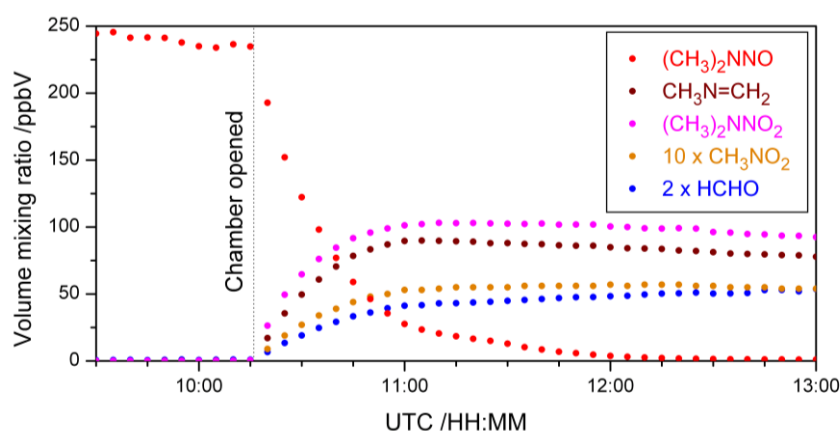

Figure 5.57. Time evolution of DMNA and its photolysis products as observed in the experiment on 2010/03/23. Only products with a yield > 1 % have been included.
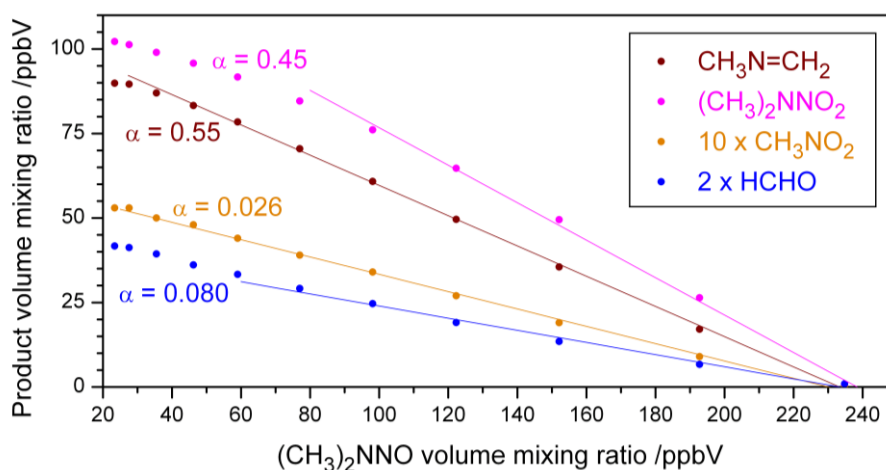
Figure 5.58. Correlations between $(CH_3)_2NNO$ and photolysis products as observed in the initial phase of the 2010/03/23 experiment.
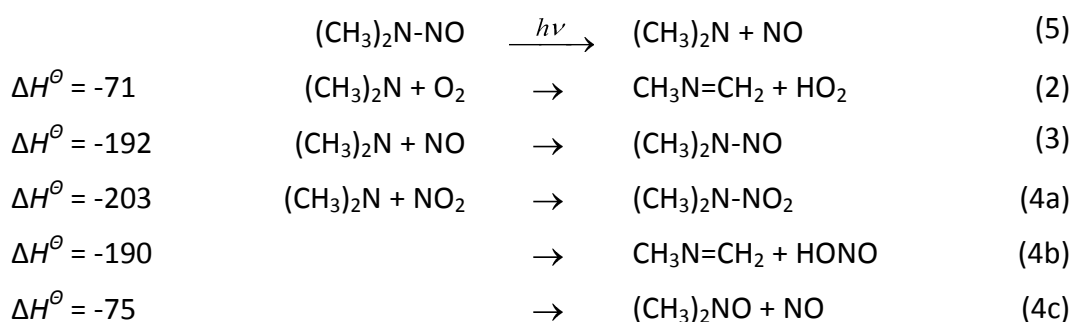
Similar plots to Figure 5.58 are obtained for the other NDMA photolysis experiments; Table 5.14 summarizes the results obtained reflecting the different NOx-conditions (see Annex 12, 15 and 16). The yields of formaldehyde and nitromethane are apparently independent of the NO_2-level suggesting they originate from the reaction between the dimethylamino radical and O_2. We note that the CH_2O : CH_3NO_2 ratio in 3 of the 4 experiments is around 3:1. In the 2010.07.01 experiment initial NDMA levels were lower resulting in a higher experimental uncertainty for HCHO.

Table 5.14. Linear regression slopes of photolysis products versus NDMA as observed in the initial phase of all $(CH_3)_2NNO$ photolysis experiments.

m/z	Ion formula	2010.03.23	2010.07.01	2010.07.02 am	2010.07.02 pm	Neutral precursor
31.0180	CH_3O^+	0.080	0.13	0.082	0.079	formaldehyde
44.0497	$C_2H_6N^+$	0.55	0.63	0.46	0.32	*N*-methyl methanimine
62.0240	$C_2H_5O_2^+$	0.026	0.024	0.022	0.028	Nitromethane
91.0500	$C_2H_7N_2O_2^+$	0.45	0.27	0.44	0.67	*N*-nitro dimethylamine

Reiterating previous relevant studies (section 1, page 15): Lindley *et al.*[33] studied the gas phase reactions of the $(CH_3)_2N$ radical with O_2, NO and NO_2 using FT-IR detection and identified *N*-nitroso dimethylamine, *N*-nitro dimethylamine and *N*-methyl methanimine as products. They further derived the relative rates $k_2/k_3 = (1.48 \pm 0.07) \times 10^{-6}$, $k_2/k_{4a} = (3.90 \pm 0.28) \times 10^{-7}$ and $k_{4b}/k_{4a} = 0.22 \pm 0.06$, from which the branching of the dimethylamino radical reactions with O_2, NO and NO_2 was determined. Lazarou *et al.*[43] studied the reactions of the $(CH_3)_2N$ radical with NO and NO_2 by the Very Low Pressure Reactor (VLPR) technique, reported the formation of *N*-nitroso dimethylamine, *N*-nitro dimethylamine and the

dimethylnitroxide radical as the main products, and derived the absolute rates of reaction $k_3 = (8.53 \pm 1.42) \times 10^{-14}$, $k_{4a} = (3.18 \pm 0.48) \times 10^{-13}$, and $k_{4c} = (6.36 \pm 0.74) \times 10^{-13}$ cm^3 molecule^{-1} s^{-1} at 300 K. Due to mass spectrometric overlap the formation of N-methyl methanimine was not verified by Lazarou et al. Tuazon et al.[37] determined the photolysis rate of NDMA relative to that of NO$_2$ to be $j_{NDMA}/j_{NO2} = 0.53 \pm 0.03$. They employed O$_3$ in large excess in their photolysis experiments to prevent back-reaction of NO with the dimethylamino radical and reported product yields of 33% CH$_3$NO$_2$, 38% HCHO (both ascribed to <u>secondary</u> reactions between N-methylmethanimine and O$_3$) and 2% CO in addition to 65% (CH$_3$)$_2$NNO$_2$. We note, however, that under such experimental conditions NO$_3$ radicals are formed and the obtained result for j_{NDMA}/j_{NO2} thus only represent an *upper* limit to the nitrosamine relative photolysis rate. The literature adds up to the subsequent reactions following the photolysis of NDMA:

$$(CH_3)_2N\text{-}NO \xrightarrow{h\nu} (CH_3)_2N + NO \qquad (5)$$

$\Delta H^{\ominus} = -71$ $\qquad (CH_3)_2N + O_2 \qquad \rightarrow \qquad CH_3N=CH_2 + HO_2 \qquad (2)$

$\Delta H^{\ominus} = -192$ $\qquad (CH_3)_2N + NO \qquad \rightarrow \qquad (CH_3)_2N\text{-}NO \qquad (3)$

$\Delta H^{\ominus} = -203$ $\qquad (CH_3)_2N + NO_2 \qquad \rightarrow \qquad (CH_3)_2N\text{-}NO_2 \qquad (4a)$

$\Delta H^{\ominus} = -190$ $\qquad\qquad\qquad\qquad \rightarrow \qquad CH_3N=CH_2 + HONO \qquad (4b)$

$\Delta H^{\ominus} = -75$ $\qquad\qquad\qquad\qquad \rightarrow \qquad (CH_3)_2NO + NO \qquad (4c)$

The reaction enthalpies listed ($\Delta H^{\ominus}$ /kJ mol^{-1}) refer to 298 K and to the lowest energy conformations of the species involved and stem from G3 calculations.[122]
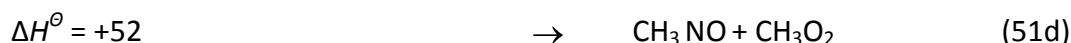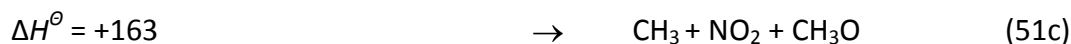
The dimethylnitroxide radical, (CH$_3$)$_2$N-NO, is apparently among the more stable organic radicals and nothing is known on its atmospheric loss. The enthalpy of dissociation (C-N scission) is quite high, and scission is not likely to be relevant under atmospheric conditions:

$\Delta H^{\ominus} = +187$ $\qquad\qquad (CH_3)_2NO \xrightarrow{\Delta} CH_3NO + CH_3 \qquad (49)$

Nitrosomethane has its n $\rightarrow$ π^* transition at around 680 nm and it will undergo very fast photolysis in the gas phase.[142]

$$CH_3NO \xrightarrow{\Delta} CH_3 + NO \qquad (50)$$

Another possibility is reaction of dimethylnitroxide with O$_2$, which may also explain the formation of nitromethane:

$\Delta H^{\ominus} = -88$ $\qquad (CH_3)_2NO + O_2 \qquad \rightarrow \qquad CH_3NO_2 + CH_3O \qquad (51a)$

$\Delta H^{\ominus} = +212$ $\qquad\qquad\qquad\qquad \rightarrow \qquad CH_3 + NO + CH_3O_2 \qquad (51b)$

$\Delta H^{\ominus} = +163$ $\qquad\qquad\qquad\qquad \rightarrow \qquad CH_3 + NO_2 + CH_3O \qquad (51c)$

$\Delta H^{\ominus} = +52$ $\qquad\qquad\qquad\qquad \rightarrow \qquad CH_3NO + CH_3O_2 \qquad (51d)$
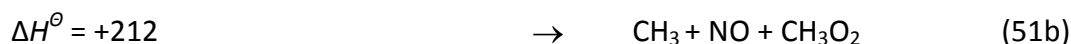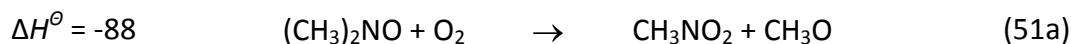
The methyl radical, the methoxy radical and the methylperoxy radical undergo a series of fast reactions to yield formaldehyde, CH$_2$O.

According to the results of Lazarou et al.[43] route (4c) should be 2 times faster than route (4a) at low pressures. The present experiments do not support route

(4c) being a dominant route in the $(CH_3)_2N+NO_2$ reaction at atmospheric pressure. The yields of formaldehyde and nitromethane in the NDMA photolysis experiments are small and not correlated to the NO_2-level. In addition, the observed mass balances do not leave room for (4c) being a a dominant reaction pathway.
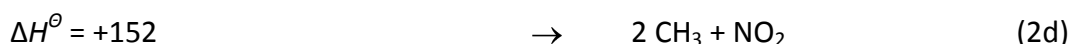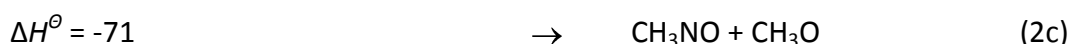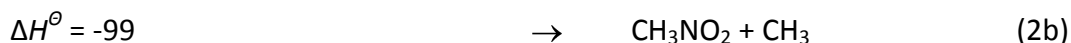
It is alternatively suggested that reaction (2) has two additional branches, (2b) and (2c). Both pathways are exothermic with $k_{2b} \approx k_{2c}$, in line with the observed 3 : 1 product ratio of CH_2O and CH_3NO_2:

$\Delta H^\ominus$ = -71	$(CH_3)_2N + O_2$	$\rightarrow$	$CH_3N=CH_2 + HO_2$	(2a)
$\Delta H^\ominus$ = -99		$\rightarrow$	$CH_3NO_2 + CH_3$	(2b)
$\Delta H^\ominus$ = -71		$\rightarrow$	$CH_3NO + CH_3O$	(2c)
$\Delta H^\ominus$ = +152		$\rightarrow$	$2 CH_3 + NO_2$	(2d)
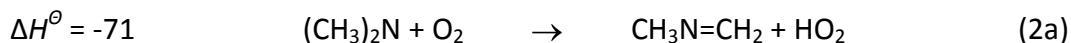
Neglecting reactions with OH radicals, the photolysis experiments have been modelled according to Scheme 5.3.
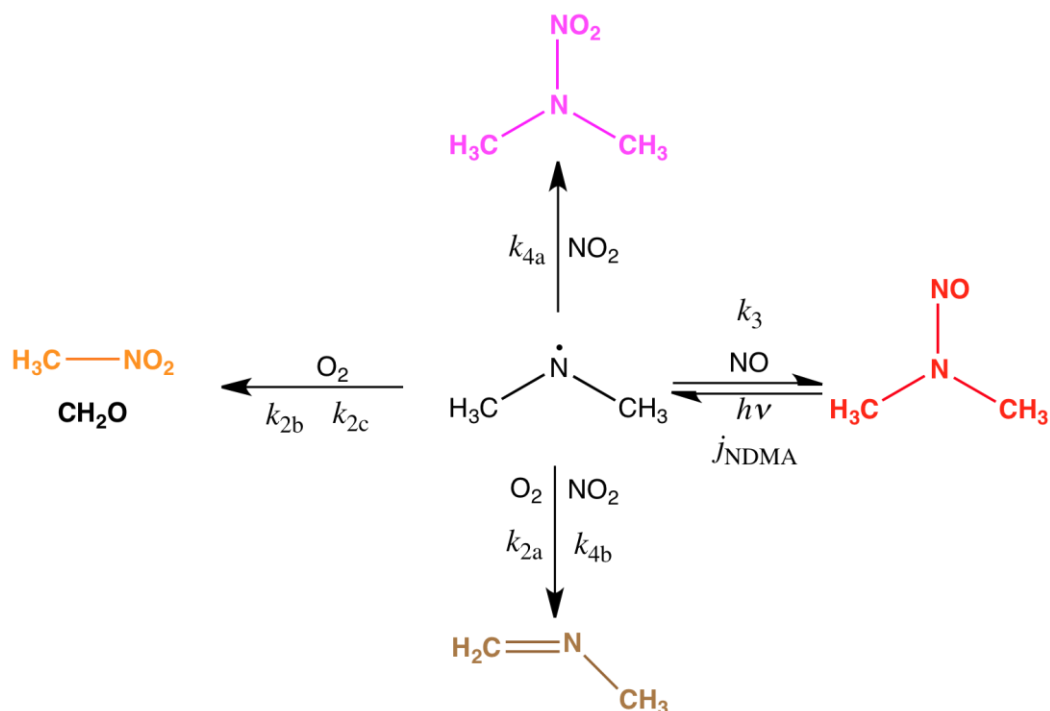
Scheme 5.4. Updated scheme for the atmospheric photolysis of *N*-nitroso dimethylamine (NDMA) and subsequent reactions with O_2 and NO_2.

The photolysis rate constant depends on the absorption cross-section, the actinic flux and the quantum yield to photolysis. Figure 5.59 shows the actinic flux measured inside the chamber during the 2010.03.23 experiment reflecting that it was a partly cloudy day in Valencia (see also Annex 12).

Figure 5.60 shows the photolysis rates of NO_2, j_{NO2}, and *N*-nitroso dimethylamine (NDMA), j_{NDMA}, which have been calculated from:

$$j_M = \int \sigma_M(\lambda) \cdot F(\lambda) \cdot \Phi_M(\lambda) \cdot d\lambda \qquad \text{(X)}$$

where $\sigma_M(\lambda)$ is the absorption cross section, $F(\lambda)$ is the actinic flux, and $\Phi_M(\lambda)$ is the quantum yield to photo-dissociation. For NO_2 the quantum yield is close to 1 over the whole absorption band. Assuming a unity quantum yield over the whole absorption band in NDMA results in the photolysis rate shown in Figure 5.61 (the UV-VIS molar extinction is shown in Figure 5.7, page 46). The relative photolysis rate of NO_2 and NDMA is nearly constant throughout the experiment: $j_{NDMA} : j_{NO2} \approx 0.55$. One may therefore, to a good approximation, scale the NDMA photolysis to that of NO_2.
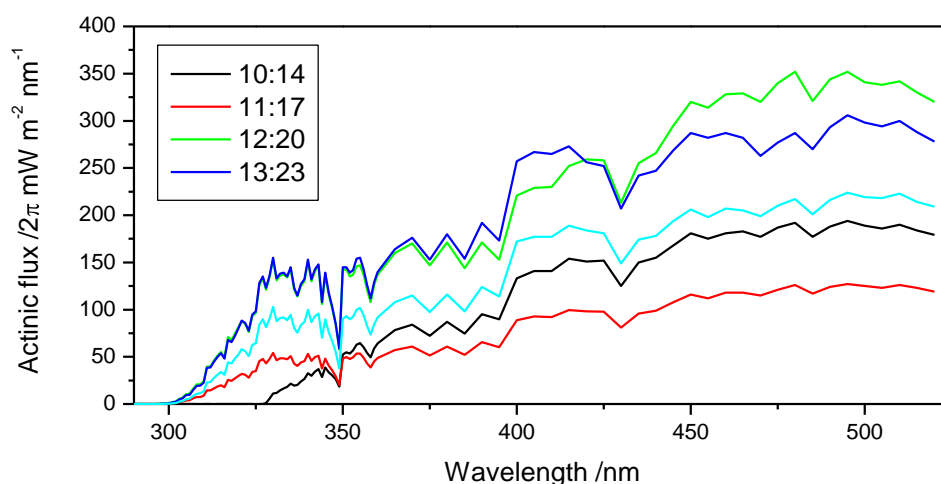
Figure 5.59. Actinic UV-A and UV-B flux on March 23, 2010.
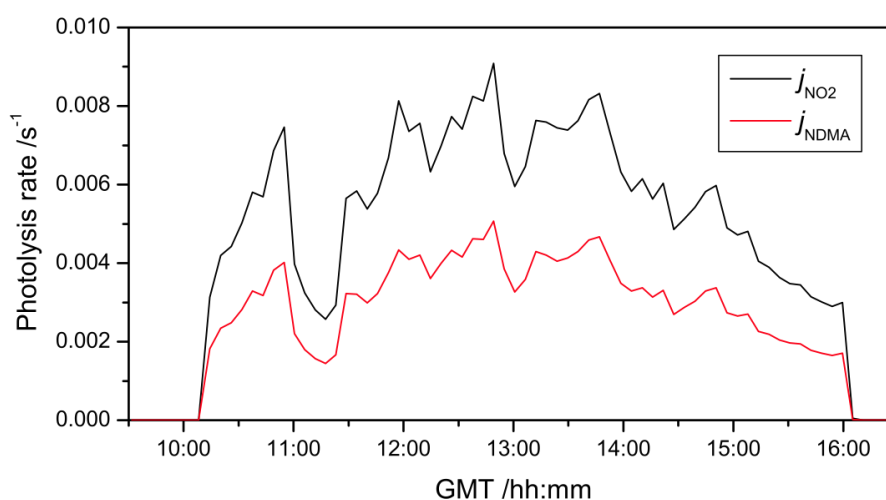
Figure 5.60. Calculated photolysis frequencies of NO_2 and $(CH_3)_2NNO$ (NDMA) during the experiment on March 23, 2010. The calculated photolysis rate of NDMA assumes a unity quantum yield over the entire absorption band.

Figure 5.61 shows the observed time profiles of NDMA in the four photolysis experiments together with the decay calculated using literature kinetic data. For all experiments it can be seen that the calculated NDMA loss is much faster than the observed decay. This can be due to either an overestimation of the quantum yield to photolysis, an underestimation of the $(CH_3)_2N+NO$ back reaction or a
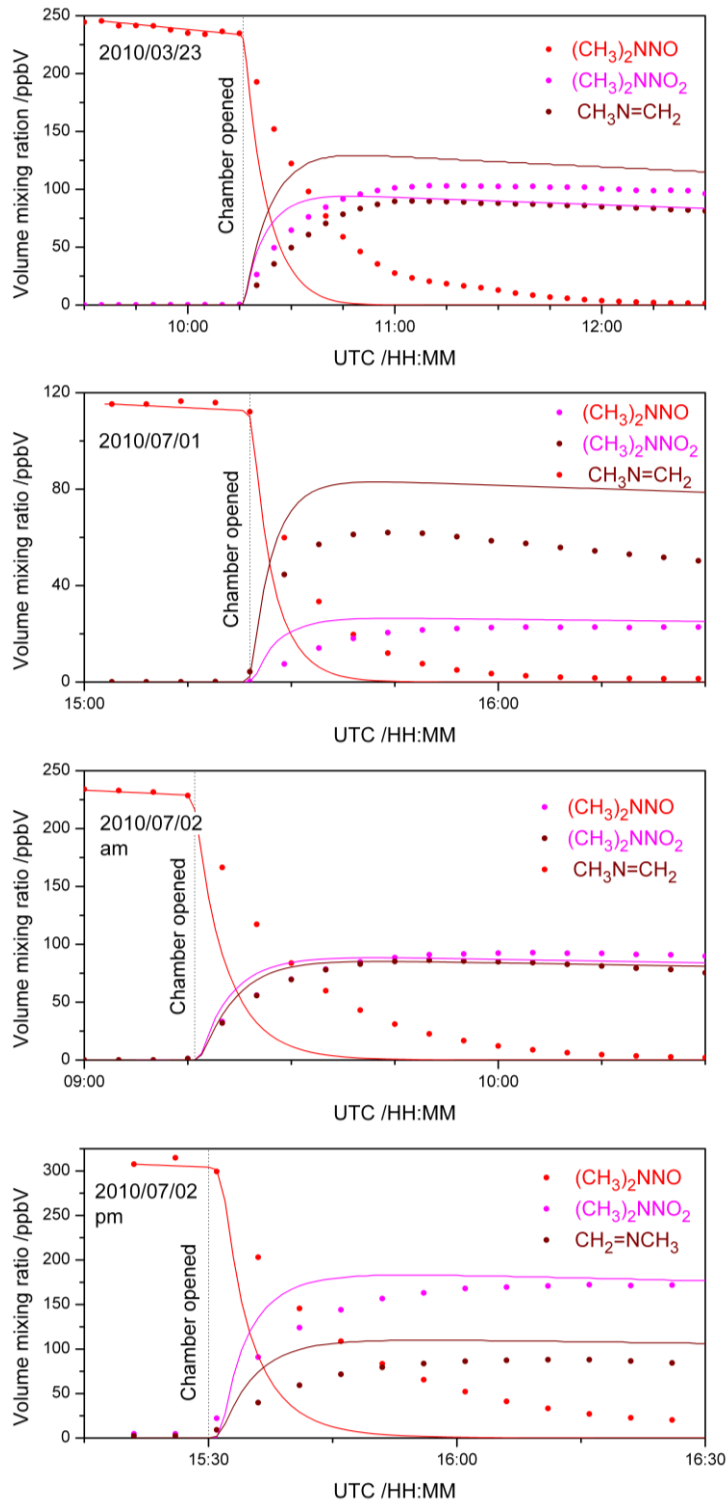
Figure 5.61. Observed and literature model mixing ratios of *N*-nitroso dimethylamine (NDMA), *N*-nitro dimethylamine (DMNA), *N*-methyl methanimine (MMI) in the 2010/03/23, 2010/07/01, 2010/07/02 a.m. and 2010/07/02 p.m. experiments.

combination of both. Considering the different NOx conditions in the four experiments it is clear that quantum yield of NDMA photolysis is less than 1.

The best fit of the available data is obtained with $k_3/k_{4a} = 0.75$, $k_{2a}/k_{4a} = 3.0 \times 10^{-7}$, $k_{4b}/k_{4a} = 0.1$, $k_{2b}/k_{4a} = k_{2c}/k_{4a} = 1.5 \times 10^{-8}$ and $j_{NDMA} : j_{NO2} = 0.25$. The latter number implies that the quantum yield to N-nitroso dimethylamine photolysis in the gas
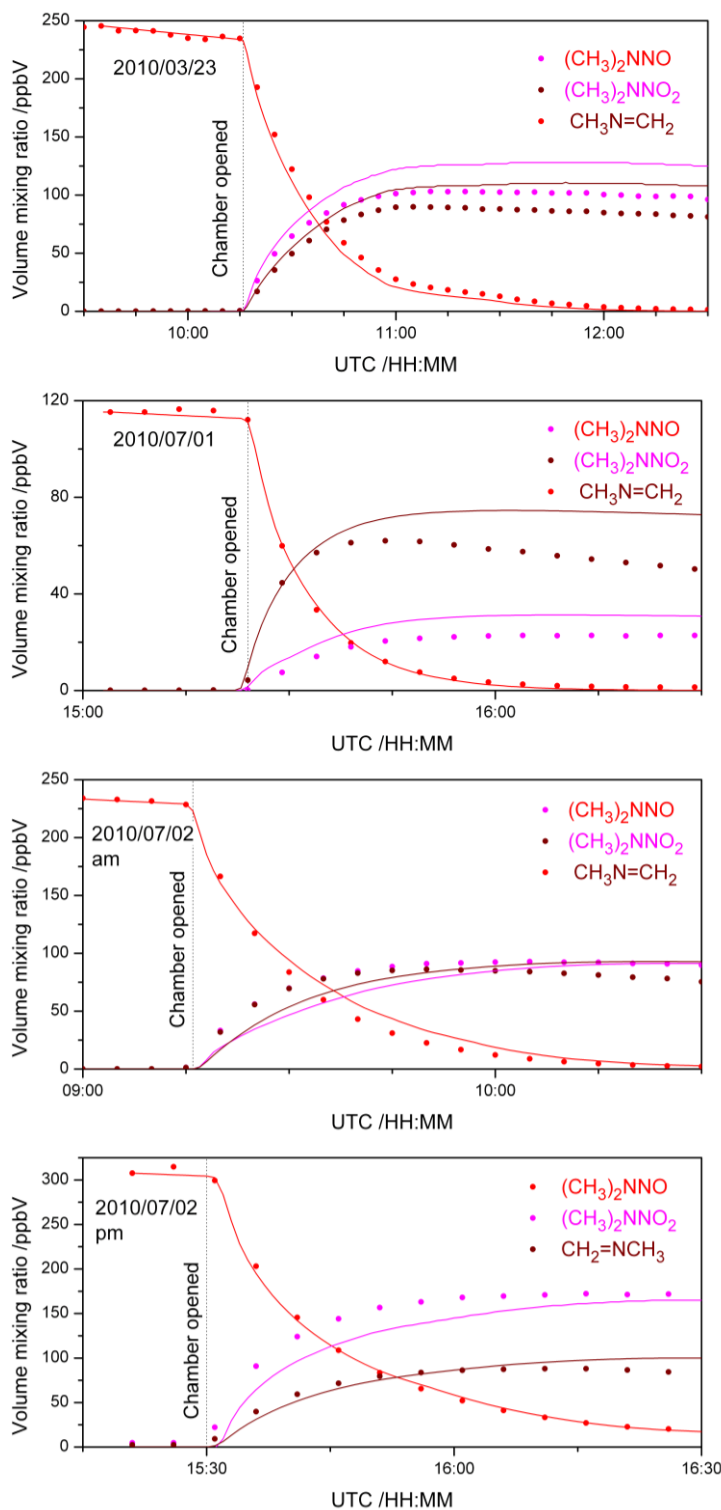
Figure 5.62. Observed and modelled mixing ratios of N-nitroso dimethylamine (NDMA), N-nitro dimethylamine (DMNA), N-methylmethanimine (MMI) in the 2010/03/23, 2010/07/01, 2010/07/02 a.m. and 2010/07/02 p.m. experiments.

phase is around 0.45. For comparison, the quantum yield to *N*-nitroso dimethylamine photolysis is reported to be 0.04-0.08 (MeOH) and 0.12 (cyclohexane).[143]

Figure 5.62 compares the observations and the modelled NDMA photolysis experiments. The present experiments unambiguously show that the photolysis rate constant of NDMA is less than half of what was reported by Tuazon *et al.*[37] That is, photolysis of N-nitroso dimethylamine is by a factor of two slower than previously believed. Further, the present experiments clearly show that CH_3NO_2 is a minor, <u>primary</u> product in the reactions following NDMA photolysis.

Table 5.15. Comparison of relative rate constants relating to the branching of the dimethylamino radical reactions in the atmosphere.

	k_2/k_{4a}	k_{4b}/k_{4a}	k_3/k_{4a}	j_5/j_{NO2}
Lindley *et al.*[33]	$(3.90 \pm 0.28) \times 10^{-7}$	0.22 ± 0.06	0.26	
Tuazon *et al.*[37]				0.53
This work	3.0×10^{-7}	0.10	0.75	0.25

5.14 CH$_3$NHNO$_2$ photo-oxidation studies

The experiments were unsuccessful in the sense that no products were detected in amounts significantly above the background artifacts from the Innsbruck chamber. The reaction of CH$_3$NHNO$_2$ and OH radicals is slower than expected which makes it difficult to observe products, which probably are more reactive than the parent molecule. Quantum chemistry studies suggest that N-nitro formamide should be the major product:

$$CH_3NHNO_2 + OH \quad \rightarrow \quad CHONHNO_2 + H_2O \tag{52}$$

The FT-IR spectra obtained during the kinetic studies (see also section 5.20, page 121) are currently being analyzed.

5.15 CH$_2$=NCH$_3$ photo-oxidation studies

The gas phase chemistry of *N*-methyl methanimine was studied under various NOx conditions. It was common to all experiments that heterogeneous reactions interfered to such an extent that it was difficult to extract explicit informations. This is exemplified in Figure 5.63 in which uncalibrated PTR-TOF data (in normalized counts) from a high-NOx experiment (>150 ppbV NO$_2$) are shown.
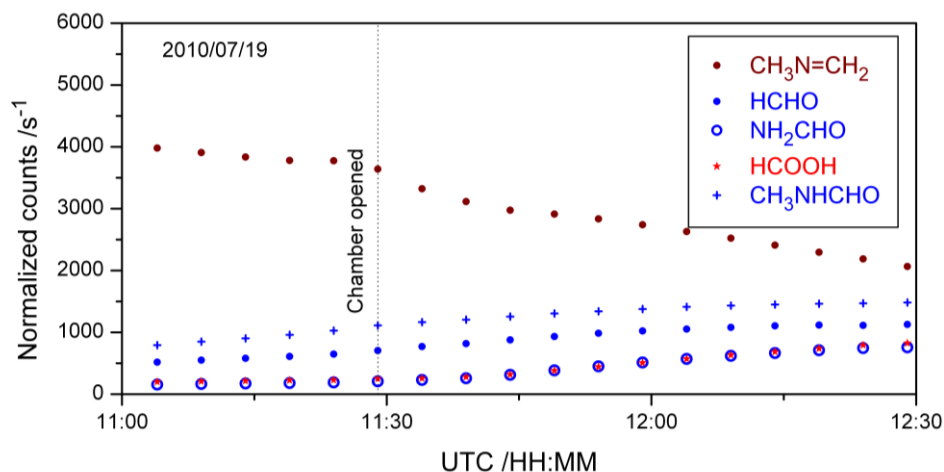
Figure 5.63. Normalized ion counts registered during the high-NOx *N*-methyl methanimine photo-oxidation experiment on 2010/07/19.

Products start to form already in the dark and there is no immediately evident gradient in product formation upon chamber opening. However, a change in the product formation becomes evident when plotting the "product" signals versus the N-methyl methanimine signal, Figure 5.64. The obtained data warrant further experimental investigations and we will at present not offer any gas phase mechanistic interpretation of the obtained results.
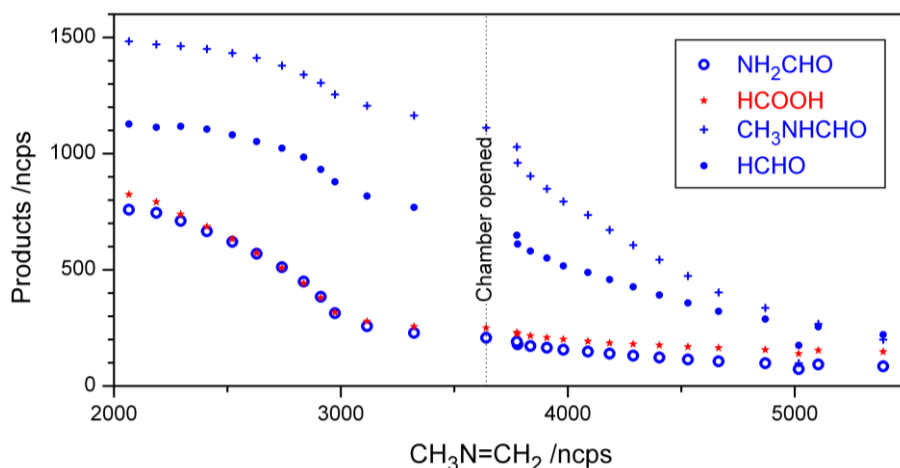
Figure 5.64. Correlation of product vs. reagent ion counts registered during the high-NOx *N*-methyl methanimine photo-oxidation experiment on 2010/07/19.

5.15.1 Analysis of aerosol formation

In all experiments with N-methyl methanimine (MMI) two nucleation events occurred. The first event occurred after addition of the substance to the chamber already containing NO_x and the second event occurred directly after opening the chamber (Figure 5.65).
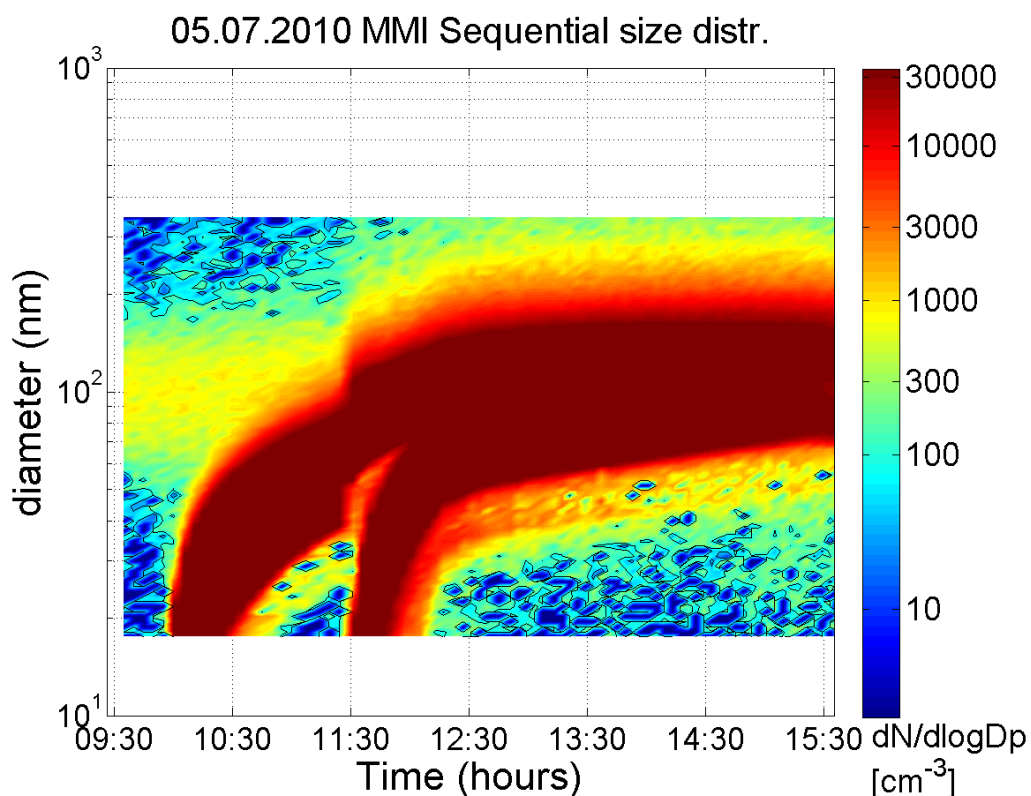
Figure 5.65. Sequential number size distribution (dN/DlogDp in # cm^{-3}) as recorded by SMPS during the experiment on July 5, 2010. SMPS lower cut-off is at 17.5 nm. A first particle burst occurred in the dark chamber after MMI addition and a second occurred directly after the canopy was opened.

In the two MMI experiments performed on July 5 and 19, 2010 the volatility of the produced aerosol increased after opening the chamber. The VTDMA data are shown in Figure 5.66 and Figure 5.67. The observed particles were different from particles which are typically produced from oxidation of organics in chamber studies and whose volatility decreases with time exposure to sunlight. In both MMI experiments the aerosol was of low volatility after exposure to sunlight for about 1 hour.
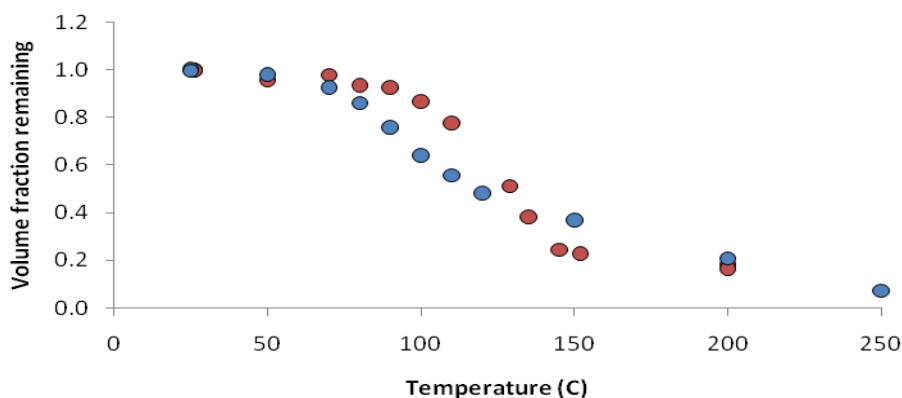
Figure 5.66. Volume fraction remaining versus evaporative temperature for one high NOx-experiment on *N*-methyl methanimine on July 19, 2010. 20 minutes before the chamber was opened (red circles) and 1 hour after the chamber was opened (blue circles).
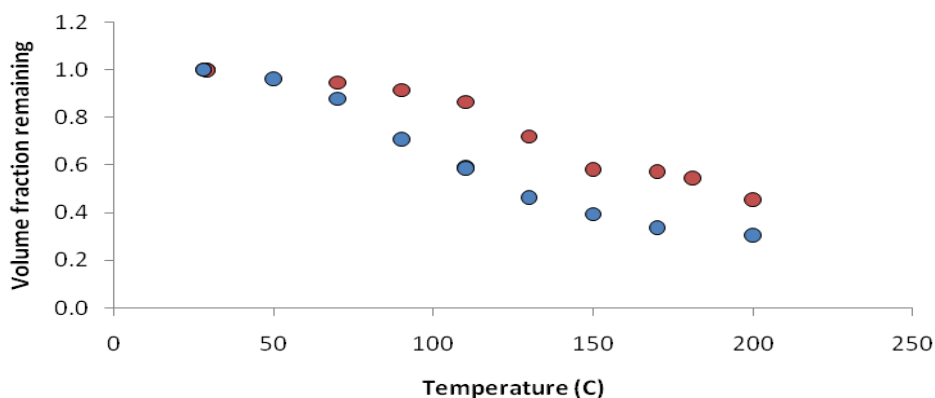
Figure 5.67. Volume fraction remaining versus evaporative temperature for one high NO$_x$-experiments on *N*-methyl methanimine on July 5, 2010. 1 hour before the chamber was opened (red circles) and 1 hour 40 minutes after the chamber was opened (blue circles).

Analysis of the AMS thermograms confirmed the low volatility of the aerosol. Two thermograms between 25°C and 200°C were performed with the AMS set up during the experiment on July 5, 2010, between 13:52 - 14:08 UTC and 15:26 - 15:48 UTC (dark conditions). During thermogram 1, 17% of initial nitrate mass was in the aerosol at 150°C and during thermogram 2, 12 % of the initial nitrate mass was still in the aerosol at 150°C.

Figure 5.68 depicts the evolution of the AMS and the SMPS data during the experiment on July 5, 2010. The experiment was performed with a controlled injection of 10 ppbV of NO_x and the addition of H_2O_2. The chamber was opened at 11:27 UTC and closed at 15:12 UTC. No *N*-methyl methanimine nitrate (MMINO$_3$) reference was available; therefore ionization efficiencies of MMANO$_3$ have been used for AMS quantification. Good agreement for the 30 eV and 70 eV AMS data was achieved. By applying an effective density D_{va}/D_m between 1.08 (10:30 UTC) and 1.20 (13:30 UTC) to the SMPS data, the AMS total aerosol mass (ammonia + nitrate+ organics) and the D_{va}/D_m corrected SMPS total concentration show good agreement. An underestimation of the AMS mass loading is visible due to the small size of the particles; i.e. the mobility diameter of the aerosol V_m starts to be larger than 100 nm at 12:00 UTC.
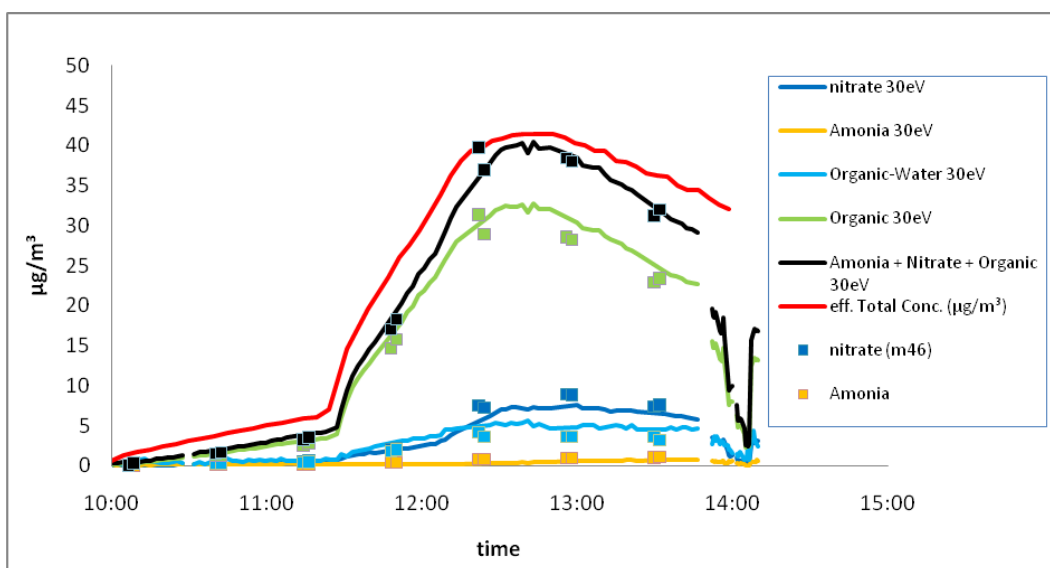
Figure 5.68. Mass loading for nitrate, ammonia, organics and organic-Water for 30 eV (lines), 70 eV (squares) and effective SMPS total concentration during the MMI experiment on July 5, 2010.

A maximum aerosol mass loading of about 39 µg/m³ has been detected around 12:40 UTC, about 1h 10min after the chamber was initially opened. At this time about 82% of the total loading was formed by organics, about 18% as nitrate, 32 µg/m³ and 7 µg/m³ respectively. Similar to other low NO_x experiments, the organic fraction dominated during the whole experiment. Due to the lack of a pure MMINO$_3$ reference, an estimation of the primary salt contribution could not be given.

Modelled particle mass concentrations obtained in a MAFOR simulation of the experiment on July 5, 2010, starting short after exposure to sunlight, overestimated the slope of the concentration increase of organics and underestimates the total concentrations of nitrates and organics at later stages of the experiment (Figure 5.69).

05.07.2010 Particle mass conc.
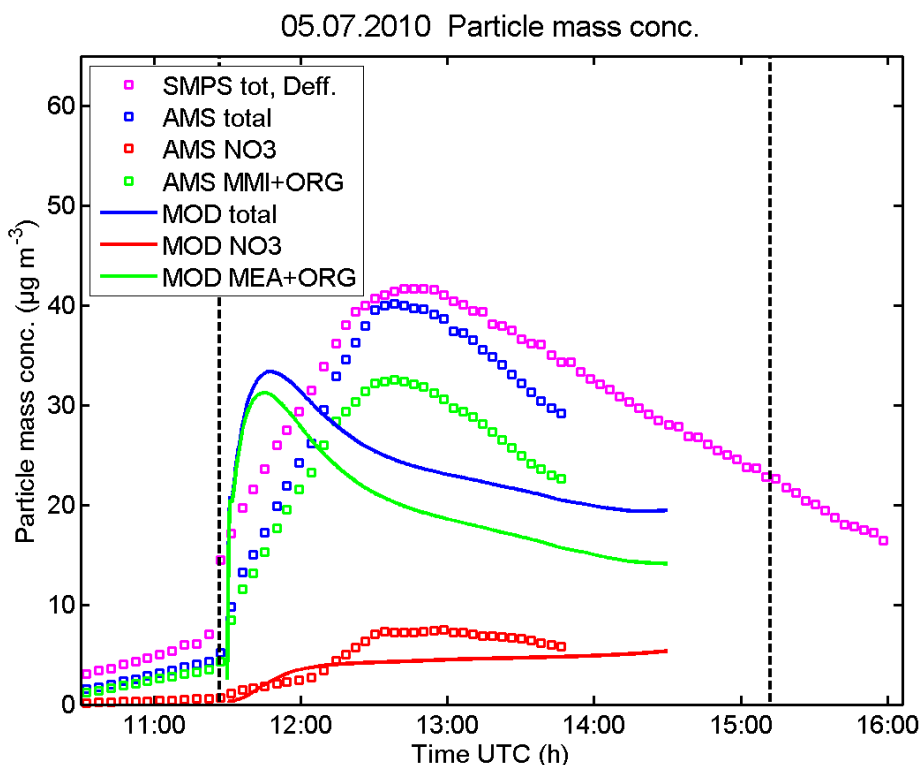
Figure 5.69. Comparison of modelled particle mass concentration (in µg m^{-3}) of aerosol components with measured mass concentrations by AMS (red, green an blue squares), and by SMPS (magenta squares) for the MMI experiment on 05 July, 2010. Increase of modelled particle mass concentration of total organics including MMI (green line) shows a steeper slope than AMS measured organics (green squares).

Summary. According to the MAFOR model, most MMI was lost to the walls during this experiment (~77%) and only a small fraction (~18%) reacted with OH radicals to produce gas phase and condensed phase compounds. About 6% ended up in the aerosol in the form of MMINO$_3$. The second increase of nitrate measured by AMS at about 13:30 UTC was not reproduced by the model indicating that this increase was from other secondarily formed, non-MMI, nitrates. SOA was formed in high yield in the oxidation of MMI (70%). The modelled increase of the concentration of particulate organics is too steep although the measured gas-phase concentration time series of MMI is fitted well by the model. At later stages in the experiment obviously other semi-volatile or low-volatile vapours contributed to the growth of the aerosol, that were either formed in secondary gas-phase reactions of MMI-products or not originating from the oxidation of MMI at all.

Observation of a nucleation event in dark conditions before significant nitrate particle formation started, suggests that the injected MMI precursor, i.e. the trimer of MMI, is a nucleating compound. The total aerosol yield in the experiment on July 5, 2010, was predicted by MAFOR to be 18%. Even with the involved uncertainties, both in the performance of the experiment and in the model simulation, it can be concluded that MMI has a high aerosol formation potential and that the formed aerosol has a low volatility.

5.16 (CH₃)₂NNO₂ photo-oxidation studies

The experiments were successful in the sense that products were detected in amounts above the background artifacts from the Innsbruck chamber. The reaction of $(CH_3)_2NNO_2$ and OH radicals is slow which makes it difficult to observe products that are more probably more reactive than the parent molecule. The major product ion m/z 105.02965 corresponds to an ion formula $C_2H_5N_2O_3^+$, in agreement with the results from quantum chemistry studies suggesting that *N*-nitro,*N*-methyl formamide should be the major product:
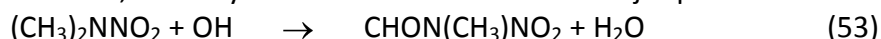
$$(CH_3)_2NNO_2 + OH \quad \rightarrow \quad CHON(CH_3)NO_2 + H_2O \tag{53}$$

The FT-IR spectra obtained during the kinetic studies (see also section 5.20, page 121) are currently being analyzed.

5.17 NH₂CHO photo-oxidation studies

Photo-oxidation experiments were carried out in the "Innsbruck-reactor" employing PTR-TOF-MS detection and in the "Oslo-reactor" employing FT-IR detection. The PTR-TOF-MS showed only one single product ion in the OH-initiated photo-oxidation at m/z 44.042, with CH_2NO^+ being the sum formula of the protonated molecule. The FT-IR spectra, Figure 5.70, identified the product as isocyanic acid, HNCO. Barnes *et al.*[52] also report HNCO as the only product in NOx-free photo-oxidation of formamide.
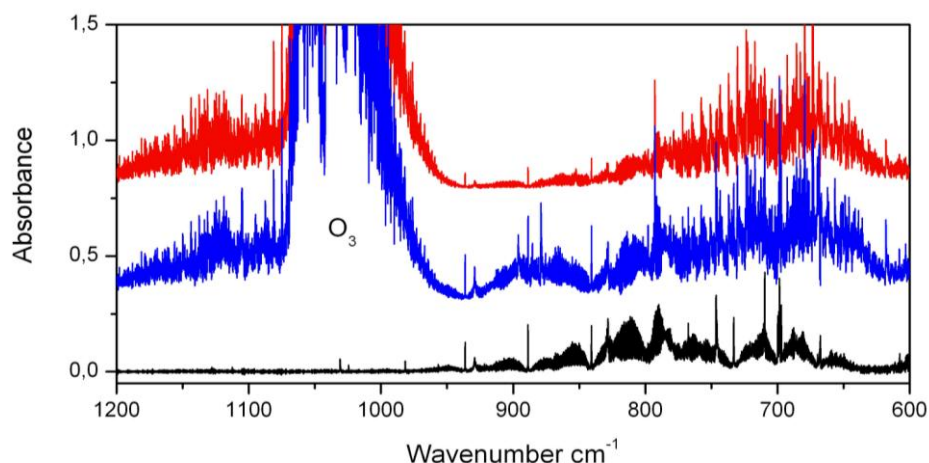
Figure 5.70. Infrared spectra of the 1200-600 cm^{-1} region of a formamide / O_3 /H_2 mixture during a photo-oxidation experiment. Red curve, after 1 min. photolysis; blue curve, after 5 min. photolysis; black curve, reference spectrum of isocyanic acid (HNCO).

There are two possible sites for the initial H-abstraction from formamide, **Scheme 5.5**, both leading to the same final product. Information about the site of initial H-abstraction is needed to obtain a structure-activity relationship for amides. Quantum chemistry calculations predict the following enthalpies of reaction:

$$\Delta H^{\ominus} = -99 \qquad NH_2CHO + OH \quad \rightarrow \quad NH_2CO + H_2O \tag{54a}$$

$$\Delta H^{\ominus} = -15 \qquad \qquad\qquad\qquad \rightarrow \quad NHCHO + H_2O \tag{54b}$$

The bond enthalpy is consequently around 80 kJ mol^{-1} higher for the N-H bond than for the C-H bond in formamide, and one therefore expects C-H abstraction to be the dominant route in the OH reaction with formamide.
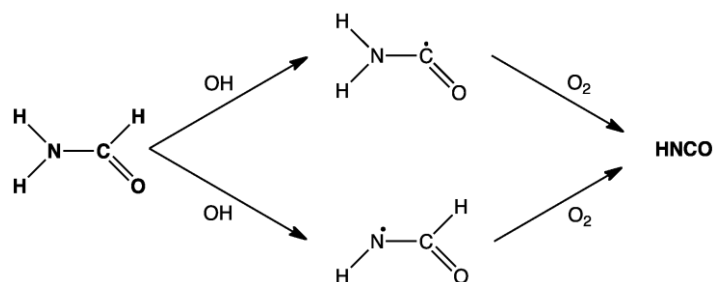
Scheme 5.5. Reaction scheme for the OH initiated photo-oxidation of formamide.

5.18 CH₃NHCHO photo-oxidation studies

Figure 5.71 shows the time-integrated molar increase in CH₃NHCHO photo-oxidation products (detected in their protonated forms at m/z 28.019, 31.018, 44.014, 46.030, 58.030, 74.024, 77.035) relative to the time-integrated decrease of *N*-methylformamide (detected in its protonated form at m/z 60.045) during the first 30 minutes of the photo-oxidation experiment. Only products with a relative increase > 2 % have been included in the figure. The observed ion signals are assigned as follows: m/z 28.019 (protonated HCN, cannot be reliably quantified without external calibration), m/z 31.018 (protonated formaldehyde, cannot be reliably quantified without external calibration), m/z 44.014 (protonated isocyanic acid), m/z 46.030 (protonated formamide), m/z 58.030 (protonated methylisocyanate), m/z 74.024 (protonated N-formyl formamide), m/z 77.035 (protonated methylnitramine). In addition, we observed the formation of methanol, acetaldehyde, formic acid and acetic acid. These are compounds which are typically formed in any smog chamber photo-oxidation

Figure 5.71.   Mass spectral difference measured during the photo-oxidation of *N*-methylformamide. Mass peaks of intensity < 2 % of $\Delta I_{60.045}$ are omitted.
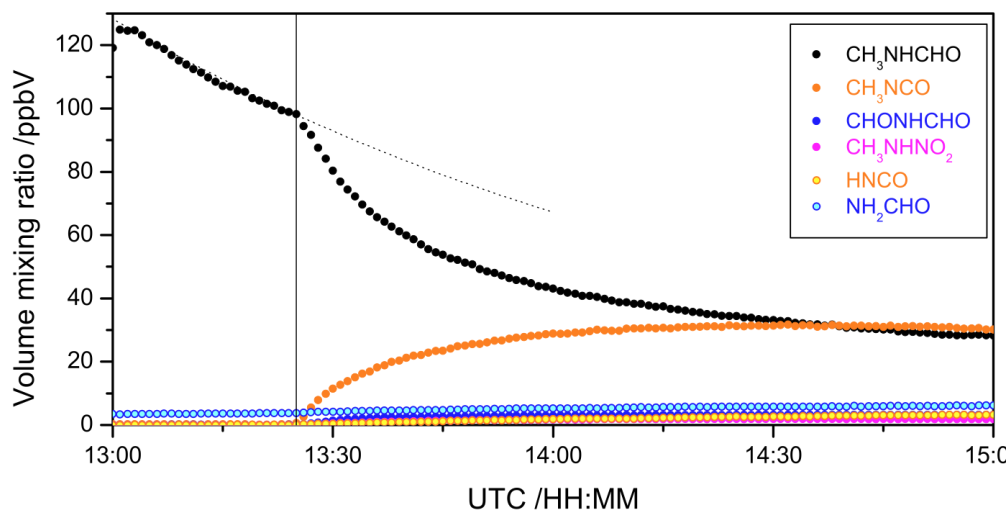
Figure 5.72.   Time evolution of *N*-methylformamide and photo-oxidation products as observed in the experiment on 2010/09/01. The dotted curve represents the extrapolated wall loss of *N*-methylformamide.

experiment, *i.e.* even in the absence of CH₃NHCHO. Figure 5.72 shows the time evolution of the main ion signals during the photo-oxidation experiment, while Figure 5.73 shows the main increasing products enhanced by a factor of 10.

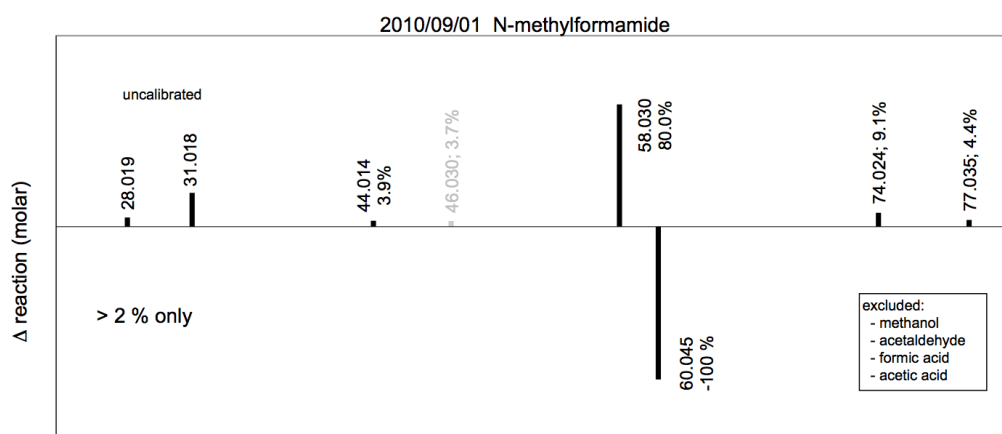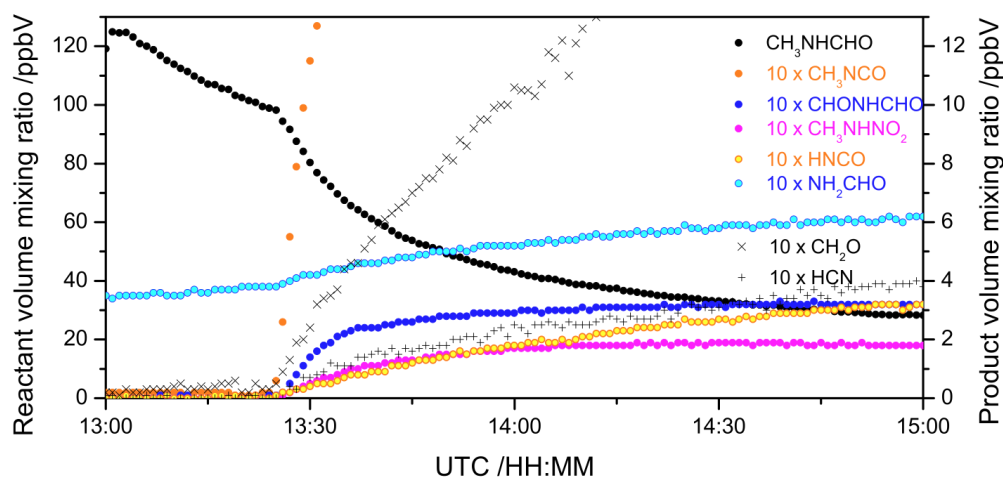**Figure 5.73**.   Time evolution of ion signals observed during photo-oxidation of *N*-methylformamide. The product ion signals have been enhanced by a factor of 10.

The wall loss of *N*-methylformamide was significant in the experiment: from the loss curve before start of photo-oxidation a loss rate of $k_{wall\ loss} \approx 1.5 \times 10^{-4}\ s^{-1}$ is extracted. In addition, the chamber temperature increased from 25 °C to 35 °C during the experiment. It can be seen that formamide was released from the chamber walls when *N*-methylformamide was added to the chamber and was therefore present from the start of the photo-oxidation experiment. Further, the HNCO signal is correlated to the formamide signal, indicating that HNCO may primarily stem from the photo-oxidation of formamide (see section 5.17, page 112). Small amounts of $CH_2=NH$, CH_2O and HCN were also observed in the experiment, the uncalibrated ion signals of the latter two species are included in Figure 5.72. The protonated methanimine signal is an order of magnitude smaller still. It is presently highly uncertain if CH_2O, HCN, NH_2CHO and HNCO are products of the *N*-methylformamide photo-oxidation or chamber artifacts due to spillover from previous experiments. In principle, both HCN and NH_2CHO may be products of methanimine photo-oxidation but no firm conclusion concerning this can, however, be made from the avilable experimental data.

A simplified scheme of the OH initiated photo-oxidation of *N*-methylformamide is shown in Scheme 5.6. The results in press by Barnes *et al.*[52] lists unquantified amounts of HN(CHO)₂, CH₃NHC(O)OONO₂ and CH₃NCO as products in the photo-oxidation of CH₃NHCHO. The present photo-oxidation experiment shows that CH₃NCO is the major primary product (~80 %) followed by *N*-formyl formamide (~10 %) and methylnitramine (~5 %). The PAN-type product, CH₃NHC(O)OONO₂, observed Barnes *et al.*,[52] is expected as a secondary product in the photo-oxidation of *N*-methylformamide. It was, however, not detected in the present experiments due to the high NO concentration in the present experiment, Figure 5.74.
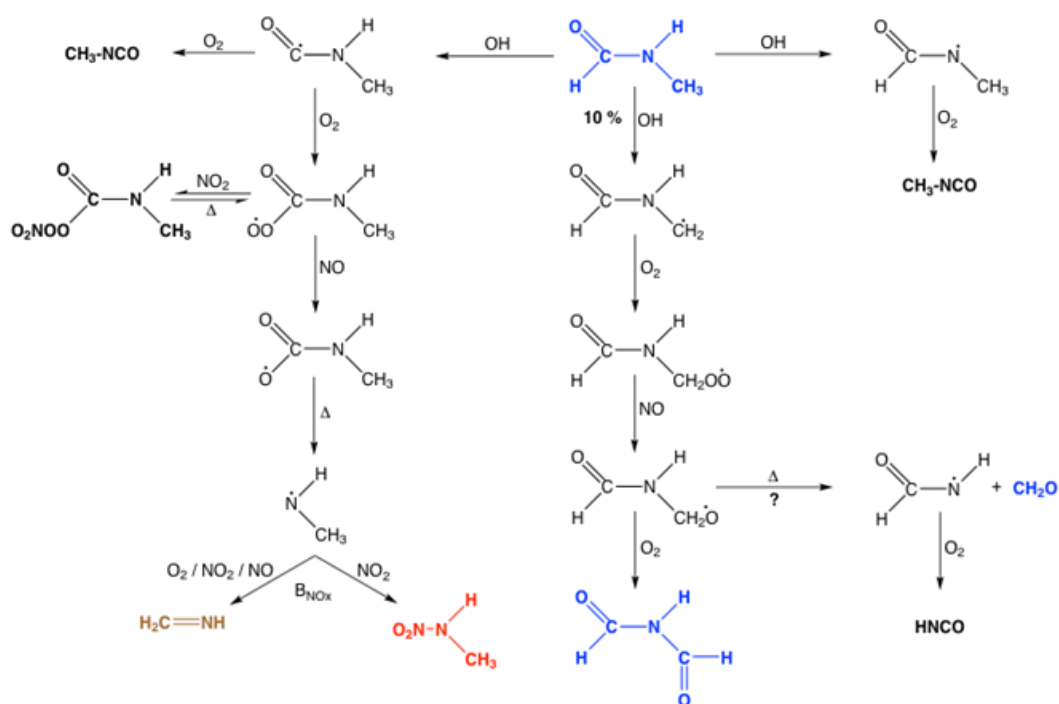
Scheme 5.6. Reaction scheme for OH initiated photo-oxidation of N-methyl formamide.

There are three possible routes of *N*-methylformamide reaction with OH radicals:
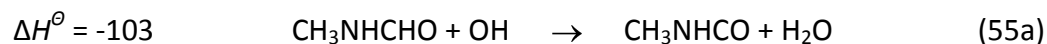
$\Delta H^{\ominus} = -103$	$CH_3NHCHO + OH$	$\rightarrow$	$CH_3NHCO + H_2O$	(55a)
$\Delta H^{\ominus} = -40$		$\rightarrow$	$CH_3NCHO + H_2O$	(55b)
$\Delta H^{\ominus} = -104$		$\rightarrow$	$CH_2NHCHO + H_2O$	(55c)

The reaction enthalpies listed ($\Delta H^{\ominus}$ /kJ mol^{-1}) refer to 298 K and to the lowest energy conformations of the species involved and stems from G3 calculations.[122] The calculated reaction enthalpies for the routes (55a) and (55c) are nearly identical, and, consequently, so are the bond enthalpies $\Delta_{bond}H_{C-H3}$ and $\Delta_{bond}H_{(O)C-H}$. Route (55b) is significantly less exothermic and the N-H bond enthalpy correspondingly larger. A first estimate of the branching in reaction (55) is therefore that routes (55a) and (55c) may be equally important, and that route (55b) can be neglected.

The unimolecular dissociation of the CHONCH$_2$O radical leading to CH$_2$O and, subsequently, to isocyanic acid is calculated to be endothermic by around 90 kJ mol^{-1}. The rate of this reaction is therefore expected to be negligible compared to the hydrogen abstraction by O$_2$. The quantum chemistry calculations therefore support that isocyanic acid is <u>not</u> a major product in the atmospheric photo-oxidation of *N*-methylformamide.

It can be seen from Scheme 5.6 that two of the initial routes, (29a) and (29b), result in same products products; the branching ratio between these routes can therefore not be determined from the observed product yields. The branching

ratio k_{29c}/k_{29} can be determined from the observed product yields assuming that *N*-formyl formamide will not react to any large extent with OH during the initial phase of the experiment, that its wall loss can also be neglected in the same time-span, and that the observed isocyanic acid stems from the formamide chamber artifact. Under these assumptions, the amount of *N*-formyl formamide formed corresponds to 9 ± 2 % of the reaction following route (29c).

The branching ratio between the two routes of the CH$_3$NH radical was discussed in section 5.10 (page 55). Given the measured NO and NO$_2$ mixing ratios shown in Figure 5.74 and the observed yield of CH$_3$NHNO$_2$ in a the photo-oxidation of *N*-methylformamide implies that 7 ± 2 % of the initial reaction follows leads to this product. Finally, the amount of CH$_3$NCO formed corresponds to 75 ± 5 % of the total reaction. The wall loss, extrapolated from the *N*-methylformamide loss before start of the reaction, and the observed products (CH$_3$NCO, CHONHCHO and CH$_3$NHNO$_2$) balances 91 % of the total *N*-methylformamide lost during the first 15 minutes of the experiment, the wall loss being associated with the major uncertainty. Normalizing the results give: 82 ± 6 % CH$_3$NCO, 8 ± 3 % CH$_3$NHNO$_2$ and 10 ± 3 % CHONHCHO ($k_{29c}/k_{29} = 0.10 \pm 0.03$).
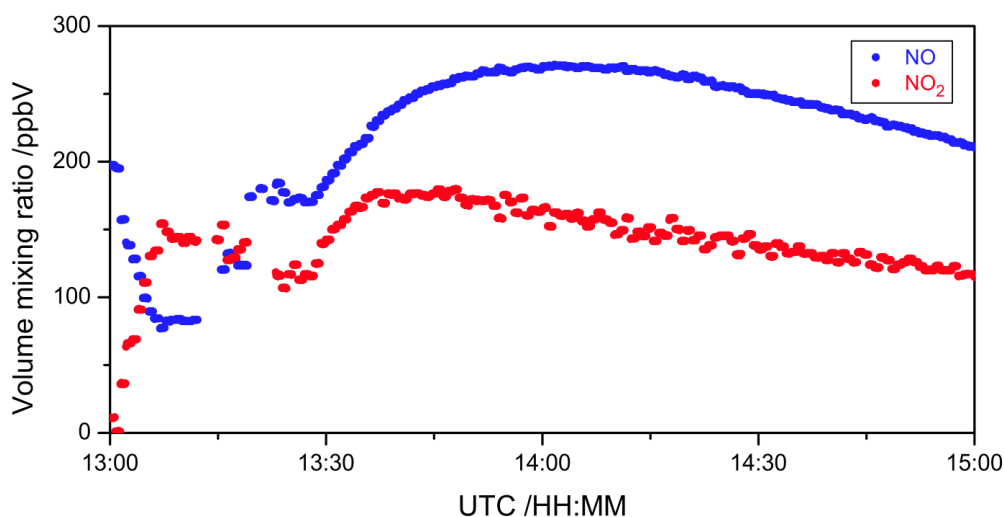
Figure 5.74.   Volume mixing ratios of NO and NO$_2$ during the photo-oxidation of *N*-methylformamide on 2010/09/01.

5.19 (CH₃)₂NCHO photo-oxidation studies

Figure 5.75 shows the time-integrated molar increase in $(CH_3)_2NCHO$ photo-oxidation products (detected in their protonated forms at m/z 31.019, 44.014, 44.050, 45.993, 58.029, 72.045, 75.055, 80.040 and 91.050) relative to the time-integrated decrease of *N,N*-dimethylformamide (detected in its protonated form at m/z 74.060) during the first 30 minutes of the photolysis experiment. Only products with a relative increase > 1 % have been included in the figure. The observed ion signals are assigned as follows: m/z m/z 31.019 (protonated form-aldehyde, cannot be reliably quantified without external calibration), m/z 44.014 (protonated isocyanic acid), m/(z 44.050 (protonated *N*-methylmethanimine), m/z 45.993 (NO_2^+ from unidentified compound), m/z 58.029 (protonated methylisocyanate), m/z 72.045 (protonated $(CH_3)_2NCO^+$, from $(CH_3)_2NC(O)OONO$?), m/z 75.055 (protonated *N*-nitroso dimethylamine), m/z 88.040 (protonated *N*-formyl,*N*-methyl formamide) and m/z 91.050 (protonated *N*-nitro dimethyl-amine). In addition, we observed the formation of methanol, acetaldehyde, formic acid and acetic acid. These are compounds which are typically formed in any smog chamber photo-oxidation experiment, *i.e.* even in the absence of $(CH_3)_2NCHO$.

31.08.2010 N,N-dimethylformamide

excluded: acetaldehyde, formic acid, acetone, acetic acid
*: potential artifact

31.019 uncalibrated
44.014 * 3.7%
44.050 8.4%
45.993 4.0%
58.029 3.2%
72.045 2.7%
75.055 16.4%
88.040 37.4%
91.050 27.9%
74.060 -100.0%

Δ reaction
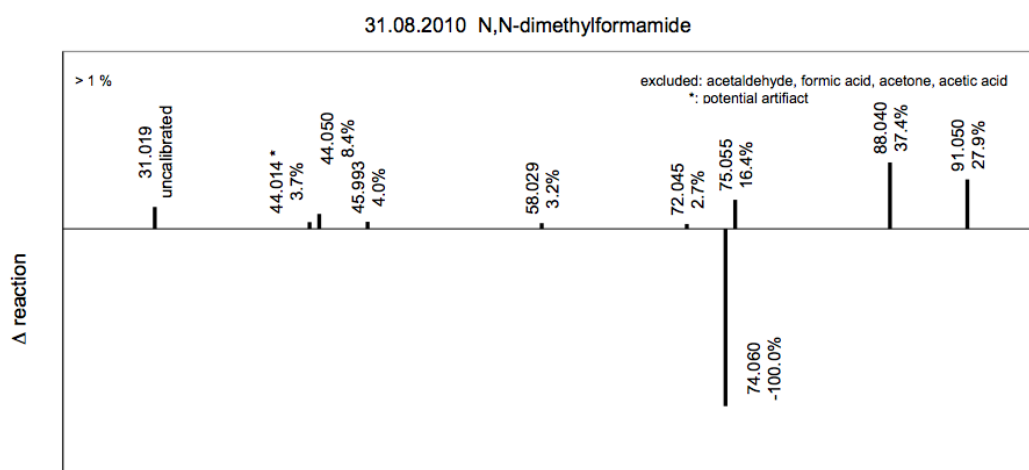
Figure 5.75. Mass spectral difference measured during the photo-oxidation of *N,N*-dimethylformamide. Mass peaks of intensity < 1 % of $\Delta I_{74.060}$ are omitted.

Figure 5.76 shows the time evolution of the main compounds during the photo-oxidation experiment, while Scheme 5.7. shows a simplified photo-oxidation scheme for *N,N*-dimethylformamide.
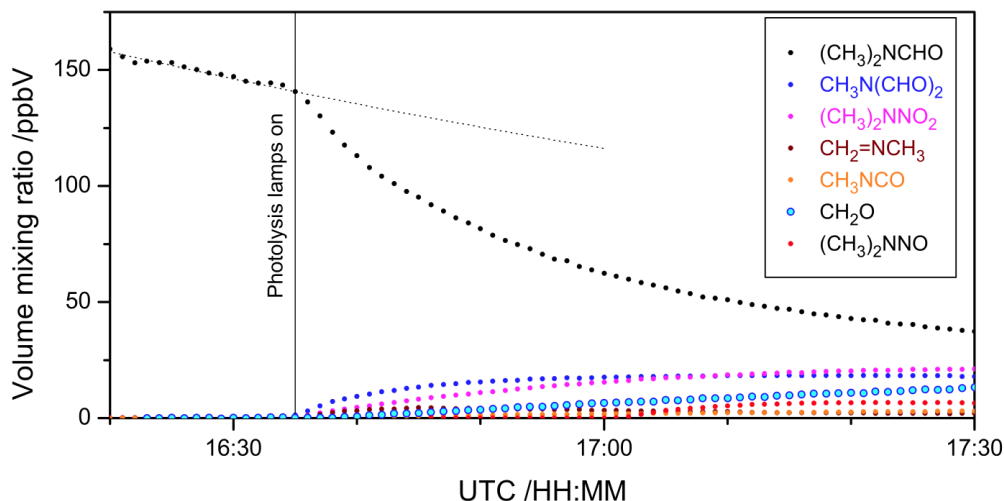
Figure 5.76. Time evolution of the main ion signals observed during photo-oxidation of *N,N*-dimethylformamide.

The results in press by Barnes *et al.*[52] lists only unquantified formation of $CH_3N(CHO)_2$ and $(CH_3)_2NC(O)OONO_2$ in the photo-oxidation of $(CH_3)_2NCHO$. The PAN-type compound, $(CH_3)_2NC(O)OONO_2$, which is expected in the photo-oxidation of $(CH_3)_2NCHO$ was not detected in the present experiments due to the high NO concentration, Figure 5.77. The two possible routes of N-methyl formamide reaction with OH radicals leads to different products. The individual product yields therefore give a direct measure of the branching ratios in the photo-oxidation, Scheme 5.7.

Scheme 5.7. Reaction scheme for OH initiated photo-oxidation of N,N-dimethyl formamide.
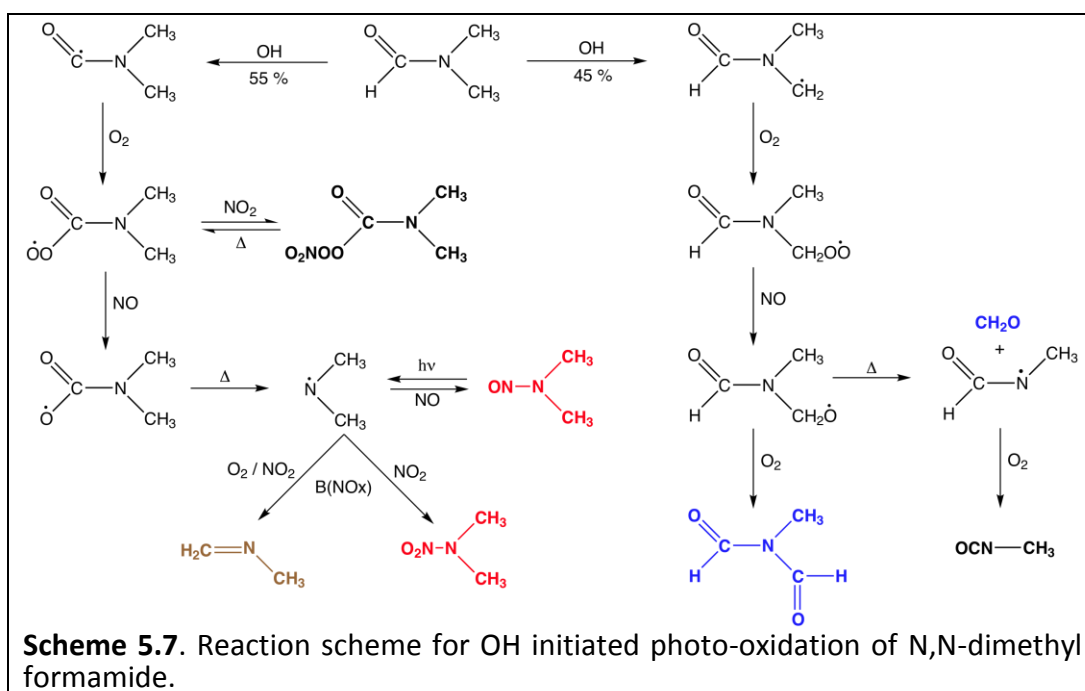
There are two routes to the photo-oxidation of *N,N*-dimethylformamide and each route has its unique products. The branching ratio in the initial reaction can therefore be determined from analysis of the product yields. Assuming that

N-formyl,*N*-methyl formamide does not react to any large extent during the initial phase of the experiment one may derive that 45 ± 5 % of the hydrogen abstraction reaction of *N,N*-dimethylformamide with OH radicals takes place at the methyl groups while 55 ± 5 % of the initial hydrogen abstraction reaction takes place from the –CHO group.
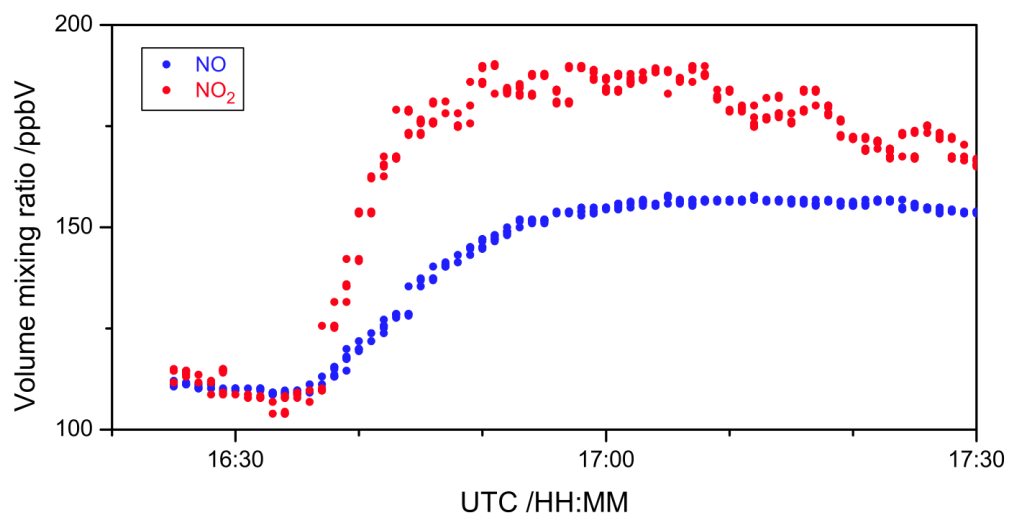
Figure 5.77.   Volume mixing ratios of NO and NO_2 during the photo-oxidation of *N,N*-dimethylformamide on 2010/08/31

5.20 Kinetic study of OH + CH₃NHNO₂ and OH + (CH₃)₂NNO₂

The kinetic study was carried out by the relative rate method in a static gas mixture, in which the removals of the reacting species are simultaneously measured as a function of reaction time. Assuming that the reactants react solely with the same radical and that none of the reactants are reformed in any side reactions, the relative rate coefficient, k_{rel}, is given according to eq (VII):

$$\ln\left\{\frac{[S]_0}{[S]_t}\right\} = k_{rel} \cdot \ln\left\{\frac{[R]_0}{[R]_t}\right\} \quad ; \quad k_{rel} = \frac{k_S}{k_R}$$

$$(XI)$$

where $[S]_0$, $[R]_0$, $[S]_t$ and $[R]_t$ are concentrations of the substrate (nitramin) and the reference compound at start and at the time t, respectively, and k_S and k_R are the corresponding rate coefficients. A plot of $\ln\{[S]_0/[S]_t\}$ vs. $\ln\{[R]_0/[R]_t\}$ will thus give the relative reaction rate coefficient $k_{rel} = k_N/k_R$ as the slope.

All experiments were carried out in synthetic air (AGA 99.99%; CH₄, CO and NO$_x$ < 100 ppbV) at 298 ± 2 K and 1013 ± 10 hPa. The experiments were repeated several times with different mixing ratios of the reactants in the range 2-10 ppmV in 1013 hPa synthetic air. Data collection was carried out in sequences: 128 scans were co-added at a nominal resolution of 0.5 cm^{-1} and Fourier transformed using boxcar apodization.

Hydroxyl radicals were generated by photolysis of O₃ in the presence of H₂ (99%, AGA). Ozone was produced from oxygen (99.995%, AGA) using a MK II ozone generator from BOC, which has a conversion efficiency of approximately 5%, and was collected in a trap filled with silica beads at 195 K. Typical partial pressures of ozone and hydrogen were 50 and 200 Pa, respectively. Photolysis of ozone was carried out at intervals of 2–10 min using two Philips TL12 UVB-lamps (λ_{max} ~ 305 nm).
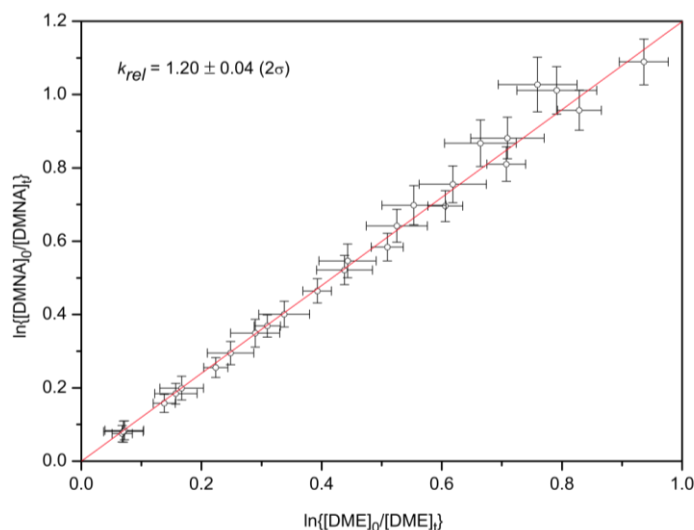
Figure 5.78. Plot of $\ln\{[(CH_3)_2NNO_2]_0/[(CH_3)_2NNO_2]\}$ *vs.* $\ln\{[CH_3)_2O]_0/[CH_3)_2O]_t\}$ during the reactions of $(CH_3)_2NNO_2$ and $(CH_3)_2O$ with OH radicals. 26 data points from 3 independent experiments were analysed to give $k_{rel} = 1.20 \pm 0.04$ (2σ)

Data from independent experiments were analyzed according to eq. (X) using a weighted least squares procedure which includes uncertainties in both reactant concentrations.[144] The uncertainties in the relative reactant concentrations were taken as 5 times the standard deviations from the least squares fitting of the experimental infrared spectra. If a dataset showed a *y*–intercept significantly different from zero, the experiment was discarded.

Figure 5.78 shows the results from 3 independent kinetic experiments in which the OH radical reaction with dimethylnitramine (DMN) was followed relative to that with dimethylether from which it is seen that $k_{OH+DMN}/k_{OH+CH3OCH3} = 1.20 \pm 0.04$ (2σ). This compares well with the previous results of Tuazon *et al.*[37] who found $k_{OH+DMN}/k_{OH+CH3OCH3} = 1.29 \pm 0.05$. Taking today's recommended absolute value for $k_{OH+CH3OCH3} = 2.8 \times 10^{-12}$ cm^3 molecule^{-1} s^{-1} at 298 K,[38] places an average value of $k_{OH+DMN} = (3.5 \pm 0.5) \times 10^{-12}$ cm^3 molecule^{-1} s^{-1}.

Figure 5.79 summarises the data from 2 experiments giving a relative rate 0.85 ± 0.04 (2σ). Taking the currently recommended value of $k_{OH+CH3OH} = (9.0 \pm 0.7) \times 10^{-13}$ cm^3 molecule^{-1} s^{-1} at 298 K[61] places $k_{OH+CH3NHNO2}$ on an absolute scale at $(7.7 \pm 0.7) \times 10^{-13}$ cm^3 molecule^{-1} s^{-1} at 298 K. For comparison $k_{OH+(CH3)2NNO2}$ is reported to be $(3.6 \pm 0.5) \times 10^{-12}$ cm^3 molecule^{-1} s^{-1}; that is OH reaction with CH_3NHNO_2 is more than 4 times slower than with $(CH_3)_2NNO_2$. Data have been obtained from relative rate experiments using $CH_3C(O)CH_3$ as reference compound and additional experiments employing CH_3OCH_3 as reference are underway to verify this somewhat unexpected result.
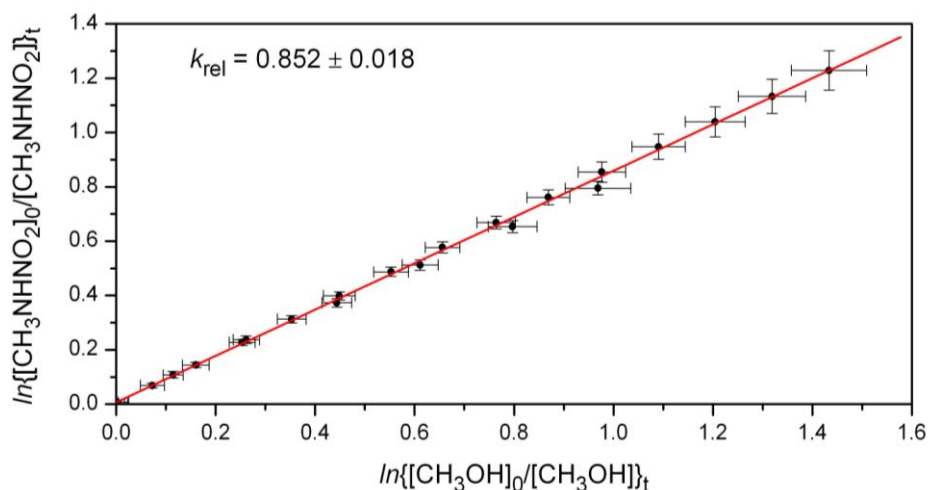
Figure 5.79.   Plot of $\ln\{[CH_3NHNO_2]_0/[CH_3NHNO_2]_t\}$ *vs.* $\ln\{[CH_3OH]_0/[CH_3OH]_t\}$ during reaction with OH radicals. 22 data points from 2 independent experiments were analysed to give $k_{rel} = 0.852 + 0.018$.

6 Conclusions from the photo-oxidation studies

The OH initiated photo-oxidation of three methylamines, monomethylamine (MMA), dimethylamine (DMA) and trimethylamine (TMA), *N*-methyl methanimine (MMI), and the photolysis of *N*-nitroso dimethylamine (NDMA) has been studied in two campaigns at the European Photochemical Reactor, EUPHORE, in Valencia (Spain). The experimental day-to-day variability spanned a wide range of conditions resulting in large differences in the various gas phase removal processes (photo-oxidation, aerosol formation, wall loss).

Branching ratios in the OH initiated photo-oxidation of MMA, DMA and TMA have been derived from the observed gas phase product distributions in the various experiments.

There are no previous results for the product distribution in the atmospheric photo-oxidation of methylamine. The present results show that around 25% of the initial OH reaction with methylamine is N-H abstraction, which in part results in nitramine formation. The other 75% of the initial OH reaction is C-H abstraction, of which only 15% results in the formation of formamide, while the remaining 85% results in imine formation ($CH_2=NH$). The amount of methylnitramine formed depends upon the NO_2 concentration. For rural areas where mixing ratios of NOx are 0.2-10 ppbV with an average ratio $NO:NO_2 = 1:2$,[145] the amount of methylnitramine formed will be less than 0.4% of the methylamine photo-oxidized. In summary, the OH-initiated atmospheric photo-oxidation of methylamine results in $\approx$10% NH_2CHO (formamide), $\approx$90% $CH_2=NH$ (methanimine) and less than 0.4% CH_3NHNO_2 (methylnitramine) under rural conditions. The atmospheric fate of $CH_2=NH$ is uncertain. Most likely the lifetime will be very short and the compound will hydrolyze in aqueous particles to give CH_2O (formaldehyde) and NH_3 (ammonia). Formamide has an estimated atmospheric lifetime of more than 1 day in the Mongstad area and the sole product of its reaction with OH radicals is HNCO (isocyanic acid). As isocyanic acid is a secondary product in the atmospheric photo-oxidation of methylamine it will by highly dispersed and it s not expected to reach any level of concern in the air masses. Isocyanic acid reacts very slowly with OH radicals and its major atmospheric fate is expected to be hydrolysis in aqueous particles forming CO and NH_3.

There are no previous results for the product distribution in the atmospheric photo-oxidation of trimethylamine. The present results show that around 40% of the initial OH reaction with trimethylamine results in the formation of N,N-dimethyl formamide. The other 60% of the initial OH reaction leads to the formation of the $(CH_3)_2N$ radical, which then, depending upon the NOx level, leads to *N*-nitroso and *N*-nitro dimethylamine formation. The major products in the OH-initiated photo-oxidation of trimethylamine are $CH_2=NCH_3$ (N-methylmethanimine) and $(CH_3)_2NCHO$ (*N,N*-dimethyl formamide). The atmospheric fate of *N*-methyl methanimine is uncertain. Most likely the lifetime will be very short and the compound will hydrolyze in aqueous particles to give CH_2O (formaldehyde) and CH_3NH_2 (methylamine). *N,N*-dimethyl formamide has

an estimated atmospheric lifetime of more than 1 day in the Mongstad area and the major product of its reaction with OH radicals includes CH_3NCO (methylisocyanate) and $CH_2=NCH_3$. As methylisocyanate is a secondary product in the atmospheric photo-oxidation of dimethylamine it will by highly dispersed and it is not expected to reach any level of concern in the air masses. Methylisocyanate reacts very slowly with OH radicals and its major atmospheric fate is expected to be hydrolysis in aqueous particles forming CO and CH_3NH_2.

For dimethylamine the present product distribution in the OH-initiated photo-oxidation is largely in agreement with the previous results of Lindley et al.[33] There has been a particular focus on the branching of the dimethylamino radical reactions with O_2, NO and NO_2 and here the present results differ significantly from the previous kinetic data of Lindley et al.[33] and the nitrosamine photolysis rate of Tuazon et al.[37]

The reactions involved in the formation of N-nitroso dimethylamine (NDMA) and N-nitro dimethylamine (DMN) from dimethylamine (DMA) are:

$$(CH_3)_2NH + OH \quad \rightarrow \quad (CH_3)_2N + H_2O \tag{1a}$$

$$\rightarrow \quad (CH_3)N(H)CH_2 + H_2O \tag{1b}$$

$$(CH_3)_2N + O_2 \quad \rightarrow \quad \textcolor{brown}{CH_2=N\text{-}CH_3} + HO_2 \tag{2}$$

$$(CH_3)_2N + NO \quad \rightarrow \quad \textcolor{red}{(CH_3)_2N\text{-}NO} \tag{3}$$

$$(CH_3)_2N + NO_2 \quad \rightarrow \quad \textcolor{magenta}{(CH_3)_2N\text{-}NO_2} \tag{4a}$$

$$\rightarrow \quad \textcolor{brown}{CH_2=N\text{-}CH_3} + HONO \tag{4b}$$

$$\textcolor{red}{(CH_3)_2N\text{-}NO} \xrightarrow{h\nu} (CH_3)_2N + NO \tag{5}$$
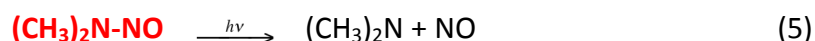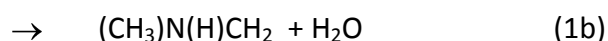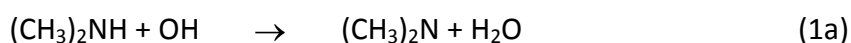
First of all the present experimental data show that the photolysis of N-nitroso dimethylamine, reaction (5), is slower by a factor of two than previously reported. Second, the nitrosamine formation, reaction (3), is three times faster relative to reaction (4a) than previous results suggested. This obviously affects the amounts of nitrosamine and nitramine that will be formed during the photo-oxidation of dimethylamine.

The present results show that around 42% of the initial OH reaction with dimethylamine is N-H abstraction, which in part result in nitrosamine and nitramine formation. The amount of nitrosamine and nitramine formed depends on the NO_2 concentration. For rural areas where mixing ratios of NOx are 0.2-10 ppbV with an average ratio $NO:NO_2 = 1:2$,[145] the amount of dimethylnitramine formed will be less than 2.5% of the dimethylamine photo-oxidized; the amout of nitrosamine formed will be discussed below. The other 58% of the initial OH reaction is C-H abstraction, of which 55% results in imine formation ($CH_2=NCH_3$), while the remaining 45% roughly divides into equal parts of CH_3NHCHO (N-methyl formamide), CH_2O (formaldehyde) $CH_2=NH$ (methanimine).

In summary, N-methyl methanimine ($CH_2=NCH_3$) is the major product in the OH-initiated photo-oxidation of dimethylamine accounting for around 70% of photo-oxidized dimethylamine. N-methyl formamide accounts for around 13% and CH_2O and $CH_2=NH$ for another 13%. The atmospheric fate of N-methyl

methanimine is uncertain. Most likely, the lifetime will be very short and the compound will hydrolyze in aqueous particles to give CH_2O (formaldehyde) and CH_3NH_2 (methylamine). *N*-methyl formamide has an estimated atmospheric lifetime of more than 1 day in the Mongstad area and the major product of its reaction with OH radicals is CH_3NCO (methylisocyanate), see above.

The amount of N-nitroso dimethylamine (NDMA) formed in the atmosphere from DMA depends on the ambient amounts of NO and NO_2, the amount of oxidizing radicals (here OH), and the actinic flux. These parameters all vary as a function of the time of day and the time of the year, and because NDMA is constantly formed and destroyed through photolysis it makes little sense to quantify the yield *per se* (the reaction of NDMA with OH radicals is slow, $\tau_{OH} \approx 3$ days, and not relevant compared to photolysis).

It is the amount of NDMA present in the atmosphere that is of interest, and this can be estimated from steady-state considerations. The differential rate laws for the formation and destruction of NDMA are:

$$\frac{d\left[(CH_3)_2NH\right]}{dt} = -k_1 \cdot \left[(CH_3)_2NH\right]\left[OH\right] \tag{XII}$$

$$\frac{d\left[(CH_3)_2N\right]}{dt} = k_{1a} \cdot \left[(CH_3)_2NH\right]\left[OH\right] + j_5\left[(CH_3)_2NNO\right]$$
$$-k_2\left[(CH_3)_2N\right]\left[O_2\right] - k_3\left[(CH_3)_2N\right]\left[NO\right] - k_4\left[(CH_3)_2N\right]\left[NO_2\right] \tag{XIII}$$

$$\frac{d\left[(CH_3)_2NNO\right]}{dt} = k_3\left[(CH_3)_2N\right]\left[NO\right] - j_5\left[(CH_3)_2NNO\right] \tag{XIV}$$

Assuming steady-state (i.e. the rate of NDMA formation equals the rate of NDMA destruction) results in the following expression for the steady-state concentration of NDMA:

$$\frac{\left[(CH_3)_2NNO\right]_{SS}}{\left[(CH_3)_2NH\right]} = \frac{k_{1a}\left[OH\right]}{j_5} \cdot \frac{k_3\left[NO\right]}{k_2\left[O_2\right] + k_4\left[NO_2\right]} \tag{XV}$$

Alternatively, normalizing to k_{4a} and introducing mixing ratios, X_i:

$$\frac{\left[(CH_3)_2NNO\right]_{SS}}{\left[(CH_3)_2NH\right]} = \frac{k_{1a}\left[OH\right]}{j_5} \cdot \frac{(k_3/k_{4a})X_{NO}}{(k_2/k_{4a})X_{O2} + (1 + k_{4b}/k_{4a})X_{NO2}} \tag{XVI}$$

The steady-state concentration varies as a function of the time of day and the time of the year. Not only will OH and j_{NDMA} (j_5) vary, but so will also NO and NO_2. Nothing is known about night-time amine chemistry, but a worst-case scenario will be that the night-time oxidation capacity towards amines equals that of the daytime. To a first approximation, annual average oxidant levels (OH at daytime, NO_3 at night-time) of 5 x 10^5 cm^{-3} and an annual average actinic flux corresponding to j_{NO2} = 6 x 10^{-5} s^{-1}, will mimic the conditions at Mongstad. Typical mixing ratios of NOx are 0.2-10 ppbV in rural areas with an average ratio NO:NO$_2$

= 1:2.[145] Such conditions result in a steady-state nitrosamine concentration of less than 0.6 % of the photo-oxidized dimethylamine and less than 1.1 % of the photo-oxidized trimethylamine. A realistic West European urban scenario will have NOx up 50 ppbV, again with an average ratio $NO:NO_2$ = 1:2, and the steady state nitrosamine concentration will be less than 2.3 % of the photo-oxidized dimethylamine and less than 4.2 % of the photo-oxidized trimethylamine.

The nitramines are minor products in the atmospheric photo-oxidation of amines. The estimated yields of nitramines formed in atmospheric photo-oxidation of methylamine, dimethylamine and trimethylamine are summarized in Table 6.1 for rural and urban scenarios (as specified above). The estimated uncertainty in the branching ratios of the OH-initiated photo-oxidation of methylamine, dimethylamine and trimethylamine is around ±15%. To reduce this uncertainty it is necessary to carry out a least squares fit of all related data simultaneously. In particular, the data from the various dimethylamine photo-oxidation experiments are currently being analyzed jointly with the *N*-nitroso dimethylamine photolysis experiments to reduce the model uncertainty in the nitrosamine and nitramine formation.

Table 6.1. Estimated yields of nitramines in the atmospheric photo-oxidation of methylamine, dimethylamine and trimethylamine assuming <OH> = $5x10^5$ cm^{-3} and $<j_{NO2}>$= 6 x 10^{-5} s^{-1}.

Amine	Rural scenario[a] /%	Urban scenario[b] /%
Methylamine	< 0.4	< 1.5
Dimethylamine	< 2.5	< 8
Trimethylamine	< 5	< 15

[a]Rural scenario: 0.2 – 10 ppbV NOx, $NO:NO_2$ = 1:2, [b]Urban scenario: 20 – 50 ppbV NOx, $NO:NO_2$ = 1:2.

The aerosol model MAFOR proved to be a useful and reliable tool for the determination of the loss terms of methylamines during photo-oxidation experiment.The loss processes of methylamines in selected photo-oxidation experiments can be characterized as follows. About 50-90% of the degradation of the three methylamines in the analyzed experiments is due the chemical reaction with OH radicals (Table 6.2). A very small fraction of the parent methylamine, about 1-2%, is lost to particles by gas-to-particle conversion processes (explained in more detail below). About 10-50% of the initial methylamine amount is lost to the walls or by dilution through the replenishment flow. Sources of uncertainty in this analysis are the rate constant of the reaction between the respective methylamine and OH radicals, the wall loss rate of the methylamine and AMS and PTR-MS instrumental uncertainties. Among these, the wall loss rate involves the highest uncertainty (50 %). The wall loss rate was characterized in each experiment and assumed to be constant during the sunlit experiment time. The rate constant for the OH-reaction with MMA, DMA, and TMA is relatively well known, and the associated uncertainty is <20%.

Table 6.2. Loss terms for methylamines and N-methyl methanimine in selected photo-oxidation experiments, given in percentage: chemical reaction, conversion to particulate phase (as aminium nitrate) and wall loss (including dilution loss). The first three hours of the sunlit experiment were used for this analysis.

Reactant	Date	Chemical reaction (%)	Particle conversion (%)	Wall loss (%)
MMA	22.03.2010	93	2	6
DMA	09.03.2010	49	1	49
DMA	11.03.2010	68	1	31
TMA	23.07.2010	54	<1	46
MMI	05.07.2010	18	6	77

In photo-oxidation experiments with initially 200-300 ppbV methylamines present, maximum total aerosol mass concentrations of 25-45 $\mu g/m^3$ were produced. The aerosol formation potential of the three methylamines was found to be substantial. Total aerosol yields obtained in EUPHORE experiments were between 8 and 14%. In general, aerosol particles formed in methylamine photo-oxidation experiments consisted of the nitrate salt of the respective methylamine (aminium nitrate salt) and secondarily produced organics. In experiments under low NO_x conditions, representative for rural air, secondary organic aerosol (SOA) was the dominant fraction in the aerosol. While the nitrate fraction of the aerosol was characterized by relative high volatility, the SOA fraction had intermediate to low volatility.

Aminium nitrate salt particles forming from the respective methylamines and other nitrate salt particles that formed in the photo-oxidation experiments are generally characterized by a high volatility. The high volatility of methyl aminium nitrate ($MMANO_3$), dimethyl aminium nitrate ($DMANO_3$) and trimethyl aminium nitrate ($TMANO_3$) salt particles that formed in the chamber experiments in EUPHORE has been confirmed in the AMS and VTDMA thermograms.

Evaporation of nitrate aerosol was observed in several experiments with increasing time of the sunlit experiment due to the decay of the (parent) methylamine. Methylamine-derived aminium nitrate particles are forming in a thermodynamic equilibrium reaction between the methylamine and HNO_3, followed by physical uptake (condensation or nucleation) of the reaction product into the particle phase. The stability of aminium nitrate particles is characterized by their solid-gas equilibrium dissociation constant, K_d. Experimental dissociation coefficients were obtained by adjusting the aerosol model MAFOR to measured particle mass concentrations of nitrate by the AMS set up and to measured particle number distributions by the SMPS. Resulting dissociation constants from selected photo-oxidation experiments in EUPHORE are provided in Table 6.3. It is noted that the temperature dependence of the dissociation coefficient of methylaminium nitrates has not yet been determined experimentally and that the derived K_d values refer to the respective mean temperature of the experiment.

Table 6.3. Solid-gas equilibrium dissociation constants (K_d) of aminium nitrates in selected methylamine photo-oxidation experiments and of the pure aminium nitrate salts. Experiment K_d values were determined by (qualitative) inverse modelling using MAFOR and measured time series from AMS and SMPS.

Reactant	Date	Mean exp. temperature T_{exp} (K)	K_d (T_{exp}) Experiment (Pa^2)	K_d (298 K) pure salt[134] (Pa^2)
MMA	22.03.2010	297.6	3.4×10^{-08}	4.54×10^{-8}
DMA	09.03.2010	290.4	3.2×10^{-11}	6.27×10^{-8}
DMA	11.03.2010	289.9	8.0×10^{-10}	6.27×10^{-8}
TMA	23.07.2010	303.4	5.3×10^{-7}	1.65×10^{-6}

Obviously, the nitrate aerosol formed in methylamine photo-oxidation experiments is composed of the aminium nitrate from the parent methylamine ("primary salt") but also of aminium nitrates from other organic compounds ("secondary salt") that are produced in the gas-phase oxidation of the methylamine. In experiments with MMA and DMA it was found that initially mainly the primary salt was formed while at later stages of the experiment, the fraction of secondary salt increased. In experiments with TMA, approximately 30% of the total nitrate mass concentration was associated to TMANO$_3$, while the remaining 70 % of the measured nitrate salt was associated to other compounds. Until now, it is not clear which organic compounds are responsible for the formation of secondary salts.

Significant amounts of secondary organic aerosol (SOA) were produced in MMA, DMA and TMA photo-oxidation experiments. In low-NO$_x$ experiments, SOA was the dominating fraction of the aerosol produced. Mass-based stoichiometric SOA yields in the photo-oxidation of MMA and DMA were 8-9% (see Table 6.4). Secondary organic aerosol (SOA) produced in MMA and DMA experiments had an intermediate volatility. In the photo-oxidation of TMA, oxygenated organics were the dominant aerosol fraction and the produced SOA had a low volatility.

Table 6.4. Mass-based yield of aminium nitrate (MANO$_3$), stoichiometric mass-based SOA yield and the total aerosol yield in selected photo-oxidation experiments, given in percentage.

Reactant	Date	MANO$_3$ yield (%) [1]	Mass-based SOA yield (%) [2]	Total aerosol yield (%) [3]
MMA	22.03.2010	2	8	9
DMA	09.03.2010	1	9	6
DMA	11.03.2010	1	8	6
TMA	23.07.2010	<1	14	8
MMI	05.07.2010	6	70	18

[1] The yield of particulate MANO$_3$ is determined by a thermodynamic equilibrium reaction between methylamine and HNO$_3$ followed by physical uptake (condensation or nucleation) of the reaction product (MANO$_3$) into the particle phase. The given values are identical with the particle conversion loss given in Table 6.1 with respect to the mass balance of methylamines.

[2] Mass-based stoichiometric yields in the reaction between methylamine and OH.

[3] Calculated as sum of the MANO$_3$ yield and of the SOA yield corrected for the fraction of methylamine that reacted with OH (see Table 6.1).

DMA photo-oxidation experiments were carried out under different NO$_x$ conditions with and without H$_2$O$_2$. In high-NO$_x$ concentrations the initial aerosol consists mostly of high volatile nitrate salts (mainly DMANO$_3$ and CNH$_4$NO$_3$) while in low-NO$_x$ concentrations an aerosol consisting of slightly less volatile secondary material (oxidized) is formed. In the high-NO$_x$ experiment nitrates and organics equally contribute to the total mass whereas the low-NO$_x$ experiment was dominated by secondary organics (~70-80% of the total mass). Aminium nitrate from dimethylamine was found to be more stable when indicated by the thermodynamic solid/gas equilibrium (experimental K_d value lower than literature K_d value). AMS thermograms recorded during the experiments (Table 6.5) show that the remaining mass fraction of total nitrate in the aerosol at 70°C was similar in DMA experiments carried out under different NO$_x$ conditions. Interestingly, it also shows that volatility of the aerosol decreased over experiment time in the low-NO$_x$ experiment (increased remaining mass fraction). Possibly, condensation of organics onto the aerosol during in the experiments formed a barrier that prevented the aminium salts from remaining at equilibrium with the gas phase and protected them against re-volatilization.

Table 6.5. Mass fraction (mf) of major aerosol components remaining at 70°C determined in thermograms using the AMS set up in selected experiments.

Reactant	Date	Time (UTC)	Organics mf (%)	Total nitrate mf (%)	MANO$_3$ mf (%)	Other nitrate mf (%)
MMA	22.03.2010	13:00	57	36	21	47
DMA	09.03.2010	17:00	53	35	36	35
DMA	11.03.2010	13:45	44	25	20	37
DMA	11.03.2010	16:45	66	49	43	57
TMA	16.07.2010	10:30	84	68	49	70
TMA	23.07.2010	10:30	89	72	87	69
MMI	05.07.2010	15:30	89	87	–	–
MMI	05.07.2010	13:30	84	76	–	–

Concurrent measurements with the AMS and the newly deployed PTR-MS particulate-phase set up revealed that, among possible nitrate-forming organic compounds, especially N-methyl methanimine (MMI) was very efficient in producing new particles upon exposure to sunlight. Additional photo-oxidation experiments with MMI demonstrated that this compound has a large particle formation potential, forming both nitrate aerosol and SOA immediately after exposure to sunlight with high yields. The total aerosol yield in a MMI photo-oxidation was estimated by MAFOR to be 18%. It is concluded that MMI has a high aerosol formation potential and that the aerosol forming in the photo-oxidation of MMI has a very low volatility. The atmospheric fate of MMI and other potential nitrate forming compounds originating in the oxidation of methylamines, such as N-methyl formamide, warrants further investigation in future photo-oxidation and aerosol studies.

7 Literature

(1)   Herzberg, G., Kölsch, R. (1933) The ultra-violet absorption of the amino group (-NH$_2$) and other groups in simple molecules in the gaseous state. *Z. Elektrochem. Angew. Phys. Chem.*, *39*, 572-3.

(2)   Bidleman, T. F. (1988) Atmospheric processes - Wet and dry deposition of organic-compounds are controlled by their vapor particle partitioning. *Environ. Sci. Technol.*, *22*, 361-67.

(3)   Wilhelm, E., Battino, R., Wilcock, R. J. (1977) Low-pressure solubility of gases in liquid water. *Chem. Rev.*, *77*, 219-62.

(4)   Christie, A. O., Crisp, D. J. (1967) Activity coefficients of n-primary secondary and tertiary aliphatic amines in aqueous solution. *J. Appl. Chem. USSR*, *17*, 11-14.

(5)   Atkinson, R. (1986) Kinetics and mechanisms of the gas-phase reactions of the hydroxyl radical with organic-compounds under atmospheric conditions. *Chem Rev.*, *86*, 69-201.

(6)   Jenkin, M. E., Saunders, S. M., Pilling, M. J. (1997) The tropospheric degradation of volatile organic compounds: A protocol for mechanism development. *Atmos. Environ.*, *31*, 81-104.

(7)   Finlayson-Pitts, B. J., Pitts, J. N. (1986) Atmospheric chemistry: Fundamentals and experimental techniques. Wiley, New York.

(8)   Logan, J. A. (1985) Tropospheric ozone - seasonal behaviour, trends, and anthropogenic influence. *J. Geophys. Res. Atmos.*, *90 (D6)*, 10463-10482.

(9)   Oltmans, S. J., Levy, H. (1994) Surface ozone measurements from a global network. *Atmos. Environ.*, *28*, 9-24.

(10)   Chameides, W. L., Fehsenfeld, F., Rodgers, M. O., Cardelino, C., Martinez, J., Parrish, D., Lonneman, W., Lawson, D. R., Rasmussen, R. A., Zimmerman, P., Greenberg, J., Middleton, P., Wang, T. (1992) Ozone precursor relationships in the ambient atmosphere. *J. Geophys. Res., 97(D5)*, 6037–6055, doi:10.1029/91JD03014.

(11)   Prinn, R. G., Weiss, R. F., Miller, B. R., Huang, J., Alyea, F. N., Cunnold, D. M., Fraser, P. J., Hartley, D. E., Simmonds, P. G. (1995) Atmospheric trends and lifetime of CH3CCl3 and global OH concentrations. *Science*, *269*, 187-92.

(12)   Logan, J. A., Prather, M. J., Wofsy, S. C., McElroy, M. B. (1981) Tropospheric chemistry - a global perspective. *J. Geophys. Res., 86 (C8)*, 7210-7254.

(13)   Pszenny, A. A. P., Fischer, E. V., Russo, R. S., Sive, B. C., Varner, R. K. (2007) Estimates of Cl atom concentrations and hydrocarbon kinetic reactivity in surface air at Appledore Island, Maine (USA), during International Consortium for Atmospheric Research on Transport and Transformation/Chemistry of Halogens at the Isles of Shoals. *J. Geophys. Res.*, *112*, D10S13, doi:10.1029/2006JD007725.

(14)   Wingenter, O. W., Kubo, M. K., Blake, N. J., Smith, T. W., Jr., Blake, D. R., Rowland, F. S. (1996) Hydrocarbon and halocarbon measurements as photochemical and dynamical indicators of atmospheric hydroxyl, atomic chlorine, and vertical mixing obtained during Lagrangian flights. *J. Geophys. Res.*, *101 (D2)*, 4331–4340, doi:10.1029/95JD02457.

(15) Wayne, R. P., Barnes, I., Biggs, P., Burrows, J. P., Canosamas, C. E., Hjorth, J., Lebras, G., Moortgat, G. K., Perner, D., Poulet, G., Restelli, G., Sidebottom, H. (1991) The nitrate radical - physics, chemistry, and the atmosphere. *Atmos. Environ. Gen. Top.*, *25*, 1-203.

(16) Winer, A. M., Atkinson, R., Pitts, J. N. (1984) Gaseous nitrate radical: Possible nighttime atmospheric sink for biogenic organic compounds. *Science*, *224*, 156-59.

(17) Vrekoussis, M., Kanakidou, M., Mihalopoulos, N., Crutzen, P. J., Lelieveld, J., Perner, D., Berresheim, H., Baboukas, E. (2004) Role of the NO_3 radicals in oxidation processes in the eastern Mediterranean troposphere during the MINOS campaign. *Atmos. Chem. Phys.*, *4*, 169-82.

(18) McLaren, R., Wojtal, P., Majonis, D., McCourt, J., Halla, J. D., Brook, J. (2010) NO_3 radical measurements in a polluted marine environment: links to ozone formation. *Atmos. Chem. Phys.*, *10*, 4187-206.

(19) Atkinson, R., Perry, R. A., Pitts, J. N., Jr. (1977) Rate constants for the reaction of the hydroxyl radical with methanethiol and methylamine over the temperature range 299-426 Deg K. *J. Chem. Phys.*, *66*, 1578-81.

(20) Carl, S. A., Crowley, J. N. (1998) Sequential two (blue) photon absorption by NO_2 in the presence of H_2 as a source of OH in pulsed photolysis kinetic studies: Rate constants for reaction of OH with CH_3NH_2, $(CH_3)_2NH$, $(CH_3)_3N$, and $C_2H_5NH_2$ at 295 K. *J. Phys. Chem. A*, *102*, 8131-41.

(21) Tuazon, E. C., Atkinson, R., Aschmann, S. M., Arey, J. (1994) Kinetics and products of the gas-phase reactions of O_3 with amines and related-compounds. *Res. Chem. Intermed.*, *20*, 303-20.

(22) Rudic, S., Murray, C., Harvey, J. N., Orr-Ewing, A. J. (2003) The product branching and dynamics of the reaction of chlorine atoms with methylamine. *Phys. Chem. Chem. Phys.*, *5*, 1205-12.

(23) Galano, A., Alvarez-Idaboy, J. R. (2008) Branching ratios of aliphatic amines + OH gas-phase reactions: A variational transition-state theory study. *J. Chem. Theory Comput., 4*, 322-27.

(24) Tian, W., Wang, W., Zhang, Y., Wang, W. (2009) Direct dynamics study on the mechanism and the kinetics of the reaction of CH_3NH_2 with OH. *Int. J. Quantum Chem.*, *109*, 1566-75.

(25) Schade, G. W., Crutzen, P. J. (1995) Emission of aliphatic-amines from animal husbandry and their reactions - Potential source of N_2O and HCN. *J. Atmos. Chem.*, *22*, 319-46.

(26) Murphy, S. M., Sorooshian, A., Kroll, J. H., Ng, N. L., Chhabra, P., Tong, C., Surratt, J. D., Knipping, E., Flagan, R. C., Seinfeld, J. H. (2007) Secondary aerosol formation from atmospheric reactions of aliphatic amines. *Atmos. Chem. Phys.*, *7*, 2313-37.

(27) Atkinson, R., Perry, R. A., Pitts, J. N., Jr. (1978) Rate constants for the reactions of the hydroxyl radical with dimethylamine, trimethylamine, and ethylamine over the temperature range 298-426 K. *J. Chem. Phys.*, *68*, 1850-3.

(28) Pitts, J. N., Grosjean, D., Vancauwenberghe, K., Schmid, J. P., Fitz, D. R. (1978) Photo-oxidation of aliphatic-amines under simulated atmospheric conditions - Formation of nitrosamines, nitramines, amides, and photo-chemical oxidant. *Environ. Sci. Technol.*, *12*, 946-53.

(29)   Hanst, P. L., Spence, J. W., Miller, M. (1977) Atmospheric chemistry of N-nitroso dimethylamine. *Environ. Sci. Technol.*, *11*, 403-5.

(30)   Glasson, W. A. (1979) An experimental evaluation of atmospheric nitrosamine formation. *Environ. Sci. Technol.*, *13*, 1145-46.

(31)   Lv, C. L., Liu, Y. D., Zhong, R., Wang, Y. (2007) Theoretical studies on the formation of N-nitrosodimethylamine. *J. Mol. Struct.: THEOCHEM*, *802*, 1-6.

(32)   Grosjean, D. (1991) Atmospheric chemistry of toxic contaminants. 6. Nitrosamines: dialkyl nitrosamines and nitrosomorpholine. *J. Air Waste Manag. Assoc.*, *41*, 306-11.

(33)   Lindley, C. R. C., Calvert, J. G., Shaw, J. H. (1979) Rate studies of the reactions of the $(CH_3)_2N$ radical with O_2, NO, and NO_2. *Chem. Phys. Lett.*, *67*, 57-62.

(34)   Price, D. J. (2010) Field and smog chamber studies of agricultural emissions and reaction products. Logan, Utah State University.

(35)   Erupe, M. E., Price, D. J., Silva, P. J., Malloy, Q. G. J., Qi, L., Warren, B., Cocker Iii, D. R. (2008) Secondary organic aerosol formation from reaction of tertiary amines with nitrate radical. *Atmos. Chem. Phys. Discuss.*, *8*, 16585-608.

(36)   Atkinson, R. (1991) Kinetics and mechanisms of the gas-phase reactions of the NO3 radical with organic-compounds. *J. Phys. Chem. Ref. Data*, *20*, 459-507.

(37)   Tuazon, E. C., Carter, W. P. L., Atkinson, R., Winer, A. M., Pitts, J. N. (1984) Atmospheric reactions of n-nitrosodimethylamine and dimethylnitramine. *Environ. Sci. Technol.*, *18*, 49-54.

(38)   IUPAC Subcommittee for Gas Kinetic Data Evaluation (2009) Evaluated kinetic data. URL: http://www.iupac-kinetic.ch.cam.ac.uk/index.html [Accessed 2010-01-20].

(39)   Zabarnick, S. S., Fleming, J. W., Baronavski, A. P., Lin, M. C. (1986) Reaction kinetics of hydroxyl with nitromethane, dimethylnitrosamine, and 1,3,5-trioxane, photolytic production of hydroxyl from nitromethane at 266 nm. *NBS Spec. Publ. (U. S.)*, *716*, 731-56.

(40)   Bamford, C. H. (1939) A study of the photolysis of organic nitrogen compounds - Part I Dimethyl- and diethyl-nitrosoamines. *J. Chem. Soc.*, 12-17.

(41)   Geiger, G., Stafast, H., Bruehlmann, U., Huber, J. R. (1981) Photodissociation of dimethylnitrosamine. *Chem. Phys. Lett.*, *79*, 521-4.

(42)   Geiger, G., Huber, J. R. (1981) Photolysis of dimethylnitrosamine in the gas-phase. *Helv. Chim. Acta*, *64*, 989-95.

(43)   Lazarou, Y. G., Kambanis, K. G., Papagiannakopoulos, P. (1994) Gas-phase reactions of $(CH_3)_2N$ radicals with NO and NO_2. *J. Phys. Chem.*, *98*, 2110-15.

(44)   Nielsen, C. J., D'Anna, B., Dye, C., George, C., Graus, M., Hansel, A., Karl, M., King, S., Musabila, M., Müller, M., Schmidbauer, N., Stenstrøm, Y., Wisthaler, A. (2010) Atmospheric Degradation of Amines (ADA). Summary Report: Gas phase photo-oxidation of 2-aminoethanol (MEA) CLIMIT project no. 193438. Kjeller, NILU (OR 8/2010).

(45)   Challis, B. C., Challis, J. A. (1982) N-nitrosamines and N-nitrosimies. In: *The chemistry of amino, nitroso, and nitro compounds and their*

derivatives. Supplement F. Ed. by: Patai, S. Chichester, Wiley. pp 1151-1223.

(46) Tang, Y., Hanrath, M., Nielsen, C. J. (2010) Do primary nitrosamines form and exist in the gas phase? A computational study of CH_3NHNO and $(CH_3)_2NNO$. *Manuscript in preparation*,

(47) Chakir, A., Solignac, B., Mellouki, A., Daumont, D. (2005) Gas phase UV absorption cross-sections for a series of amides. *Chem. Phys. Lett.*, *404*, 74-78.

(48) Koch, R., Palm, W. U., Zetzsch, C. (1997) First rate constants for reactions of OH radicals with amides. *Int. J. Chem. Kinet.*, *29*, 81-87.

(49) Solignac, G., Mellouki, A., Le Bras, G., Barnes, I., Benter, T. (2005) Kinetics of the OH and Cl reactions with N-methylformaraide, N,N-dimethylformaraide and N,N-dimethylacetamide. *J. Photochem. Photobiol. Chem.*, *176*, 136-42.

(50) Aschmann, S. M., Atkinson, R. (1999) Atmospheric chemistry of 1-methyl-2-pyrrolidinone. *Atmos. Environ.*, *33*, 591-99.

(51) El Dib, G., Chakir, A. (2007) Temperature-dependence study of the gas-phase reactions of atmospheric NO3 radicals with a series of amides. *Atmos. Environ.*, *41*, 5887-96.

(52) Barnes, I., Solignac, G., Mellouki, A., Becker, K. (2010) Aspects of the atmospheric chemistry of amides. *ChemPhysChem, 11,* 3844–3857.

(53) Patai, S. (1970) The chemistry of the carbon-nitrogen double bond. London, Interscience.

(54) Teslja, A., Nizamov, B., Dagdigian, P. J. (2004) The electronic spectrum of methyleneimine. *J. Phys. Chem. A*, *108*, 4433-39.

(55) Nguyen Minh, T., Sengupta, D., Ha, T.-K. (1996) Another look at the decomposition of methyl azide and methanimine: How is HCN formed? *J. Phys. Chem.*, *100*, 6499-503.

(56) Layer, R. W. (1963) Chemistry of imines. *Chem Rev.*, *63*, 489-510.

(57) Tully, F. P., Perry, R. A., Thorne, L. R., Allendorf, M. D. (1989) Free-radical oxidation of isocyanic acid. *Symp. (Int.) Combust., [Proc.]*, *22nd*, 1101-1106.

(58) Glarborg, P., Kristensen, P. G., Jensen, S. H., Damjohansen, K. (1994) A flow reactor study of HNCO oxidation chemistry. *Combust. Flame*, *98*, 241-58.

(59) Wooldridge, M. S., Hanson, R. K., Bowman, C. T. (1996) A shock tube study of CO+OH->CO2+H and HNCO+OH->products via simultaneous laser adsorption measurements of OH and CO2. *Int. J. Chem. Kinet.*, *28*, 361-72.

(60) Woo, S.-C., Liu, T.-K. (1935) The absorption spectra and dissociation energies of cyanic acid and some isocyanates. *J. Chem. Phys.*, *3*, 544-46.

(61) Atkinson, R., Baulch, D. L., Cox, R. A., Crowley, J. N., Hampson, R. F., Hynes, R. G., Jenkin, M. E., Rossi, M. J., Troe, J. (2006) Evaluated kinetic and photochemical data for atmospheric chemistry: Volume II - gas phase reactions of organic species. *Atmos. Chem. Phys.*, *6*, 3625-4055.

(62) Nielsen, C. J., D'Anna, B., Atsumi, M., Aursnes, M., Boreave, A., Dye, D., George, C., Hallquist, M., Matthias Karl, Mikoviny, T., Maguta, M. M., Müller, M., Schmidbauer, N., Skov, H., Sellevåg, S. R., Salo, K., Stenstrøm, Y., Tang, Y., Wisthaler, A. (2010) Atmospheric Degradation of Amines (ADA). Progress report April 2010: Gas phase photo-oxidation of

methylamine, dimethylamine and trimethylamine. CLIMIT project no. 201604.

(63) Nielsen, C. J., D'Anna, B., Aursnes, M., Boreave, A., Bossi, R., Dye, C., Hallquist, M., Karl, M., Mikoviny, T., Maguta, M. M., Müller, M., Skov, H., Salo, K., Stenstrøm, Y., Wisthaler, A. (2010) Atmospheric Degradation of Amines (ADA) Progress report June 2010: Gas phase photo-oxidation of methylamine, dimethylamine and trimethylamine. CLIMIT project no. 201604.

(64) Carter, W. P. L., Atkinson, R. (1985) Atmospheric chemistry of alkanes. *J. Atmos. Chem.*, *3*, 377-405.

(65) Atkinson, R., Perry, R. A., Pitts, J. N., Jr. (1978) Rate constants for the reaction of hydroxyl radicals with carbonyl sulfide, carbon disulfide and dimethyl thioether over the temperature range 299-430 K. *Chem. Phys. Lett.*, *54*, 14-18.

(66) Gorse, R. A., Jr., Lii, R. R., Saunders, B. B. (1977) Hydroxyl radical reactivity with diethylhydroxylamine. *Science*, *197*, 1365-1367.

(67) Harris, G. W., Pitts, J. N. (1983) Rates of reaction of hydroxyl radicals with 2-(dimethylamino)ethanol and 2-amino-2-methyl-1-propanol in the gas-phase at 300 +- 2 K. *Environ. Sci. Technol.*, *17*, 50-51.

(68) Anderson, L. G., Stephens, R. D. (1988) Kinetics of the reaction of hydroxyl radicals with 2-(dimethylamino)ethanol from 234-364-K. *Int. J. Chem. Kinet.*, *20*, 103-10.

(69) Koch, R., Kruger, H. U., Elend, M., Palm, W. U., Zetzsch, C. (1996) Rate constants for the gas-phase reaction of OH with amines: tert-butyl amine, 2,2,2-trifluoroethyl amine, and 1,4-diazabicyclo[2.2.2]octane. *Int. J. Chem. Kinet.*, *28*, 807-15.

(70) Tuazon, E. C., Winer, A. M., Graham, R. A., Schmid, J. P., Pitts, J. N. (1978) Fourier-transform infrared detection of nitramines in irradiated amine-Nox systems. *Environ. Sci. Technol.*, *12*, 954-58.

(71) Pitts, J. N., Smith, J. P., Fitz, D. R., Grosjean, D. (1977) Enhancement of photochemical smog by N, N'-diethylhydroxylamine in polluted ambient air. *Science*, *197*, 255-57.

(72) Grosjean, D. (1980) Atmospheric chemistry of selected nitrogenous pollutants. *Calif. Air Environ.*, *7*, 12-15.

(73) Karl, M. (2010) Atmospheric Degradation of Amines (ADA). Amines in aerosol - A review. CLIMIT project no. 210604. Kjeller, NILU (OR 60/2010).

(74) Karl, M., Gross, A., Leck, C., Pirjola, L. (2010) New particle formation in the High Arctic: Observations and model simulations. *Geophys. Res. Abstr.*, *12*, EGU2010-8393.

(75) Karl, M., Gross, A., Leck, C., Pirjola, L. (2010) A new flexible multicomponent model for the study of aerosol dynamics in the marine boundary layer. *Tellus Ser. B. Under review.*

(76) Pirjola, L., Kulmala, M. (2000) Aerosol dynamical model MULTIMONO. *Boreal Environ. Res.*, *5*, 361-74.

(77) Pirjola, L., Tsyro, S., Tarrason, L., Kulmala, M. (2003) A monodisperse aerosol dynamics module, a promising candidate for use in long-range transport models: Box model tests. *J. Geophys. Res.*, *108 (D9)*, 4258, doi:10.1029/2002JD002867.

(78) Karl, M., Gross, A., Leck, C., Pirjola, L. (2007) Intercomparison of dimethylsulfide oxidation mechanisms for the marine boundary layer: Gaseous and particulate sulfur constituents. *J. Geophys. Res.*, *112, D15304*, doi:10.1029/2006JD007914.

(79) Sandu, A., Verwer, J. G., VanLoon, M., Carmichael, G. R., Potra, F. A., Dabdub, D., Seinfeld, J. H. (1997) Benchmarking stiff ODE solvers for atmospheric chemistry problems-I. Implicit vs explicit. *Atmos. Environ.*, *31*, 3151-66.

(80) Zador, J., Turanyi, T., Wirtz, K., Pilling, M. J. (2006) Measurement and investigation of chamber radical sources in the European Photoreactor (EUPHORE). *J. Atmos. Chem.*, *55*, 147-66.

(81) Naumann, K. H. (2003) COSIMA - a computer program simulating the dynamics of fractal aerosols. *J. Aerosol Sci.*, *34*, 1371-97.

(82) Jacobson, M. Z. (2005) Fundamentals of atmospheric modeling. Cambridge, Cambridge University Press.

(83) Odum, J. R., Hoffmann, T., Bowman, F., Collins, D., Flagan, R. C., Seinfeld, J. H. (1996) Gas/particle partitioning and secondary organic aerosol yields. *Environ. Sci. Technol.*, *30*, 2580-85.

(84) Jacobson, M. Z. (1997) Numerical techniques to solve condensational and dissolutional growth equations when growth is coupled to reversible reactions. *Aerosol Sci.Technol.*, *27*, 491-98.

(85) Meng, Z. Y., Dabdub, D., Seinfeld, J. H. (1998) Size-resolved and chemically resolved model of atmospheric aerosol dynamics. *J. Geophys. Res. Atmos.*, *103*, 3419-35.

(86) Pankow, J. F. (1994) An absorption-model of gas-particle partitioning of organic-compounds in the atmosphere. *Atmos. Environ.*, *28*, 185-88.

(87) Pankow, J. F. (1994) An absorption-model of the gas aerosol partitioning involved in the formation of secondary organic aerosol. *Atmos. Environ.*, *28*, 189-93.

(88) Bowman, F. M., Odum, J. R., Seinfeld, J. H., Pandis, S. N. (1997) Mathematical model for gas-particle partitioning of secondary organic aerosols. *Atmos. Environ.*, *31*, 3921-31.

(89) Seinfeld, J. H., Pankow, J. F. (2003) Organic atmospheric particulate material. *Annu. Rev. Phys. Chem.*, *54*, 121-40.

(90) Bilde, M., Svenningsson, B., Monster, J., Rosenorn, T. (2003) Even-odd alternation of evaporation rates and vapor pressures of C3-C9 dicarboxylic acid aerosols. *Environ. Sci. Technol.*, *37*, 1371-78.

(91) Becker, K. H. (1996) The European photoreactor EUPHORE. Design and technical development of the European photoreactor and first experimental results, Final Report of the EC-Project Contract EV5V-CT92-0059. Wuppertal, BUGH Wuppertal.

(92) Magneron, I., Thevenet, R., Mellouki, A., Le Bras, G., Moortgat, G. K., Wirtz, K. (2002) A study of the photolysis and OH-initiated oxidation of acrolein and trans-crotonaldehyde. *J. Phys. Chem. A*, *106*, 2526-37.

(93) Volkamer, R., Platt, U., Wirtz, K. (2001) Primary and secondary glyoxal formation from aromatics: Experimental evidence for the bicycloalkyl-radical pathway from benzene, toluene, and p-xylene. *J. Phys. Chem. A*, *105*, 7865-74.

(94) Klotz, B., Sorensen, S., Barnes, I., Becker, K. H., Etzkorn, T., Volkamer, R., Platt, U., Wirtz, K., Martin-Reviejo, M. (1998) Atmospheric oxidation

of toluene in a large-volume outdoor photoreactor: In situ determination of ring-retaining product yields. *J. Phys. Chem. A*, *102*, 10289-99.

(95)   Wenger, J. C., Le Calve, S., Sidebottom, H. W., Wirtz, K., Reviejo, M. M., Franklin, J. A. (2004) Photolysis of chloral under atmospheric conditions. *Environ. Sci. Technol.*, *38*, 831-37.

(96)   Jordan, A., Haidacher, S., Hanel, G., Hartungen, E., Mark, L., Seehauser, H., Schottkowsky, R., Sulzer, P., Mark, T. D. (2009) A high resolution and high sensitivity proton-transfer-reaction time-of-flight mass spectrometer (PTR-TOF-MS). *Int. J. Mass Spectrom.*, *286*, 122-28.

(97)   Mikoviny, T., Kaser, L., Wisthaler, A. (2010) Development and characterization of a high-hemperature proton-transfer-reaction mass spectrometer (HT-PTR-MS). *Atmos. Meas. Tech. Discuss.*, *3*, 185-202.

(98)   Hellen, H., Dommen, J., Metzger, A., Gascho, A., Duplissy, J., Tritscher, T., Prevot, A. S. H., Baltensperger, U. (2008) Using proton transfer reaction mass spectrometry for online analysis of secondary organic aerosols. *Environ. Sci. Technol.*, *42*, 7347-53.

(99)   Jonsson, A. M., Hallquist, M., Saathoff, H. (2007) Volatility of secondary organic aerosols from the ozone initiated oxidation of alpha-pinene and limonene. *J. Aerosol Sci.*, *38*, 843-52.

(100) Salo, K., Jonsson, Å. M., Andersson, P. U., Hallquist, M. (2010) Aerosol volatility and enthalpy of sublimation of carboxylic acids. *J. Phys. Chem. A*, *114,* 4586-4594.

(101) Kalberer, M., Paulsen, D., Sax, M., Steinbacher, M., Dommen, J., Prevot, A. S. H., Fisseha, R., Weingartner, E., Frankevich, V., Zenobi, R., Baltensperger, U. (2004) Identification of polymers as major components of atmospheric organic aerosols. *Science*, *303*, 1659-62.

(102) Offenberg, J. H., Kleindienst, T. E., Jaoui, M., Lewandowski, M., Edney, E. O. (2006) Thermal properties of secondary organic aerosols. *Geophys. Res. Lett.*, *33*, L03816, doi:10.1029/2005GL024623.

(103) An, W. J., Pathak, R. K., Lee, B. H., Pandis, S. N. (2007) Aerosol volatility measurement using an improved thermodenuder: Application to secondary organic aerosol. *J. Aerosol Sci.*, *38*, 305-14.

(104) Drewnick, F., Hings, S., DeCarlo, P., Jayne, J., Gonin, M., Fuhrer, K., Weimer, S., Jimenez, J., Demerjian, K., Borrmann, S., Worsnop, D. (2005) A new time-of-flight aerosol mass spectrometer (TOF-AMS) - Instrument description and first field deployment. *Aerosol Sci.Technol.*, *39*, 637-58.

(105) Müller, M., Graus, M., Ruuskanen, T. M., Schnitzhofer, R., Bamberger, I., Kaser, L., Titzmann, T., Hörtnagl, L., Wohlfahrt, G., Karl, T., Hansel, A. (2010) First eddy covariance flux measurements by PTR-TOF. *Atmos. Meas. Tech.*, *3*, 387-95.

(106) Griffith, D. W. T. (1996) Synthetic calibration and quantitative analysis of gas phase infrared spectra. *Appl. Spectros.*, *50*, 59-70.

(107) Rothman, L. S., Gordon, I. E., Barbe, A., ChrisBenner, D., Bernath, P. F., Birk, M., Boudon, V., Brown, L. R., Campargue, A., Champion, J.-P., Chance, K., Coudert, L. H., Danaj, V., Devi, V. M., Fally, S., Flaud, J.-M., Gamache, R. R., Goldmanm, A., Jacquemart, D., Kleiner, I., Lacome, N., Lafferty, W. J., Mandin, J.-Y., Massie, S. T., Mikhailenko, S. N., Miller, C. E., Moazzen-Ahmadi, N., Naumenko, O. V., Nikitin, A. V., Orphal, J., Perevalov, V. I., Perrin, A., Predoi-Cross, A., Rinsland, C. P., Rotger, M., Simeckova, M., Smith, M. A. H., Sung, K., Tashkun, S. A., Tennyson, J.,

Toth, R. A., Vandaele, A. C., VanderAuwera, J. (2009) The HITRAN 2008 molecular spectroscopic database. *J. Quant. Spectrosc. Radiat. Transfer, 110*, 533-72.

(108) Zhao, Y. Y., Boyd, J., Hrudey, S. E., Li, X. F. (2006) Characterization of new nitrosamines in drinking water using liquid chromatography tandem mass spectrometry. *Environ. Sci. Technol.*, *40*, 7636-41.

(109) Lee, H. L., Wang, C. Y., Lin, S., Hsieh, D. P. H. (2007) Liquid chromatography/tandem mass spectrometric method for the simultaneous determination of tobacco-specific nitrosamine NNK and its five metabolites. *Talanta*, *73*, 76-80.

(110) Krauss, M., Hollender, J. (2008) Analysis of nitrosamines in wastewater: Exploring the trace level quantification capabilities of a hybrid linear ion trap/orbitrap mass spectrometer. *Anal. Chem.*, *80*, 834-42.

(111) Brunauer, S., Emmett, P. H., Teller, E. (1938) Adsorption of gases in multimolecular layers. *J. Am. Chem. Soc.*, *60*, 309-19.

(112) Salo, K., Jonsson, A. M., Andersson, P. U., Hallquist, M. (2010) Aerosol volatility and enthalpy of sublimation of carboxylic acids. *J. Phys. Chem. A*, *114*, 4586-94.

(113) Monster, J., Rosenorn, T., Svenningsson, B., Bilde, M. (2004) Evaporation of methyl- and dimethyl-substituted malonic, succinic, glutaric and adipic acid particles at ambient temperatures. *J. Aerosol Sci.*, *35*, 1453-65.

(114) Bird, R. B., Stewart, W. E., Lightfoot, E. N. (1960) Transport phenomena. New York, Wiley.

(115) Mylrajan, M., Srinivasan, T. K. K., Sreenivasamurthy, G. (1985) Crystal structure of monomethylammonium nitrate. *J. Chem. Crystallogr.*, *15*, 493-500.

(116) Walden, P. (1914) Molecular weights and electrical conductivity of several fused salts. *Bull. Acad. Imp. Sci. St.-Petersbourg*, 405-422.

(117) Cottrell, T. L., Gill, J. E. (1951) The preparation and heats of combustion of some amine nitrates. *J. Chem. Soc.*, 1798-800.

(118) Lydersen, A. L. (1955) Estimation of critical properties of organic compounds by the method of group contributions. Madison, WI, College of Engineering, University of Wisconsin (Eng. Exp. Sta. Rep., 3).

(119) Nannoolal, Y., Rarey, J., Ramjugernath, D. (2007) Estimation of pure component properties. Part 2. Estimation of critical property data by group contribution. *Fluid Phase Equil.*, *252*, 1-27.

(120) Brandner, J. D., Junk, N. M., Lawrence, J. W., Robins, J. (1962) Vapor pressure of ammonium nitrate. *J. Chem. Eng. Data*, *7*, 227-28.

(121) Hildenbrand, D. L., Lau, K. H., Chandra, D. (2010) Thermochemistry of gaseous ammonium nitrate, NH4NO3(g). *J. Phys. Chem. B*, *114*, 330-32.

(122) Curtiss, L. A., Raghavachari, K., Redfern, P. C., Rassolov, V., Pople, J. A. (1998) Gaussian-3 (G3) theory for molecules containing first and second-row atoms. *J. Chem. Phys.*, *109*, 7764-76.

(123) Frisch, M. J., Trucks, G. W., Schlegel, H. B., Scuseria, G. E., Robb, M. A., Cheeseman, J. R., Montgomery, J., J. A., , Vreven, T., Kudin, K. N., Burant, J. C., Millam, J. M., Iyengar, S. S., Tomasi, J., Barone, V., Mennucci, B., Cossi, M., Scalmani, G., Rega, N., Petersson, G. A., Nakatsuji, H., Hada, M., Ehara, M., Toyota, K., Fukuda, R., Hasegawa, J., Ishida, M., Nakajima, T., Honda, Y., Kitao, O., Nakai, H., Klene, M., Li, X., Knox, J. E., Hratchian, H. P., Cross, J. B., Bakken, V., Adamo, C.,

Jaramillo, J., Gomperts, R., Stratmann, R. E., Yazyev, O., Austin, A. J., Cammi, R., Pomelli, C., Ochterski, J. W., Ayala, P. Y., Morokuma, K., Voth, G. A., Salvador, P., Dannenberg, J. J., Zakrzewski, V. G., Dapprich, S., Daniels, A. D., Strain, M. C., Farkas, O., Malick, D. K., Rabuck, A. D., Raghavachari, K., Foresman, J. B., Ortiz, J. V., Cui, Q., Baboul, A. G., Clifford, S., Cioslowski, J., Stefanov, B. B., Liu, G., Liashenko, A., Piskorz, P., Komaromi, I., Martin, R. L., Fox, D. J., Keith, T., Al-Laham, M. A., Peng, C. Y., Nanayakkara, A., Challacombe, M., Gill, P. M. W., Johnson, B., Chen, W., Wong, M. W., Gonzalez, C., Pople, J. A. (2004) Gaussian 03, Revision C.02. Wallingford, CT, Gaussian, Inc.

(124) Larry, A. C., Paul, C. R., Krishnan, R., Vitaly, R., John, A. P. (1999) Gaussian-3 theory using reduced Møller-Plesset order. *J. Chem. Phys.*, *110*, 4703-09.

(125) Becke, A. D. (1993) Density-functional thermochemistry. III. The role of exact exchange. *J. Chem. Phys.*, *98*, 5648-52.

(126) Lee, C., Yang, W., Parr, R. G. (1988) Development of the Colle-Salvetti correlation-energy formula into a functional of the energy density. *Phys. Rev. B*, *37*, 785-89.

(127) Vosko, S. H., Wilk, L., Nusair, M. (1980) Accurate spin-dependent electron liquid correlation energies for local spin-density calculations - a critical analysis. *Can. J. Phys.*, *58*, 1200-11.

(128) Stephens, P. J., Devlin, F. J., Chabalowski, C. F., Frisch, M. J. (1994) Ab-initio calculation of vibrational absorption and circular-dichroism spectra using density-functional force-fields. *J. Phys. Chem.*, *98*, 11623-27.

(129) Dunning, T. H., Jr. (1989) Gaussian basis sets for use in correlated molecular calculations. I. The atoms boron through neon and hydrogen. *J. Chem. Phys.*, *90*, 1007-23.

(130) Haszeldine, R. N., Jander, J. (1954) Spectroscopy. VI. Ultraviolet and infrared spectra of nitrosoamines, nitrites, and related compounds. *J. Chem. Soc.*, 691-5.

(131) Chow, Y. L., Wu, Z. Z., Lau, M. P., Yip, R. W. (1985) On the singlet and triplet excited-states of nitrosamines. *J. Am. Chem. Soc.*, *107*, 8196-201.

(132) Plumlee, M. H., Reinhard, M. (2007) Photochemical attenuation of N-nitrosodimethylamine (NDMA) and other Nitrosamines in surface water. *Environ. Sci. Technol.*, *41*, 6170-76.

(133) Padhye, L., Wang, P., Karanfil, T., Huang, C. H. (2010) Unexpected role of activated carbon in promoting transformation of secondary amines to N-nitrosamines. *Environ. Sci. Technol.*, *44*, 4161-68.

(134) Ge, X., Wexler, A. S., Clegg, S. L. (2011) Atmospheric amines - Part II. Thermodynamic properties and gas/particle partitioning. *Atmos. Environ.*, *45,* 561-577.

(135) Su, F., Calvert, J. G., Shaw, J. H. (1979) Mechanism of the photo-oxidation of gaseous formaldehyde. *J. Phys. Chem.*, *83*, 3185-91.

(136) Burrows, J. P., Moortgat, G. K., Tyndall, G. S., Cox, R. A., Jenkin, M. E., Hayman, G. D., Veyret, B. (1989) Kinetics and mechanism of the photooxidation of formaldehyde. 2. Molecular modulation studies. *J. Phys. Chem.*, *93*, 2375-82.

(137) Veyret, B., Lesclaux, R., Rayez, M. T., Rayez, J. C., Cox, R. A., Moortgat, G. K. (1989) Kinetics and mechanism of the photooxidation of formaldehyde. 1. Flash-photolysis study. *J. Phys. Chem.*, *93*, 2368-74.

(138) Zabel, F., Sahetchian, K. A., Chachaty, C. (1987) Electron spin-resonance spectra of free-radicals formed during the gas-phase photooxidation of formaldehyde - thermal-stability of the HOCH2OO radical. *Chem. Phys. Lett.*, *134*, 433-37.

(139) Barnes, I., Becker, K. H., Fink, E. H., Reimer, A., Zabel, F., Niki, H. (1985) FTIR spectroscopic study of the gas-phase reaction HO2 with H2CO. *Chem. Phys. Lett.*, *115*, 1-8.

(140) Su, F., Calvert, J. G., Shaw, J. H., Niki, H., Maker, P. D., Savage, C. M., Breitenbach, L. D. (1979) Spectroscopic and kinetic studies of a new metastable species in the photo-oxidation of gaseous formaldehyde. *Chem. Phys. Lett.*, *65*, 221-25.

(141) Veyret, B., Rayez, J. C., Lesclaux, R. (1982) Mechanism of the photo-oxidation of formaldehyde studied by flash-photolysis of CH_2O-O_2 mixtures. *J. Phys. Chem.*, *86*, 3424-30.

(142) Tarte, P. (1954) Spectroscopic investigation on nitroso compounds. *Bull. Soc. Chim. Belg.*, *63*, 525-41.

(143) Gowenlock, B. G., Pfab, J., Williams, G. C. (1978) Quantum yields for the photolysis of some nitrosamines in solution. *J. Chem. Res. (S)*, 362-3.

(144) York, D. (1966) Least-squares fitting of a straight line. *Can. J. Phys.*, *44*, 1079-86.

(145) National Research Council. Committee on Tropospheric Ozone Formation and Measurement (1991) Rethinking the ozone problem in urban and regional air pollution. Washington, D.C., National Academy Press.

Norwegian Institute for Air Research

REPORT SERIES SCIENTIFIC REPORT	REPORT NO. OR 2/2011	ISBN: 978-82-425-2357-0 (print) 978-82-425-2358-7 (electronic) ISSN: 0807-7207	
DATE 28.1.2011	SIGN.	NO. OF PAGES 140	PRICE NOK 150.-
TITLE Atmospheric Degradation of Amines (ADA). Summary Report: Photo-oxidation of Methylamine, Dimethylamine and Trimetahylamine. Climit project no. 201604		PROJECT LEADER Matthias Karl	
		NILU PROJECT NO. O-110043	
AUTHOR(S) Claus Jørgen Nielsen, Barbara D'Anna, Matthias Karl, Marius Aursnes, Antoinette Boreave, Rossana Bossi, Arne Joakim Coldevin Bunkan, Marianne Glasius, Mattias Hallquist, Anne-Maria Kaldal Hansen, Kasper Kristensen, Tomas Mikoviny, Mihayo Musabila Maguta, Markus Müller, Quynh Nguyen, Jonathan Westerlund, Kent Salo, Henrik Skov, Yngve Stenstrøm, Armin Wisthaler		CLASSIFICATION * A	
		CONTRACT REF. CLIMIT project no. 201604	
REPORT PREPARED FOR CLIMIT Gassnova SF Dokkvegen 19, N-3920 Porsgrunn 2700			

ABSTRACT
The atmospheric gas phase photo-oxidation of methylamine (CH_3NH_2), dimethylamine (($CH_3)_2NH$) and trimethylamine (($CH_3)_3N$) has been studied under pseudo natural conditions at the European Photochemical Reactor, EUPHORE, in Valencia, Spain. Major products in the photo-oxidation were imines (methanimine and N-methyl-methanimine) and amides (formamide, N-methyl formamide and N,N-dimethyl formamide). Total aerosol yields obtained in EUPHORE experiments were between 8 and 14%. Mimicking conditions at Mongstad results in a steady-state nitrosamine concentration of less than 0.6 % of photo-oxidized dimethylamine and less than 1.1 % of photo-oxidized trimethylamine. For rural regions it is predicted that the formation yield of the corresponding nitramine in the atmospheric oxidation of CH_3NH_2, ($CH_3)_2NH$ and ($CH_3)_3N$ is less than 0.4 %, 2.5 % and 5 %, respectively. The major uncertainties in the current understanding of the fate of amines emitted to the atmosphere are related to night-time chemistry, to the chemistry of imines, and to chemistry in the aqueous aerosol.

NORWEGIAN TITLE

Gassfase fotooksidasjon av methylamin, dimethylamin og trimethylamin

KEYWORDS Methylamines	KEYWORDS Atmospheric Chemistry	KEYWORDS Aerosol

ABSTRACT (in Norwegian)
Atmosfærisk fotooksidasjon av methylamin (CH3NH2), dimethylamin ((CH3)2NH) og trimethylamin ((CH3)3N) har blitt studert under pseudonaturlige forhold ved "European Photochemical Reactor", EUPHORE, i Valencia (Spania). Hovedproduktene i fotooksidasjonen var iminer (methanimin og N-methyl-methanimin) og amider (formamid, N-methyl formamid og N, N-dimethyl formamid). Total aerosoldannelse i EUPHORE-eksperimentene var mellom 8 og 14 %. Etterligning av forholdene på Mongstad resulterte i en "steady-state" konsentrasjon av kreftfremkallende nitrosaminer som var mindre enn 0.6 % per fotooksidert dimethylamin og mindre enn 1.1 % av fotooksidert trimetylamin. For landlige områder er det antatt at dannelsen av tilsvarende nitraminer i den atmosfæriske oksidasjonen av CH3NH2, (CH3)2NH og (CH3)3N er mindre enn henholdsvis 0.4 %, 2.5 % og 5 %. De største usikkerhetene i nåværende kunnskap om aminutslipp til atmosfæren er knyttet til natt- kjemi, til kjemien av iminer og til kjemien i vannfase aerosoler.

* Classification	A	Unclassified (can be ordered from NILU)
	B	Restricted distribution
	C	Classified (not to be distributed)

NILU is an independent, nonprofit institution established in 1969. Through its research NILU increases the understanding of climate change, of the composition of the atmosphere, of air quality and of hazardous substances. Based on its research, NILU markets integrated services and products within analyzing, monitoring and consulting. NILU is concerned with increasing public awareness about climate change and environmental pollution.

NILU Norsk institutt for luftforskning
Norwegian Institute for Air Research